The use of cervical gene therapy for the prevention of infection-related preterm birth

Dr Natalie Suff

Thesis submitted for completion of a Doctorate in Philosophy

Institute for Women's Health

University College London

Declaration

I, Natalie Suff confirm that the work presented in this thesis is my own. Where information has been derived from other sources, I confirm that this has been indicated in the thesis.

Acknowledgements

I wish to thank, first and foremost, my supervisors Donald, Simon and Suzy. Thank you all for believing in me! Donald, thank you for your constant support, helpful career guidance and motivation. Simon, thank you for being my stats guru and for your amazing advice. You inspired me to become a better scientist and researcher. Suzy, thank you for your life chats, encouragement and endless proof reading.

To my lab buddies, Raj, Jo, Dany, Juan and Julien. Thank you for guiding me through experiments and for laughing with me when things failed (as they often did!). I look forward to continuing to work with you in the future. To Roz, thanks for being there for my regular lunchtime moans, you helped me get through the tough PhD times! To Mona, thanks for our fun science chats, you constantly inspired me and encouraged me to be better. To Mark Tangney and Peter Taylor, thanks for providing the glowing bugs which are central to this thesis. To Dagmar and Grace, thank you for all your expert advice and analysis of the microbiome data. Thank you to the Wellbeing of Women and the Priory Foundation for providing the funding for this research.

To my family, thank you for being there for me all the time. I love you all. To Mike, my cheerleader, I could not have done this without your endless support.

Abstract

Introduction

Approximately 40% of preterm births are preceded by microbial invasion of the intrauterine space, with ascent from the vagina being the most common pathway. Antimicrobial peptides (AMPs), in combination with mucin and other immune cells, constitute a barrier within the cervical canal which prevents ascending infection. I investigate whether overexpression of human beta-defensin 3 (HBD-3), a potent AMP, in the cervical mucosa prevents bacterial ascent from the vagina into the uterine cavity of pregnant mice.

Methods

Models of ascending infection and preterm birth

Mice received *E.coli* (non-pathogenic K12 or pathogenic K1 with integrated luxABCDE operon) intra-vaginally at E16.5 and bacterial ascension was monitored by live whole body bioluminescence imaging.

AAV gene therapy

An adeno-associated virus vector (AAV8) containing the HBD-3 transgene was synthesised (AAV8-HBD3). AAV8-HBD3 or control vector AAV8-GFP control was administered intravaginally into E13.5 pregnant mice. This was followed by induction of ascending infection at E16.5 as described above.

Results

Following vaginal infection with *E.coli* K12, bioluminescence imaging showed bacterial ascent into the uterine cavity but this did not lead to preterm birth. Following vaginal infection with *E.coli* K1, bioluminescence showed bacterial ascent into the uterine cavity leading to subsequent premature delivery and a reduction in pups born alive, compared with uninfected controls.

Following intravaginal infection with *E.coli* K12 or K1, there was significantly less uterine bioluminescence in the AAV8-HBD3 treated mice at 24 and 48 hours after infection compared with the AAV8-GFP controls, signifying reduced uterine bacterial ascent in the AAV8-HBD3 treated mice. Although there was no increase in the gestation length in the *E.coli* K1 dams following AAV8-HBD3 treatment, there was an increase in the proportion of live pups at delivery compared with AAV8-GFP controls.

Conclusion

AAV-HBD3 may be a promising candidate for augmenting cervical innate immunity to prevent ascending infection-related preterm birth.

Table of Contents

List of tables

List of figures

Chapter 1 Introduction

1.1. Summary

Preterm birth is defined by the World Health Organization as delivery before 37 completed weeks of pregnancy. It is associated with serious neonatal morbidity and mortality, particularly for those infants born before 32 weeks gestation (Moore et al. 2012).

Intrauterine infection accounts for at least 40% of cases of spontaneous preterm birth. The most common route of pathogen entry into the uterine cavity is believed to be ascent from the microbial diverse environment of the vagina. There are currently no treatments that significantly and consistently prevent preterm birth and so there is a serious need to develop novel preventative treatments.

The cervix and its mucus plug play an important role in preventing ascending infection by providing a mechanical and immunological barrier that protects the uterine cavity from infectious insult. The plug contains numerous innate immune peptides known as antimicrobial peptides which contribute to its role in the prevention of infection. It is believed that a compromise in this specialised immune barrier confers an increased risk of infection-related preterm birth. I will investigate the novel hypothesis that expression of human antimicrobial peptides in the murine cervix using conventional virus-based gene transfer technology will prevent bacteria, which are capable of inducing preterm birth, from ascending the cervical canal and accessing the intrauterine space.

1.2. Preterm Birth

Preterm birth is defined by the World Health Organization as delivery before 37 completed weeks of pregnancy (WHO 2015). It is associated with serious neonatal morbidity and mortality, particularly for those infants born before 32 weeks gestation (Moore et al. 2012). Preterm birth is the single largest direct cause of neonatal mortality in the United Kingdom and worldwide, being responsible for more than 1 million neonatal deaths globally (NICE 2015; Blencowe et al. 2013). There are 54,000 cases of preterm birth per year in England and Wales, which accounts for approximately 8% of all live births and a quarter of these are associated with preterm deliveries before 32 weeks gestation (NICE 2015). Worldwide, 15 million babies are born prematurely, representing a preterm birth rate of 11.1% (Blencowe et al. 2013; Blencowe et al. 2012).

Despite extensive preterm birth research there has been no decline in preterm birth rates in the United Kingdom over the last ten years and these rates appear to be increasing in the developing world (NICE 2015; Blencowe et al. 2013).

The Millennium Development Goal-4 (1990-2015) set out to reduce the mortality rate in children under 5 years old by at least two thirds. Unfortunately this goal was not achieved, with the slow decline in neonatal mortality being largely responsible for this; neonatal deaths account for greater than 42% of deaths in under 5 year olds (Lawn et al. 2010). Prematurity is the direct cause of approximately 30% of the 4 million neonatal deaths every year and acts as a risk factor for many other causes of neonatal death, such as infection (Blencowe et al. 2013).

There is currently no effective treatment for the prevention of preterm birth (Iams et al. 2008). Even if we employed all of the five current interventions for preterm birth in high-income countries there would only be a 5.2% reduction in preterm birth rates (from 9.59% to 9.07% of livebirths) (Chang et al. 2013). Recent work from the March of Dimes preterm birth working group using an analytical model to evaluate preterm birth interventions found that new

research will be the most promising intervention to reduce preterm birth rates worldwide (Ferrero et al. 2016; Martin et al. 2017) (Figure 1.1.1). Interestingly the least promising intervention was found to be maximising or altering current preventative interventions. This highlights the serious necessity for research into the pathogenesis of preterm birth to enable us to develop novel preventative preterm birth treatments.

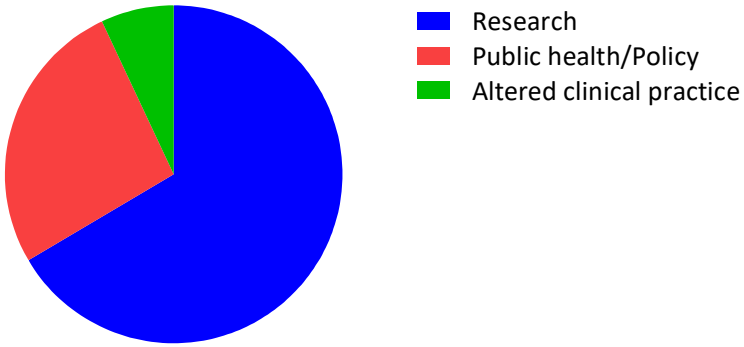

Figure 1.1: The areas of intervention and their potential effect on reducing the rates of preterm birth. Research accounts for 59-74% of the potential reduction effect whilst Public health/Policy accounts for 14-39%. Altered clinical practice is the smallest intervention group to provide potential beneficial effects on PTB rates accounting for a 2-12% effect with the current knowledge levels. Adapted from (Martin et al. 2017)

1.3. Epidemiology of Preterm Birth

The incidence of preterm birth varies between countries, ranging from 5-13% of all live births, resulting in approximately 15 million premature deliveries every year (Koullali et al. 2016). Mortality and morbidity of babies born preterm decreases with increasing gestational age. Preterm birth is ranked 5th in the leading cause of disease burden over time in the 2015 Global burden of Disease study (GBD 2015 DALYs and HALE Collaborators et al. 2016). Children born prematurely are three times more likely to have vision problems and they are also at increased risk of hearing impairment (O'Connor & Fielder 2007; Marlow et al. 2005). Furthermore, they are likely to have respiratory problems ranging from reduced exercise tolerance to needing

supplementary home oxygen (Greenough 2012; Bolton et al. 2012; Fawke et al. 2010). The cardiovascular consequences of prematurity have not been fully described although babies born extremely preterm (below 28 weeks gestation) are likely to be at increased risk of cardiovascular disease in the future (McEniery et al. 2011). Unsurprisingly, preterm birth leads to significant financial costs amounting to approximately £1 billion per year in England and Wales (Mangham et al. 2009).

It is not only the child that is affected by prematurity, it can also have a huge impact on the mother and other family members. The mother, for example, has an increased risk of preterm birth in the future which could put even more of a financial and health burden on the family (Laughon et al. 2014). Furthermore, there is a high prevalence of post-traumatic stress disorder in mothers following preterm birth and this can influence their coping mechanisms and future mental health (Ghorbani et al. 2014; Misund et al. 2014).

There are numerous risk factors associated with preterm birth (Table 1.1). The strongest predictor of preterm birth is a previous preterm birth or late miscarriage; these are associated with a 32% chance of a recurrent preterm birth (Laughon et al. 2014). BMI and low socio-economic status are associated with poor pregnancy outcomes, including preterm birth (Thompson et al. 2006). Connective tissue disorders, such as rheumatoid arthritis and Ehler Danlos syndrome, are associated with an increased risk of preterm birth, as are uterine anomalies (Wallenius et al. 2015; Khander et al. 2017). A short interpregnancy interval, IVF and multiple pregnancy are all obstetric factors which are associated with preterm birth (Shachar et al. 2016; Kindinger et al. 2016; Pandey et al. 2012).

Mid-trimester cervical shortening is strongly associated with premature delivery, with a cervical length below 25mm being highly predictive of preterm birth in both low and high risk women (Iams et al. 1996; Owen et al. 2001). Cervical length screening is common practice in the high risk population, however its use as a screening tool in low risk pregnancies is not

routinely recommended due to its low sensitivity (van der Ven et al. 2015; Orzechowski et al. 2014).

Fetal fibronectin is a glycoprotein found in placental tissue, amniotic fluid and the extracellular matrix of the decidua basalis, and it is believed to be released in response to inflammatory or mechanical damage to the membranes or placenta (Honest et al. 2002). Fetal fibronectin testing has a role in predicting the risk of preterm birth in symptomatic women, having a high negative predictive value for delivery within two weeks (Abbott et al. 2013). Furthermore, it is useful as a screening tool in combination with cervical length measurements in asymptomatic high risk women (Abbott et al. 2015).

	Risk factor	Reference
Maternal characteristic	Extremes of BMI	(Lynch et al. 2014; Cnattingius et al. 2013)
	Smoker	(Mei-Dan et al. 2015)
	Black ethnicity	(Schaaf et al. 2013)
	Low socio-economic status	(Thompson et al. 2006)
Medical history	Cervical surgery	(Kyrgiou et al. 2014; Bevis & Biggio 2011)
	Connective tissue disorders	(Wallenius et al. 2015)
	Uterine anomalies	(Khander et al. 2017; Takami et al. 2014)
Obstetric history	Previous preterm birth	(Khander et al. 2017; Takami et al. 2014)
	Previous late miscarriage > 16 weeks gestation	(Khander et al. 2017)
	Short interpregnancy interval	(Shachar et al. 2016)
Current pregnancy	IVF	(Sabban et al. 2017; Pandey et al. 2012)
	Multiple pregnancy	(Kindinger et al. 2016)
	Short cervix	(Hezelgrave et al. 2016)

Table 1.1: The risk factors associated with preterm birth. Previous preterm birth is the strongest predictor of a further preterm birth.

1.4. Pathogenesis of Preterm Birth

Preterm birth can be either spontaneous or iatrogenic (indicated early due to a maternal or fetal complication). Spontaneous preterm birth which includes preterm pre-labour rupture of membranes, accounts for approximately three quarters of preterm births in the UK, whilst the remaining quarter are classified as iatrogenic (Moutquin 2003).

The pathogenesis of spontaneous preterm birth and preterm pre-labour rupture of membranes remains poorly understood. There is accumulating evidence that preterm birth is a complex syndrome which is attributable to multiple pathological processes. These processes include intrauterine infection, stress, vascular disorders and uterine over-distension (Romero 2011). It is believed that these different pathophysiological processes lead to preterm labour by prematurely activating the common pathway of parturition. Intrauterine infection is the only known pathogenesis that has a definite causal link with spontaneous preterm birth (Minkoff 1983, Romero et al. 1988, Romero et al. 2001). Approximately 25-40% of cases of spontaneous preterm birth and preterm pre-labour rupture of membranes have been associated with infection and this number is thought to be even greater in cases of preterm birth occurring before 32 weeks gestation (Romero et al. 2001; Moore et al. 2012; Goldenberg et al. 2008; Goldenberg et al. 2000).

1.4.1. Intrauterine infection as a cause for preterm birth

There is a large body of evidence for the role of infection in preterm birth. As mentioned above, infection is associated with approximately 25-40% of cases of preterm birth, although this is likely to be an underestimate due to sample and culture selection bias (Goldenberg et al. 2000; Goldenberg et al. 2008). Histological chorioamnionitis, the hallmark of intrauterine infection, is found in around 66% of preterm births between 20 to 24 weeks and around 16% of preterm births at 34 weeks (Lahra & Jeffery 2004). For many years bacteria was often not detected in

cases of histological chorioamnionitis using traditional culturing techniques. However, the advent of molecular techniques in microbiology using the 16S rRNA gene meant that we were able to detect bacteria in the uterine cavity (Jones et al. 2009). Interestingly, the majority of bacteria found to be associated with preterm birth are fastidious organisms that are notoriously difficult to culture. In clinical studies, the uterine cavity is thought to be largely sterile, minimal bacteria is detected in term elective caesarean section or indicated preterm deliveries (Jones et al. 2009). Bacteria is seen in both term and preterm fetal membranes following vaginal delivery. In preterm samples, however, there is increased prevalence, diversity and distribution of bacterial species.

From an evolutionary perspective, infection-related preterm birth is likely to occur to improve the chance of maternal survival and reproductive fitness by allowing the mother to expel infected tissue. Evidence from animal models has shown that inoculation of the intrauterine cavity with live bacteria or bacterial toxins, such as lipopolysaccharide (LPS) leads to preterm birth, for example intrauterine LPS administration in mice (Migale et al. 2015; Rinaldi et al. 2015) and trans-cervical *E.coli* inoculation in rabbits (Fidel et al. 2003). Furthermore, extra-uterine systemic infections, such as malaria and pyelonephritis, are associated with preterm birth (Kalanda et al. 2006; Kaul et al. 1999). This is supported by evidence in rodent models where systemic administration of live bacteria or LPS cause preterm birth (Celik & Ayar 2002; Lee et al. 2003).

The current understanding is that microbes invade the choriodecidual space, activating the decidua and the fetal membranes to produce inflammatory cytokines, including interleukin-1β (IL-1β), interleukin-6 (IL-6), interleukin-8 (IL-8) and tumour necrosis factor-α (TNF-α) (Goldenberg et al. 2000; Gonzalez et al. 2011). These cytokines recruit immune cells to the area, such as neutrophils and macrophages and then stimulate prostaglandin synthesis (which is responsible for inducing myometrial contractions). This inflammatory process also leads to the synthesis of metalloproteases which can cause membrane rupture and remodelling of the

cervix leading to cervical dilatation. Supporting evidence is shown in animal models of preterm birth where administering pro-inflammatory cytokines, such as IL-1β and TNF-α, into the uterine cavity are sufficient to cause premature labour (Sadowsky et al. 2006; Nadeau-Vallée et al. 2017).

1.4.2. Ascending vaginal infection

There are multiple potential routes by which bacteria can gain access into the intrauterine cavity;

1) By ascending infection from the vagina via the cervix
2) By haematogenous dissemination from the maternal blood via the placenta
3) By retrograde seeding from the peritoneal cavity through the fallopian tubes
4) By an invasive procedure, such as an amniocentesis or chorionic villus sampling

Ascending vaginal infection is believed to be the most common pathway (Figure 1.2). The main supporting evidence for this pathway is based on the association between the bacterial species identified in the fetal membranes and placenta and those normally found in the lower genital tract by 16S ribosomal DNA PCR studies (Jones et al. 2009; Doyle et al. 2017). These species include *Ureaplasma urealyticum*, *Ureaplasma parvum* and *Streptococcus agalactiae* (also known as Group B *Streptococcus*). It has also been found that histological chorioamnionitis is more common and more severe at the site of membrane rupture, supporting an ascending route of microbial entry (Romero et al, 1989).

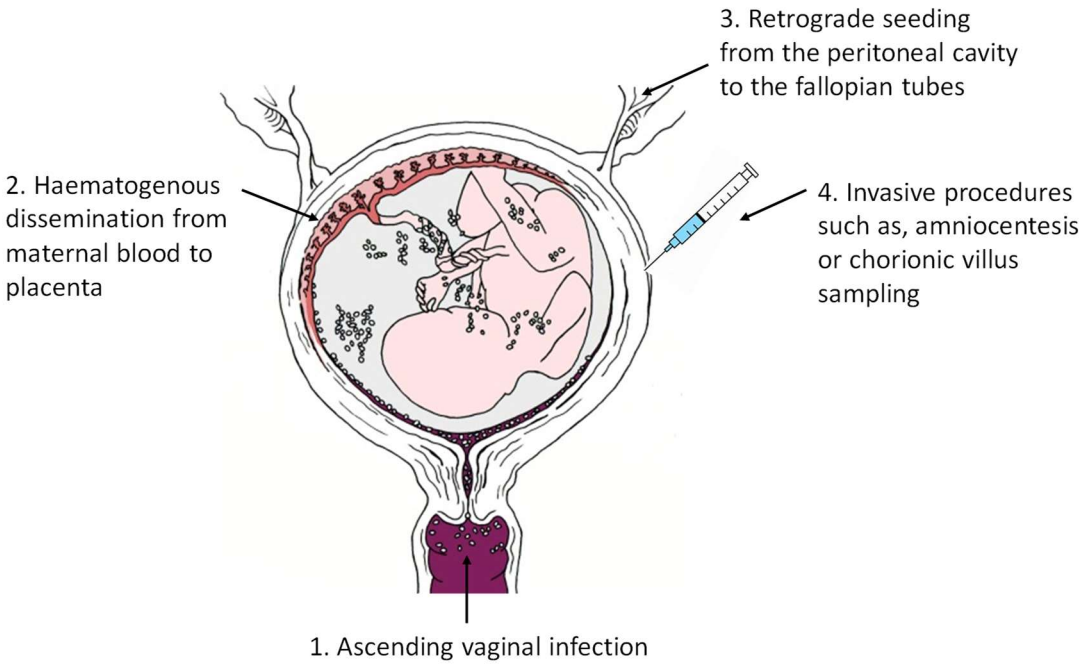

Figure 1.2: Routes of entry of pathogens into the pregnant uterine cavity. By ascending infection from the vagina via the cervix (1), by haematogenous dissemination from the maternal blood via the placenta (2), by retrograde seeding from the peritoneal cavity through the fallopian tubes (3) or by an invasive procedure, such as an amniocentesis or chorionic villus sampling (4). Ascending vaginal infection is thought to be the most common route of entry.

There are two theories describing how bacteria ascend into the uterine cavity (Figure 1.3):

1. Bacteria ascend into the choriodecidual space where they replicate and cause inflammation followed by subsequent passage through the chorioamniotic membranes to reach the intraamniotic cavity (Grigsby et al. 2010; Adams Waldorf et al. 2011).
2. Bacteria ascend to the decidua of the supracervical region, followed by subsequent passage through a distinct region of the chorioamniotic membranes to reach the intraamniotic cavity (Steel et al. 2005; Kim et al. 2009). Chorioamnionitis is thought to occur as a secondary step in this process.

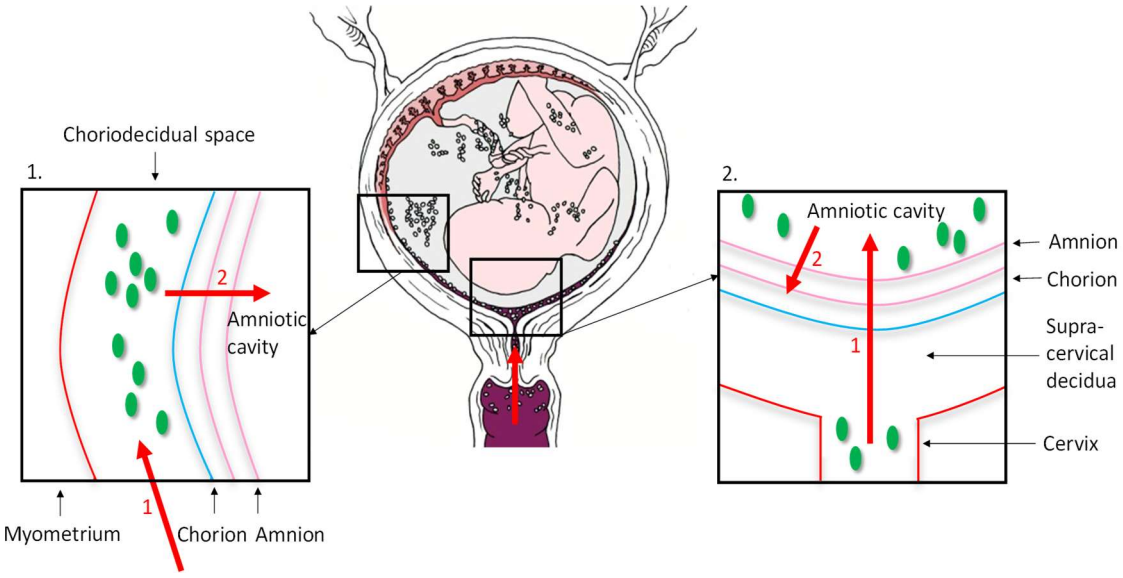

Figure 1.3: Ascending vaginal infection - two theories describing the trafficking of bacteria into the chorioamniotic membranes during microbial invasion of the amniotic cavity. (1) Widespread bacterial invasion along the choriodecidual and chorioamniotic planes prior to entering the amniotic cavity. **(2)** Initial intraamniotic entry of bacteria through a restricted supracervical region leading to intraamniotic invasion and subsequent bacterial movement into the amnion and chorion.

It is unknown why some women are more at risk of developing ascending infection leading to subsequent preterm birth, but the interaction between cervical mucosal immunity and the diverse vaginal microbiome may play a key role. Bacterial vaginosis, a vaginal infection where normal lactobacillus-predominant vaginal flora is replaced with an overgrowth of anaerobic bacteria, has been associated with preterm birth (Hillier et al. 1995). Furthermore, certain gene-environment interactions are thought to confer an increased risk of preterm birth; polymorphism in the tumour necrosis factor promoter region and concurrent bacterial vaginosis (Macones et al. 2004). More recent evidence has shown that specific bacterial virulence factors, such as β-haemolysin/cytolysin in Group B *Streptococcus*, also make bacterial

ascension and infection of the intrauterine cavity more likely (Randis et al. 2014). Furthermore, concurrent viral infection may alter cervical mucosal immunity and predispose to ascending vaginal infection (Racicot et al. 2013).

It is also not clear what comes first in the mechanistic pathway of infection-related preterm labour; ascending infection or cervical dilatation. Ascending infection may lead to inflammatory changes in the cervix which result in cervical shortening and dilatation or alternatively the cervix may dilate initially and allow for pathogens to ascend into the uterine cavity. Preterm birth has been linked to cervical treatment for cervical intra-epithelial neoplasia and this risk appears to be proportional to the volume of cervical tissue removed (Castanon et al. 2014; Kyrgiou et al. 2014). The reduction in cervical epithelium may lead to an impairment in the mechanical and structural integrity of the cervix resulting in an increased risk of ascending vaginal infection or alternatively, the reduction in cervical epithelial surface area may cause an impairment in the host innate immune defence to combat ascending vaginal infection. In addition, cervical intra-epithelial neoplasia is caused by an inability to clear high-risk human papilloma virus and it has been postulated that cervical human papilloma virus infection alone confers a risk of preterm birth (Reilly et al. 2012). This points towards an inherent impairment in cervical antimicrobial defence as the cause of preterm birth.

1.4.3. The vaginal microbiome and preterm birth

A healthy vaginal microbiome in pregnant and non-pregnant women is associated with low bacterial diversity and lactobacillus dominance. Lactobacillus species are thought to provide protection against pathobiont colonization through lactic acid excretion, hydrogen peroxide excretion and antimicrobial production of bacteriocins (Aroutcheva et al. 2001). An association between lactobacillus depletion and vaginal dysbiosis leading to poor pregnancy outcomes, such as preterm birth and late miscarriage, has long been reported (Hillier et al. 1995; Donders et al. 2009; Murphy & Mitchell 2016). However, recent evidence suggests that dominance of a

certain lactobacillus species, *Lactobacillus iners* (*L.iners*), at 16 weeks gestation is associated with increased rates of preterm birth instead of bacterial vaginosis (Petricevic et al. 2014; Kindinger et al. 2017), whilst a dominance of *Lactobacillus crispatus* is associated with a reduced risk of preterm birth (Kindinger et al. 2017). Interestingly, *L.iners* is often associated with bacterial vaginosis as its dominance in the vagina confers a less stable microbiota with a tendency to transition to a bacterial vaginosis-associated state (Verstraelen et al. 2009; Tamrakar et al. 2007). Older studies looking at the link between vaginal dysbiosis and preterm birth were unable to differentiate the lactobacillus species and so may have missed this important association (Hillier et al. 1995; Leitich et al. 2003).

Lactobacillus species appear to have differing effects on the vaginal mucosa which may contribute to the mechanisms by which *L.iners* leads to preterm birth. These effects include host-bacterial metabolite interactions whereby *L.iners* produces more L-Lactic acid compared with *L.crispatus* which produces more D-lactic acid (Witkin et al. 2013). L-lactic acid has been shown to promote vaginal extracellular matrix metalloproteinase inducer, as well as matrix metalloproteinase-8 which may lead to subsequent cervical remodelling resulting in ascending infection and/or preterm birth. Furthermore, *L.iners* has been shown to induce pro-inflammatory cytokines, such as IL-8, in human vaginal epithelial cells *in vitro* (Anahtar et al. 2016).

1.4.4. The morbidity and mortality of the premature infant

Preterm birth is now the leading cause of death in infants under 5 years old (Liu et al. 2015) with the risk of mortality and the severity of preterm birth complications being inversely related to gestation at delivery (Moore et al. 2012). Prematurity is associated with complications in a number of organ systems including cognitive and neurological disability, such as cerebral palsy, respiratory conditions and gastrointestinal disease (Moore et al. 2012; Marlow & Budge 2005; Goldenberg et al. 2008).

As mentioned above, intrauterine infection and inflammation is commonly associated with preterm birth, particularly at the earlier gestations (Moore et al. 2012). Whilst some of the complications observed in babies born preterm relate to immaturity, there is substantial evidence that perinatal exposure to infection and inflammation leads to further damage. Bacteria and inflammatory mediators, such as cytokines, can reach the fetus directly by transplacental transmission or indirectly via ingestion from the amniotic fluid (Adams Waldorf & McAdams 2013).

Neurodevelopmental consequences of prematurity include cerebral palsy, sensorineural hearing loss, blindness and severe intellectual disability (Chang 2015). Cerebral palsy is often seen in the setting of diffuse white matter injury and/or cystic periventricular leukomalacia. Prematurity has also been linked to neuropsychological conditions such as schizophrenia and autism (Meldrum et al. 2013; Meyer et al. 2011). The preterm brain is particularly susceptible to inflammation; any dysregulation in the normal production of cytokines appears to influence brain development. Pro-inflammatory cytokines either cause a direct insult to oligodendrocytes and neurons; there is evidence TNF-α is toxic to oligodendrocytes (Li et al. 2008), or they cause secondary injury by activating microglia leading to local cytokine and free radical release (Burd et al. 2012). This is supported by clinical data in which placental infection and inflammation alone was found to be a predictor of diparetic cerebral palsy in the very preterm infant (Leviton et al. 2010). Interestingly, Elovitz et al., have reported evidence of fetal brain injury and subsequent long-term neurological sequelae in a mouse model of intrauterine inflammation even in the absence of preterm birth (Elovitz et al. 2011; Dada et al. 2014). Furthermore, fetuses of rabbits transcervically inoculated with *E.coli* have been shown to develop white matter brain injury, which is similar to the pathology we see clinically in preterm babies, within 5 days of infection (Yoon et al. 1997).

1.4.5. Current treatments for preterm birth

In view of the clear link between intra-uterine infection and preterm delivery, the use of antibiotics has been one of the main focuses of preterm birth research. Clinical studies investigating the use of systemic antibiotics for preterm birth prevention has shown inconclusive results (Subramaniam et al. 2012). In particular, there is no evidence that antibiotics cause a delay to delivery in women with established preterm birth (Kenyon et al. 2001; King & Flenady 2002). Furthermore, there is evidence that antibiotic use may be associated with an increased risk of cerebral palsy in the infant (Kenyon et al. 2008). It is likely that antibiotic use at this late stage may only mask the damaging inflammation which has already occurred and therefore lead to more severe pathology. This data has unsurprisingly resulted in a significant barrier to further research into antibiotic use in a clinical setting.

The treatment of bacterial vaginosis (which has been linked to preterm birth) with antibiotics has not been found to significantly reduce the rates of preterm birth in a Cochrane review of 21 trials (Brocklehurst et al. 2013). This is supported by data in which metronidazole treatment was not found to reduce preterm birth rates (and may even lead to higher rates) in women greater than 24 weeks gestation who were at high risk of preterm birth (Shennan et al. 2006). Following antibiotic treatment for bacterial vaginosis, the vaginal microbiota has been found to be predominately composed of the lactobacillus species, *L.iners* (Ferris et al. 2007). In view of the recent data linking a *L.iners* dominant vaginal microbiota to an increased risk of preterm birth it is possible that antibiotic treatment for bacterial vaginosis may be doing more harm than good (Kindinger et al. 2017).

Cervical cerclage, the placement of a suture in the cervix, is commonly performed in women at high risk of preterm birth who have a reduced cervical length. There is evidence that it leads to a reduction in preterm birth in this group of women (Berghella et al. 2011) but this benefit is less convincing in other groups of high risk women (To et al. 2004). Although the underlying

mechanism is unknown it is believed to have a role in maintaining the integrity of the cervical barrier and mucus plug. There is, however, evidence that the type and the location of the cervical suture has an effect on the length of gestation (Kindinger et al. 2016; Cook et al. 2017).

Progesterone has long been used as a preventative treatment for women at high risk of preterm birth, possibly due to its anti-inflammatory effects. The OPPTIMUM study, a large randomised controlled trial on vaginal progesterone use in women at high risk of preterm birth, showed no reduction in risk of preterm birth or improvement in neonatal outcomes (Su et al. 2014; Norman et al. 2016). However, a recent meta-analysis of vaginal progesterone in preterm birth, including data from OPPTIMUM, showed evidence of a reduced risk of preterm birth in a sub-group of high risk women who have a cervical length ≤ 25mm (Romero et al. 2016). These studies highlight the need to develop novel preventative therapies for preterm birth.

1.4.6. Animal models of infection-related preterm birth

Animal models of infection-related preterm birth provide useful insight into the mechanisms that regulate infection, inflammation and preterm parturition. An ideal research model for preterm birth would have similar reproductive biology as a human, mimic what occurs clinically and have comparable fetal and neonatal development. The non-human primate would represent a near-ideal species in which to investigate preterm birth although their use is limited due to cost and ethical considerations. Nevertheless, the rhesus macaque has been used to model infection-related preterm birth by infiltration of group B streptococcus, as well as inflammatory cytokines, into the amniotic cavity and choriodecidual space (Grigsby et al. 2010; Waldorf et al. 2011; Elst et al. 1991; Sadowsky et al. 2006).

In the human and the non-human primate, systemic progesterone withdrawal does not seem essential for parturition to occur, however in the lower mammalian species, such as the mouse,

rat and rabbit, term labour occurs after involution of the corpus luteum which results in progesterone withdrawal (Challis et al. 2000). This has been supported by evidence in which blocking progesterone using RU486 (a competitive progesterone receptor antagonist) induces preterm birth in rodents (Garfield et al. 1987; Dudley et al. 1996). This was initially thought to be a concern when using lower mammalian species as preterm birth models but it has since been shown that progesterone withdrawal is not an essential step in the preterm labour process following bacterial inoculation in mice (Hirsch & Muhle 2002).

Rodents, mainly mice, have been used as models of infection-related preterm birth for many years. Large numbers can be used, they are relatively cheap to maintain and they have short breeding cycles making them a practical animal model for preterm birth research. Furthermore, more transgenic mouse models are available compared to other animal species so the specific genes and pathways involved in parturition can be interrogated. Systemic administration of LPS was initially used to induce preterm birth in mice (Lee et al. 2003; Kaga et al. 1996). These models tend to mimic the systemic extra-uterine infections, such as pyelonephritis or malaria, which are associated with preterm birth clinically. To model the localised intrauterine inflammatory process seen more commonly in human preterm birth, models were developed by administering intrauterine LPS (Migale et al. 2015; Elovitz et al. 2003; Elovitz & Mrinalini 2005; Edey et al. 2016; Rinaldi et al. 2014). More recently a less invasive but equally efficient model has been developed which uses ultrasound, instead of laparotomy, to target the injection site (Rinaldi et al. 2015).

The use of animal models to mimic the ascending vaginal infection in preterm birth is much less common. Intravaginal LPS administration in pregnant mice has been shown to cause cervical inflammation and remodelling (Gonzalez et al. 2011; Gonzalez et al. 2014). A murine model of Group B *Streptococcus* (GBS) colonization and ascending infection has been

developed (Randis et al. 2014). Furthermore, intravaginal application of *E.coli* (055) has been used to develop a model of preterm birth in mice (Akgul et al. 2014).

Intravaginal application of a laboratory strain of *E.coli*-tagged with a red fluorescent protein and *Ureaplasma urealyticum* has been used to model ascending vaginal infection with the added benefit of being able to track bacterial ascent (Racicot et al. 2013). Interestingly, these bacteria were not able to ascend into the pregnant uterine cavity unless the cervix had prior exposure to viral infection.

Bacteria that are commonly implicated in preterm birth clinically include the genital mycoplasmas, *Streptococcus agalactiae* (Group B streptococcus) and commensal species of the oral cavity such as *Fusobacterium nucleatum* (Witt et al. 2005; Nguyen et al. 2004; Kataoka et al. 2006; Feikin et al. 2001; DiGiulio et al. 2008; Han et al. 2009). *Escherichia coli* (*E.coli*) is commonly used in animal models of preterm birth, whether as live bacteria or as an *E.coli* strain of LPS endotoxin, however, it is not classically associated with preterm birth clinically. Although interestingly a recent systemic review of data published on the intraamniotic microbiome of women who delivered preterm found *E.coli* to be present in the amniotic fluid of 7% of women who delivered preterm, whilst a bacteria more commonly associated with preterm birth, *Ureaplasma urealyticum*, was only found in 11% (Mendz et al. 2013). Furthermore, *E.coli* is easily obtained and cultured so provides a convenient infectious agent for preterm birth modelling, as well as proving to be efficient in inducing premature delivery in mice. As with all animal models, they do not exactly mimic the same condition as humans but they provide an understandable and easily manipulated model that is consistent with the 3Rs of animal research (nc3Rs 2014).

The development of animal models of ascending vaginal infection is particularly important for preterm birth research to provide mechanistic data, as well as a means of reliably testing novel

preventative treatments which could be clinically translated into pregnancies at risk of delivering prematurely.

1.5. The innate immune system

The innate immune system compromises the rapid, non-specific and primitive part of the immune system (Figure 1.4). It provides the first line of host defence in all multicellular organisms and it results in swift immune responses as it does not rely on antigen recognition like the adaptive immune system. The innate immune system in humans includes the complement system, neutrophils, macrophages, cytokines, chemokines and the naturally occurring antimicrobial peptides (AMPs) (Tosi 2005). The main role of the innate immune system is the fast elimination of pathogens and the activation of a stereotypical inflammatory response. This system has evolved to recognise foreign pathogens by pathogen-recognition receptors which are found on the surface of epithelial cells, innate immune cells such as neutrophils and macrophages and are also found secreted into tissue fluids or the bloodstream (Janeway & Medzhitov 2002). These receptors bind to specific pathogen-associated molecular patterns found in groups of microorganisms. The main pathogen-recognition receptors involved in the innate immune system are the toll-like receptors. Toll-like receptor signalling leads to immune cell recruitment as well as the production and secretion of endogenous AMPs (Takeda et al. 2003).

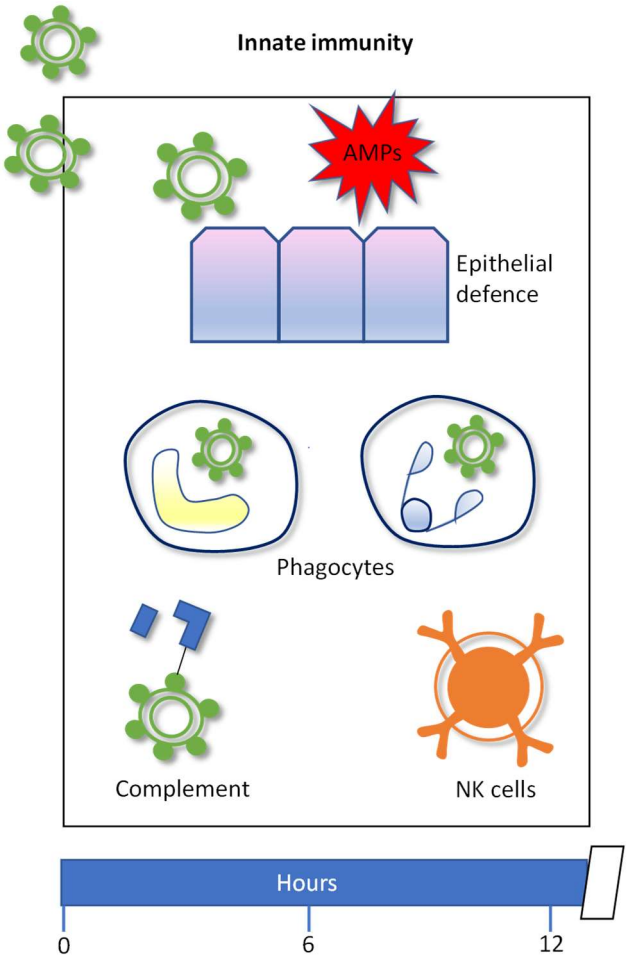

Figure 1.4: The innate immune system. The innate immune system is the rapid, non-specific and primitive part of the immune system. The innate immune system comprises of epithelial cell barriers. As well as producing substances such as, mucus which can trap pathogens, these cells can express antimicrobial peptides which have direct antimicrobial activity and specific immunomodulatory roles. The immune cells involved in innate immunology are the phagocytes; neutrophils, macrophages and dendritic cells. They can phagocytose invading pathogens and macrophages and dendritic cells specifically have a role in antigen presentation, linking the innate and acquired immune systems. Natural killer cells also have a role in innate immunity by non-specifically killing virus and tumour infected cells. The complement system is an important part of the immune system, being the major humoral defence mechanism by participating in opsonization, chemotaxis and activation of leucocytes and cytolysis of infected cells.

1.5.1. Natural antimicrobial peptides (AMPs)

AMPs, as discussed above, are important effector molecules of the innate immune system. Over 1200 AMPs have been discovered so far with the common unifying function of killing microbes at physiological concentrations (Bevins et al. 1999). They are found abundantly in the host defence systems of all plants and animals (Borregaard et al. 2000). The majority of these peptides consist of 10-50 amino acid residues and their common features include a positive charge whilst maintaining a hydrophobic and amphipathic structure. It is thought that these features allow them to interact with the negatively charged phospholipid groups and hydrophobic fatty acid chains of microbial membranes to form lytic pores and therefore facilitate the subsequent release of cytosol contents (Latal et al. 1997).

AMPs appear to play a key role in linking the innate and adaptive immune system firstly by activating immune cells such as dendritic cells, T lymphocytes and monocytes and secondly by inducing specific cytokine release (Yang et al. 1999; Biragyn 2011). There are two main types of AMPs in humans; defensins and cathelicidins; humans possess a single cathelicidin gene, whilst there are numerous defensin genes (Ganz 2003; de Souza et al. 2007) (Table 1.2).

.

	LL-37	α-defensins	β-defensins
Structure	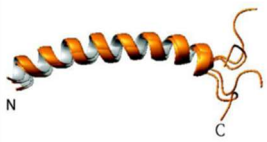 • Linear amphipathic α-helix	 • β-sheets • 6 cysteine motifs with disulphide bridges (C 1-6, 2-5, 3-5)	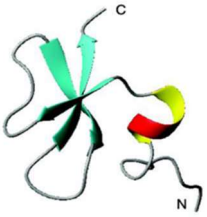 • β-sheets • 6 cysteine motifs with disulphide bridges (C 1-5, 2-4, 3-6)
Source	• Epithelial cells • Leucocytes	• HNP 1-4; neutrophil granules • HD5-6; Paneth cells of small intestine	• Epithelial cells
Regulation	• Constitutive and inducible	• Constitutive	• Constitutive and inducible
Antimicrobial properties	• Broad spectrum	• Broad spectrum	• Broad spectrum

Table 1.2: The main AMPs in humans are the cathelicidin and the defensins. This table describes the structure, types, locations and properties of these AMPs. The structural peptide images have been adapted from (Wang & Guangshun 2014)**.**

Defensins are widely distributed in epithelial cells and neutrophils. They are part of the cysteine rich beta-sheet peptide family which includes the two main subfamilies the α and β-defensins. They share a common structure of six disulphide-linked cysteine bridges forming the characteristic β-sheet (Ganz 2003). They differ in the pattern of their cysteine pairings (Wiesner & Vilcinskas 2010). These small cationic peptides have a broad range of antimicrobial activity against a wide range of bacteria including gram negative bacteria, gram positive bacteria and fungi (Miyasaki & Lehrer 1998). Their main mechanism of antimicrobial killing is by the formation of pores in the lipid bilayer of the microbe (Latal et al. 1997).

So far, 6 α-defensins have been discovered; human neutrophil peptides 1-4 (isolated from azurophilic granules in human neutrophils) and α-defensins 5 and 6 (found in intestinal paneth cells) (Wiesner & Vilcinskas 2010; Ghosh et al. 2002). The beta-defensins (HBD), on the other hand, are found at all mucosal surfaces, either constitutively or inducibly expressed. Their synthesis and release is regulated by bacteria, viruses and inflammatory cytokines. HBDs are highly conserved peptides which are thought to have evolved from a single ancestral beta-defensin gene (Dhople et al. 2006). There are four human beta-defensins. HBD-1 is constitutively expressed in some tissues, whilst HBD-2, HBD-3 and HBD-4 are inducible, usually in response to a pro-inflammatory stimulus (Pazgier et al. 2006). Their charge-dependent microbial killing mechanism can occur at micromolar concentrations but this is inhibited under conditions of increased ionic strength.

Cathelicidin is stored in secretory granules of neutrophils and macrophages, as well as in epithelial cells. Humans and mice possess a single cathelicidin gene, the *CAMP* gene, which produces the LL-37 and CRAMP proteins respectively. Exons 1 to 3 of the *CAMP* gene encode the signal precursor and the pro-sequence domain, whilst exon 4 encodes the mature antimicrobial peptide (Zanetti et al. 2000; Pestonjamasp et al. 2001). Cleavage of the inactive precursor by proteinase-3 or elastase to release the mature C-terminal antimicrobial peptide occurs upon degranulation of activated neutrophils (Panyutich et al. 1997; Sørensen et al. 2001) however, the cleavage process in epithelial cells is less well understood (Pestonjamasp et al. 2001).

The antimicrobial activity of cathelicidin is rapid and broad spectrum, effectively killing many common antibiotic-resistant strains of bacteria (Zanetti et al. 2002). The mechanism of microbial killing is, like defensins, through disruption of the microbe's membrane integrity (Boman et al. 1993).

1.5.2. Human beta-defensin-3 (HBD-3)

HBD-3 has potent antimicrobial activity against multiple bacteria, fungi and viruses (Table 1.3) and appears to be resistant to high salt environments (Harder et al. 2001). HBD-3 also has the potential to bind and neutralise LPS leading to anti-toxin properties (Lee et al. 2010). Importantly, it is able to inhibit HIV replication by acting as an endogenous CXCR-4 antagonist (Feng et al. 2006).

In addition to its antimicrobial activities, it also has important immunomodulatory properties. It has a chemoattractant role which is mediated through its effector ligands for chemokine receptor CCR6 on T-lymphocytes and immature dendritic cells (Wu et al. 2003). This allows HBD-3 to link the innate and adaptive immune systems. There is, however, significant controversy as to whether HBD-3 exerts pro- or anti-inflammatory effects *in vivo*. It has been found to increase pro-inflammatory cytokines such as IL-6, IL-8 and IL-1β by dendritic cells and monocytes, as well as inhibiting the production of the anti-inflammatory cytokine IL-10 by monocytes (Tewary et al. 2013; Funderburg et al. 2011). Furthermore, recent evidence has supported this pro-inflammatory effect by showing that HBD-3 can cause an exacerbated IFN-β response in human and mouse macrophages in response to the viral ligand mimic polyinosinic:polycytidylic acid (Semple et al. 2015).

In contrast, HBD-3 has numerous anti-inflammatory effects. In addition to its ability to neutralise the LPS toxin by direct binding, it can also inhibit TNF-α and IL-6 in LPS stimulated cells (Semple et al. 2010; Bedran et al. 2014). The underlying mechanism has been shown to be the inhibition of pro-inflammatory gene transcription within TLR-4 stimulated cells (Semple et al. 2011). Furthermore, HBD-3 can attenuate pro-inflammatory cytokine responses to the oral pathogen *Porphyromonas gingivalis* in mucosal secretions (Pingel et al. 2008). In addition, HBD-3 and LL-37 appears to work synergistically to reduce inflammatory cytokine production in an *in vitro* model of periodontitis (Bedran et al. 2014).

Antimicrobial activity of HBD-3	
Escherichia coli	(Hoover et al. 2003)
Pseudomonas aeruginosa	(Harder et al. 2001)
Klebsiella pneumoniae	(Sahly et al. 2006)
Staphylococcus aureus	(Hoover et al. 2003)
Streptococcus pyogenes	(Harder et al. 2001)
Streptococcus pneumoniae	(Scharf et al. 2012)
Enterococcus faecium	(Harder et al. 2001)
Porphyromonas gingivalis	(Shelburne et al. 2005)
Staphylococcus carnosus	(Hoover et al. 2003)
Saccharomyces cerevisiae	(Hoover et al. 2003)
Candida albicans	(Harder et al. 2001)
Candida parapsilosis	(Harder et al. 2001)
Candida krusei	(Harder et al. 2001)
HIV-1	(Feng et al. 2006)

Table 1.3: Antimicrobial activity of HBD-3. HBD-3 has broad spectrum antimicrobial activity; it is particularly microbicidal against gram negative bacteria.

1.5.3. Cervical innate immunity in pregnancy

The innate immune system of the female reproductive tract is a unique and specialized system that functions to support and protect the fetus as well as protecting against potential pathogens. The cervix has a particularly important role in pregnancy as it acts as the gatekeeper to the uterus by protecting the largely sterile decidua from the diverse microbial environment of the vagina. During pregnancy, the cervix produces a specialised cervical mucus plug which contributes to its important immuno-protective role. The cervical mucus plug is a large, viscous structure that occupies the cervical canal during pregnancy. The key component

which contributes to its structural and immunological properties is the mucinous glycoproteins. These mucins sterically inhibit the diffusion of larger molecules, such as bacteria and fungi, as well as providing ligands for cytokines and chemokines. Importantly, these mucins are negatively charged oligosaccharides which help to retain positively charged molecules, including the endogenously occurring AMPs (Becher et al. 2009). A number of AMPs have been found in the cervical mucus plug; secretory leucocyte protease inhibitor (SLPI), elafin, lysozyme, human neutrophil peptides 1-3 and human beta-defensin 1 (Hein et al. 2002; Hein et al. 2001; Stock et al. 2009). The cervical mucus plug appears to function as a structural and immunological barrier preventing ascending vaginal bacteria from gaining access into the uterine cavity.

1.5.4. AMPs and preterm birth

The role of cervical AMPs in the pathogenesis of preterm birth is not entirely clear. Bacterial vaginosis in pregnancy which has been linked to an increased risk of preterm birth is associated with low cervico-vaginal levels of elafin (Hillier et al. 1995; Stock et al. 2009). Furthermore, low levels of SLPI and elafin have also been found in the amniotic fluid and fetal membranes of woman with preterm pre-labour rupture of membranes (King et al. 2007). It is thought that these low AMP levels may reflect a reduced capacity of these women to respond to and to combat vaginal infection. Polymorphisms of the elafin gene have been identified which are associated with reduced elafin secretion, although this has not been investigated in women at risk of preterm birth (Tejera et al. 2009). Recent data has shown a reduction in cervical HBD-1 and SLPI in women after cervical excision for cervical intra-epithelial neoplasia (Mitra et al. Society of Reproductive Investigation, 2016, unpublished data). Cervical excision for cervical intra-epithelial neoplasia, as mentioned previously, is a major risk factor for preterm birth and this represents an interesting potential mechanistic link.

In contrast to this, SLPI and elafin have also been found to be raised in the cervico-vaginal fluid of women in the second trimester who subsequently develop cervical shortening and spontaneous preterm birth (Abbott et al. 2014). In addition, SLPI has been shown to act as a marker of impending delivery in normal term deliveries (Samejima et al. 2015). Increased expression of SLPI, elafin and human neutrophil peptide mRNA has been found in the cervical cells of women who were admitted in preterm labour (Itaoka et al. 2015; Xu et al. 2008; Lucovnik et al. 2011). It is likely that these women are responding to subclinical vaginal infection by increasing endogenous levels of cervical AMPs, so as to enhance their host defence mechanisms. This is in contrast to the increased levels being a cause of the premature parturition. In support of this, cathelicidin has been shown to be increased in cervico-vaginal fluid in women with bacterial vaginosis during pregnancy and have a protective role in resolving the dysbiosis (Frew et al. 2014). The fact that cathelicidin levels have been found to return to normal after bacterial vaginosis treatment would also support this protective role (Valore et al. 2006).

Ureaplasma species, which colonize the vagina in some women, have been associated with preterm birth (Witt et al. 2005). Interestingly, it has been found that these bacterial species can manipulate host defence by downregulating AMP gene expression (Xiao et al. 2014).

1.6. Gene therapy: novel therapeutic strategies for preterm birth

The use of gene transfer therapy is increasingly considered to be a realistic treatment option for a variety of single gene defect disorders and there are successful clinical trials using gene therapy for the treatment of inherited immunodeficiency, Leber's congenital amaurosis and haemophilia (Gaspar et al. 2011; Bainbridge et al. 2015; Russell et al. 2017; Nathwani et al. 2014). In recent years, acquired diseases such as cardiovascular disease, cancer and infectious diseases have been the subject of most of the gene therapy research rather than inherited monogenic disorders due to the larger numbers of affected patients and advancements in the

field (Ginn et al. 2013). Of most relevance to obstetrics research, is the development of a therapy for fetal growth restriction using adenoviral vector-delivered vascular endothelial growth factor to the maternal arteries during pregnancy ((Mehta et al. 2014), http://everrest-fp7.eu/). This exciting advancement in gene therapy for fetal growth restriction has lead the way for the development of gene therapies for other pregnancy disorders. Furthermore, the above study has performed patient-led focus groups to discuss the acceptability of gene therapy for pregnancy disorders and overall this type of therapy was found to be generally favourable.

1.6.1. Viral vector-based gene therapy

Gene transfer can be achieved by viral and non-viral vectors. Viral vectors have been more successful up to now, due to their increased efficiency of gene delivery, and they have been used in all of the successful gene therapy clinical trials so far (Bainbridge et al. 2015; Nathwani et al. 2012). The most common viral vectors used are lentiviruses, adenoviruses and adeno-associated viruses (AAV). Lentiviral vectors, a subclass of retroviruses, naturally integrate into both dividing and non-dividing cells as well as showing stable and long-term expression. Adenoviral vectors have high packaging capacity, are non-integrating and can deliver short-term gene transfer however, a serious safety concern was raised after an adenoviral vector caused the death of a patient in the late 1990s. This was found to be caused by the adenoviral capsid leading to a cytokine storm which resulted in subsequent multi-organ failure. The majority of adenovirus research now focuses on its use as a targeted oncolytic agent, vascular disease and as a vaccine delivery vector, rather than as an intravenous treatment of genetic diseases (Appaiahgari & Vrati 2015; Bradshaw & Baker 2013; Mehta et al. 2014).

AAV vectors, on the other hand, are becoming increasingly popular for the treatment of genetic disease due to their ability to produce safe and stable long term expression *in vivo.* AAVs are non-enveloped, single stranded DNA parvoviruses that were first discovered 50 years

ago (Rose et al. 1969; Rose et al. 1966). Their popularity is linked to their low immunogenicity and the fact that they predominantly remain as an non-integrating extrachromosomal episome in the majority of cells (Nakai et al. 2001). They have shown success in dozens of gene therapy clinical trials and they have been approved as a treatment for lipoprotein lipase deficiency in Europe (Wierzbicki & Viljoen 2013).

1.6.2. Adeno-associated virus

AAV was discovered in 1965 as contaminant DNA viral particles in adenoviral preparations (Atchison et al. 1965; Hoggan et al. 1966). It is a small, non-enveloped icosahedral virus with a diameter of approximately 25nm (Chapman 2006). It belongs to the *Dependovirus* genus of the family Paroviridae. They are considered to be naturally replication deficient due to the need for a helper virus, such as adenovirus or herpes virus, for replication and generation of virions (Samulski et al. 1982; Handa & Carter 1979). The life cycle of wild-type AAV is biphasic; lytic, when co-infected with a helper virus, or latent, when there is absence of helper virus (Figure 1.5).

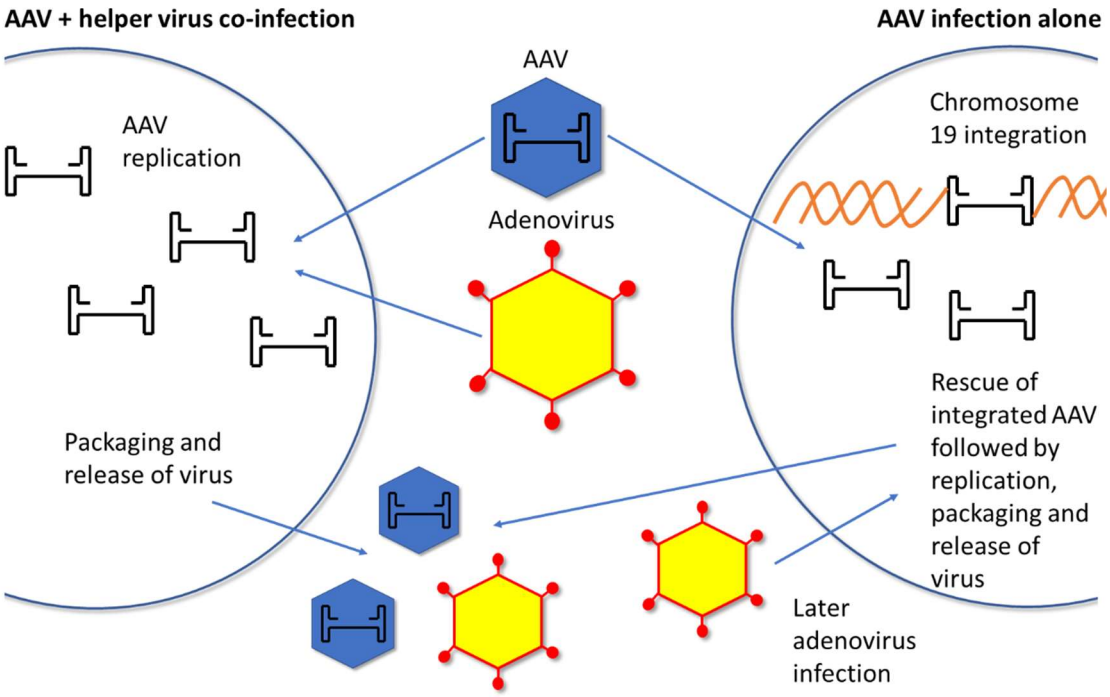

Figure 1.5: Life cycle of wild-type AAV. Upon entry into the host cell nucleus, AAV can follow one of two pathways of its life cycle; the lytic or the latent. The lytic pathway occurs when there is co-infection with a helper virus, such as adenovirus. This results in genome replication, viral gene expression, packaging and release of virions. The latent pathway occurs in the absence of helper virus co-infection. Latency occurs by preferential integration of the virus genome into the AAVS1 locus on chromosome 19 (Kotin et al. 1990). Helper virus infection of an AAV latently infected cell can result in subsequent replication, packaging and release of AAV virions.

The wild-type AAV genome consists of a linear single stranded DNA molecule of approximately 4.7 kilobases which includes the viral *rep* and *cap* genes flanked by 145 nucleotide long inverted terminal repeats (ITRs) (Koczot et al. 1973; Rose et al. 1969) (Figure 1.6). The ITRs act as self-priming hairpins that enable genome replication (Bohenzky et al. 1988). The four rep proteins are essential for replication, transcription, integration and encapsidation (Trempe et al. 1987). The three structural capsid proteins assemble in a VP1:VP2:VP3 ratio of 1:1:10 into

a 60 subunit icosahedral with the help of an assembly activating protein (Naumer et al. 2012). As the ITRs contain the necessary *cis*-acting sequences, the viral coding sequences can be removed from the wildtype AAV genome and a DNA sequence of choice can be inserted between the flanking ITRs to develop a recombinant AAV (rAAV) gene delivery vector. Replication and assembly of virions is then achieved by addition of the AAV *rep* and *cap* proteins in *trans* and the adenoviral helper plasmid (Samulski et al. 1982).

In rAAV transduced cells, vector genomes are predominantly maintained as concatenated episomes (Xiao et al. 1996), although they can undergo integration into the genome (Cunningham et al. 2008). At least 12 serotypes of AAV have been identified from humans and primates with variable cellular tropisms (Zincarelli et al. 2008). Several of these serotypes have been reported to bind to a primary cell surface receptor, such as heparan sulphate proteoglycan for AAV2 (Summerford & Samulski 1998), for initial attachment to the cell surface followed by the subsequent binding of a secondary receptor that enables viral internalization. Recently published work using a loss-of-function genetic screening approach has identified a universal AAV receptor that appears to be an essential receptor for multiple AAV serotypes, which is capable of endocytosing from the plasma membrane and trafficking to the trans-Golgi network (Pillay et al. 2016). The different cellular tropisms of AAV serotypes are thought to result from unique interactions with this universal AAV receptor (Pillay et al. 2017). How this receptor fits in to our previous understanding of AAV attachment and entry into the host cell still needs to be clarified but it has huge potential to improve our understanding of the AAV-host cell interaction and to enable the development of more effective AAV gene therapy treatments.

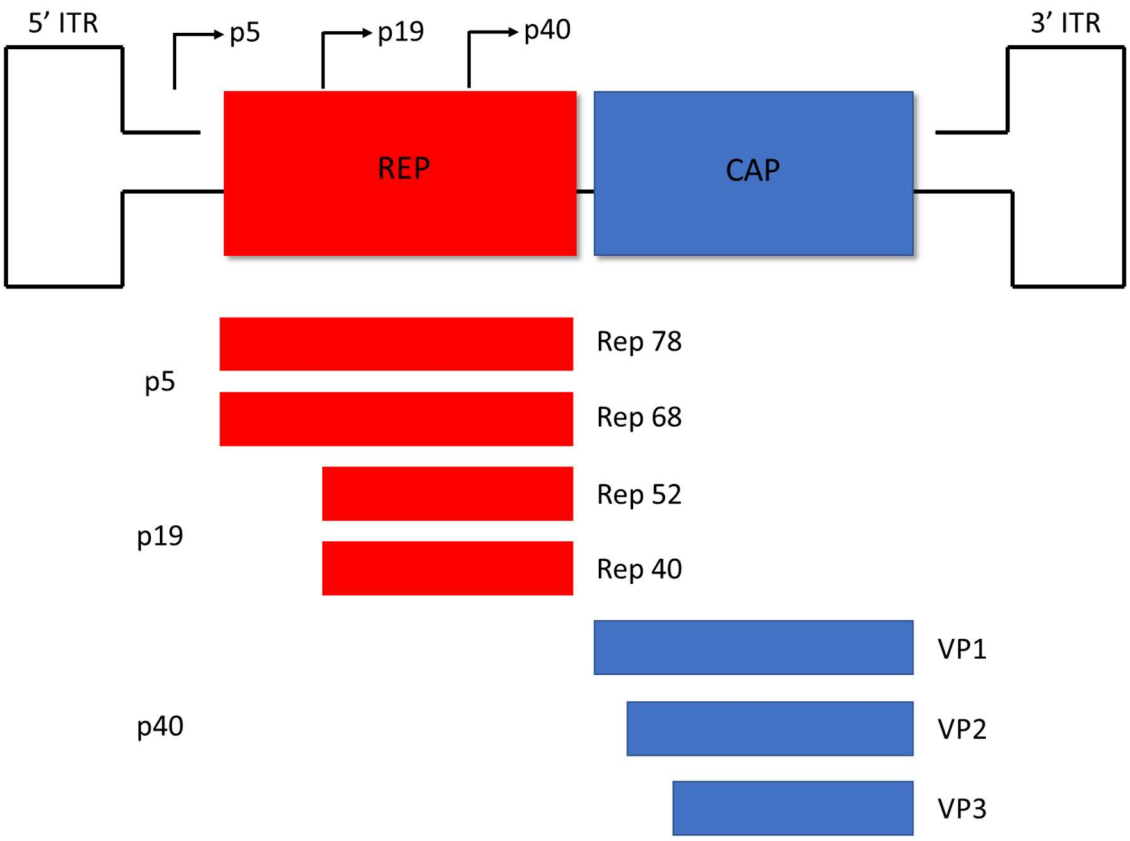

Figure 1.6: AAV viral genome. Two ITRs flank the AAV ssDNA genome which encodes the *rep* and *cap* genes. The *rep* gene encodes the four non-structural rep proteins; Rep 78, Rep 68, Rep 52 and Rep 40. The *cap* gene encodes the three structural proteins; VP1, VP2 and VP3 (adapted from (Drouin & Agbandje-McKenna 2013)).

1.6.3. Clinical translation of AAV gene therapy

As mentioned previously, AAV gene therapy has led to many successful clinical trials and is the first gene therapy vector to be approved by the European medicines agency for the treatment for lipoprotein lipase deficiency (Wierzbicki & Viljoen 2013; Nathwani et al. 2014; Bainbridge et al. 2015). rAAVs can infect dividing and non-dividing cells, and they have been shown to provide stable and long-lasting expression. The main concerns for translating gene therapy into

humans include gene silencing, insertional mutagenesis, phenotoxicity, immunotoxicity, horizontal and vertical transmission of delivered DNA.

Gene silencing is thought to occur through mechanisms such as promoter methylation (Li & Dinauer 1998). Recent evidence has shown that inhibition of histone deacetylation and DNA methylation can improve gene expression (Kia et al. 2013). Insertional mutagenesis appears to be minimal after AAV transduction as the transferred genomes tend to persist in an episomal non-integrated form, but even if the AAV does integrate there have been no vector-induced malignancies reported in humans (Kaeppel et al. 2013; Schnepp et al. 2003; Li et al. 2011).

AAV is often described as the least immunogenic of the commonly used viral vectors as the innate immune responses are considered to be minimal compared with other vectors, particularly adenoviral vectors (Zaiss et al. 2002). The innate immune signalling TLR9-MyD88 pathway appears to be responsible for the immune response to AAV (Zhu et al. 2009). In some situations AAV can avoid innate immune responses by inefficiently activating TLRs or limiting antigen-presenting cell transduction, which can help to reduce cytotoxic T cell responses (Zaiss et al. 2002; Hensley & Amalfitano 2007; Jooss & Chirmule 2003; Zhang et al. 2000; Somanathan et al. 2010). There does appear to be a critical threshold by which AAV leads to CD8+ T cell priming resulting in immunotoxicity and how this threshold is reached is largely unknown, although the combination of capsid, transgene and inflammatory environment within the host tissue is thought to play an important role in this (Wu et al. 2014; Manno et al. 2006). There is accumulating evidence that the cytokine milieu of the host tissue can dictate T cell priming, for example, an anti-inflammatory environment can induce an immune tolerant environment by inducing T regulatory cells (Cao et al. 2007; Mingozzi et al. 2007). Strategies to reduce T cell responses include reduction of vector doses and induction of transient immunosuppression with, for example, a short course of steroid treatment (Jiang et al. 2006; Mingozzi et al. 2013; Nathwani et al. 2014)

The humoral immune response caused by pre-existing neutralising antibodies (70% of the human population are seropositive for AAV2 neutralising antibodies) can be problematic, leading to the inhibition of gene transfer (Boutin et al. 2010). There has been increasing interest in developing AAV variants from animals, such as AAVrh.10 from the rhesus macaque, as humans will ideally have no or minimal pre-existing neutralising antibodies to these AAV vectors (Thwaite et al. 2015; Sondhi et al. 2007).

Horizontal transmission of donated DNA has often been of concern for gene therapy translation in situations where virus is more likely to be shed into the environment, such as the respiratory system. Preclinical studies demonstrate vector shed in bodily fluids after intravenous injection in the non-human primate is no longer infectious by 72 hours after injection (Favre et al. 2001). Germline vertical transmission of delivered DNA is also of concern, but a rabbit model has shown no evidence of germline transmission in male gametes following systemic AAV2 and AAV8 administration (Schuettrumpf et al. 2006; Favaro et al. 2009).

1.6.4. Cervical gene therapy

The main focus of cervical and vaginal targeted gene transfer research up to now has been in the prevention of infectious diseases. Adenoviral vectors encoding interferon-ϒ, IL-12 and MCP-1 cytokines have been used as an intravaginal treatment for vaginal candidiasis, unfortunately their use did not protect against candida vaginitis (Wozniak et al. 2005). Prevention of genital herpes simplex virus (HSV) infection using RNA interference strategies has showed promise, for example, the use of lipoplexes carrying small-interfering RNAs (siRNA) that target essential HSV-2 genes (Palliser et al. 2006) or the use of HSV-1 vectors carrying short-hairpin RNA (shRNA) that target HSV-2 DNA polymerase. Anti-HIV antibodies have been delivered using AAV vectors to human cervical and vaginal cells *in vitro* and also to the lower genital tract of the rhesus macaque to successfully prevent mucosal acquisition of HIV infection

in vivo (Abdel-Motal et al. 2014; Abdel-Motal et al. 2011). A gene therapy approach has not been explored for preterm birth prevention.

1.6.5. AMP gene therapy

The many important functions of AMPs and their association with human disease point towards these peptides as a new therapeutic target. However, these peptides are very expensive to produce and purify chemically, and they are relatively unstable *in vivo*. Therefore, gene transfer of AMPs has been explored as a way of overcoming these potential problems for the treatment of infectious diseases and other immune disorders. In support of this, there is evidence that gene delivery of cathelicidin is significantly more effective than purified cathelicidin peptide in an infected burn model (Jacobsen et al. 2005).

The antimicrobial activity of AMPs makes them useful as localised antibiotic treatments, especially in situations where there are multiple antibiotic resistances. HBD-2 gene therapy has been tested in a rodent urinary tract infection model and chronic otitis media model (Zhao et al. 2011; Woo et al. 2014). Natural venoms contain AMPs and it has been discovered that spider venom in particular contains several different types of AMPs (Vassilevski et al. 2009). Interestingly, plasmids containing 6 spider venom AMP genes were used to transduce HEK 293T cells which resulted in strong anti-chlamydial affects (Lazarev et al. 2011).

The defensins' ability to influence the adaptive immune system means they have a potential role as immunomodulators in inflammatory disorders and cancer. HBD-2 transduced tumours demonstrated chemotactic activity of immature dendritic cells leading to significant inhibition in tumour growth (Li et al. 2014).

β-defensins have been discovered to play a key role in wound repair; stimulating the migration and proliferation of keratinocytes in areas of skin damage (Supp et al. 2004; Niyonsaba et al. 2007). Therefore, an adenovirus expressing HBD-3 has been used to transduce keratinocytes

in a porcine diabetic wound model (Hirsch et al. 2009). This was found to reduce bacterial load within the wound and also improve re-epithelialisation leading to better wound closure.

The use of cathelicidin in gene therapy, like defensins, has been mainly for its microbial killing properties. Diminished antimicrobial function of cathelicidins and defensins have been implicated in cystic fibrosis patients where it is thought that the abnormal salt environment of the cystic fibrosis airway reduces AMP function (Smith et al. 1996). To combat this, adenoviral vectors expressing the human cathelicidin gene have been used to transduce human bronchial xenografts from cystic fibrosis patients (Bals et al. 1999). This overexpression of cathelicidin was sufficient to restore bacterial killing in the airway fluid to that of normal controls. Furthermore, adenovirus expressing human cathelicidin was used in a mouse model of *Pseudomonas aeruginosa* lung infection (a common pathogen in cystic fibrosis lungs) which led to a significant reduction in bacterial load and airway inflammation (Bals et al. 1999).

As well as its role in microbial killing, cathelicidin can bind and neutralise LPS (Cironei et al. 2003). This enables it to reduce the systemic inflammatory response by inhibiting endotoxaemia. This important function has been utilised in a mouse model of LPS and *E.coli* sepsis in which an adenoviral vector encoding the cathelicidin gene improves sepsis survival rates (Bals et al. 1999). Cathelicidin's role in immune modulation has also been utilised in a mouse model of ulcerative colitis (Tai et al. 2012). A plasmid containing the murine cathelicidin gene was intra-rectally applied to a dextran sulfate sodium-induced colitis mouse and this lead to a reversal in the elevated interleukin1-beta (IL1-β) and tumour necrosis factor-alpha (TNF-α) levels, neutrophils and apoptotic cells seen in this model.

Elafin is a serine elastase inhibitor AMP which is produced constitutively from epithelial cells (Pfundt et al., 1996). As well as its antimicrobial role, elafin is also able to attenuate inflammatory processes by inhibiting elastase and proteinase-3 (Korkmaz et al. 2008; Baranger

et al. 2008). Adenoviral delivered elafin to inflamed endothelial cells resulted in reduced IL-8 production and cytotoxicity (Henriksen et al. 2004).

There is also the potential for synergistic antimicrobial function using gene therapy with a combination of multiple AMPs, particularly in view of the small size of the AMP genes. HBD-2 in combination with cathelicidin can synergistically augment microbial killing in transduced human keratinocytes (Carretero et al. 2004).

1.7. Bioluminescence imaging

Bioluminescence imaging (BLI) is a powerful technology for studying cellular immune responses *in vivo*; light is emitted when luciferase enzymes catalyse their substrates. Bioluminescence imaging detects this light as a surrogate marker for protein expression using a comparatively inexpensive cooled charge-coupled device (CCCD) camera. Unlike conventional reporter gene methods which require analysis of large numbers of animal cohorts at different time points, BLI allows for continual analysis in the same cohort. This reduces the number of animals needed (in accordance with the 3Rs principle of the NCRs) and also increases the fidelity of the data by reducing inter-animal variation (nc3Rs 2014). Continual BLI for pathogen colonization and treatment response is a well-established tool in infectious disease research (Suff & Waddington 2017).

1.7.1. Bioluminescent pathogens

Bioluminescent pathogens can be genetically engineered by transfer of the *luxCDABE* operon from bacteria such as *Photorhabdus luminescens* or *Xenorhabdus luminescens* which confers them with constitutive bioluminescence. The bacterial lux operon contain 5 genes; *luxA* and *luxB* encode the luciferase enzyme that oxidises a long-chain aldehyde and a reduced flavin mononucleotide to produce oxidised flavin, the reaction which emits light at 490nm, and the *luxC*, *luxD* and *luxE* genes encode a multienzyme complex responsible for the regeneration of

the aldehyde substrate required for the light-emitting reaction (Figure 1.7) (Baldwin et al. 1984). The main advantage of the lux operon system is that the use of an exogenous substrate is unnecessary which reduces the problem of substrate bioavailability.

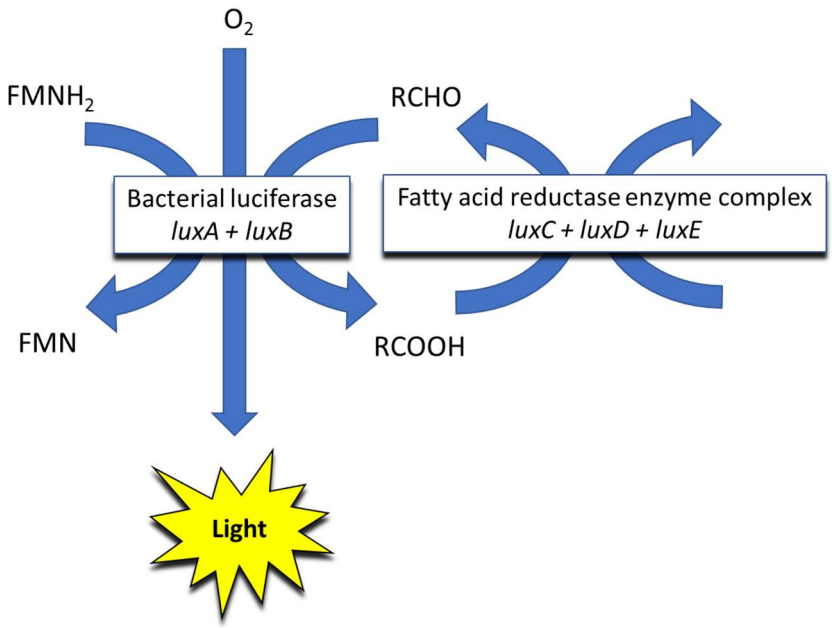

Figure 1.7: The lux operon (*luxCDABE*) reaction emits light. *luxA* and *luxB* encode the luciferase enzyme that oxidises a long-chain aldehyde and a reduced flavin mononucleotide to produce oxidised flavin, the reaction which emits light at 490nm. *luxC*, *luxD* and *luxE* genes encode a multienzyme complex responsible for the regeneration of the aldehyde substrate required for the light-emitting reaction. *FMH- flavin mononucleotide, $FMNH_2$- reduced flavin mononucleotide, RCHO- N-decanol, RCOOH- N-decanoic acid.*

1.8. Project hypothesis and aims

Central to this thesis are the following hypotheses:

(1) That the augmentation of endogenous antimicrobial peptides within the murine cervix using conventional virus-based gene transfer technology will prevent bacteria which are capable of inducing preterm birth from ascending the cervical canal and accessing the intrauterine space.

(2) That reducing or preventing bacterial presence in the intrauterine space through increasing cervicovaginal AMP expression prolongs gestational length and improves the survival of the offspring.

The specific aims are:

1. To develop and characterise models of ascending vaginal infection and to assess the effect this has on pregnancy and pup survival.
2. To determine the most effective viral vector (as well as optimising additional factors) to achieve successful gene transfer to the cervical epithelium of female mice.
3. To design and produce a gene therapy AMP construct and use this to overexpress an AMP in murine cervical epithelium *in vivo.*
4. To determine the effect of this AMP overexpression in the cervix on bacterial survival, motility and ascent into the uterus.
5. To determine the effect of this AMP overexpression in the cervix on gestation, pup survival and outcomes.

Chapter 2 Methods

2.1. Developing and characterising the ascending infection model

2.1.1. Bacterial culture: *Escherichia coli* K12 MG1655-*luxCDABE*

Escherichia coli K12 MG1655-*luxCDABE* (*E.coli K12*) were kindly gifted from Dr Mark Tangney, University College Cork. *E.coli K12* were inoculated in 10ml of Luria Bertani (LB) broth, supplemented with 300µg/ml Erythromycin. It was grown overnight at 37^{o}C at 200rpm (0.6g). The following morning the culture was diluted to an OD_{600} of 0.1 in LB broth with erythromycin. This was grown for 2 to 3 hours at 37^{o}C and 200rpm (0.6g) to mid-logarithmic phase. The bacteria were harvested when the OD_{600} was between 0.5 and 0.7. They were centrifuged for 1 minute at 18000g and the pellet was washed twice with 10mM PB. The pellet ($1x10^{9}$ CFU) was then resuspended in 30µl of 10mM PB. CFU was determined by serial dilutions and plating on LB plus erythromycin agar plates.

2.1.2. Bacterial culture: *Escherichia coli* K1 A192PP-*luxABCDE*

Escherichia coli K1 A192PP-*luxABCDE* (*E.coli* K1) were kindly gifted from Professor Peter Taylor, University College London. *E.coli* K1 were inoculated in 10ml of LB broth, supplemented with 50µg/ml Kanamycin. It was grown overnight at 37^{o}C at 200rpm (0.6g). The following morning the culture was diluted down to an OD_{600} of 0.01 in LB broth and kanamycin. This was grown for 2 to 3 hours at 37^{o}C and 200rpm (0.6g) to mid-logarithmic phase. The bacteria were harvested when the OD_{600} was between 0.5 and 0.7. They were centrifuged for 1 minute at 18000g and the pellet was washed twice with 10mM PB. The pellet ($1x10^{9}$ CFU) was then diluted to $1x10^{5}$ CFU in 10 mM PB and 20µl of this was aliquoted (approximately $2x10^{2}$ CFU). CFU was determined by serial dilutions and plating on LB plus kanamycin agar plates.

2.1.3. Motility studies

SIM (Sulfide, Indole, Motility) medium agar was mixed into 100ml of ddH_20 and placed into 15ml Falcon® centrifuge tubes. Each tube was inoculated in the centre of the media to a depth of 2cm with 2-3 bacterial colonies using a sterile needle. They were incubated at 37^oC overnight. The following day the bacterial motility was assessed. A positive motility test is indicated by a diffuse zone of bacterial growth spreading from the central inoculation zone.

2.1.4. Ascending vaginal infection

The mice used in this study were supplied by Charles River. All animal experiments conducted were in agreement with the Home Office guidelines and institutional guidelines at University College London and under project licence held by Dr Simon Waddington (PPL 70/8030). The mice strains used include CD-1, BALB-C, C57BL/6 and C57BL/6N-Tyr$^{c\text{-}Brd}$ (albino BL/6).

Adult female mice (6-8 weeks old) received 20µl bacteria (preparation described above) intra-vaginally using a sterile 200µl pipette tip under anaesthesia (isoflurane in 100% oxygen with a flow rate of 2L/min). This was followed by 10µl of F127 pluronic gel intravaginally (Sigma Aldrich, UK) and quinine powder to the introitus (Boughter et al. 2005), to deter the mice from cleaning the bacterial suspension. To obtain pregnant mice, stock animals were time mated and the following morning was described as embryonic day 0.5 (E0.5). Pregnant dams received bacterial suspensions on either E14.5, E15.5 or E16.5.

2.1.5. Whole body bioluminescence imaging

Mice were anaesthetised with isoflurane (in 100% oxygen with a flow rate of 2L/min) and bioluminescent images were captured using an IVIS imaging system (IVIS Lumina II, PerkinElmer, USA) at different time points. To measure photon radiance quantitatively, regions of interest (ROI) were preselected on the mouse body using an automatic ROI and expressed

as photons per second per centimetre squared per steradian (photons/second-cm2/sr) using Living Image software (Perkin Elmer, Coventry, UK).

2.1.6. Transformation of competent bacterial cells

ccdB or One Shot Stbl3™ chemically competent *E.coli* cells were thawed on ice prior to each transformation. 10pg to 100ng of DNA was added to each 50µl vial, gently mixed and incubated on ice for 30 minutes. The cells were heat shocked for 45 seconds at 42°C. The cells were placed on ice for 2 minutes, after which 250µl of SOC media was added and the cells shaken at 200rpm (0.6g), 37°C for 1 hour. The cells were spread on LB agar plates containing ampicillin (100µg/mL) or kanamycin (50µg/mL). The plates were incubated over night at 37°C, after which colonies were selected by using a sterile 10µl pipette tip and grown overnight in LB broth (plus antibiotic) at 200rpm (0.6g) and 37°C. Plasmid DNA was prepared using Qiagen Mini-prep kits following the manufacturer's instructions. Larger volumes of plasmid DNA were prepared using Qiagen Maxi-prep kits following the manufacturer's instructions. For long term storage, bacterial cultures were stored at -80°C in a 1:3 ratio of glycerol.

Plasmid DNA concentrations were measured using a FluoStar Omega LVIS plate spectrophotometer (BMG Labtech, Buckinghamshire, UK) by measuring the ratio of the absorbance of light at wavelength 260nm and 280nm.

2.1.7. Cell culture

Cell lines End1/E6E7 and human embryonic kidney (HEK) 293T cells were obtained from the America Tissue Culture Collection (Manassas, VA, USA). End1/E6E7 were maintained in Keratinocyte Serum Free medium, supplemented with 0.1ng/ml human recombinant epidermal growth factor, 0.05mg/ml bovine pituitary extract and calcium chloride 44.1mg/ml at 37^{o}C in 5% CO_2. HEK 293T cells were maintained in DMEM, supplemented with 10% fetal calf serum.

2.1.8. Production of lentiviral vectors

Lentiviral plasmids were gifted from Dr Stephen Howe, UCL and Dr Juliette Delhove, St George's University. To generate the lentiviral plasmid with the NF-κB response element, a Gateway® cloning system (Life Technologies, Glasgow, UK) was used by Dr Delhove. The lentiviral backbone which was used contained a minimal promoter upstream of the NF-κB response element, followed by a 3xFLAG, FLuc (firefly luciferase), and 2A-eGFP (enhanced GFP) (Buckley et al. 2015) (Figure 2.1).

To produce a second generation lentivirus a three plasmid system was used (Demaison et al. 2002) (Figure 2.2). Envelope plasmids VSV-G (pMD.G2; Vesicular Somatitis Virus glycoprotein) and the packaging plasmid pCMVΔR8.74 containing the gag and pol genes were used (kindly gifted from Dr Stephen Howe, UCL). The packaging plasmid allows the lentivirus carrying the transgene to integrate into the host genome. The envelope and the packaging plasmids were produced in large scale by Aldevron (North Dakota, USA).

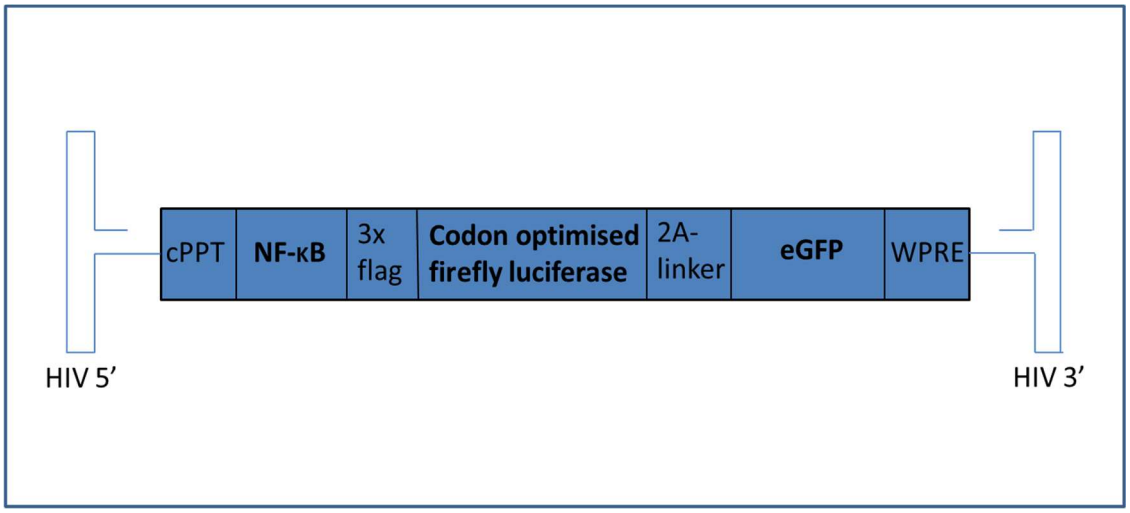

Figure 2.1: An example of a lentiviral plasmid with the NF-κB response element. The plasmid was generated with Gateway® cloning technology.

2.1.8.1. Lentiviral transfection

Lentiviral preparations were made using three plasmids with the standard second generation lentivirus system (Figure 2.2).

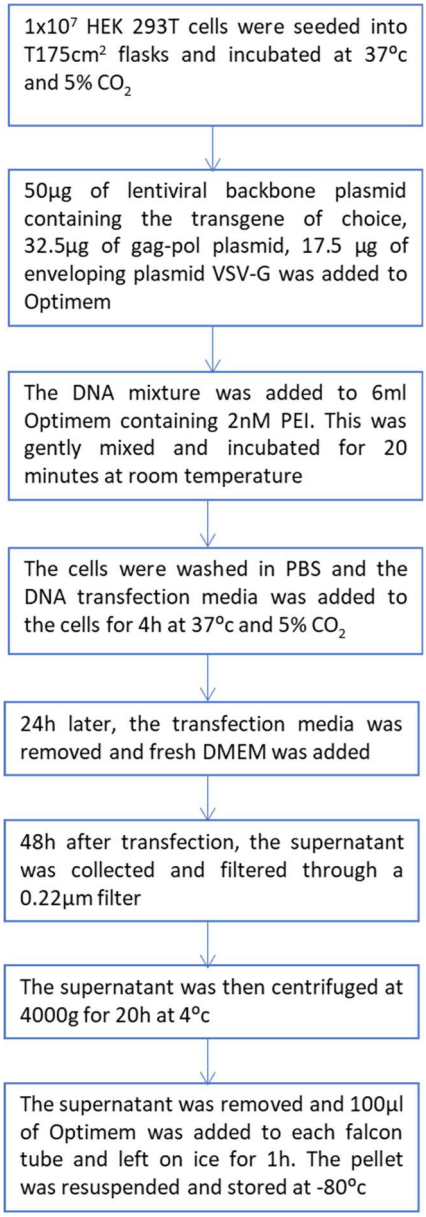

Figure 2.2: Lentivirus preparation using the standard second generation lentiviral system.

2.1.8.2. Titration of lentiviral vector

The lentiviral vector was titrated using the p24 antigen ELISA kit. Lentiviral vectors were diluted; 1:1 x 10^6, 1:5 x 10^6 and 1:1 x 10^7 and added to the antibody coated wells. Standards were also prepared following the manufacturer's instructions. The absorbance of each well

was then read at 450nm and the quantity of p24 antigen was calculated. Viral titre was then expressed as genomic copies; GC/ml.

2.1.9. Production of AAV 8 viral vectors

The AAV viral vector is produced following the three plasmid transient transfection protocol described below (Binny & Nathwani 2012) (Figure 2.3). The three plasmids include the helper, the packaging and the genome plasmids. Genome plasmids were provided by Vector Biolabs and Aldevron (USA). The helper plasmid, pHGTI, contains the key adenoviral genes to support efficient AAV replication and packaging (Streck et al. 2005). The packaging plasmid expresses the two AAV genes *rep* and *cap*. These genes are not flanked by ITRs so they cannot be packaged into new AAV capsids. The genome plasmid contains the promoter and transgene of choice flanked by ITRs. This will be packaged into the AAV vector. All viral vectors used in this study are pseudotyped; an AAV 6 or AAV 8 capsid containing a ssDNA genome consisting of the chosen promoter and transgene flanked by ITRs derived from AAV 2. For NF-κB biosensor experiments a AAV 8 serotype vector containing a minimal promoter upstream of the NF-κB response element, followed by a FLuc (firefly luciferase) and 2A-eGFP (enhanced GFP) transgene was developed (Karda et al., *unpublished data*) (Buckley et al. 2015).

2.1.9.1. AAV 8: Three plasmid AAV transfection

The AAV vector is produced following the three plasmid transient transfection protocol described below (Figure 2.3).

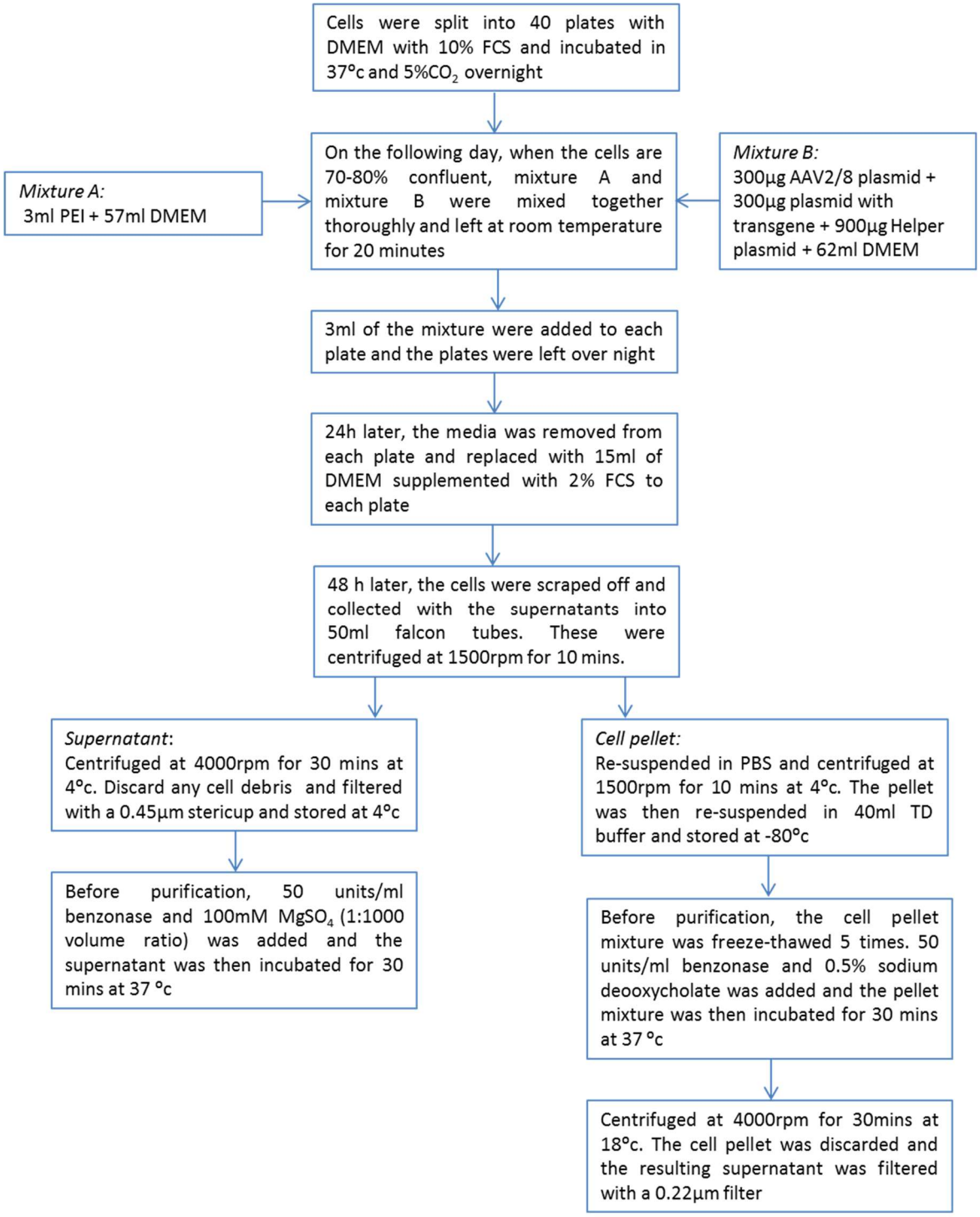

Figure 2.3: AAV three plasmid transient transfection protocol.

2.1.9.2. AAV purification with HPLC (High Performance Liquid Chromatography)

AAV particles were purified by affinity chromatography using an ÄKTA HPLC system (GE Healthcare UK Ltd, Buckinghamshire, UK) with a sepharose (GE Healthcare UK Ltd, Buckinghamshire, UK) packed column (Generon, Maidenhead, UK).

All the HPLC fluid lines were washed with filtered 20% ethanol followed by PBS (pH 7.5) through line A and 50mM of Glycine (pH 2.7) through line B. After which the Sepharose column was attached and equilibrated with PBS using a flow rate of 1mL/min. The prepared AAV supernatant and cell lysates were then run through the Sepharose column. After this, PBS was run through the column to remove the unbound protein and DNA. To elute the viral particles from the column, 50mM of Glycine (pH 2.7) was run through Line B. The elution fractions were collected in 1mL FACS tubes with 30µl of 1M Tris (pH 8.8) to neutralise the glycine. The fractions containing virus were identified by the peaks in absorbance at 260nm and 280nm. The viral fractions were then collated and injected into a 10KDa dialysis cassette. This was left spinning overnight in PBS to neutralise the acidic pH.

2.1.9.3. AAV concentration

Amicon Centrifugal 100KDa filter was initially primed with 5ml PBS. This was centrifuged for 5 minutes at 3000g at 4°C. The PBS was discarded and the collected AAV virus was added to the filter and again centrifuged for 5 minutes at 3000g at 4°C. The concentrated virus in the Amicon ultra membrane was removed and placed in a 1.5mL micro-centrifuge tube. The membrane was washed with 200µl of PBS to collect further virus remaining on the filter. The concentrated virus was sterilised using a 1.5mL micro-centrifuge tube with a 0.22µm filter. The virus was stored either at -80°C for long term storage or at 4°C for short-term storage (<4 weeks).

2.1.9.4. AAV batch validation

A coomassie gel was performed to detect the three structural viral capsids: VP1, VP2 and VP3. A NuPAGE pre-cast gel was placed into a gel tank with MOPS buffer. 20µL of concentrated virus was mixed with 20µL of Laemlli loading buffer and heated for 5 minutes at 95°C. This was loaded onto the gel with a 5µL prestained protein ladder. The gel was run at 125 volts for approximately 30 minutes. The gel was placed into the Coomassie blue dye, protected with aluminium foil and shaken on a platform shaker for 2 hours. The Coomassie dye was removed and destain solution was placed on the gel for a further 2 hours on a platform shaker. The gel was visualised using white light (Bench top UV trans-illuminator, UVP BioDoc-It^2 Imaging system, Cambridge, UK) to detect the three structural proteins.

2.1.9.5. Denaturing alkaline gel electrophoresis to titre viral DNA

The alkaline electrophoresis buffer, power pack and electrophoresis gel tank were placed into the fridge to cool them down to 4°C. The alkaline gel was prepared with 0.8g agarose and 98ml ddH20. Once cooled below 50 °C, 2ml 50x alkaline electrophoresis buffer was added and the gel was left to set in a gel tray. 25µl of concentrated AAV, as well as serial dilutions in PBS, were then added to 8.5 µl of alkaline sample loading buffer. The samples were cooled down on ice and loaded onto the gel, alongside a 5µl Hyperladder. The gel was then run at 20 volts overnight at 4°C. The following day, the gel was placed into 0.1M Tris and shaken for 1 hour on a platform shaker. It was transferred into 4x Gelred in 0.1M sodium chloride and was shaken for 2 hours covered in aluminium foil. The gel was rinsed briefly in dd$H_2$0 and the image captured using a UV transilluminator. The gel image was analysed in Image J, where the viral DNA band intensity is compared against DNA standards in the HyperLadder™ to calculate viral titre (GC/ml).

2.1.10. Injection of AAV and lentiviral vectors and bioluminescence imaging after intravenous and intracranial injections

For intravenous injections, postpartum day 0 female neonates were intravenously injected with 10µl of $1x10^{12}$ viral vector genomic copies/ml. For neonatal intracranial injection, unilateral intracranial injections of 2.5 µl of $1x10^{12}$ viral vector were performed on postpartum day 0 neonates. For in utero fetal intracranial injections, a mid-line laparotomy was performed on pregnant mice at embryonic day 15.5 under isoflurane anaesthesia (procedures performed by Dr Simon Waddington). A subcutaneous injection of morphine (5mg/kg) and bupivacaine (2mg/kg) was given for analgesia. Uterine horns were exteriorized and kept moist with a sterile PBS swab. Intracranial injections of the fetuses were performed and then the uterine horns were replaced into the abdomen and the peritoneum and skin were sutured in two layers. Mice recovered in a heated chamber and were then singly housed with regular monitoring.

For bioluminescent imaging mice were anesthetised with isoflurane and received an intraperitoneal injection of 10-300µl (volume dependent on the stage of development of mice) of 15mg/mL of D-luciferin. Mice were left for 5 minutes before they were imaged using the IVIS machine as mentioned previously (section 2.1.5.

2.1.11. Protein extraction

Extracted tissues were frozen in 100µl of lysis buffer (Reporter gene assay lysis buffer, Roche, Burgess Hill, UK). Samples were defrosted and homogenised with a hand-held homogenizer (Proscientific, Oxford, CT, USA). They were centrifuged for three minutes to separate cell debris and the supernatant was collected and stored at -20^{o}C.

2.1.12. Protein assay

Protein assays were performed using the Pierce BCA Protein Assay Kit (Thermo-Scientific, Glasgow, UK). Samples were loaded alongside BSA standards, described in the manufacturer's protocol. The samples were loaded into a 96 well plate and 200µl of BCA protein assay reagent (1 part BCA reagent B to 50 part BCA reagent A) was added to each sample, including the standards. The plate was incubated at 37°C for 30 minutes and absorbance was then read at 562nm using a FluoStar Omega microplate reader. Results were analysed in MARS data analysis data software.

2.1.13. Cytokine ELISAs: IL1-β, IL-6 and TNF-α

Samples were processed using the R&D systems ELISA kit according to manufacturer's protocols. Samples and antibodies were diluted with reagent diluent (1% BSA in PBS, pH 7.4). For the IL-1β standards; the lower and upper limits of detection were 15.6pg/ml and 1000pg/ml, respectively. For the Il-6 standards; For the TNF-α standards; 31.3pg/ml and 2000pg/ml, respectively. The plate was read at absorbance 450nm using the FluoStar Omega microplate reader. Results were analysed in MARS data analysis data software.

2.1.14. Inflammation and neutrophil influx immunohistochemistry and quantification

2.1.14.1. Tissue processing and sectioning of organs

Mice were anaesthetised using isoflurane. Sacrifice perfusion was performed by incising the right atrium and injecting 10mL of sterile PBS into the left ventricle. Tissues were removed and stored in 4% PFA for 48 hours, then transferred to 30% sucrose at 4°C until microtome sectioning. For brain tissue, the brain within the intact skull was transferred to 4% PFA for 24

hours, followed by removal of the skull and a further 48 hours in fresh 4% PFA prior to transfer into 30% sucrose.

The samples were frozen in blocks of embedding matrix OCT and then mounted onto the microtome platform (Thermo-fisher, Glasgow, UK). Transverse sections were cut at 10-40µm (depending on the organ) and stored in TBSAF at 4°C.

For processing of embryos and placentas, tissues were removed and stored in 10% neutral-buffered Formalin solution (Sigma-Aldrich, Dorset, UK) for 48 hours followed by storage at 4°C in 70% ethanol. Tissue was then paraffin-embedded and sectioned at 5µm.

2.1.14.2. Immunohistochemistry

Representative sections of the organ were selected, mounted onto double-coated chrome gelatin Superfrost slides (VWR, Leicestershire, UK) and left to dry for two hours. The slides were placed in 4% PFA for 10 minutes followed by washing three times in TBS. They were treated with 30% H_2O_2 in 1xTBS, to block endogenous peroxidase activity, for 30 minutes at room temperatures. The slides were washed again and the edge painted with a DAKO pen to contain the antibody solutions. The slides were blocked with 15% serum (animal specificity dependent on the secondary antibody) in 0.1% TBS-T for 30 minutes at room temperature. This was followed by incubation in primary antibody (in 10% serum in 0.1% TBS-T) overnight at 4°C. The slides were washed again three times and secondary antibody in 10% serum in 0.1% TBS-T was added. This incubation period was for 2 hours at room temperature. Following this the slides were incubated for a further 2 hours in ABC Vectastain (Vector Labs, Peterborough, UK). Slides were transferred into DAB solution (0.05% 3.3'-diaminobenzidine (DAB) in TBS with 30% H_2O_2 and left for 2 to 3 minutes. The reaction was stopped by transferring the slides to a cuvette containing ice-cold TBS. The slides were allowed to air dry and were dehydrated for 15 minutes in 100% ethanol. The slides were then placed into Histoclear for 30 minutes, followed by cover slipping with DPX mounting solution. Antibody dilutions detailed in (Appendix 10.3.

2.1.14.3. Immunofluorescence staining

A similar protocol was followed for immunofluorescence, sections were mounted onto double-coated chrome-gelatin Superfrost slides (VWR, Leicestershire, UK) and then left to dry. Sections were fixed in 4% PFA for ten minutes followed by washing three times in TBS. The slides were blocked with 15% serum (animal specificity dependent on the secondary antibody) in 0.1% TBS-T for 30 minutes at room temperature. This was followed by incubation in primary antibody (in 10% serum in 0.1% TBS-T) overnight at 4°C. The slides were washed again three times and secondary antibody in 10% serum in 0.1% TBS-T was added. After the secondary antibody was incubated for 2 hours away from direct light, DAPI was prepared in TBS using a 1:5000 concentration. The sections were incubated with DAPI for 2 to 3 minutes and then washed in TBS. The sections were allowed to dry away from direct sunlight and then cover-slipped using Fluoromount-G. Sections were stored in 4°C.

For paraffin embedded slides, slides were placed in Histoclear for 10 minutes and then rehydrated in 100% ethanol for 10 mins, 95% ethanol for 5 mins and 75% ethanol for 5 mins. Antigen retrieval was then performed by boiling the slides in citrate buffer for 20 minutes followed by washing in 1xTBS. The remaining steps then followed the above protocol from the blocking step.

2.1.14.4. Terminal deoxynucleotidyl transferase (TdT) dUTP Nick-End Labelling (TUNEL) assay

Brain sections were selected and mounted on to double-coated gelatin-chrome Superfrost-plus glass slides (VWR) and left to dry overnight. When dry, slides were placed in histology slide cuvettes and covered with 50 ml 4% PFA, left for 5 min, and washed with 0.1M PB. Methanol with 10% H_2O_2 was poured in the cuvettes and left for 15 minutes at room temperature. After this incubation, slides were transferred to clean cuvettes and covered in 0.1M PB. TUNEL staining solution was prepared on ice. Incubation was allowed for 2.5 hours at room temperature. TUNEL stop solution was then applied and left for 10 min to block the reaction.

This was followed by incubation in Vectastain ABC solution (1:1000 in 0.1M PB, Vector Laboratories) for 1 hour at room temperature. A 3,3'-diaminobenzidine Cobalt-Nickel solution was made and filtered with a 0.2 µm filtered aspirator and poured in designated cuvettes. Slides were washed three times in 10 mM PB and transferred to the DAB cuvettes, where reaction was timed and monitored under the microscope (for approximately 5 min). Slides were washed in 10 mM PB and left to dry overnight for subsequent coverslipping. The next day, sections were dehydrated for 5-10 min in absolute ethanol, cleared in a Histoclear for 10-15 min and immediately coverslipped using DPX mounting medium.

2.1.14.5. Neutrophil influx quantification

The uterine horn sections were visualised using a x5 objective lens and the epithelium and sub-epithelial stromal areas were identified (Figure 2.4). 5 random fields of view were selected using a x40 objective lens. The numbers of neutrophils were counted per area. 5 sections were counted per mouse and the number of neutrophils counted per area averaged per mouse.

2.1.14.6. Intestinal villus height

A random section of jejunum-ileum was selected per mouse using a x40 objective lens. Villus height was measured from the basal layer of the submucosa to the ending of the villus. 5 villi were counted in each section and the height was averaged per mouse.

2.1.14.7. ICAM-1 and CD-68 immunohistochemistry thresholding

The uterine horn or brain sections were visualised using a x5 objective lens and the desired area was identified (Figure 2.4 & Figure 2.5). 5 random fields of view were selected using a x40 objective lens. Using ImageJ software the percentage of DAB stained area was determined.

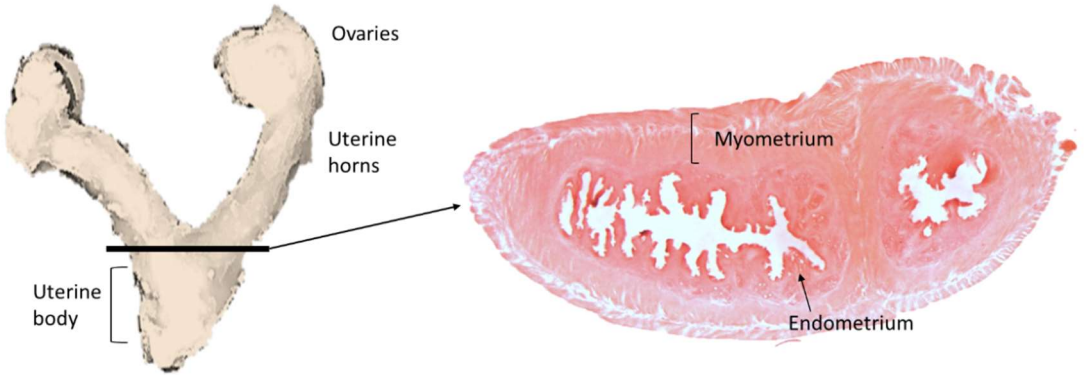

Figure 2.4: Anatomical diagram of the murine uterus and a transverse section of the uterine body showing the myometrial and endometrial layers (H&E stained).

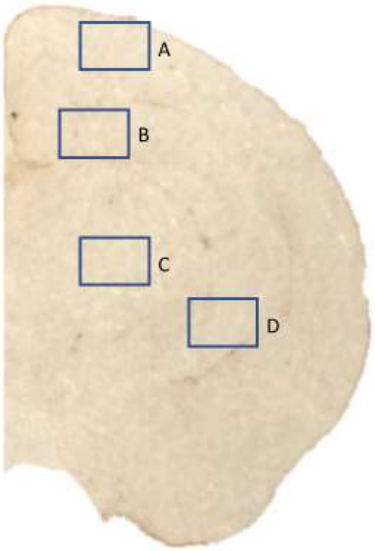

Figure 2.5: P6 left hemisphere of the brain on a coronal section with specific brain regions identified. A=Cortex, B=Hippocampus, C=Thalamus, D=Striatum

2.1.15. Inflammatory cytokine mRNA expression

2.1.15.1. Tissue collection

Pregnant mice were sacrificed by cervical dislocation 18 hours after intravaginal *E.coli* infection (see section 2.1.1, 2.1.2 and 2.1.4). Uterus, placenta and fetal membranes were collected and stored in *RNAlater* (Sigma Aldrich, Dorset, UK) at -80°c for quantitative PCR (qPCR) analysis.

2.1.15.2. RNA extraction

Total RNA was extracted from the uterus, fetal membranes, and placental tissue, using the RNeasy mini kit (Qiagen, Crawley, UK) as per the manufacturer's guidelines. Tissue was initially homogenized in RNA lysis buffer using a sterile needle and syringe. RNA was then quantified using the FluoStar Omega LVis reader followed by storage at -80°C.

2.1.15.3. cDNA synthesis

10µl of RNA was reverse transcribed with the High Capacity cDNA Reverse Transcription kit (Applied Biosystems, Life Technologies Ltd., Paisley, UK). 10µl RNA was added to a 96 well microplate with 10µl RT mastermix in each well (Table 2.1). The plate was sealed, centrifuged briefly to eliminate air bubbles and then transferred to the thermal cycler on ice (Table 2.2). cDNA was quantified using the FluoStar Omega LVIS reader, diluted 1:10 and stored in aliquots at -20°C.

Reverse Transcription Mastermix x1	Amount per 20 µl reaction (µl)
10X RT buffer	2.0
25X dNTP buffer	0.8
10X random primers	2.0
Multiscribe reverse transcriptase	1.0
RNAse inhibitor	1.0
Nuclease free H_20	3.2

Table 2.1: Reverse Transcription mastermix

T°C	25	37	85	4
Time (min)	10	120	5	∞

Table 2.2: Reverse transcription cycling conditions

2.1.15.4. Quantitative polymerase chain reaction (qPCR)

Primer sets were obtained from Life Technologies based on validated primers (see appendix) (Edey et al. 2016). Quantitative PCR was performed in the presence of SYBR green using the KAPA biosystems SYBR® fast qPCR kit (Sigma Aldrich) (Table 2.3 and Table 2.4).

qPCR Mastermix x1	Amount/µl
2X RT KAPA Fast SYBR mastermix	10.0
Forward primer (20µM)	0.4
Reverse primer (20µM)	0.4
Rox light	0.4
Nuclease free H_20	6.8
cDNA	2.0

Table 2.3: qPCR mastermix

T°C	Time	Cycles
95	3 min	1
95	15 s	
60	20 s	40
72	20 s*	

Table 2.4: qPCR cycling conditions.

***data acquisition from green channel**

Standard curve amplifications (for PCR reaction efficiency) were determined for each primer and the PCR efficiencies were confirmed to be 90-110% (Figure 2.6).

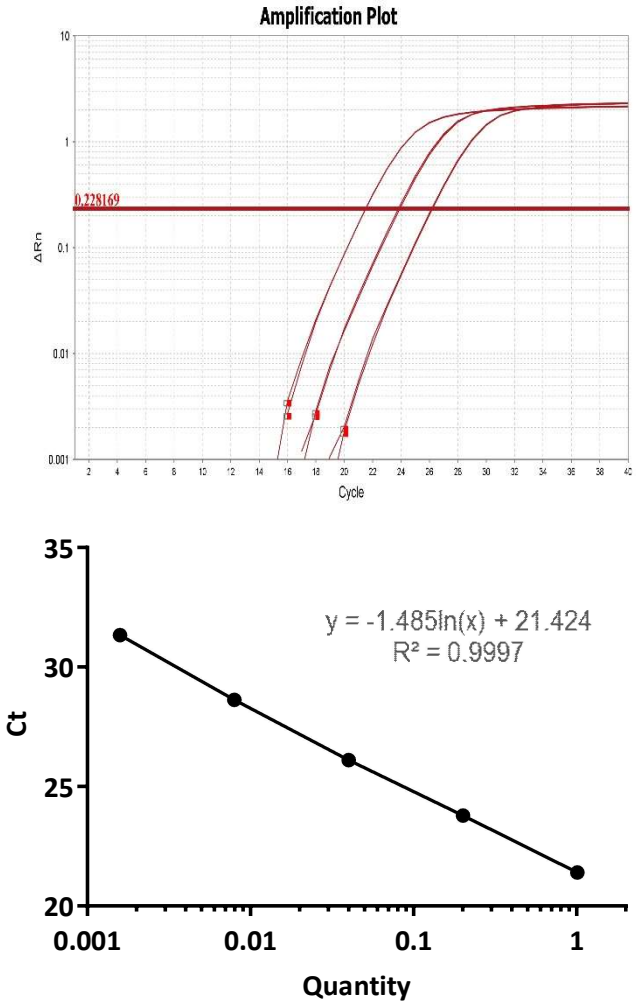

Figure 2.6: Example of standard curve amplification for GAPDH.

Target gene expression was normalized for RNA loading by using GAPDH, and the expression in each sample was calculated relative to a calibrator sample, using the $2^{-\Delta\Delta Ct}$ method of analysis. All qPCR analyses were performed on an Applied Biosystems Quant Studio 3 instrument (Applied Biosystems, Life Technologies Ltd., Paisley, UK).

2.2. Cervical epithelium transduction *in vivo*

2.2.1. *In vivo* viral marker studies

2.2.1.1. Viral vectors

The following vectors were obtained for *in vivo* experiments:

Viral vector	**Company**
AAV2/6 CMV-GFP	*Vector Core, University of Pennsylvania, USA*
AAV2/8 CMV-GFP	*Vector Core, University of Pennsylvania, USA*
AAV2/6 CMV-Luciferase	*Vector Biolabs, Malvern, USA*
AAV2/8 CMV-Luciferase	*Vector Core, University of Pennsylvania, USA and Vector Biolabs, Malvern, USA*
Recombinant adenovirus CMV-Luciferase	*Vector Core, University of Pennsylvania, USA*
Lentiviral VSV-G CMV-Luciferase	*Kindly provided by Dr Stephen Howe*

2.2.1.2. Injection of viral vectors in vivo

Adult (6-8 weeks old) female C57BL/6N-Tyr$^{c\text{-}Brd}$ mice were anaesthetised with isoflurane. 10µl of virus (diluted in PBS if necessary) to a concentration of 1x10^{12} genomic copies/mL was administered intravaginally using a 200µl sterile pipette tip. This was either applied in combination or plugged with 20µl of F127 thermosensitive pluronic gel or AK12 thermosensitive pluronic gel. The pluronic gel was allowed to harden, which takes approximately 2 to 3 minutes before removing the mouse from the anaesthetic.

2.2.2. *Ex-vivo* luminometry

Tissue samples were lysed with 500µl of 1x Lysis buffer (Promega) followed by homogenisation. The homogenates were centrifuged for 10 minutes at 18000g and the supernatants collected. Each sample was loaded on to a white 96 well plate. 1.5mM of luciferase (Promega) was added at a 1:1 volume ratio to the sample. FluoStar Omega microplate reader (BMG labtech) was used to read the luminescence and the results were analysed using MARS data analysis data software (BMG labtech).

2.2.3. Immunohistochemistry and Immunofluorescence

Samples were prepared as described above in section 2.1.14.1, except that transverse sections of the vagina, cervix and uterus were obtained and cut at 40µm. The protocol used is described in section 2.1.14.2 and 2.1.14.3. Antibody dilutions detailed in Appendix 10.3.

2.2.4. GFP ELISA

Primary antibody (monoclonal anti-GFP antibody) was diluted 1:10000 in bicarbonate buffer. 100µl was added to each well of a 96-well plate and incubated at 4°C overnight. The plate was washed 3 times. 300µl of block solution was added to each well and incubated at 37°C for 1 hour, followed by 3 washes. The samples and standards were diluted in wash buffer and 100µl

was added to the wells in duplicate followed by incubation at 37°C for 1 hour. The plate was washed three times and then a biotin conjugated secondary antibody (polyclonal anti-GFP antibody) diluted 1:500 in block solution was added to each well. This was incubated for 1 hour at 37°C followed by 3 washes. Streptavidin-HRP diluted 1:20000 in block solution was added to each well and incubated at 37°C for 1 hour. The plate was washed 3 times and then TMB substrate solution was added and incubated for 10 minutes at room temperature away from direct light. A stop solution of 2.5M H_2SO_4 was added and the plate was read at an absorbance of 450nm using the FluoStar Omega microplate reader. The results were analysed in MARS data analysis data software.

2.3. Designing and developing AMP viral vectors

2.3.1. Designing a HBD-3 construct

A bicistronic AAV plasmid was designed containing the human-beta defensin 3 transgene (*defb103*) and the enhanced GFP transgene under the control of separate CMV promoters (Figure 2.7). The plasmid was made by Vector Biolabs (Malvern, USA). See the appendix for the plasmid map (Appendix 10.5).

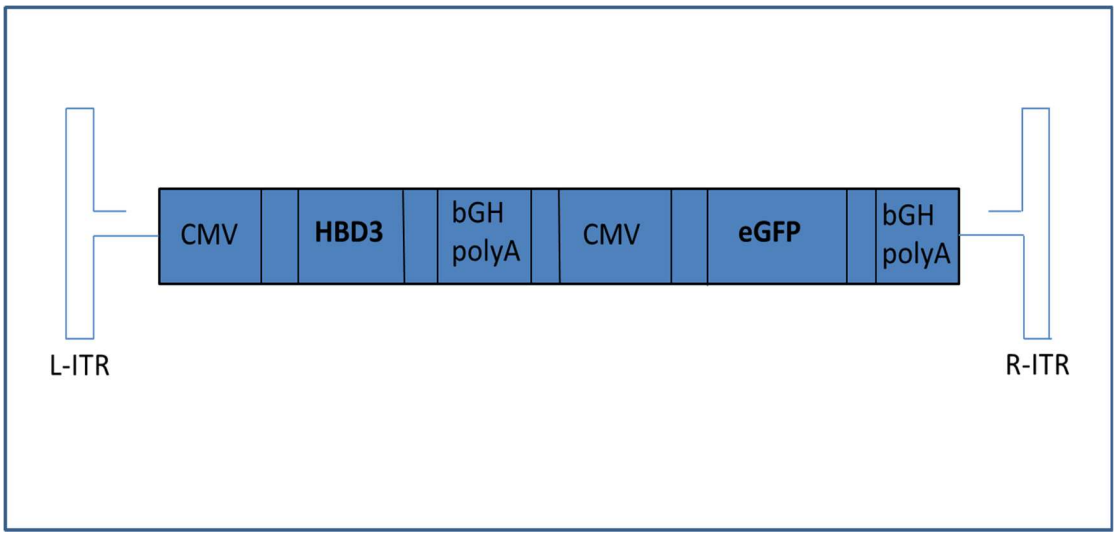

Figure 2.7: Bistronic AAV HBD-3 GFP plasmid.

2.3.2. Plasmid transient transfections

$1x10^5$ cells were seeded per well in DMEM supplemented with 10% FCS and incubated overnight at 37°C and 5% CO_2. A transfection mixture containing; 250µl of serum free OptiMEM media, 1µg of plasmid containing transgene and 1. 5µl of 40µM PEI per well was prepared. This was mixed and incubated for 20 minutes at room temperature. The media was removed from the cells and they were washed in serum free OptiMEM media. 250µl of transfection mix was added per well and left to incubate for 4 hours at 37°C and 5% CO_2. After this incubation time, the transfection mix was removed and replaced with 500ml of DMEM supplemented with 10% FCS. The cells were incubated for 72 hours until protein extraction.

2.3.3. Supernatant and cell lysate AMP extraction

Supernatants and cell lysates were placed in 20% acetic acid overnight at 4°C. The following day the samples were centrifuged at 18000g for 10 minutes. The cell debris was discarded and the resulting supernatants placed into micro-centrifuge tubes. These samples were lyophilized overnight and the extracted protein was resuspended in 10mM acetic acid.

2.3.4. AAV production

The AAV 2/8 viral vector containing the HBD-3 and GFP transgenes was produced as described above (section 2.1.9.) and also made by Vector Biolabs (Malvern, UK). The AAV 2/6 viral vector containing the HBD-3 and GFP transgenes was made by Vector Biolabs (Malvern, UK).

2.3.5. AMP protein detection and quantification

2.3.5.1. AMP western blotting

The samples were added to 2.5µl of 4x SDS buffer, 2µl of Dithiothreitol (DTT) and the total volume made up to 12µl with dH_20. The protein samples were heat shocked at 100°C for 5 minutes and briefly centrifuged at 9500g. A 4-20% Mini Protean TGX stain-free gel (BioRad,

UK) was placed into a western blot tank containing MOPS buffer, where 10µl of the samples were loaded. 5µl of a Precision plus protein all blue ladder was also loaded. The gel was then run for 30 minutes at 300V. The gel was transferred on to a pre-prepared PVDF membrane (Trans-Blot turbo pack: BioRad, UK) and placed into a transfer chamber for 3 minutes. The membrane was incubated in a blocking buffer (5% milk powder in 0.01% PBS-T) for 1 hour. This was followed by 3 washes in PBS-T. The membrane was then incubated with primary antibody (anti-rabbit HBD-3: 1:1000 concentration) in 1% milk in PBST on a roller shaker overnight at 4°C. The membrane was washed the following morning and then incubated with the secondary HRP-conjugated antibody in 1% milk in PBS-T for 1 hour on a roller shaker. After further washes, the membrane was added to Chemiluminescence solution for 3 minutes followed by visualisation on a BioRad ChemiDoc imager.

2.3.5.2. AMP ELISAs

Samples were processed using the Peprotech HBD3 ELISA kit according to manufacturer's protocol. Samples and antibodies were diluted with reagent diluent (1% BSA in PBS, pH 7.4). For the HBD-3 standards; the lower and upper limits of detection were 63pg/ml and 4000pg/ml, respectively. The plate was read at an absorbance of 405nm using the FluoStar Omega microplate reader. The results were analysed in MARS data analysis data software.

2.3.6. AMP functional killing assays

E.coli K12 was grown to mid-logarithmic phase and diluted to $1x10^5$ CFU/ml. The bacteria were centrifuged at 14000g for 3 minutes. The pellet was washed once in 10mM PB followed by further centrifugation and then re-suspended in 10mM phosphate buffer. In a 96 well plate, 90µl of the resuspended bacteria was mixed with 10µl recombinant HBD-3 protein, prepared supernatant, extracted cell lysate samples or vaginal lavage. The plate was incubated for 30 minutes at 37°C. 20µl of each sample was then mixed with PBS (to inhibit further AMP activity).

Serial dilutions were then plated and placed at 37°C overnight. CFU were counted the following morning.

In vitro killing assays were performed by inoculating transfected cell media with 100µl of $1x10^5$ CFU/ml *E.coli*-K12 at 72 hours after plasmid transfection. This was placed at 37°C and 5% CO_2 for 2 hours. Bioluminescence was determined prior to inoculation and then at 2 hours after inoculation using the FluoStar Omega microplate reader. The results were analysed in MARS data analysis data software. The fold change in bioluminescence was used as a measure of bacterial viability.

2.4. Microbiome studies using next generation sequencing

Culture-independent profiling of bacterial communities relies on the amplification and sequencing of the universal prokaryotic 16S ribosomal RNA (rRNA) gene. The rRNA gene is 1500bp long and contains nine hypervariable regions interspersed between conserved regions (Figure 2.8). This study uses the V3-V4 hypervariable region for sequencing. Next generation sequencing can generate $1x10^7$ sequences from a single sample and so allow for an extensive description of microbial DNA. It involves amplification of a PCR library with barcoded primers, followed by clean up and normalisation steps and then subsequent sequencing on a MiSeq™ (Illumina, Cambridge, UK). After sequencing, downstream bioinformatics is necessary to demultiplex samples, cluster sequences to operational taxonomic units (OTUs), quality filter and analyse data. The Quantitative Insights into Microbial Ecology (QIIME) software platform was used for the bioinformatics in this study.

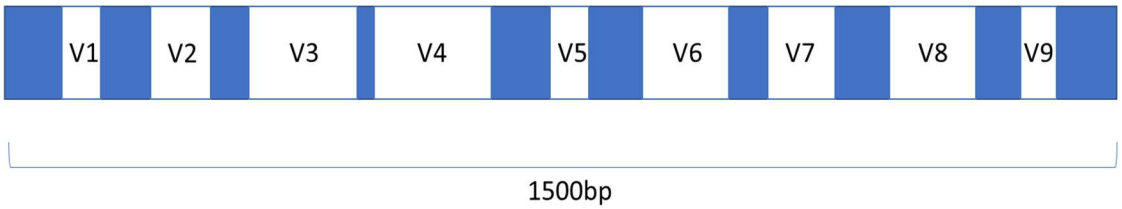

Figure 2.8: 16S rRNA gene with 9 hypervariable regions interspersed between conserved regions (blue).

2.4.1. Vaginal lavage

Vaginal lavage samples were obtained by administering 100µl of sterile PBS into the vagina of the mouse and pipetting in and out 10 times. Samples were put into a sterile Eppendorf and snap frozen in dry ice, followed by storage in -80°C.

2.4.2. DNA extraction of vaginal lavage samples

DNA extraction was performed using a QIAmp DNA mini kit (Qiagen, Manchester, UK) according to manufacturer's guidelines. Pipettes and AE buffer were placed under the UV light for 20 minutes prior to extraction in the dedicated microbiome extraction area. 20µl of proteinase K followed by 100µl sample was added to a lysis matrix B tube (MP biomedicals, Santa Ana, US). 200µl of AL-buffer was added and mixed by vortexing for 15 seconds. The samples were incubated at 56°C for 10 minutes. Bead beating at 50 oscillations for 1 minute was then performed using a Tissue-Lyser LT (Qiagen, Manchester, UK). Samples were centrifuged at 6600g for 1 minute and then 200µl of 70% ethanol was added followed by mixing by inversion. The contents are then applied to the column provided in the kit and centrifuged at 6600g for 1 minute. The column was placed in a new collection tube and 500µl of AW1 buffer was added followed by centrifuging at 6600g for 1 minute. The column was subsequently placed in a new collection tube and 500 µl of AW2 buffer was added followed by centrifuging at 6600g for 3 minutes. The column was next placed into a sterile Eppendorf and 50µl of AE buffer was added followed by centrifuging at 6600g for 1 minute. DNA was then

quantified using the Qubit DNA high sensitivity assay kit and Qubit 2.0 machine (Thermo Fisher Scientific, UK), followed by freezing at -80°C.

2.4.3. Broad range 16S rRNA gene qPCR

Broad range 16S rRNA gene qPCR was performed to confirm gene expression and to determine DNA inhibition. The qPCR mastermix was prepared using POWER SYBR® Green master mix (Applied Biosystems, Cheshire, UK) (Table 2.5). Primers are detailed in 10.4. DNA samples were run as neat, 1/10 and 1/100 dilution to check for DNA inhibition. qPCR was performed on a Biorad CFX96 Touch™ Real-Time PCR Detection System (Biorad, Watford, UK) with the following cycling conditions (Table 2.6).

qPCR Mastermix x1	**Amount per 20 µl reaction (µl)**
POWER SYBR Green Master Mix	12.5
Forward primer (0.7pmol/µl)	0.9
Reverse primer (0.24pmol/µl)	0.3
Nuclease free H_20	9.3
Cdna	2.0

Table 2.5: 16S rRNA gene qPCR mastermix

T°C	**Time**	**Cycles**
95	10 min	1
95	15 s	45
60	30 s*	

Table 2.6: 16S rRNA gene qPCR cycling conditions.

***data acquisition from green channel**

2.4.4. Next generation sequencing

2.4.4.1. V3-V4 16s rRNA gene amplicon PCR

The mastermix without the DNA template and primers was made up and 42.5µl was added to each well of a 96-well plate (Table 2.7). Barcoded forward and reverse primers were added (see 10.4.), making sure to change tips between wells. DNA template was added before briefly spinning the plate and running in the PCR machine (Biorad T100 Thermal cycler) (Table 2.8).

Amplicon PCR Mastermix x1	**Amount per 50 µl reaction (µl)**
10x PCR buffer	5.0
Forward primer (0.5µM) with barcode attached-different for every samples	1.25
Reverse primer (0.5µM) with barcode attached-different for every sample	1.25
dNTP mix	1
Taq DNA polymerase	0.25
Nuclease free H_20	36.25
Cdna	5.0

Table 2.7: Amplicon PCR mastermix

T°C	**Time**	**Cycles**
95	3 min	1
95	30 s	
50	30 s	30
72	30 s	
72	10 min	1

Table 2.8: Amplicon PCR cycling conditions

2.4.4.2. PCR clean-up

35µl of AMPure beads (Beckman Coulter, High Wycombe, UK) was added to each well containing PCR products. Once mixed, this was incubated for 5 minutes at room temperature. The plate was then placed onto a magnetic stand (Beckman Coulter, High Wycombe, UK) for 2 minutes or until the supernatant becomes clear. The supernatant is removed and then the beads were washed twice in 200µl of 80% ethanol. The plate was then removed from the magnetic stand and 50µl of AE buffer was added to each well and mixed. After a 2-minute incubation period, the plate was then placed back onto the magnetic stand for 2 minutes or until the supernatant becomes clear. The supernatant with the PCR clean product was removed and transferred to a new 96 well plate and was stored for 1 week at -20°C.

2.4.4.3. Next generation sequencing

The DNA from the above step was quantified using a Qubit DNA high sensitivity assay kit and Qubit 2.0 machine (Thermo Fisher Scientific, UK). The DNA concentration in each well was normalised to the lowest concentration sample. The DNA was then pooled including negative DNA extraction controls. This library was diluted to 0.4nM after quantification using the Qubit 2.0, standard curve qPCR and an Agilent high sensitivity DNA kit with the Agilent 2200 Tapestation instrument (Agilent genomics, Santa Clara, US) (Figure 2.9). The library was subsequently loaded onto the MiSeq™ sequencer (Illumina, Cambridge, UK) as per manufacturer's guidelines using the 500 cycle V2 MiSeq™ reagent kit (Illumina) with the addition of custom sequencing primers and a 15% PhiX control spike (12pM).

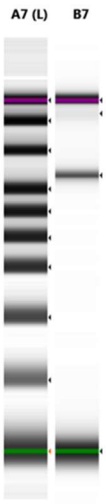

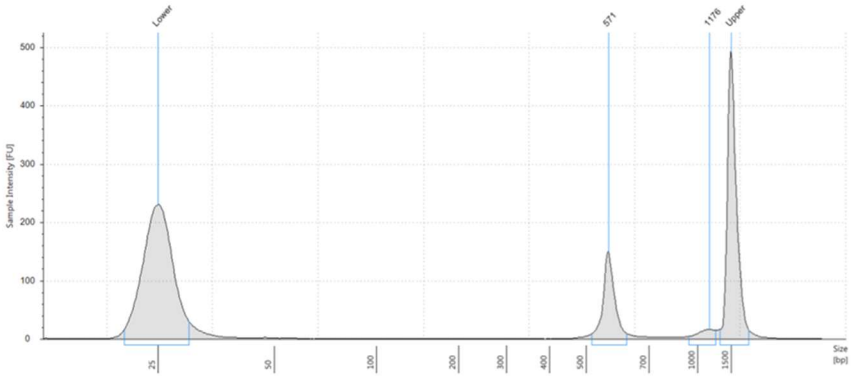

Sample Table

Well	Conc. [pg/µl]	Sample Description	Alert	Observations
B7	109			

Peak Table

Size [bp]	Calibrated Conc. [pg/µl]	Assigned Conc. [pg/µl]	Peak Molarity [pmol/l]	% Integrated Area	Peak Comment	Observations
25	385	-	23700	-		Lower Marker
571	93.9	-	253	85.94		
1176	15.4	-	20.1	14.06		
1500	250	250	256	-		Upper Marker

Figure 2.9: DNA quantification using the Agilent Tapestation method. The 571 peak represents the bacterial DNA library using the V3-V4 barcoded primers.

2.5. Cervical AMP gene therapy in ascending vaginal infection and preterm birth models

Adult female mice (6-8 weeks) C57BL/6N-Tyr$^{c\text{-}Brd}$ were mated overnight with stud males. The day a copulatory plug was observed was designated embryonic Day 0.5. Intravaginal AMP gene therapy (1x10^{12} genomic copies/ml) was injected on embryonic day 13.5 using a sterile 200µl pipette followed by application of AK12 pluronic gel (Polyvivo, US). 72 hours later, intravaginal injection of bioluminescent *E.coli* was performed, followed by daily bioluminescence imaging (Figure 2.10). Following injections, mice were placed in individual cages and continuously monitored with individual closed circuit television cameras and a digital video recorder. Time to delivery was recorded and defined as the number of hours from the time of injection to delivery of the first pup. The number of live and dead pups were recorded.

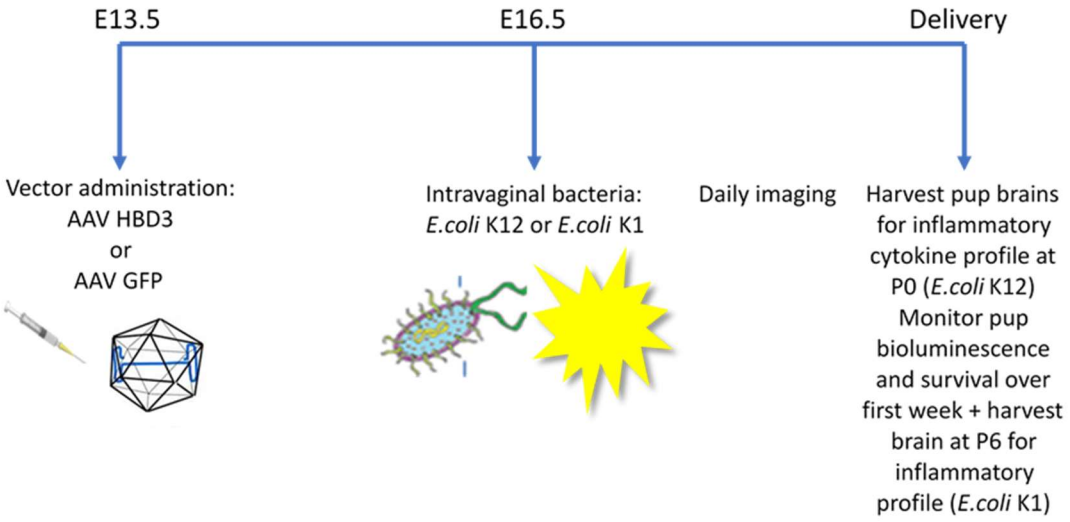

Figure 2.10: Schematic representation of AMP gene therapy experiments. Vector is administered on E13.5, followed by intravaginal bacterial administration 72 hours later on E16.5. Imaging is performed daily until delivery.

2.6. Statistical analysis

Data are expressed as means ± standard deviation. Data were checked for normality using the Shapiro-Wilk normality test. Data that was normally distributed was analysed with unpaired *t*-tests, one-way ANOVA and two-way repeated measure ANOVA with Bonferroni post hoc tests. Non-parametric data was analysed with Mann-Whitney rank tests and Kruskal-Wallis tests with Dunn's post hoc tests. All statistical analyses were performed with GraphPad Prism software version 7.0 (GraphPad, San Diego, CA). $P < 0.05$ was considered statistically significant. Next generation sequencing data was kindly analysed by Dr Grace Logan using QIIME software.

Chapter 3 Developing a mouse model of ascending vaginal infection and preterm birth

3.1. Summary

Mouse models of disease in pregnancy are important research tools as mice are relatively inexpensive, have short gestation periods (19-21 days) and there is considerable homology between the human and mouse genomes and gene function. As ascending vaginal infection is believed to be an important factor in many cases of spontaneous preterm birth, it is imperative to create a mouse model capable of mimicking this infection. This type of model would enable testing of a cervically-targeted therapy for preterm birth prevention. It is also important that we consider the principles of the 3Rs (replacement, reduction and refinement) as a framework when developing these mouse models. With this in mind, I tested the hypothesis that with an appropriate mode of administration, choice of bacteria and mouse strain, a repeatable model of bacterial ascending vaginal infection could be established in pregnant mice.

In this chapter I describe the development of an ascending infection model system using bioluminescent *E.coli* (K12 and K1 strain) in non-pregnant and more relevantly pregnant mice, that enabled the tracking of bacterial ascent without the need to sacrifice animals at multiple time points. *E.coli* K12 is a non-pathogenic laboratory strain of *E.coli* that is commonly used in molecular biology and is not known to cause disease. *E.coli* K1, on the other hand, is a pathogenic stain which is known to cause neonatal sepsis and meningitis in humans (Simonsen et al. 2014). Intravaginal administration of *E.coli* K12 did not lead to premature delivery but

E.coli K1 resulted in premature delivery in approximately 60% of dams within 48 hours of administration. These model systems enabled the interrogation of the mechanisms leading to premature delivery as well as providing a useful model to test preventative therapies for preterm birth.

3.2. Bioluminescent *E.coli* strains K12 and K1 show constitutive expression of the lux operon

E.coli K12 and K1 bacteria were diluted in LB broth (plus appropriate antibiotic) and grown at 37°C and 200rpm. Strains were assessed for absorbance (OD_{600}) and bioluminescence at 30-minute intervals. Both *E.coli* K12 and K1 produce a bioluminescent signal over the growth cycle that correlates with absorbance, indicative of constitutive lux operon expression (Figure 3.1).

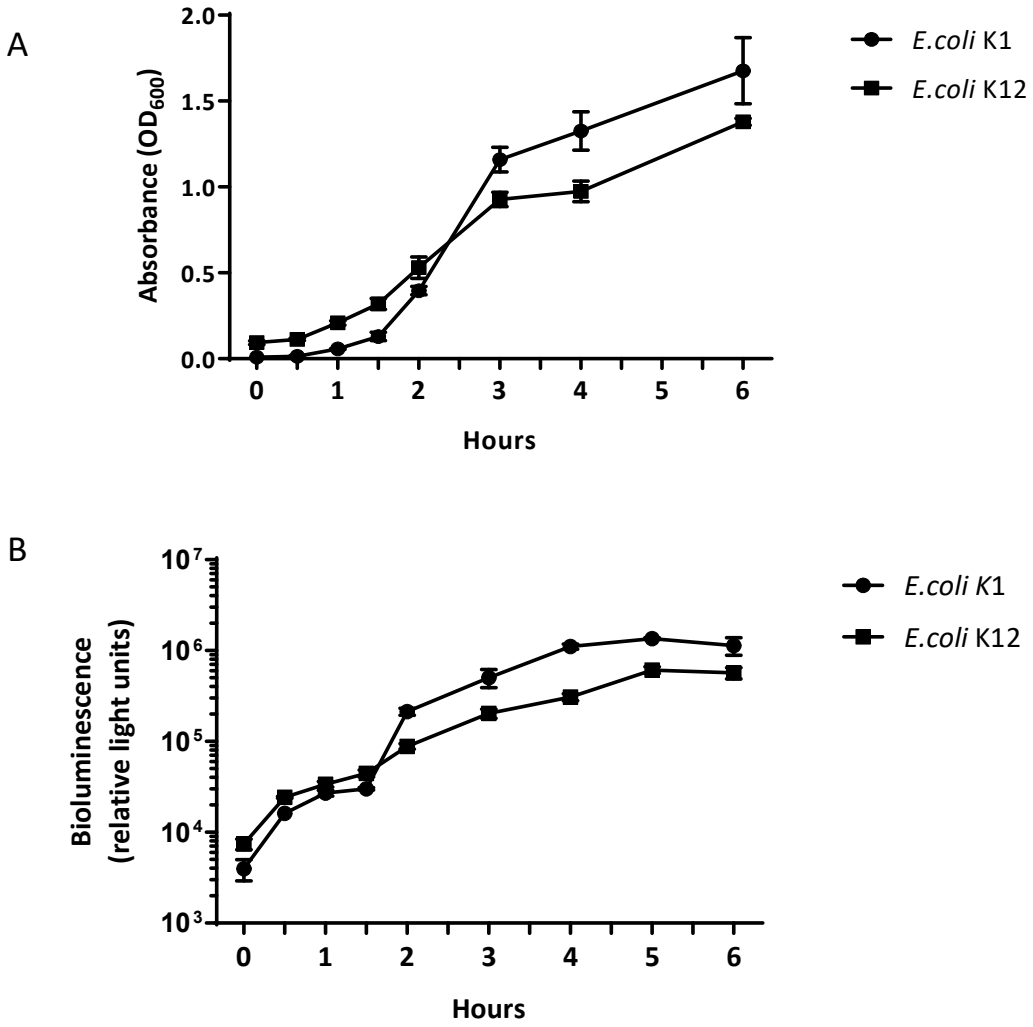

Figure 3.1: Characterization of *E.coli* K12 and *E.coli* K1 growth. (A) Growth of *E.coli* k12 and *E.coli* K1 in LB broth at 37°C and 200rpm, over time. There is an increase in OD_{600} absorbance over time. **(B)** Bioluminescent signal from *E.coli* K12 and *E.coli* K1 during the growth cycle. Bioluminescent signal correlates with the growth phase (as determined by absorbance), indicating constitutive lux operon expression. n=3.

3.3. Bioluminescent *E.coli* strains K12 and K1 are motile

Bioluminescent *E.coli* (K12 and K1) was assessed for normal motility patterns using specialised motility media (SIM media) to confirm its potential for ascension into the uterine cavity. After 24 hours incubation at 37°C, there was a diffuse spread in bacteria from the central inoculation in the motility agar medium, confirming that this strain of bacteria is motile (Figure 3.2).

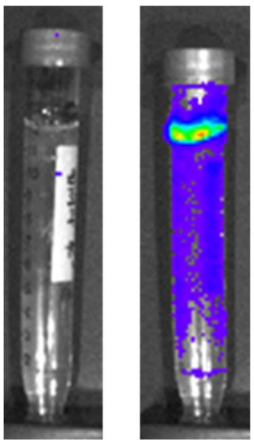

Figure 3.2: *E.coli* K1 and K12 are motile. Bacterial bioluminescence at inoculation (left) and 24h after inoculation (right). There is bacterial growth and movement to the outer edges of the falcon tube after 24 hours.

3.4. The C57BL/6N-*Tyr*$^{c\text{-}Brd}$ mouse strain is best for modelling ascending vaginal infection

Initial experiments were performed using bioluminescent *E.coli* K12 in CD1 outbred mice. Bacterial luminescence could only be detected transiently in CD1 mice which had received vaginal inoculation of *E.coli* K12 (Figure 3.3).

Figure 3.3: CD1 mice do not show ascending infection 24 hours after *E.coli* K12 vaginal administration. These are representative images at the time of *E.coli* K12 intravaginal administration and after 24 hours in CD1 mice. There was no obvious *E.coli* K12 bioluminescence in CD1 mice 24 hours after administration.

Other studies which assessed bacterial infection in the vagina and cervix used the C57BL/6 strain of mouse (Gupta et al. 2014). Therefore, ascending vaginal infection with E.coli K12 was compared with three different mouse strains (CD-1, BALB/c and C57BL/6) and a spontaneous albino mutant of the C57BL/6 strain (C57BL/6N-*Tyr*$^{c\text{-}Brd}$) (Figure 3.4). The C57BL/6N-*Tyr*$^{c\text{-}Brd}$ strain was identified as a potential candidate because as it has been reported that there is at least a 10-fold quenching of bioluminescent signal from mice with black fur (Campbell et al. 2014). There was significantly increased bacterial infection seen in C57BL/6N-*Tyr*$^{c\text{-}Brd}$ mice compared to CD-1 mice at the 6, 18 and 24 hour time points (*P=0.0049, P=0.0024* and *P=0.0007,* respectively) and compared to BALB/c mice at the 18 and 24 hour time points (*P=0.0063* and *P=0.0002,* respectively) (Figure 3.4C). This trend was also seen in the C57BL/6 mice but was only significant at 24 hours (compared with CD-1 mice; *P=0.0011*, and compared with BALB/c mice; *P=0.0004*). In view of these results C57BL/6N-Tyr$^{c\text{-}Brd}$ mice were used for the subsequent experiments.

A

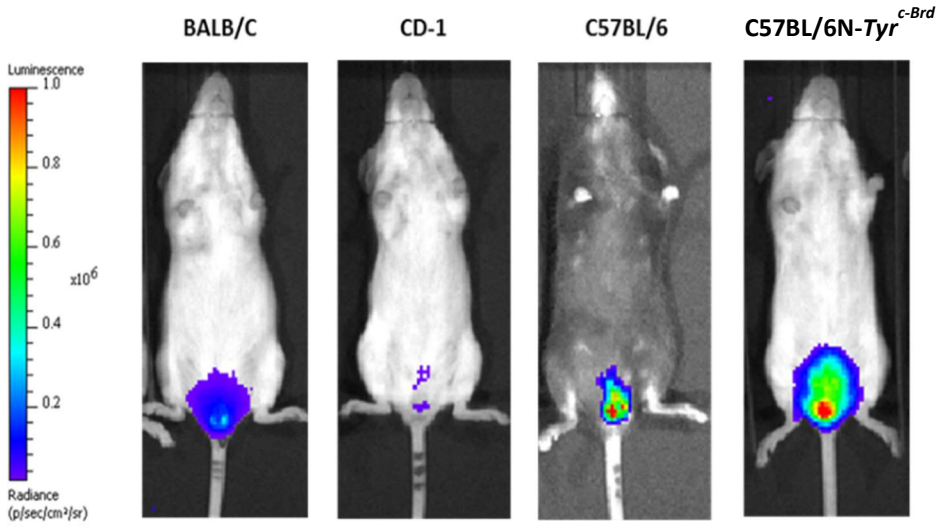

B

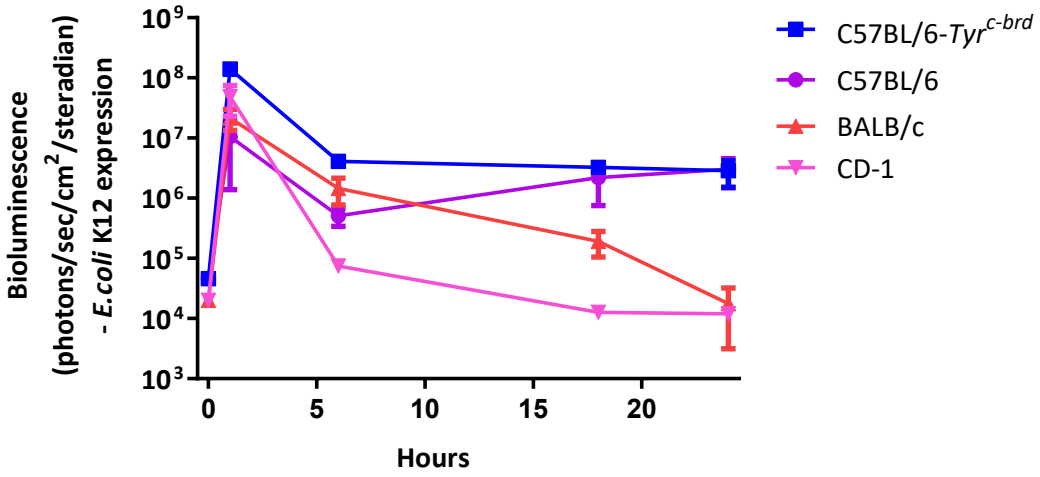

C

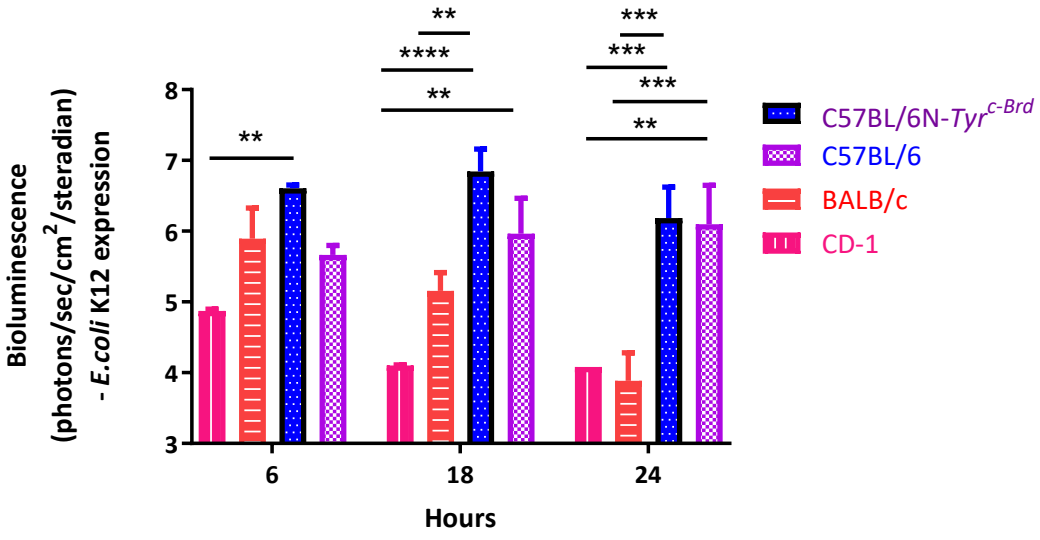

Figure 3.4: The C57BL/6N-Tyr$^{c\text{-}Brd}$ mouse strain is best for modelling ascending vaginal infection. (A) Representative images of *E.coli* K12 infection 24 hours after administration, showing increased bioluminescent signal in C57BL/6N-*Tyr*$^{c\text{-}Brd}$ mice. **(B)** *E.coli* K12 bioluminescence over time in different mouse strains**.** ***(C)*** *E.coli* K12 bioluminescence at different time points. There is increased bioluminescent signal in the C57BL/6N-*Tyr*$^{c\text{-}Brd}$ mice at all time points. n=3, data $\log_{10}$ transformed and analysed with a two-way repeated measures ANOVA with post hoc Bonferroni test,**P<0.05, **P<0.01, ***P<0.001, ****P<0.0001*

3.5. Bacteria ascend into the non-pregnant uterine cavity

Non-pregnant mice were culled and their reproductive tracts were imaged at 6, 18, 24 and 48 hours after receiving intravaginal injection of *E.coli* K12 (Figure 3.5). Bacteria were detected in the upper vagina and cervix at 6 hours, ascending the uterine horns at 18 to 24 hours and diminished by 48 hours.

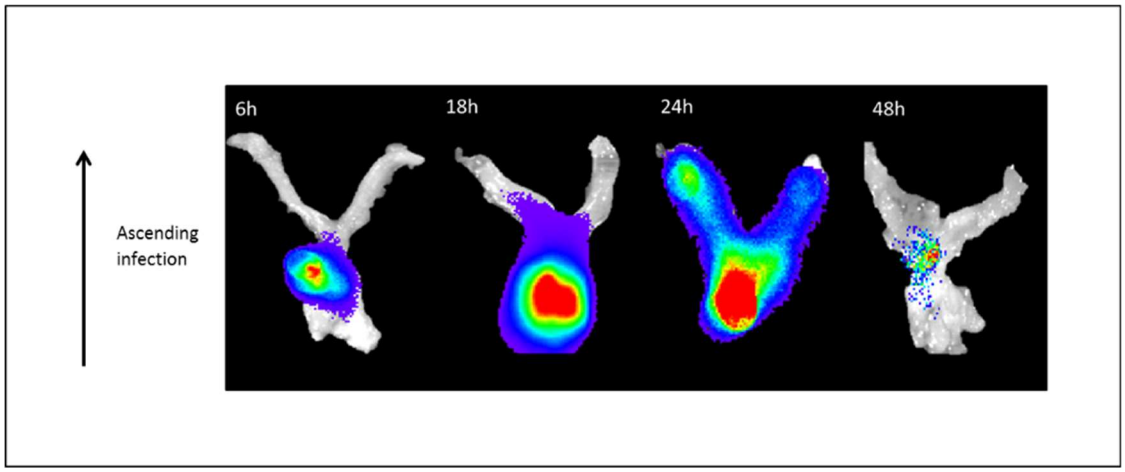

Figure 3.5: Bacteria traverse the cervical barrier of the non-pregnant uterus by 6 hours and then ascend to the top of the uterine horns by 24 hours. Representative images of the time course of ascending bacterial infection in the non-pregnant reproductive tract following intravaginal *E.coli* K12 administration.

3.6. Local inflammatory studies in non-pregnant mice

In the majority of spontaneous preterm birth cases, there is no obvious overwhelming infection in the mother and it is only during retrospective pathological examination of the placenta and fetal membranes that we see evidence of chorioamnionitis and funisitis (Wu et al. 2009). There is now strong evidence that the initiation of labour, term and preterm, is associated with an increased production of pro-inflammatory cytokines and an influx of neutrophils and macrophages in the cervix, uterus and fetal membranes (Rinaldi et al. 2014). Therefore, I hypothesised that these inflammatory markers would be elevated in the uterus of the mice after ascending bacterial infection.

3.6.1. Pro-inflammatory cytokines are not increased in the uterus of infected mice

The pro-inflammatory cytokine profile of the cervix and uterus was characterized by quantifying TNF-α and IL-1β cytokines. These cytokines are typically produced in response to bacterial infection. There was a non-significant increase in uterine IL-1β and TNF-α in the ascending *E.coli*-K12 infected model compared to the controls (Figure 3.6).

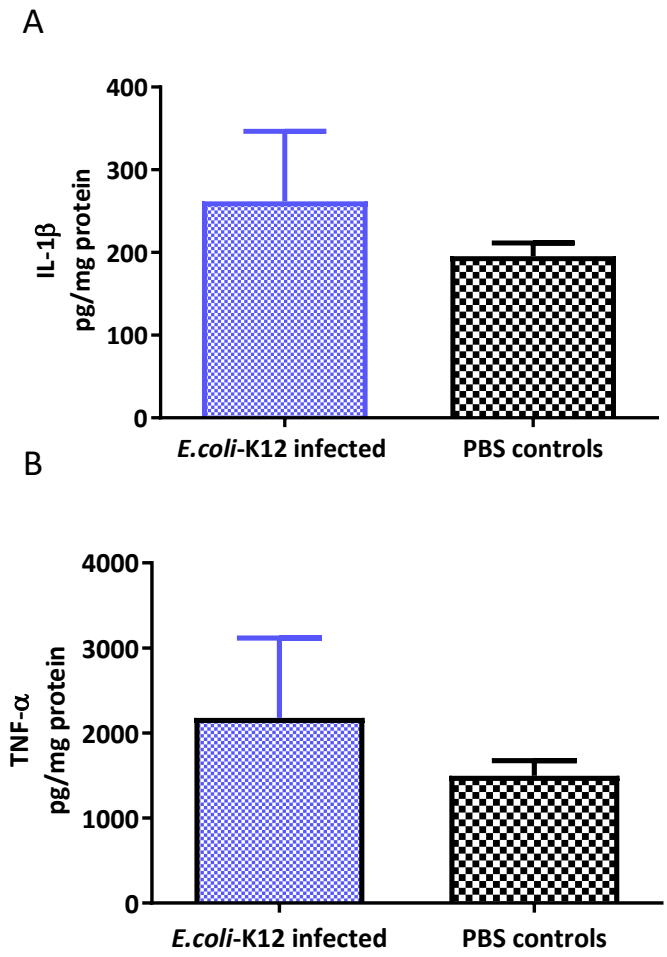

Figure 3.6: There is a non-significant increase in TNF-α and IL-1β in uterine homogenates 24 hours after intravaginal *E.coli* K12 administration. (A) Uterine IL-1β protein expression 24 hour after intravaginal *E.coli* K12 infection. **(B)** Uterine TNF-α expression 24 hour after intravaginal *E.coli* K12 infection. n=15, E.coli K12-infected; n=10, PBS controls; data not normally distributed therefore analysed with a one-tailed Mann-Whitney rank test, *P=0.16*.

3.6.2. There is an influx of neutrophils into the uterine horns of infected mice

To determine whether intravaginal *E.coli*-K12 infection resulted in neutrophil influx into the uterine tissues, anti-Ly-6g immunohistochemistry was performed on uterine horn samples collected 24 hours after intravaginal infection (Figure 3.7A). There was a significant increase in neutrophil influx in the *E.coli* K12 infected uterine horns, compared to the control horns (*P=0.0022*) (Figure 3.7B).

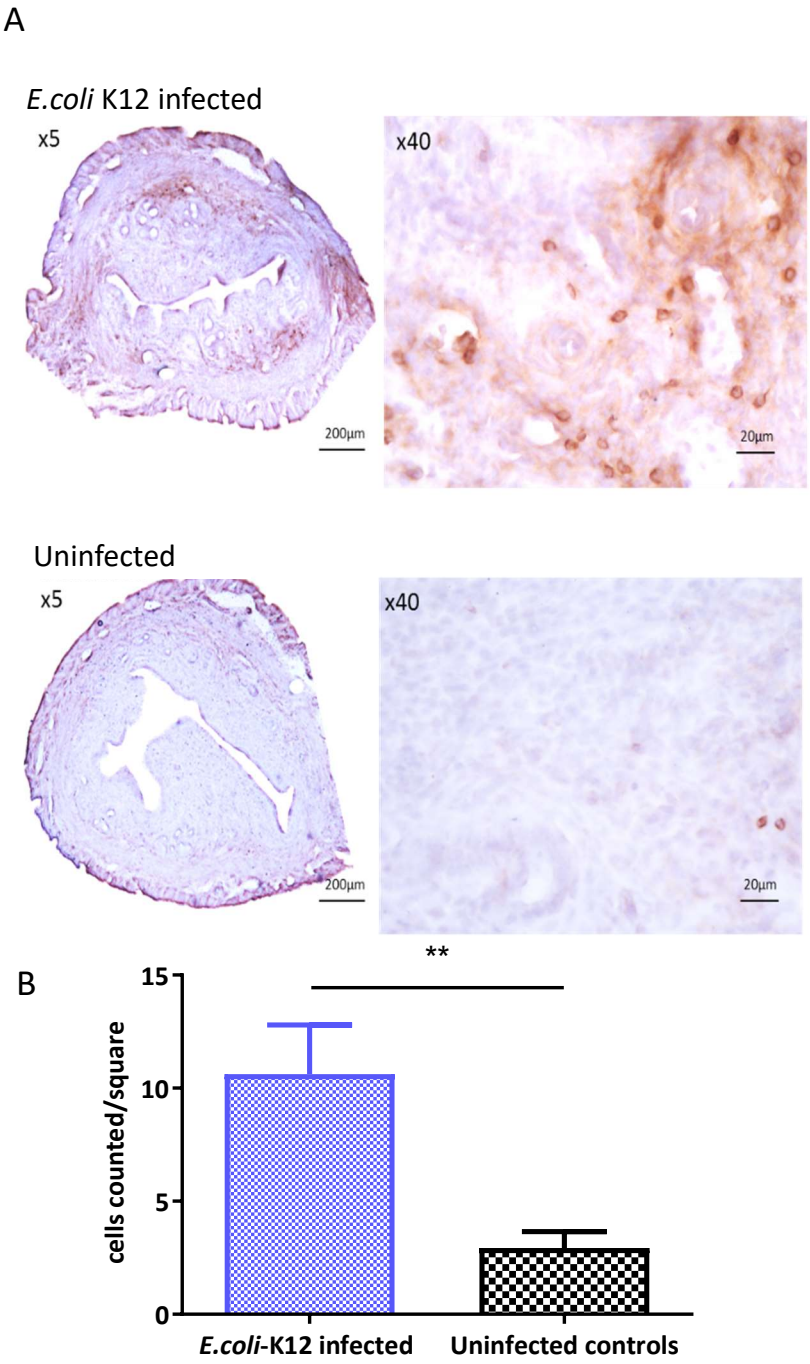

Figure 3.7: There is an increase in neutrophils in the sub-epithelial stroma of the uterine horns 24 hours following intravaginal *E.coli* K12. (A) Representative images of neutrophil localization using immunohistochemical staining of Ly-6g with haematoxylin counterstain. Brown coloration depicts DAB-positive cells. **(B)** There is an increase in sub-epithelial stroma neutrophil counts in the *E.coli* K12-infected group compared with uninfected controls. n=3; unpaired t-test, ***P<0.005*.

3.6.3. ICAM-1 Immunohistochemistry is upregulated in the uterine horns of infected mice

ICAM-1 is a cell surface glycoprotein that is a ligand for the leucocyte adhesion protein-1. It is present at low concentrations on leucocytes and endothelial cells and facilitates the migration of leucocytes from the blood into tissues. Pro-inflammatory cytokines, such as IL-1β and TNF-α greatly increase the concentration of these proteins to allow for increased migration of these cells into infected and inflamed tissues. I hypothesised that intravaginal *E.coli*-K12 would increase ICAM-1 expression in the uterus 24 hours after administration. ICAM-1 immunohistochemistry was performed on uterine tissue 24 hours after intravaginal E.*coli* K12 administration and showed ICAM-1 upregulation compared with uninfected PBS controls (*P<0.0001*) (Figure 3.8).

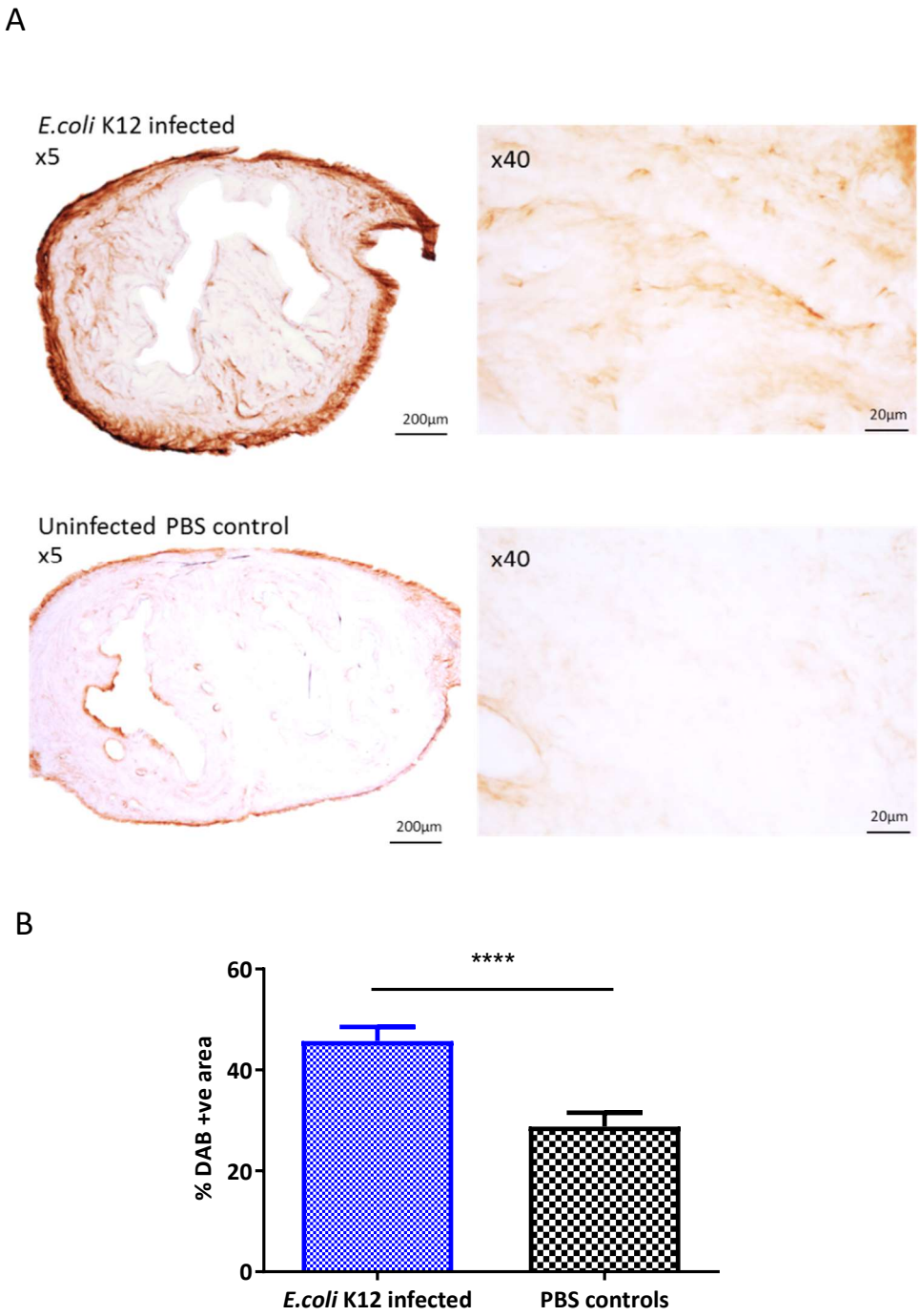

Figure 3.8 ICAM-1 is upregulated in the uterine horns 24 hours following intravaginal *E.coli* K12. (A) Representative images of neutrophil localization using immunohistochemical staining of ICAM-1. Brown coloration depicts DAB-positive cells. **(B)** There is increased ICAM-1 upregulation in the uterine horns 24 hours after intravaginal administration *E.coli* K12. n=3; unpaired t-test, ****$P<0.0001$.

3.7. Ascending vaginal bacterial infection is possible in pregnant mice using bioluminescent *E.coli* K12

To mimic the type of infection that is believed to occur in cases of spontaneous preterm birth, intravaginal infection with bioluminescent *E.coli* K12 was performed in pregnant mice. Mice received *E.coli* K12 on embryonic day 16.5 as described above (Figure 3.9). Embryonic day 16.5 was initially chosen as the day of bacterial administration based on previously published work (Rinaldi et al. 2014; Rinaldi et al. 2015; Edey et al. 2016). Pregnant mice were visualised at the time of injection and then at 6 hours after injection, followed by daily imaging. Bacteria were seen in the upper vagina after administration as would be expected (Figure 3.10A). 6 hours after bacterial administration, bacteria were seen in the left uterine horn. This is followed by bacteria being present throughout the uterine cavity at 24 and 48 hours after bacterial administration (Figure 3.10A). After delivery (P0) the bacteria begin to clear until they are not visible at 96 hours after bacterial administration. The pups were born with no evidence of bacterial colonization or infection (Figure 3.10B).

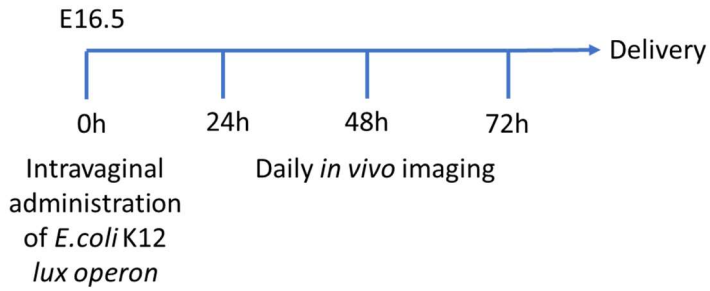

Figure 3.9: Mice were injected with bioluminescent *E.coli* K12 on E16.5 using a sterile pipette (20µl of 1x10^9 CFU) and bacterial movement was then assessed by daily in vivo bioluminescence imaging. Mice were also filmed using a continuous closed-circuit television recording system to determine gestation at delivery of first pup.

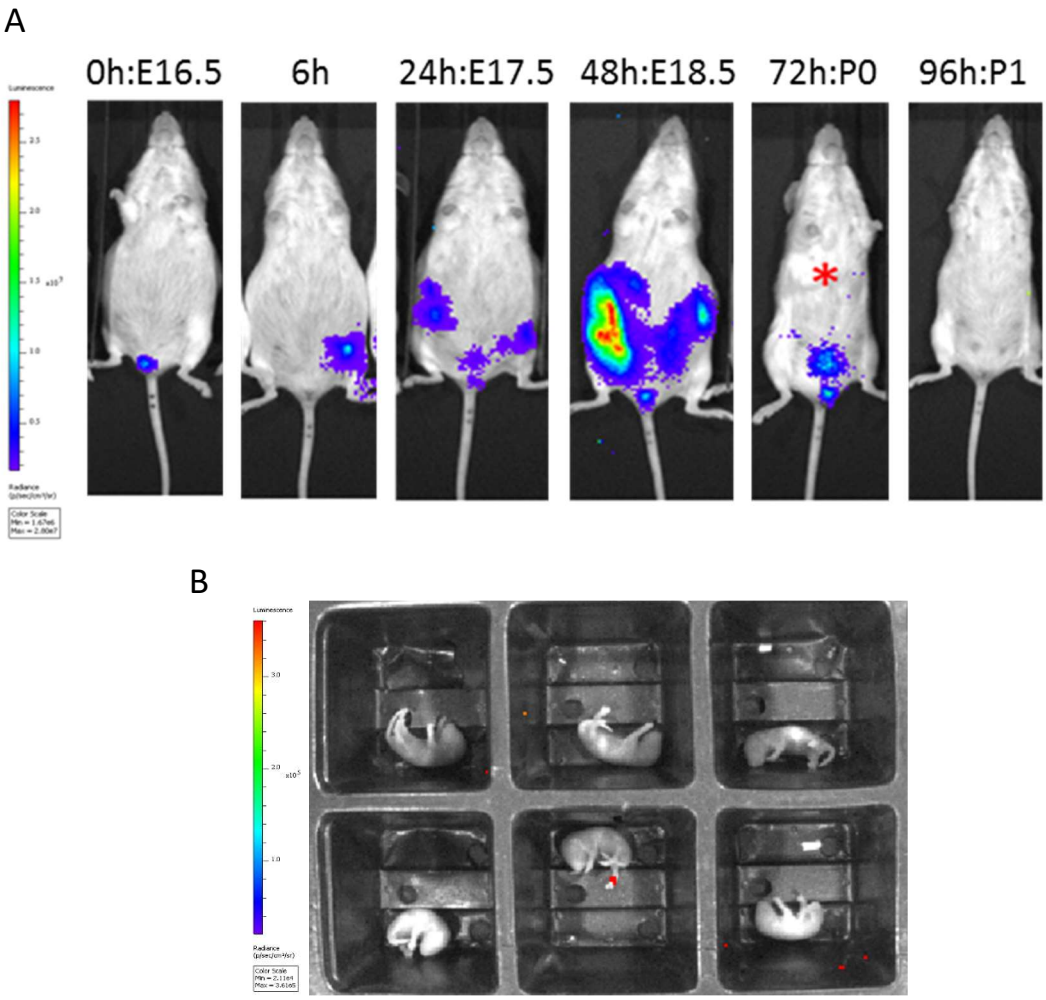

Figure 3.10: *E.coli* K12 ascends into the pregnant uterine cavity over 24 hours but does not infect pups. (A) Pregnant mice were administered intravaginal *E.coli* K12 on embryonic day 16.5. At 0h (the time of injection) bacteria are visible in the vagina. By 6 hours after injection bacteria is seen ascending into the uterine cavity. At 24 hours, embryonic day 17.5, the bacteria is visible in both uterine horns and this bacterial load increases by 48 hours, embryonic day 18.5. The following day, the pups were born and there is now minimal bacteria seen in the uterus or vagina (P0). On postpartum day 1 (P1) the bacteria have been cleared. * indicates the day of birth (P0) 24 hours later; on embryonic day 17.5, bacteria have ascended into the uterine horns. Bacteria clears by the second postpartum day. **(B)** There is no *E.coli* K12 present in pups born to infected dams. Representative images of pups on the day of birth (P0).

3.8. Pregnant mice intravaginally infected with *E.coli* K12 do not deliver prematurely or have reduced litter sizes

An ideal model of ascending vaginal bacterial infection in pregnant mice would also result in premature delivery. Therefore, delivery timings were determined in infected pregnant mice compared with controls injected with PBS. There was no difference in time to delivery between these two groups (*P=0.35)* (Figure 3.11A). To explore this ascending infection model further, intravaginal administration of *E.coli* K12 was performed at different gestational ages; embryonic day 14.5 and embryonic day 15.5. There was no obvious difference in bacterial ascent into the uterine cavity with bioluminescence imaging. In support of this, there was no difference in time to delivery between these administration gestations and PBS controls (*P=0.39* and *P=0.19*, respectively) (Figure 3.11B & Figure 3.11C). In view of this, the E16.5 time point was used for bacterial administration in subsequent experiments. The litter size was determined in *E.coli* K12 infected dams compared to PBS controls. There was no difference in litter size between the groups (*P=0.39*) (Figure 3.11D).

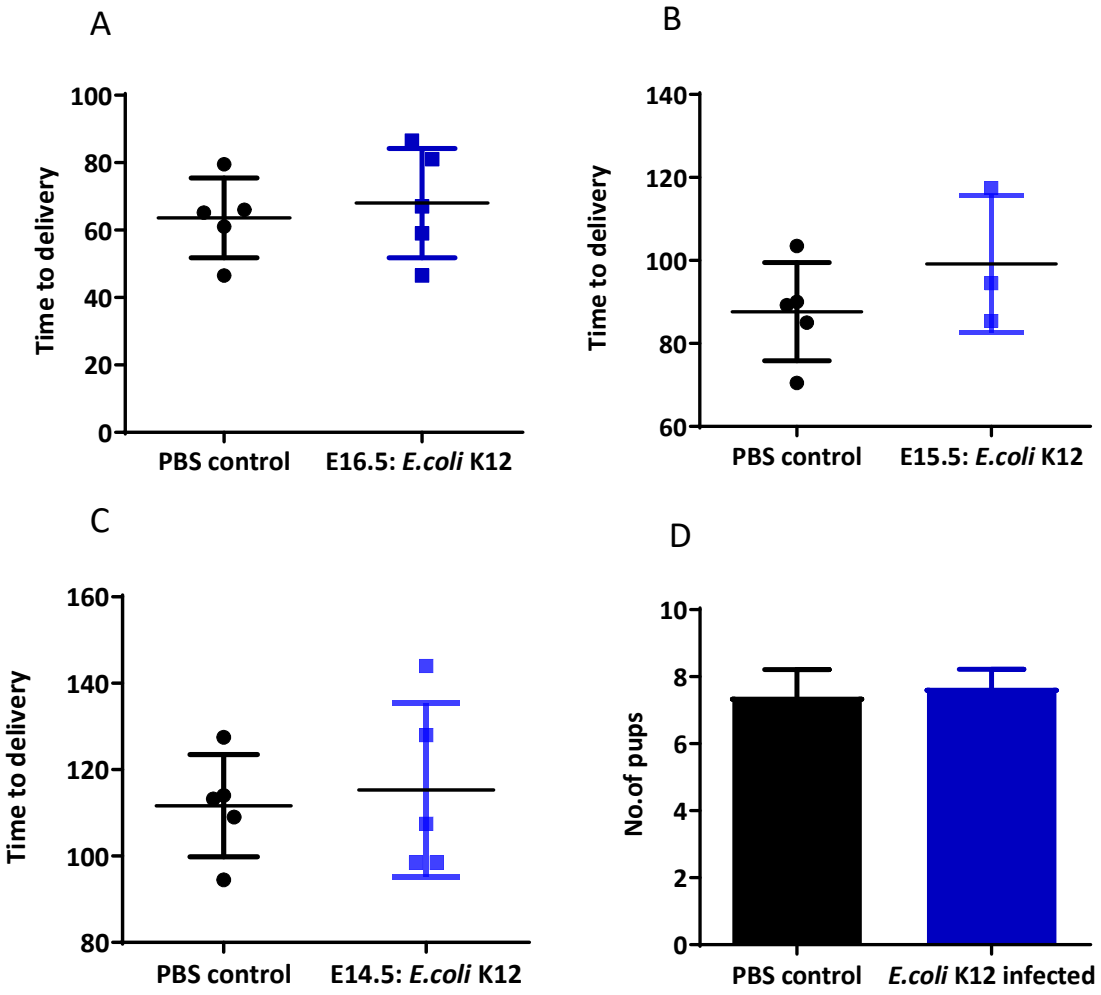

Figure 3.11: Pregnant mice intravaginally infected with *E.coli* K12 do not deliver prematurely or have reduced litter sizes. (A) Delivery time after intravaginal *E.coli* K12 infection at embryonic day 16.5. n=5; data log transformed, unpaired t-test, *P=0.35.* **(B)** Delivery time after intravaginal *E.coli* K12 infection at embryonic day 15.5. n=3, infected group; n=5, uninfected control group; data log transformed, unpaired t-test, P=0.19. **(C)** Delivery time after intravaginal *E.coli* K12 infection at embryonic day 14.5. n=5; data log transformed, unpaired t-test, *P=0.39*. **(D)** The litter size between *E.coli* K12 infected dams and uninfected control dams, following intravaginal administration at E16.5. n=5; data log transformed, unpaired t-test, *P=0.39.*

3.9. *E.coli* is detected in the placenta from pups of *E.coli* K12 infected dams

Embryos were removed from the dam 48 hours after *E.coli* K12 intravaginal administration. The embryos were imaged with their membranes, placenta and cord intact. Bacteria was detected in the placenta but not in the embryo (Figure 3.12). *E.coli* immunofluorescence staining revealed *E.coli* bacterial presence on the maternal and fetal sides of the placenta, as well as the placental origin of the umbilical cord (Figure 3.13).

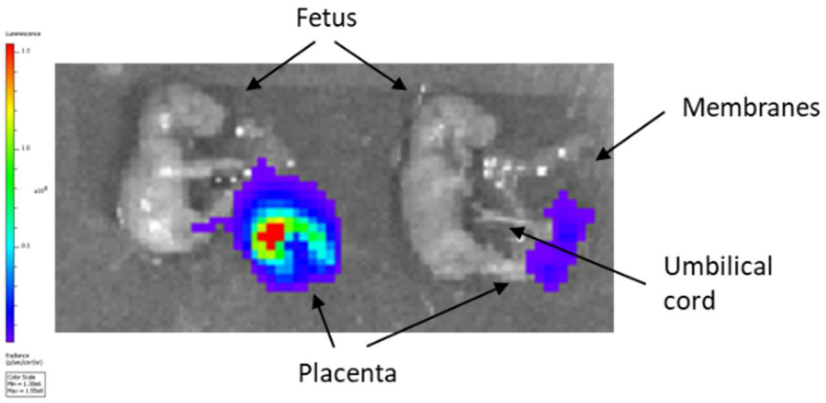

Figure 3.12: *E.coli* is detected in the placenta of pups from *E.coli* K12 infected dams. Representative images of two embryos on embryonic day 18.5 (48 hours after infection).

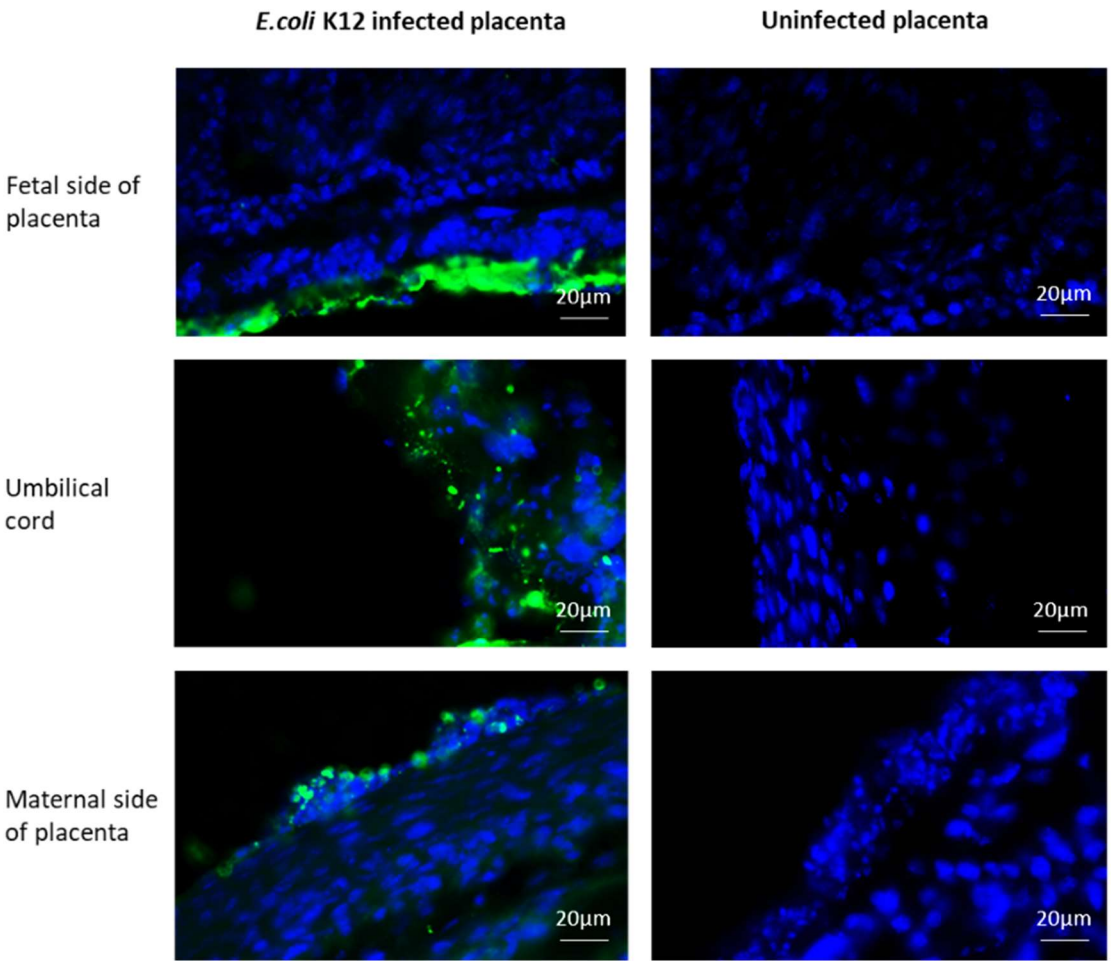

Figure 3.13: *E.coli* is detected in the placenta of pups from *E.coli* K12 infected dams. Representative images of anti-*E.coli* immunofluorescence staining of *E.coli* K12 infected placentas and uninfected controls (10x magnification). *E.coli* is present on the maternal and fetal sides of the placenta and at the placental origin of the umbilical cord. *E.coli* - green fluorescence*, DAPI nuclear stain* - blue fluorescence.

3.10. Pathogenic bioluminescent *E.coli* K1 ascends into the pregnant uterine cavity and causes preterm birth

As *E.coli* K12 did not induce preterm delivery in pregnant mice, the effects of a more pathogenic strain of *E.coli*, *E.coli* K1, were examined. *E.coli* K1 is responsible for causing neonatal meningitis and sepsis in humans and is dependent on vertical transmission from the mother (Ba-Thein et al. 2002; Witcomb et al. 2015). Bioluminescent *E.coli* K1 was intravaginally administered into pregnant mice on embryonic day 16.5 as described above (Figure 3.9). Different bacterial counts were administered to determine the effect on bacterial ascent and time to delivery ($2x10^2$ and $2x10^3$). Intravaginal administration of *E.coli* K1 lead to ascending infection in the uterine cavity by 24 hours after injection (Figure 3.14A & Figure 3.14B). The higher bacterial count lead to increased bacteria in the uterine cavity, however, these dams had much higher rates of systemic infection post-partum requiring the animal to be culled (4/10 with $2x10^3$CFU versus 2/10 with $2x10^2$CFU, n=10 dams). Therefore, $2x10^2$ CFU of *E.coli* K1 was used for intravaginal administration in subsequent experiments. Intravaginal *E.coli* K1 (lower dose; $2x10^2$CFU) resulted in premature delivery compared with PBS controls (time to delivery; 49 hours ± 9.9 hours vs. 66 hours ± 6.3 hours, *P=0.0007*) (Figure 3.14C). Furthermore, there was a reduction in the proportion of pups born alive in the *E.coli* K1 infected group compared with PBS controls (0.64 ± 0.4 vs. 0.98 ± 0.05, *P=0.0077*) (Figure 3.14D).

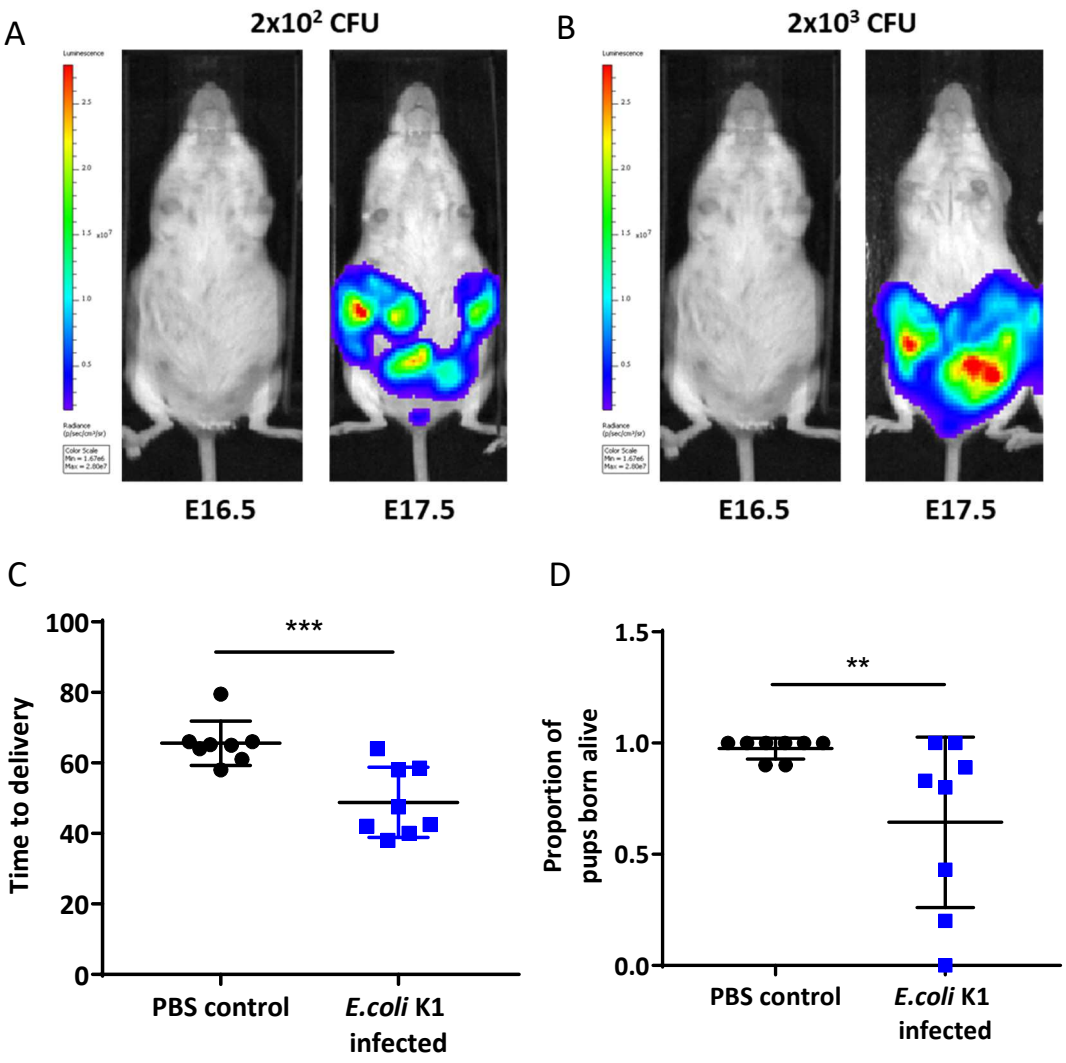

Figure 3.14: *E.coli* K1 ascends into the pregnant uterine cavity over 24 hours and leads to preterm birth and a reduced proportion of pups born alive. Representative images of *E.coli* K1 ascending into the uterine cavity of pregnant mice. **(A)** $2x10^2$ CFU (low dose) of *E.coli* K1. **(B)** $2x10^3$ (high dose) CFU OF E.coli K1. The higher bacterial count ($2x10^3$) leads to increased bacterial bioluminescence in the uterine cavity but increased rates of postpartum systemic infection. **(C)** *E.coli* K1 infected dams (lower dose; $2x10^2$ CFU) deliver earlier than PBS controls. Time to delivery after bacterial administration; 49 hours ± 9.9 hours in *E.coli* K1 dams vs. 66 hours ± 6.3 hours in PBS controls. n=8, data log transformed, unpaired t test, **** P=0.0007*. **(D)** *E.coli* K1 infected dams (lower dose; $2x10^2$ CFU) have a lower proportion of pups born alive. The proportion of pups born alive are 0.64 ± 0.4 in *E.coli* K1 infected dams versus 0.98 ± 0.05 in PBS controls. n=8, data *arcsin* transformed, unpaired t-test, ** *P=0.0077*.

3.11. *E.coli* K1 was detected in the placenta, fetal membranes and amniotic fluid 18 hours after bacterial administration

Dams were sacrificed 18 hours after intravaginal administration of *E.coli* K1, the intact uterine horns were imaged *ex vivo* and bacteria were detected within the uterine cavity (Figure 3.15A). On closer inspection, bacteria were detected in the placenta, membranes and amniotic fluid surrounding the fetus (Figure 3.15C). The placenta and fetal membranes were highly bioluminescent, whilst the amniotic fluid appeared less bioluminescent suggesting that the bacteria may infect the placenta and membranes first and then traverse the membranes to reach the amniotic fluid (Figure 3.15B).

E.coli was detected on both sides of the placenta and appeared to be present in the giant cell layer on the maternal side and the chorionic plate on the fetal side (Figure 3.16). It appeared that the bacteria were invading from both sides of the placenta as they are clearly present on the outer placental edges with the central labyrinth region containing only minimal amounts of bacteria.

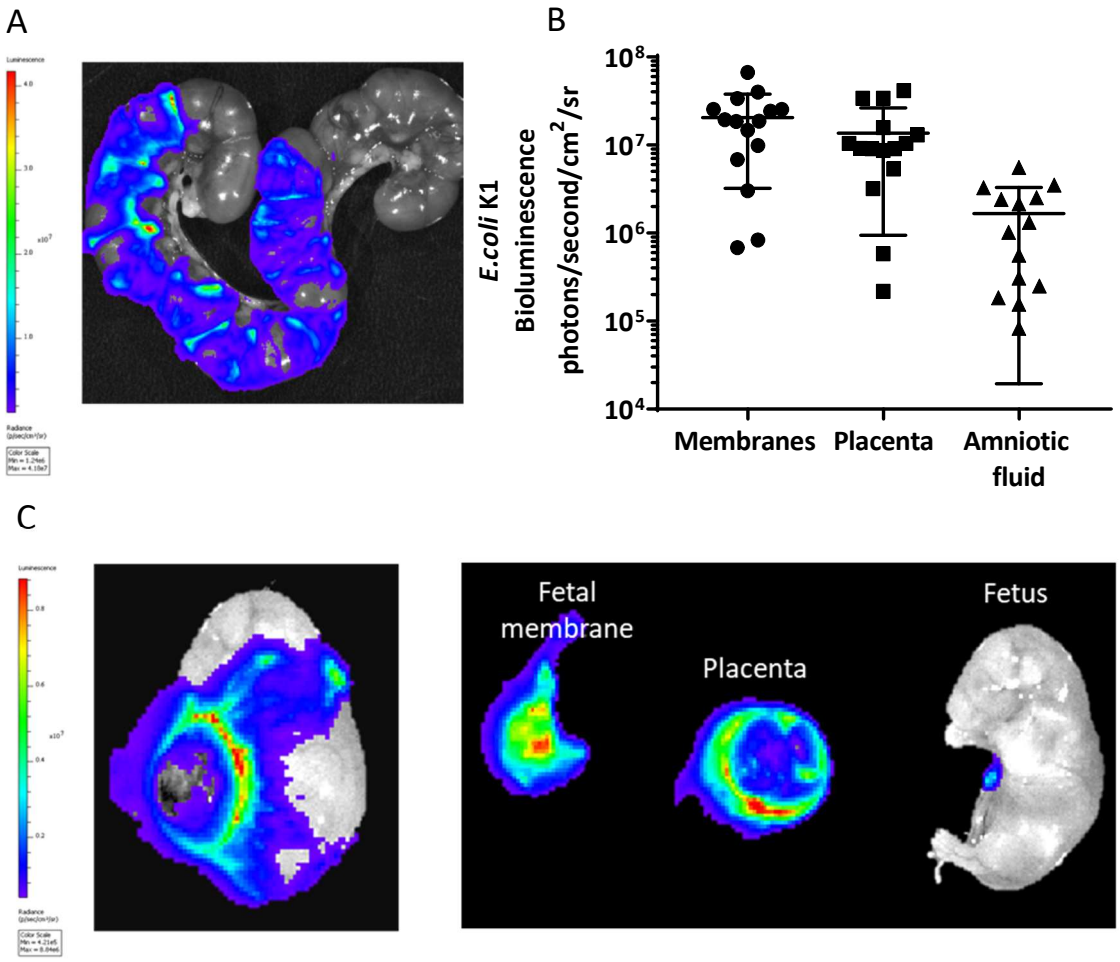

Figure 3.15 : *E.coli* K1 was detected in the placenta, fetal membranes and amniotic fluid 18 hours after bacterial administration. (A) Representative ex-vivo image of the uterus 18 hours after intravaginal *E.coli* K1 administration. **(B)** *Ex vivo* bacterial bioluminescent signal from the fetal membranes, placenta and amniotic fluid 18 hours after intravaginal *E.coli* K1. The placenta and fetal membranes are highly bioluminescent, whilst the amniotic fluid is less bioluminescent. n=15 from >3 dams. **(C)** Representative image of a fetus within its sac and separated into membrane, placenta and fetus 18 hours after infection. Bacteria is detected in the placenta, membranes, umbilical cord and within the amniotic fluid.

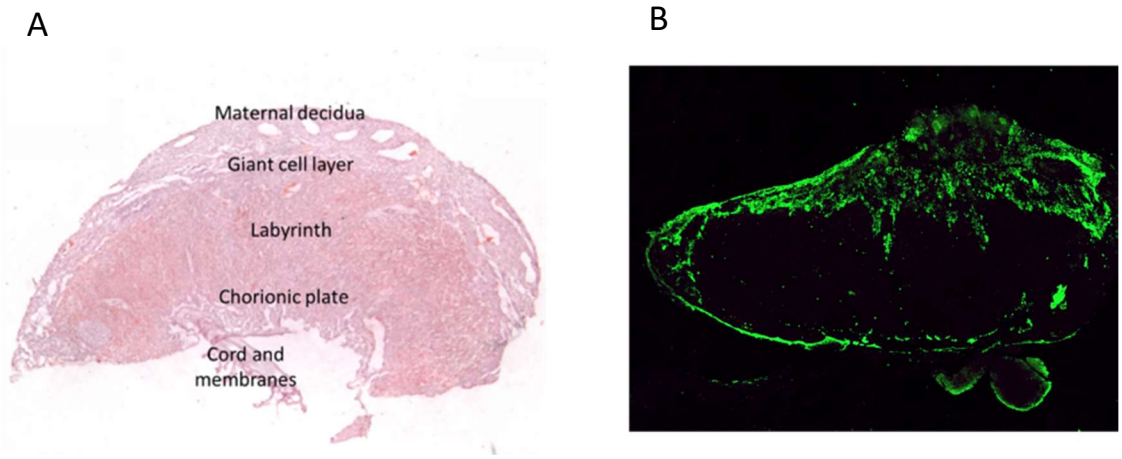

Figure 3.16: *E.coli* is detected on both side of the placenta following *E.coli* K1 administration. Representative image of *E.coli* immunofluorescence of an *E.coli* K1 infected placenta. **(A)** H&E stained placenta showing the different placental regions. **(B)** Anti-*E.coli* antibody immunofluorescence staining of an E.coli K1 infected placenta.

3.12. Bacteria is detected in the fetus by 24 hours after administration

Dams were sacrificed 24 hours after intravaginal administration of *E.coli* K1, the fetuses were imaged. Bacteria was detected within the fetus by this time point (Figure 3.17). Bacteria appears to be present in the umbilical cord, gastrointestinal tract and respiratory tract.

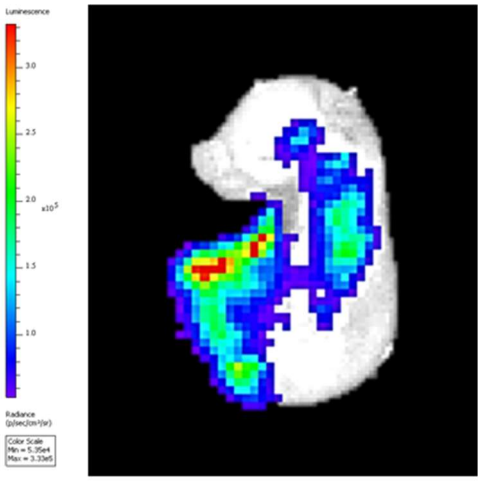

Figure 3.17: Bacteria is detected in the fetus 24 hours after intravaginal administration of *E.coli K1.* Representative image of a fetus 24 hours after maternal intravaginal *E.coli* K1.

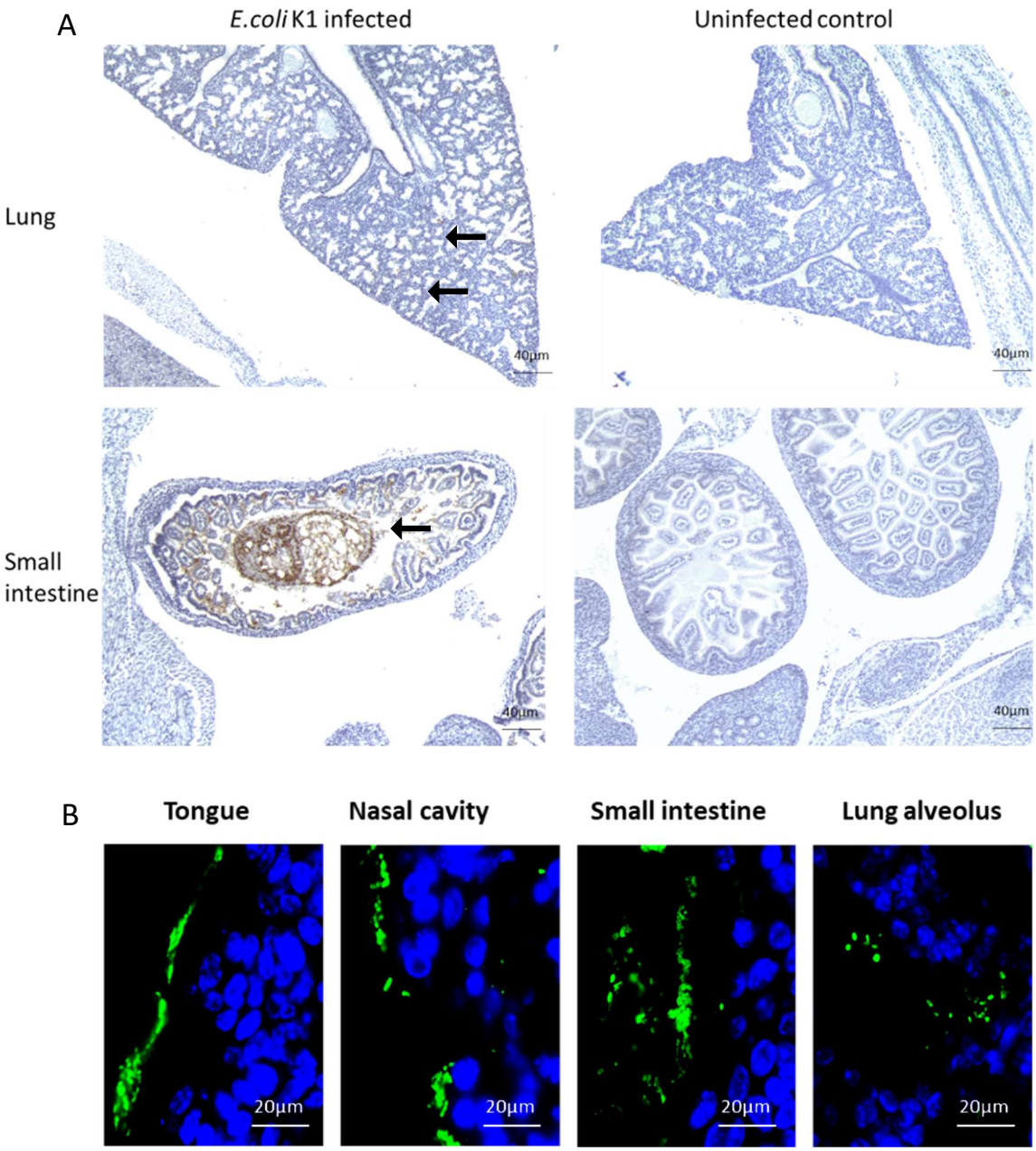

Figure 3.18: *E.coli* is present in the respiratory and gastrointestinal tract of the infected fetus 24 hours after intravaginal administration of *E.coli* K1 to the pregnant dam. (A) Representative images of anti-*E.coli* immunohistochemistry of the lung and small intestine of *E.coli* K1 infected fetuses and uninfected controls (10x magnification). Brown discoloration/arrows depicts DAB positive cells. **(B)** Representative images of anti-*E.coli* immunofluorescence staining in fetuses 24 hours after maternal intravaginal administration (x40 magnification).

Bacteria is seen in the small intestine and lungs on whole fetus anti-*E.coli* immunohistochemistry (Figure 3.18A). Bacteria is specifically seen throughout the gastrointestinal and respiratory tracts using immunofluorescence staining (Figure 3.18B).

3.13. Intravaginal administration of *E.coli* K1 and *E.coli* K12 leads to an upregulation of inflammatory cytokine mRNA expression in the uteroplacental tissues

mRNA expression of inflammatory cytokines of the uteroplacental tissues (uterine myometrium, fetal membranes and placenta) were determined in the pregnant mice 18 hours following intravaginal administration of *E.coli* K1, E.coli K12 or PBS (Figure 3.19).

There was significant upregulation of *Il1b*, *Cxcl2* and *Cxcr2* expression in the *E.coli* K1 uteri compared with uninfected PBS controls (*P<0.0001*, *P<0.0001* and *P=0.0003* respectively). There was also upregulation of *Il1b* and *Cxcl2* in the *E.coli* K12 uteri compared with uninfected PBS controls (*P=0.0007 and P=0.004*) (Figure 3.19A).

There was upregulation of *Il1b* and *Cxcl2* expression in *E.coli* K1 fetal membranes compared with uninfected PBS controls (*P<0.0001* and *P=0.014*, respectively). There were no significant differences in inflammatory cytokine mRNA expression between the *E.coli* K12 fetal membranes and the uninfected PBS controls (Figure 3.19B).

In the placenta, there was upregulation of *Il1b*, *Il6* and *Cxcl1* expression in the *E.coli* K1 placentas compared with uninfected PBS controls (*P<0.0001, P=0.02* and *P=0.0006* respectively). There was an upregulation of *Tnfa*, *Il6* and *Cxcl1* expression in the *E.coli* K12 placentas compared with uninfected PBS controls (*P=0.03*, *P=0.02* and *P=0.0079* respectively (Figure 3.19C).

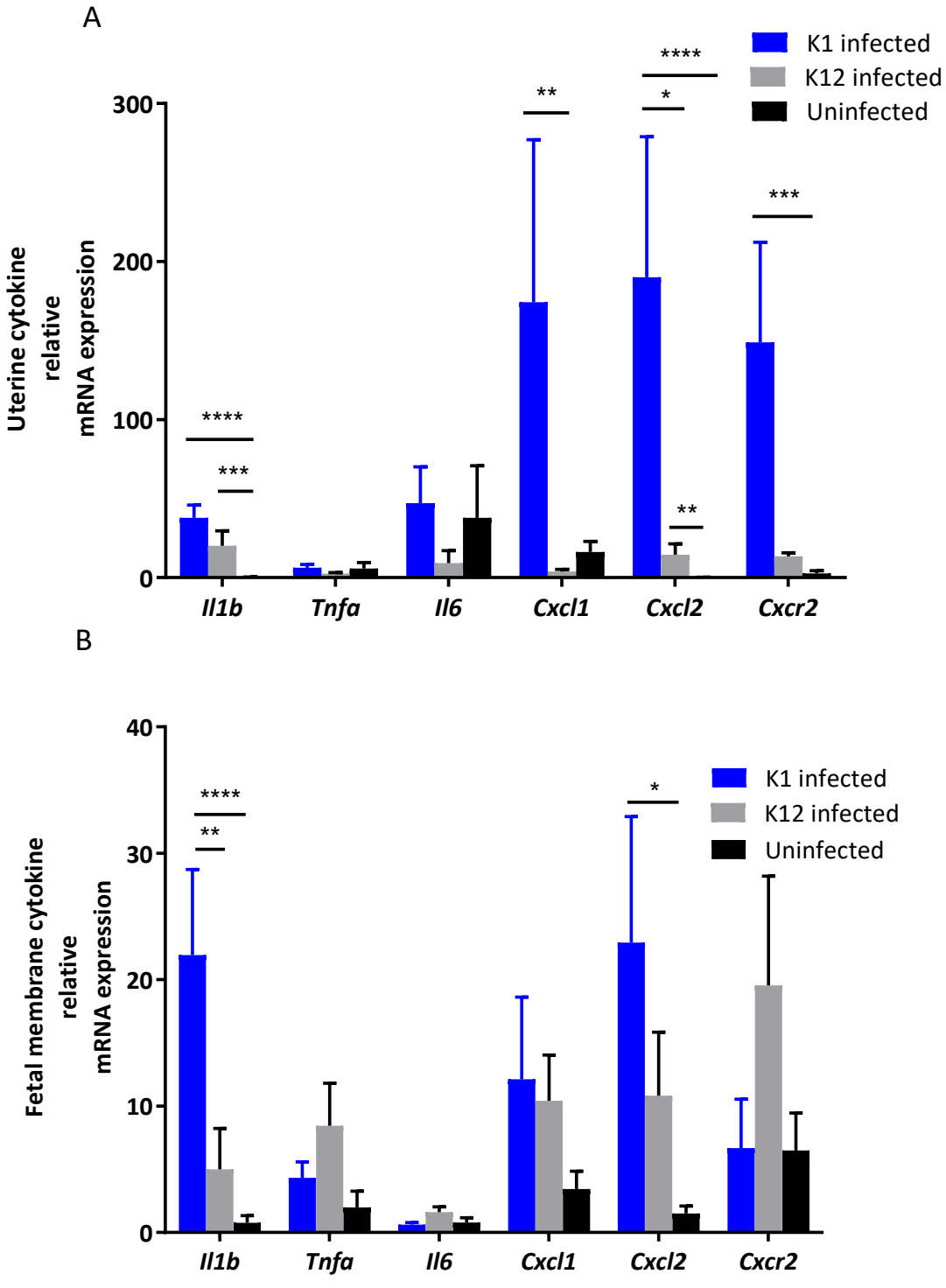
A
K1 infected
K12 infected
Uninfected
Uterine cytokine relative mRNA expression
300
200
100
0
****
***
**
*
****
**
***
Il1b
Tnfa
Il6
Cxcl1
Cxcl2
Cxcr2
B
Fetal membrane cytokine relative mRNA expression
40
30
20
10
0
****
**
*
Il1b
Tnfa
Il6
Cxcl1
Cxcl2
Cxcr2

C

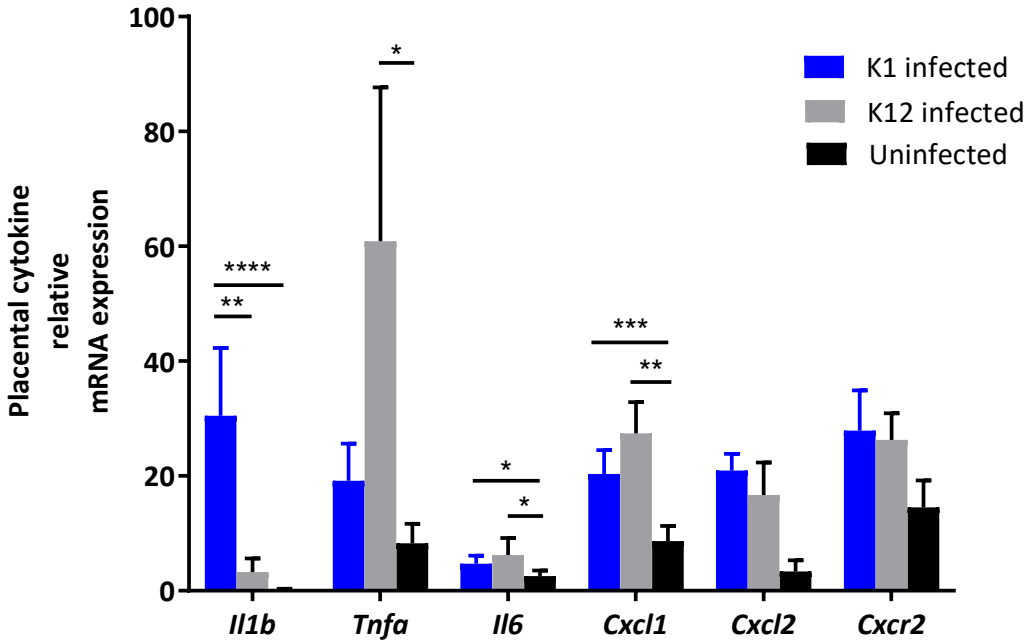

Figure 3.19: Uterine, fetal membrane and placental inflammatory cytokines are upregulated after intravaginal administration of *E.coli* K1 and *E.coli* K12. (A) Uterine inflammatory cytokine relative mRNA expression**.** n=3. **(B)** Fetal membrane inflammatory cytokine relative mRNA expression. n=8, *E.coli* K1 group; n=6, *E.coli* K12 and PBS uninfected group. **(C)** Placental inflammatory cytokine relative mRNA expression. n=8, *E.coli* K1 group; n=6, *E.coli* K12 and PBS uninfected group (from > 3 dams). Data are shown as relative mRNA expression to GAPDH ($2^{-\Delta CT}$), data not normally distributed therefore log transformed prior to analysis with a two-way ANOVA and post-hoc Bonferroni test, *$P<0.05$, **$P<0.005$, *** $P<0.001$, ****$P<0.0001$.

To interrogate the mechanisms behind preterm parturition following intravaginal *E.coli* K1, I determined the fold change differences of inflammatory cytokine expression between this group and the *E.coli* K12 group (which does not lead to premature delivery) (Figure 3.20). *Cxcl1* and *Cxcl2* expression was significantly increased in *E.coli* K1 uteri compared with *E.coli* K12 uteri (*Cxcl1* 32.8 fold, *P=0.0024* and *Cxcl2* 16.3 fold, *P=0.0174*). There was an increase in CXCR-2 expression but this is not significant (*Cxcr2* 9.6 fold, *P=0.06*). Looking at the fetal membranes and placental tissues, there was a significant increase in *Il1b* (fetal membranes 16.5 fold, *P=0.0011* and placenta 13.9 fold, *P=0.0013*).

	Uterine tissues	**Fetal membranes**	**Placental tissues**
Il1b	2.2	16.5**	13.9**
Tnfa	2.3	-2.2	-2.6
Il6	3.6	-2.5	2
Cxcl1	32.8**	-1.9	-1.39
Cxcl2	16.4*	2.4	1.26
Cxcr2	9.6	-5.6	1.11

Figure 3.20: Fold change in inflammatory cytokine mRNA expression of *E.coli* K1 tissues compared with *E.coli* K12 tissues. Data shown as fold change in mRNA expression ($2^{-\Delta\Delta CT}$), analysis performed on $2^{-\Delta CT}$ data as described above, **P<0.05*. ***P<0.0005*.

3.14. Increased neutrophil influx into the uterus 18 hours after intravaginal *E.coli* K1

Neutrophils were localised within the uterine decidua 18 hours after administration of *E.coli* K1, *E.coli* K12 or PBS (Figure 3.21). There appeared to be increased numbers of neutrophils in the *E.coli* K1 infected uteri, although neutrophil counts were not quantified.

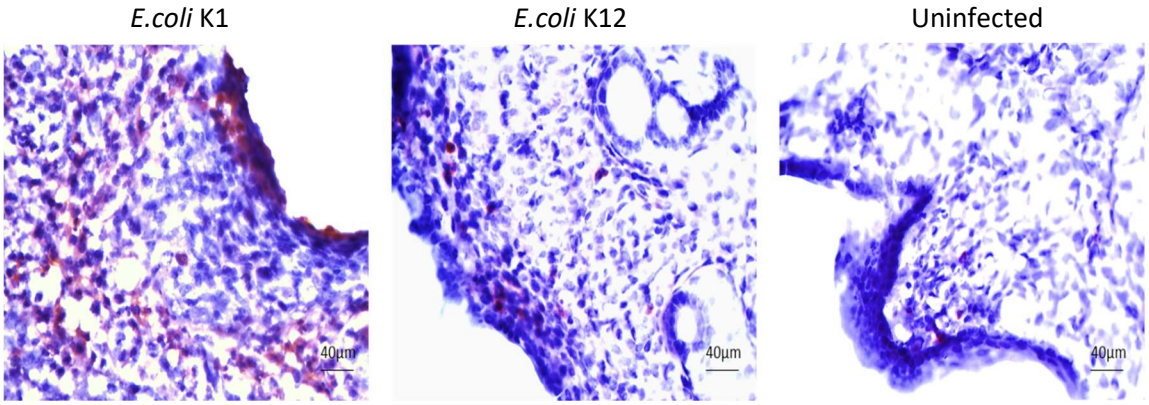

Figure 3.21: There is increased neutrophil influx into the uterus 18 hours after intravaginal *E.coli* K1. Representative images of neutrophil localization in the uterine decidua 18 hours after intravaginal administration of *E.coli* K1, *E.coli* K12 or PBS uninfected controls (x10 magnification). Anti-ly6G immunohistochemistry with haematoxylin counterstain, brown coloration depicts DAB positive cells.

3.15. Discussion

This chapter describes the development of an ascending vaginal infection and preterm birth model in the pregnant mouse.

An ascending infection model of preterm birth

Preterm birth mouse models are invaluable in understanding the mechanisms behind inflammation, bacterial infection and preterm birth and in investigating novel therapeutic approaches for the prevention of preterm birth. Successful preterm birth mouse models using local delivery of bacteria, bacterial products or inflammatory mediators have been developed (Table 3.1). These models have provided insight into the pathogenesis of preterm birth, for example, by discovering the important role of activator terminator-1 protein in mediating infection-related preterm birth (MacIntyre et al. 2014). These models have also recapitulated the process of ascending vaginal infection (Akgul et al. 2014; Racicot et al. 2013; Vornhagen et al. 2016). The models developed here complement the existing models and add to knowledge in the field. This model is less invasive than laparotomy models and also allows for cervical targeted therapies to be studied. The use of bioluminescent pathogens confers several advantages to this model; the ability to track pathogens longitudinally within the same cohort of mice, the ability to improve our understanding of how pathogens infiltrate the uterine cavity and the ability to use bioluminescence imaging to test response to novel therapies by tracking bacterial colonization and ascent. This model also supports two of the 3Rs of animal research, reduction and refinement; reducing the number of animals needed and the minimally-invasive nature of the model helps to improve animal welfare (nc3Rs 2014).

The mouse strain, C57BL/6N-Tyr$^{c\text{-}Brd}$, is best for modelling ascending vaginal infection using bioluminescent E.coli

The C57BL/6N-Tyr$^{c\text{-}Brd}$ (albino form of BL6) mouse strain was found to be the most efficient and reproducible strain for modelling ascending infection determined by *in vivo* bioluminescence (Figure 3.4). The C57BL/6 strain is often used in mice models of infection, including other models of ascending vaginal infection in the literature, because it has been found to have increased susceptibility to bacterial infection (Backstrom et al. 1992; Campbell et al. 2014) (Table 3.1). It is thought that the strain possesses a mild immunosuppressed phenotype as a result of a deficiency of cathepsin E, which has a role in antigen processing in immune cells and in the regulation of toll-like receptor expression (Tulone et al. 2007; Tsukuba et al. 2006).

Cervical viral infection is not required for bacteria to ascend into the uterine cavity

Other studies show that the pregnant murine cervix requires priming with viral infection to allow for bacterial ascent of *U.urealyticum* into the uterine cavity (Racicot et al. 2013). Interestingly, they found that this was not the case in the non-pregnant cervix, which allowed free movement of *E.coli* into the uterine horns without viral priming. They showed that cervical viral infection during pregnancy decreased the amount of TLRs, cytokines and antimicrobial peptides in the cervix and essentially reduces the antimicrobial capacity of the mucus plug allowing bacteria to breach the cervical barrier. Here we show that viral priming is not required for ascending vaginal infection with *E.coli* in pregnant mice (of note, mice were tested for murine parvovirus and found to be negative). This is consistent with data reporting the use of intravaginal *E.coli* 0:55 in pregnant mice to induce preterm birth (Akgul, et al. 2014). In the model described here, I applied quinine powder topically to the vagina after bacterial administration to prevent mice from cleaning the administered bacteria (as quinine is an aversive tastant to mice (Boughter et al. 2005). Interestingly, quinolone antimalarials (the group of drugs in which quinine is part of) have been shown to inhibit toll-like receptor 3 (TLR-

3) and toll-like receptor 9 (TLR-9) signalling (Kužnik et al. 2011; Cui et al. 2013). TLR-9 recognises CpG dinucleotides, common in bacterial and some viral nucleic acids and has a role in activating antigen-presenting dendritic cells thus, linking the innate and acquired immune responses (Wagner 2002). Whilst TLR-3 recognises dsRNA, a common product of viral replication, and so has an important role in host defence against viruses (Sen & Sarkar 2005). TLR-3 and TLR-9 have been found to be expressed in cervical mucosal epithelial cells and have a role in regulating proinflammatory cytokines and antiviral immune responses in the lower reproductive tract (Andersen et al. 2006). Racicot *et al.*, showed decreased expression of TLRs in the cervix, including TLR-3 and TLR-9, following systemic murine herpes infection and this contributed to the reduced antimicrobial capacity of the cervix allowing ascending bacterial infection to occur (Racicot et al. 2013). Therefore, it is possible that the use of quinine in this model is acting in a similar way. However, in contrast to Racicot *et al.*, in this study there appears to be much less variation in bacterial colonization and ascent in pregnant mice compared with non-pregnant mice, although a direct comparison was not performed. I speculate that the mechanism is likely to be more simple, such as vaginal anatomical variation between pregnant and non-pregnant mice, as I found bacterial application into the posterior fornix of a pregnant mouse vagina much easier.

Non-pathogenic E.coli K12 versus pathogenic E.coli K1 ascending infection

Intravaginal administration of *E.coli* K12 does not induce premature parturition (Figure 3.11). The bioluminescent *E.coli* K12 used in this study is the common molecular biology strain MG1655. It is integrated with the luxABCDE operon from the plasmid p16S*lux; a* single copy of the lux operon is present in the 16s rDNA site in the chromosome of the *E.coli* (Cronin et al. 2012). This site-specific integration means that there is no interference in the behaviour of the bacteria. The mature LPS of this *E.coli* K12 strain is known to lack the O antigen as a result of mutations within the *rfb* locus. The lack of the O antigen on its LPS renders this strain non-

pathogenic by making it less resistant to hostile environments and less likely to colonize hosts and cause disease (Browning et al. 2013). Therefore, it is not surprising that it does not induce the inflammatory response necessary to induce premature delivery in pregnant mice. In support of this, there is evidence that different virulent *E.coli* LPS serotypes used to induce preterm birth in pregnant mice elicit differing TLR-4 mediated inflammatory responses which result in varying premature delivery timings (Migale et al. 2015).

In this model, *E.coli* K12 is only detected on placental tissue *in vivo* (Figure 3.12). This is interesting as this bioluminescent strain was originally developed for tumour research using the bacteria's ability to naturally home to tumours following systemic administration (Cronin et al. 2016; Cronin et al. 2012; Murphy et al. 2017). It is thought that the tumour-specific nature of bacterial growth is due to tumours having regions of hypoxia, increased vascularity, local immune suppression and growth factor, such as VEGF, availability. Placentas share many of the same properties as tumours so it is unsurprising that *E.coli* K12 are attracted to this organ *in vivo*. The bacteria do not appear to invade the placental tissue and are seen as clusters on the outer edges of maternal decidual side and fetal side of the placenta. This is consistent with the non-invasive nature of this strain and is also seen in tumours where the injected bacteria grow in the stromal region of the tumour external to the tumour cells (Cronin et al. 2012).

The K1 strain of *E.coli* is the leading cause of neonatal sepsis and meningitis (Bonacorsi & Bingen 2005). This study uses the *E.coli* 018:K1 A192PP strain with the luxCDABE transposon integrated by mini-Tn5 mutagenesis (Witcomb et al. 2015). Intravaginal administration of this bacteria leads to premature delivery in approximately 50% of pregnant mice within 48 hours (Figure 3.14). This is consistent with data produced from other PTB models using intravaginal live bacteria administration; E.coli 055:B5 - 50% of dams deliver within 48 hours (Akgul, et al. 2014), GBS – 25-50% of dams deliver within 72 hours (Vornhagen et al. 2016; Randis et al. 2014).

The movement of bacteria into the uterine cavity following vaginal ascent

There is conflicting evidence as to where vaginal pathogens ascend to once they have breached the cervical barrier; some believe bacteria invade the chorioamniotic and choriodecidual spaces prior to entering the amniotic cavity, whilst others believe that bacteria traverse the fetal membranes through a restricted supracervical region and directly enter the amniotic cavity first (Grigsby et al. 2010; Goldenberg et al. 2000). Clinical data supporting direct amniotic cavity invasion has shown that 16S rRNA gene copy number in the amnion was significantly greater than in the chorion (Kim et al. 2009). In addition to this, in some women with chorioamnionitis there was bacteria identified in the amniotic cavity but not in the chorioamniotic membranes. However, more recent evidence has shown that in a quarter of women with preterm chorioamnionitis there was no evidence of intra-amniotic bacterial invasion or inflammation (Oh et al. 2017). The use of bioluminescent *E.coli* in these models enabled me to longitudinally track the bacterial movement over time. *E.coli* K1 was initially seen within the cervical canal by approximately 6 hours after intravaginal infection, followed by subsequent detection within the placenta and fetal membranes by 18 hours. Bacteria was also present in the amniotic fluid at this time but this has significantly less bioluminescent signal than in the placenta or membranes (Figure 3.15). Therefore, this indicates that the bacteria are likely to reach the choriodecidual space first where they replicate and then spread to the placenta and membranes eventually traversing the fetal membranes to colonize the amniotic cavity. This is further supported by the fact that bacteria are subsequently detected within the fetal respiratory and gastrointestinal tract 24 hours after vaginal administration by ingestion and inhalation from the amniotic fluid. It has been shown that this bacteria takes up to 3 hours to colonize the gastrointestinal tract in neonatal rats which is consistent with the

movement of bacteria into the amniotic cavity occurring after choriodecidual invasion (Witcomb et al. 2015) (Figure 3.17).

Pro-inflammatory cytokine gene upregulation in uteroplacental tissues

Intravaginal *E.coli* K1 leads to an upregulation of a number of inflammatory genes in the uteroplacental tissues that are commonly associated with preterm parturition (Goldenberg et al. 2000; Rinaldi et al. 2015; Edey et al. 2016; Migale et al. 2015) (Figure 3.19). *Il1b* appears to be an important mediator of preterm labour in all of the uteroplacental tissues infected by *E.coli* K1. This is supported by studies in which IL-1β has been used to induce premature delivery in mice, followed by subsequent inhibition of its receptor to prevent premature labour (Sadowsky et al. 2006; Nadeau-vallée et al. 2017). Furthermore, Il-1β has been shown to increase prostaglandin F2-α receptor mRNA expression, a gene involved in uterine contractility during labour, in myometrial cells (Zaragoza et al. 2006).

Interestingly, the expression of the chemokines *Cxcl1*, *Cxcl2* and the chemokine receptor *Cxcr2* are increased in the preterm *E.coli* K1 group compared with the non-preterm *E.coli* K12 group (Figure 3.20). This is consistent with data from preterm birth models where LPS is administered intrauterine (Rinaldi et al. 2014; Diamond et al. 2007; Pirianov et al. 2009). The expression of these chemokines CXCL-1 and CXCL-2, as well as CXCL-5 and CXCL-8 have been shown to be upregulated in the human myometrium during labour (Bollopragada et al. 2009; Hamilton et al. 2013). The CXC chemokines, via their interaction with the neutrophil expressed CXCR-1 and CXCR-2 receptors, mediate the extravasation of neutrophils into the myometrium. This data is supported by the large neutrophil influx seen in the decidua of *E.coli* K1 dams 24 hours after administration of intravaginal bacteria (Figure 3.17). Neutrophil influx into gestational tissue has been associated with term and preterm labour (Osman et al. 2003; Shynlova et al. 2013). This is supported by a study in which administration of a broad-spectrum chemokine inhibitor delayed LPS-induced preterm labour by reducing neutrophil influx and LPS-induced

upregulation of IL-1β, IL-6, IL-12, CXCL-1 and CXCL-2 (Shynlova et al. 2014). Recent data, however, has shown that depletion of neutrophils in preterm birth mouse models has no effect on premature parturition (Rinaldi et al. 2014; Filipovich et al. 2015). Interestingly, it was found that neutrophil-depleted mice delivered earlier than controls following intrauterine LPS, suggesting that neutrophil influx may be involved in ameliorating the inflammatory response and thus have a positive effect on inflammation-associated preterm birth. Of note, these studies used LPS or killed *E.coli* as the infectious agent and so the inflammatory response leading to premature parturition associated with live *E.coli*, as in this model, may be different. Furthermore, in this study uteroplacental tissue sampling was performed at 18 hours after *E.coli* injection, consistent with previous intrauterine LPS studies, but this model takes longer to cause premature delivery (approximately 12-24 hours). This may explain why other pro-inflammatory cytokines known to be upregulated in LPS-induced PTB, such as IL-6 and TNF-α, are not found to be upregulated in this study.

Cervical inflammation and remodelling in this model

An interesting model of preterm birth which utilises intravaginal administration LPS has been developed (Gonzalez. et al. 2014; Gonzalez et al. 2011). It appears to rely on inflammatory changes at the cervical level which lead to subsequent cervical remodelling as a mechanism for premature delivery. Complement activation and macrophage infiltration was found to have a role in cervical remodelling (Gonzalez et al. 2011). Although the cervix was not specifically assessed in this study, (data in Results Chapter 6; Figure 6.8 shows no evidence of cervical neutrophil or macrophage infiltration in *E.coli* K12 mice) it may be interesting to determine the effects of *E.coli* K1 ascending vaginal infection on cervical remodelling in further studies.

Conclusion

In conclusion I show that bioluminescent *E.coli* can be used to model ascending vaginal infection and preterm birth in pregnant mice. These models provide interesting insights into

the mechanisms behind preterm parturition as well as providing a novel means of testing cervical or vaginal-targeted therapies.

Table 3.1: Mouse models of infection and inflammation associated preterm birth. Models with systemic routes of infectious agent administration are not included. Embryonic day has been modified for comparison (E0.5 describes the day the vaginal plug is observed).

Route of administration	Advantages	Infectious or Inflammatory agent	Amount	Mouse strain	Technique	Embryonic day on administration	Comments	References
Intrauterine	• Reliably causes premature delivery • Useful for testing systemic or uterine treatment • Useful for assessing mechanisms of labour and preterm labour	LPS (*E.coli* O111:B4)	20µg	CD-1	Laparotomy; injection on the right horn between the upper 2 gestational sacs	E16.5		(Pirianov et al. 2009; MacIntyre et al. 2014; Edey et al. 2016; Rinaldi et al. 2014)
		LPS (*E.coli* O55:B5)	250µg	CD-1	Laparotomy; injection on the right horn between the lower 2 gestational sacs	E15.5		(Elovitz & Wang 2004; Elovitz & Mrinalini 2005)
		IL-1β	1µg	CD-1	Laparotomy; injection in the right horn between the lower 2 gestational sacs	E16.5		(Nadeau-vallée et al. 2017; Nadeau-Vallée et al. 2015)
		E.coli (O55:B5)	10^9 killed *E.coli*	C57BL/6, B6129F2	Laparotomy; injection in the midsection of the right uterine horn between 2 gestational sacs	E14.5		(Filipovich et al. 2016; Filipovich et al. 2015)

Route of administration	Advantages	Infectious or Inflammatory agent	Amount	Mouse strain	Technique	Embryonic day on administration	Comments	References
		LPS (*E.coli* O111:B4)	20µg	C57Bl/6	Direct injection into intra- uterine space between 2 gestational sacs under ultrasound guidance	E16.5	• Ultrasound guided – less invasive • As reliable in causing PTB as laparotomy model	(Rinaldi et al. 2015)
		LPS (*E.coli* O111:B4, O55:B5, O127:B8, and O128:B12)	20µg	CD-1	Laparotomy; injection on the right horn between the upper 2 gestational sacs	E16.5	• Disparity in inflammatory response amongst LPS serotypes shown	(Migale et al. 2015)
Intracervical	• Mimics microbial breaching of the cervical barrier	LPS or *E.coli*		CD-1, HS, C57BL/6	Direct endoscopic intracervical inoculation	E13.5		(Reznikov et al. 1999)
Intravaginal	• Mimics what is thought to occur in human preterm birth • Less reliable inducer of PTB (Rinaldi et al. 2015) • Enables vaginal or cervical-targeted treatment to be assessed	*U.urealyticum*	10^4 CFU	C57BL/6	Intravaginal administration	E15.5	• Prior cervical infection with MHV68 required to enable ascending infection • Gestation at delivery not assessed – may not be a preterm birth model	(Racicot et al. 2013)

Route of administration	Advantages	Infectious or Inflammatory agent	Amount	Mouse strain	Technique	Embryonic day on administration	Comments	References
		E.coli (O55:B5)	10^4 CFU	C57BL6/129Sv	Intravaginal administration	E16.5		(Akgul et al. 2014)
		Group B streptococcus	10^8 CFU	C57BL/6	Intravaginal administration, followed by inversion of mice for 5 minutes	E15.5		(Vornhagen et al. 2016)
		LPS (*E.coli* O55:B5)	250µg	C57BL/6	Intravaginal administration	E15.5	• Pathogenesis is cervical remodelling not ascending infection	(Gonzalez et al. 2011; Pedroni et al. 2014; Gonzalez, et al. 2014)
		Group B streptococcus	10^6 CFU	C57BL/6	Intravaginal administration mixed with 10% gelatin	E13.5	• All dams culled on E17.5 • PTB outcome: delivery prior to E17.5	(Randis et al. 2014)

Chapter 4 Neonatal effects following maternal ascending vaginal infection

4.1. Summary

Preterm birth is associated with serious morbidity in the premature infants. These include neurological impairment such as cerebral palsy, learning difficulties, respiratory disease and gastrointestinal complications (Goldenberg et al. 2008; Back 2017). These infants are also at increased risk of chronic disease later in life such as obesity, diabetes and schizophrenia (Meyer et al. 2011; Rubens et al. 2014).

As discussed earlier, preterm birth is associated with inflammation and infection in at least 40% of cases (Goldenberg et al. 2000). The presence of an inflammatory *in utero* environment can lead to fetal inflammatory response syndrome (FIRS) resulting in subsequent fetal injury. Bacteria or inflammatory mediators are thought to reach the fetus either indirectly through placental transmission or directly through the amniotic fluid (Adams Waldorf & McAdams 2013).

This chapter explores the outcomes of neonates born to dams following intravaginal administration of the non-pathogenic *E.coli* K12 and the pathogenic *E.coli* K1. I hypothesise that pups from *E.coli* K1 infected dams will show evidence of brain and intestinal inflammation, representing models of preterm brain injury and necrotising enterocolitis.

Interestingly I found evidence of brain inflammation and cell death in pups born from *E.coli* K1 infected dams as well as pups from *E.coli* K12 infected dams.

4.2. Half of all the pups born alive from dams infected with *E.coli* K1 survive the first week of birth

64% of pups are born alive from *E.coli* K1 infected dams (Figure 31D). Of these surviving pups, 48.6% survive to 7 days of life, compared with 100% of pups from *E.coli* K12 infected dams and uninfected dams (Figure 4.1A). There is no bacterial bioluminescent signal detected in pups from *E.coli* K12 infected dams (Figure 4.1B). The pups from *E.coli* K1, however, have evidence of *E.coli* K1 colonisation *in utero* within 24-48 hours after bacterial administration (Figure 3.17). After birth, bacterial bioluminescent signal from the *E.coli* K1 pups decreases over the first week of life (Figure 4.1C and Figure 4.1D). This is consistent with reduced bacterial colonisation and infection over time due to the death of infected pups. By 14 days of life, the pups that have survived have cleared any *E.coli* K1 colonisation or infection (observational data, not shown).

A

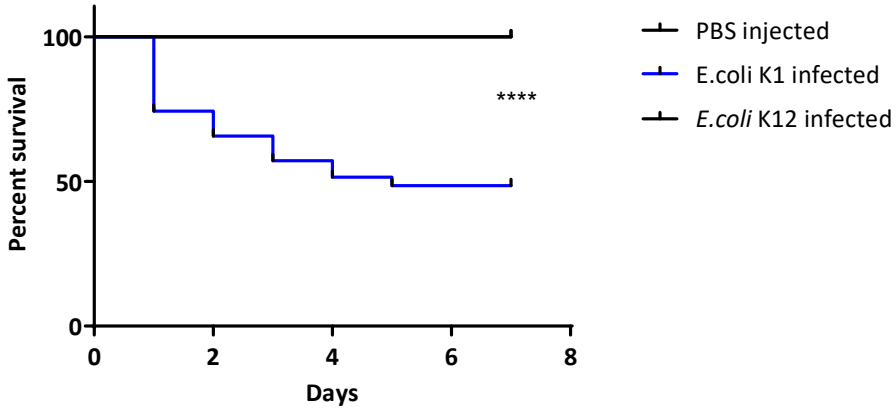
100
50
0
Percent survival
0
2
4
6
8
Days
****
PBS injected
E.coli K1 infected
E.coli K12 infected

B

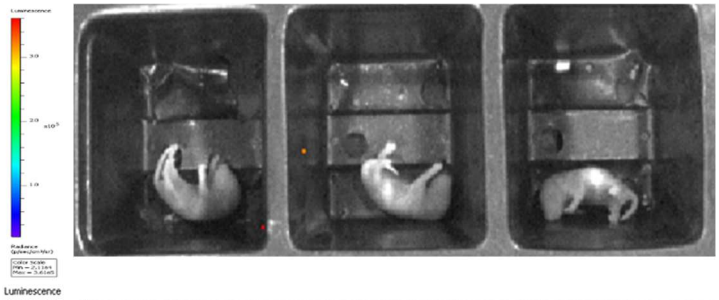
Luminescence

C

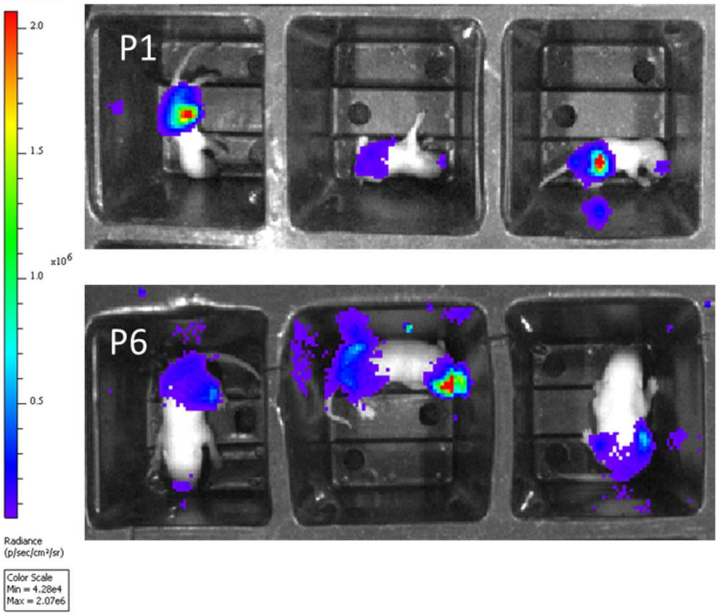
P1
P6
2.0
1.5
1.0
0.5
x10^6
Radiance (p/sec/cm²/sr)
Color Scale
Min = 4.28e4
Max = 2.07e6

D

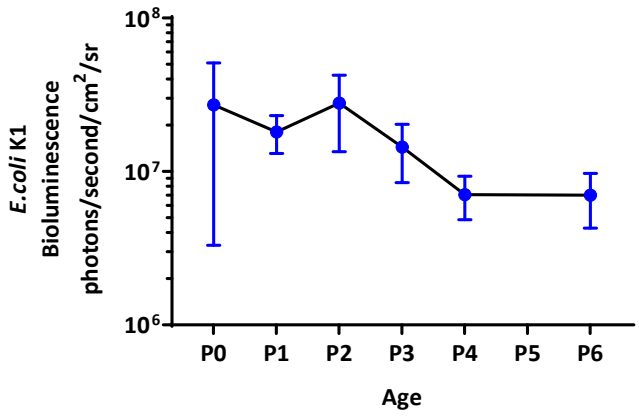
E.coli K1 Bioluminescence photons/second/cm²/sr
10^8
10^7
10^6
P0
P1
P2
P3
P4
P5
P6
Age

Figure 4.1: Half of all the pups born alive from dams infected with *E.coli* K1 survive the first week of birth. (A) Survival of neonates from *E.coli* K1 and *E.coli* K12 infected dams. Of the pups born alive, approximately 48.6% survived to postnatal day 6 compared with 100% of pups in the *E.coli* K12 group and the uninfected control group. n=25-35 pups from n=6 dams; log rank test *****P<0.0001*. **(B)** Representative images of *E.coli* K12 pups on the day of birth (P0). There is no bioluminescent *E.coli* K12 detected in pups born to *E.coli* K12 infected dams. **(C)** Representative images of bacterial bioluminescence in *E.coli* K1 postnatal day 1 pups (top row) and subsequently on postnatal day 6 (bottom row). **(D)** Bacterial colonization of neonates from *E.coli* K1 infected dams. Bacteria was detected in the pups at birth and bacterial bioluminescence levels reduced slowly over the first week. n=4-7 pups from 2 infected dams; pup numbers decrease over 7 days.

4.3. Pathogenic *E.coli* K1

4.3.1. Pro-inflammatory cytokines increase in the brain of neonates from *E.coli* K1 infected dams

Brains were harvested on the day of birth from *E.coli* K1 infected pups and uninfected controls for cytokine protein analysis. There was a significant increase in IL-1β, IL-6 and TNF-α in the brains of *E.coli* K1 infected pups compared with uninfected controls (*P=0.0004*, *P=0.03* and *P=0.04* respectively) (Figure 4.2).

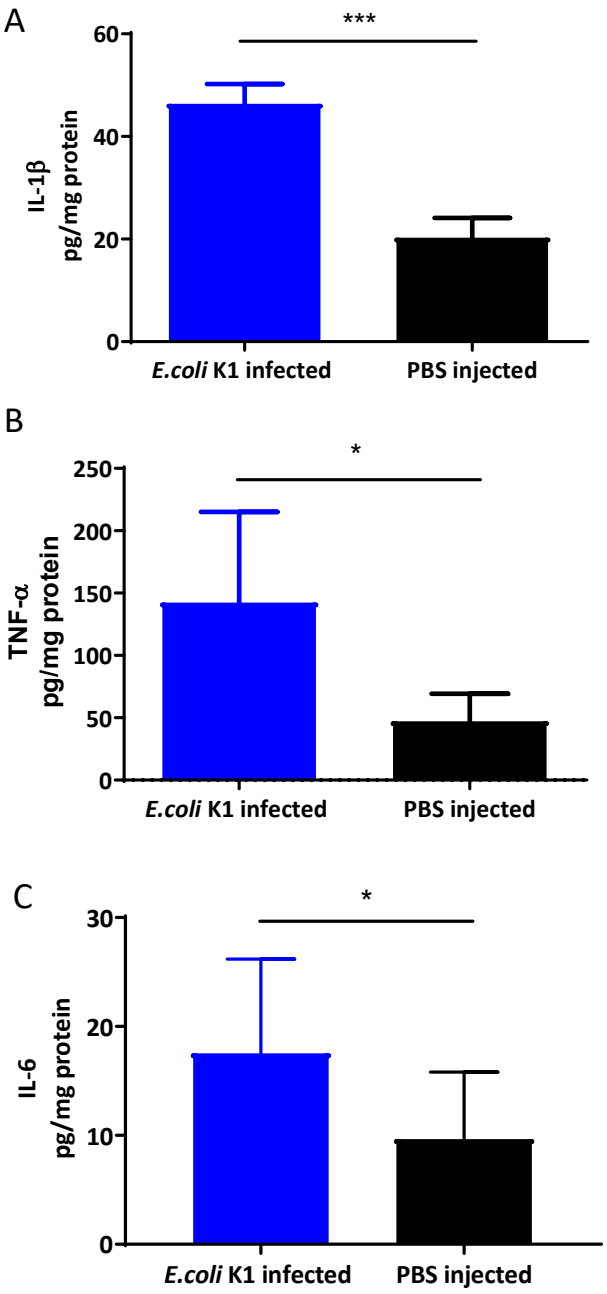

Figure 4.2: Inflammatory cytokines are increased in the brains of neonates born to *E.coli* K1 infected dams and uninfected dams. Brains were collected on the day of birth. Brain cytokine expression from neonates born to *E.coli* K1 infected dams and uninfected dams: **(A)** IL-1β. **(B)** TNF-α. **(C)** IL-6. n=5 in the *E.coli* K1 group, n=9 in the uninfected group, from >3 dams, unpaired t-test, data not normally distributed for TNF-α cytokine results therefore analysed with Mann Whitney rank test, **P<0.05, ***P<0.0005.*

4.3.2. There is evidence of brain inflammation in the brain of 7 day old pups from *E.coli* K1 infected dams

Brains were harvested from postnatal day 6 pups from *E.coli* K1 infected dams and uninfected controls for TUNEL assay and CD68 immunohistochemistry (to assess microglial activation). There was evidence of apoptosis in the cortex, thalamus and striatum of *E.coli* K1 infected pups (*P<0.0001*, *P=0.0043* and *P<0.0001* respectively) (Figure 4.3A). Furthermore, there was increased microglial activation in the cortex of *E.coli* K1 infected pups compared to controls (*P=0.0013*) (Figure 4.3B & Figure 4.3C).

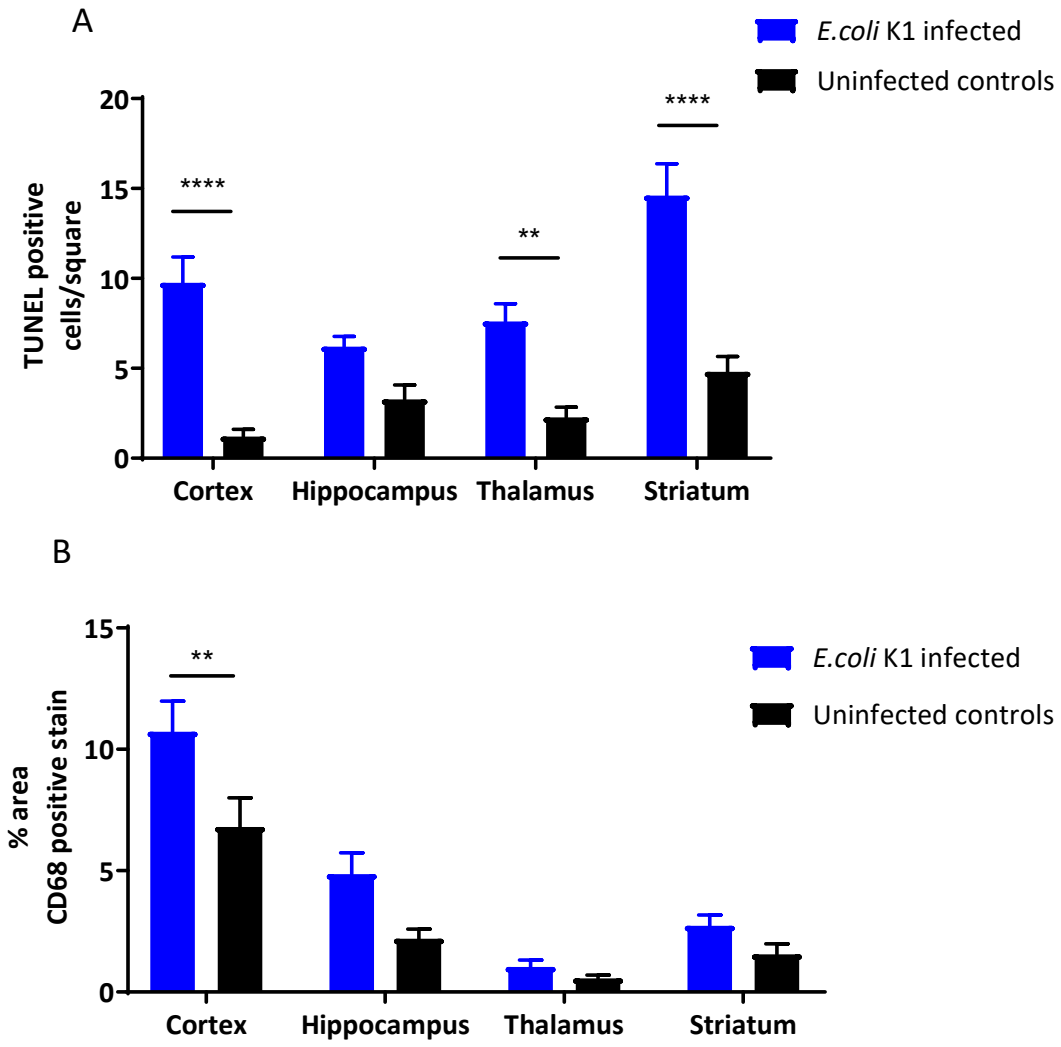

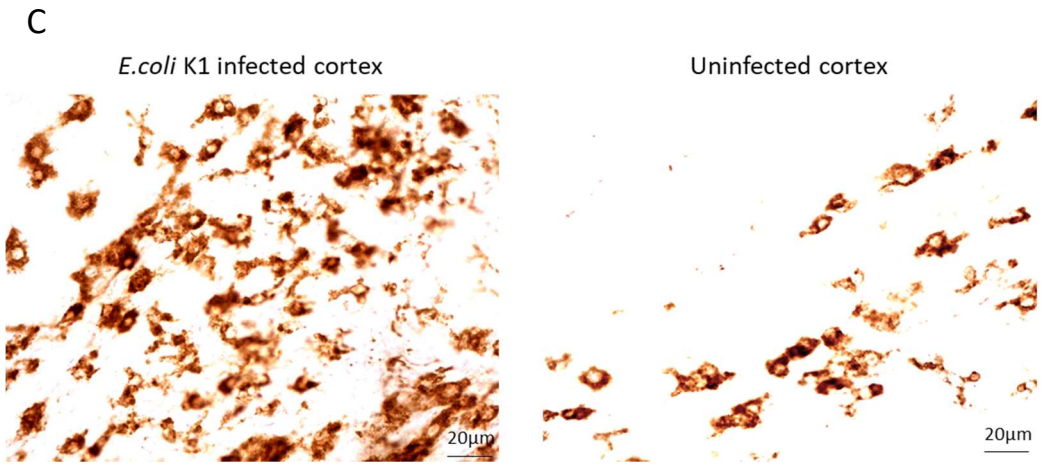

Figure 4.3: There is evidence of brain inflammation in pups born to *E.coli* K1 infected dams and uninfected dams. (A) Quantification of TUNEL positive cells in the cortex, thalamus and striatum in the neonates from *E.coli* K1 infected dams on postnatal day 6 compared with uninfected controls. n=3; two-way ANOVA (overall P value 0.01) with post hoc Bonferroni test, ***P<0.01*, *****P<0.0001*. **(B)** CD68 quantification in specific brain regions of pups born to *E.coli* K1 infected dams and uninfected dams. n=3 from 3 separate dams; two-way ANOVA (overall P value 0.07) with post hoc Bonferroni test, ***P=0.005*. **(C)** Representative images of CD68 immunohistochemistry from the cortex of *E.coli* K1 infected pups and uninfected controls.

4.3.3. There was no difference in intestinal villus height between *E.coli* K1 infected pups and controls

The small intestines were harvested from postnatal day 6 pups from *E.coli* K1 infected dams and uninfected controls to assess for villi shortening, associated with intestinal inflammation. There is no difference in villus height between the *E.coli* K1 and the uninfected group (*P=0.4*) (Figure 4.4).

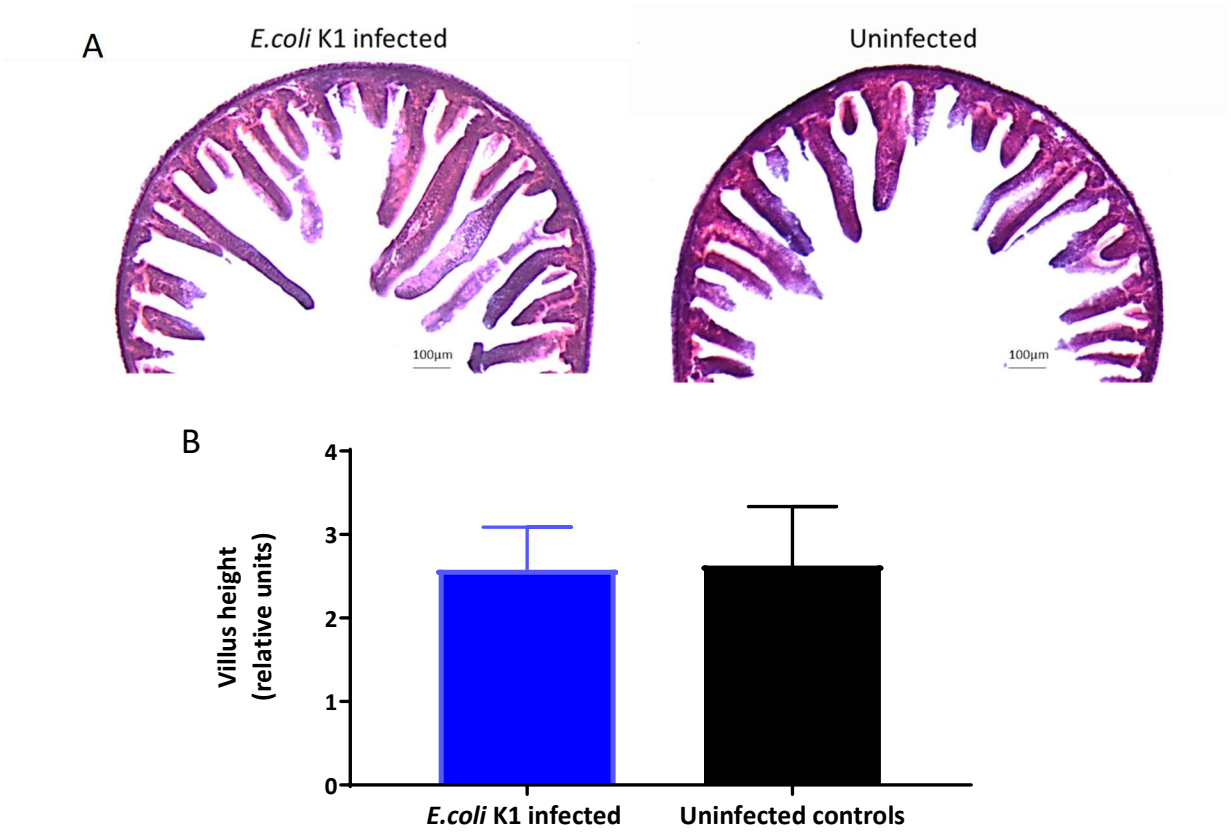

Figure 4.4: There is no difference in intestinal villus height between *E.coli* K1 infected and control pups. (A) Representative images of H&E stained small intestine (jejunum-ileum) on postnatal day 6 from *E.coli* K1 infected pups and uninfected pups (x5 magnification). **(B)** Villus height of *E.coli* K1 infected small intestine compared with uninfected controls. There is no difference in the villus height between the two groups. n=3-5; unpaired t-test.

4.4. Non-pathogenic *E.coli* K12

4.4.1. Inflammatory cytokines are not increased in the brains of neonates born to E.coli K12 infected dams and uninfected dams.

There was no difference in IL-1β and IL-6 in the brains of *E.coli* K12 infected pups compared with uninfected controls (*P=0.4* and *P=0.29* respectively), however there was a small increase in TNF-α levels (*P=0.04*) (Figure 4.5).

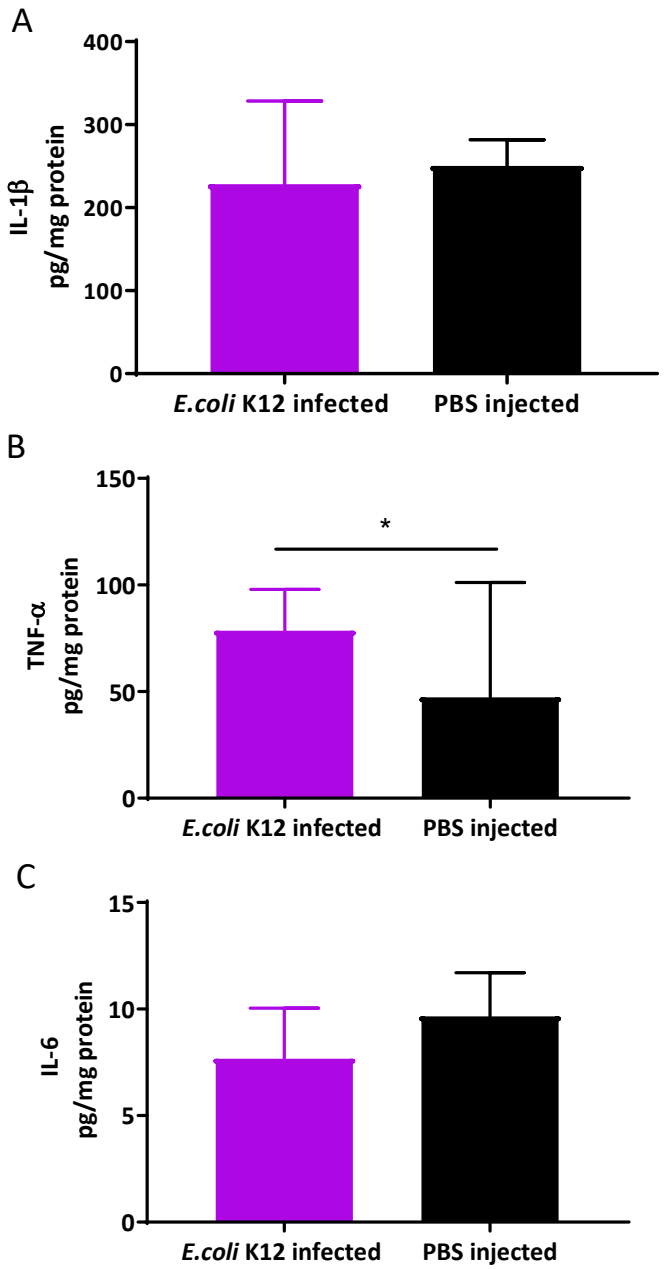

Figure 4.5: Inflammatory cytokines are not increased in the brains of neonates born to *E.coli* K12 infected dams and uninfected dams. Brains were collected on the day of birth. **(A)** Brain IL-1β protein expression of neonates born to E.coli K12 infected dams and uninfected dams. **(B)** Brain TNF-α protein expression of neonates born to E.coli K12 infected dams and uninfected dams. **(C)** Brain IL-6 protein expression of neonates born to E.coli K1 infected dams and uninfected dams. n=5 in the E.coli K1 group, n=9 in the uninfected group, from >3 dams, unpaired t-test, data not normally distributed for IL-1β and TNF-α cytokine results therefore analysed with Mann Whitney rank test, *$P<0.05$*.

4.4.2. There was evidence of brain inflammation in 7 day old pups from *E.coli* K12 infected dams

Brains were harvested from postnatal day 6 pups from *E.coli* K12 infected dams and uninfected controls for TUNEL assay and CD68 immunohistochemistry. There is evidence of apoptosis in the cortex, thalamus and striatum of *E.coli* K12 infected pups compared with uninfected controls (*P<0.0001* and *P<0.0001* respectively) (Figure 4.6A). There is increased microglial activation in the hippocampus and striatum of *E.coli* K12 infected pups compared to controls (*P=0.02* and *p=0.009* respectively) (Figure 4.6B)

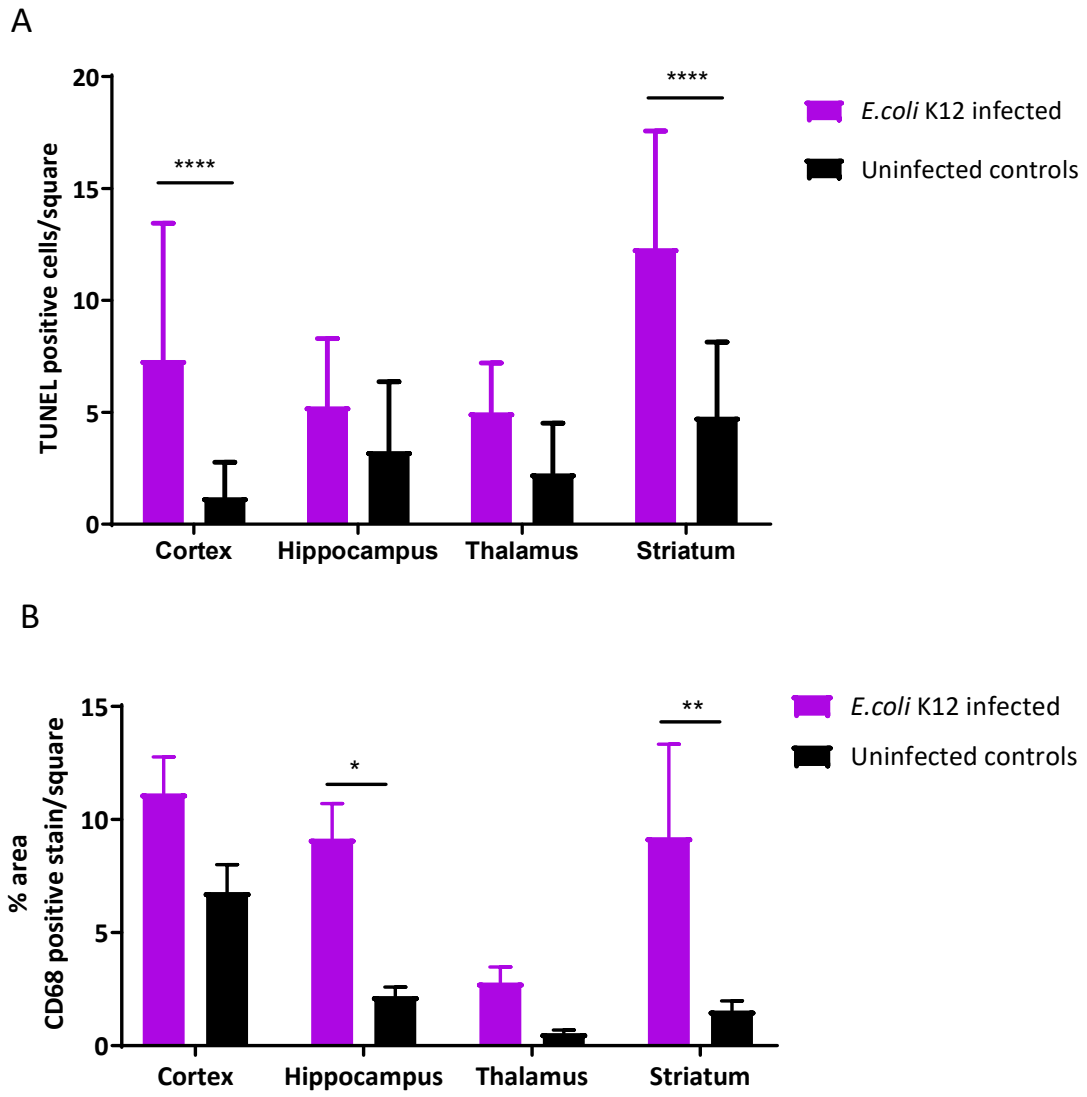

Figure 4.6: There is evidence of brain inflammation in 7 day old pups from *E.coli* K12 infected dams. (A) TUNEL quantification in specific brain regions of pups born to *E.coli* K12 infected dams and uninfected dams. n=3 from separate dams; two-way ANOVA (overall P=0.01) with post hoc Bonferroni test, *****P<0.0001*. **(B)** CD68 quantification in specific brain regions of pups born to *E.coli* K1 infected dams and uninfected dams. n=3 from separate dams; two-way ANOVA (overall P=0.38) with post hoc Bonferroni test, **P<0.05*, ***P<0.005*.

4.5. Discussion

Preterm birth is the most common cause of infant mortality worldwide with at least 40% of preterm births being associated with inflammation. Moreover, chorioamnionitis is an independent risk factor for neonatal brain injury including neurodevelopmental impairment, such as cerebral palsy, and cognitive deficits (Lee et al. 2015). In this chapter, I show that these models may also be used to model and study brain inflammation and injury in pups as a result of intra-uterine inflammation and prematurity. Numerous mouse models of perinatal brain inflammation and injury have been developed (summarised in Table 4.1) and despite the differences between brain development in mice and humans, for example delayed myelination in rodents, they can offer insights into specific pathogenic mechanisms that lead to preterm brain injury (Semple et al. 2013).

Pro-inflammatory cytokines in the brain

The brains of *E.coli* K1 infected pups show increased pro-inflammatory cytokine levels; IL-1β, IL6 and TNF-α at birth (Figure 4.2). This data is consistent with the brain inflammatory cytokine gene profile in a intrauterine LPS model of preterm birth (Burd et al. 2010). Brain IL-1β expression, in particular, was found to be significantly increased, similar to the data shown here. These pro-inflammatory cytokines are implicated in fetal inflammatory response syndrome and in particular, their presence in the amniotic fluid clinically is associated with subsequent cerebral palsy and bronchopulmonary dysplasia (Yoon et al. 1997a; Yoon et al. 1997b).

Intra-uterine inflammation, prematurity and brain injury

Whilst some of the neurological complications observed in babies born preterm relate to immaturity, there is substantial evidence that perinatal exposure to infection and inflammation leads to damage to the developing brain (Paton et al. 2017; Elovitz et al. 2011; Migale et al. 2015; Fidel et al. 2003). This is supported by our data, in which pups from non-pathogenic *E.coli* K12

dams, that do not deliver preterm, show evidence of neuroinflammation (Figure 4.6). Interestingly, in clinical studies, placental inflammation alone has been found to be a predictor of brain injury (Leviton et al. 2010). In the *E.coli* K12 model, there is upregulation of mRNA expression of TNF-α, IL-6 and CXCL-1 in the placenta 18 hours after administration followed by a small increase in TNF-α levels in the brains of the delivered pups 48 hours later. Consistent with this, Elovitz *et al.* showed that intrauterine administration of LPS, at an insufficient dose to cause preterm birth, resulted in increased pro-inflammatory cytokine expression in the fetal brains as well as reduced neuronal arborization in primary neuronal culture of these brains (Elovitz et al. 2011).

Placental inflammation and brain injury

The TUNEL and microglial data from the *E.coli* K1 and *E.coli* K12 pups was surprising as I expected that *E.coli* K1 would have had increased inflammatory effects in the brain (i.e. increased microglial activation and apoptotic cells), however they both induced very similar effects (Figure 4.3 & Figure 4.6). A possible explanation for this is that the more sick or the very preterm pups from *E.coli* K1 dams, that would have had more neuroinflammation, actually died or had to be culled prior to brain harvesting for these analyses and so we are seeing a cohort of "healthier" pups.

If this is the case, it would suggest that the inflammatory effects seen with these brain analyses is caused by bacterial presence in the uterus, regardless of whether the bacteria are pathogenic, rather than direct systemic or CNS bacterial infection (as we know that *E.coli* K12 does not infect the pups, Figure 3.12). It is known that systemic inflammation can cause rapid derogatory effects on the central nervous system before any peripheral organ dysfunction and even in the absence of direct bacterial invasion (Helderman et al. 2010). Placental inflammation, as mentioned previously, is a strong predictor for subsequent brain injury (Leviton et al. 2010). Of interest, the ELGAN study showed that even when low virulence microorganisms were isolated from the

placenta, it could predict subsequent neonatal brain lesions and long-term diparetic cerebral palsy (Leviton et al. 2010). How intrauterine inflammation leads to fetal brain injury inflammation is poorly understood but many animal studies have shown that, regardless of the type of pathogen used, inflammatory cytokines are likely to be the link between preterm birth and brain injury (Bell & Hallenbeck 2002; Bell et al. 2004; Nadeau-vallée et al. 2017). The neurodevelopmental process can be affected by any imbalance in the expression of cytokines within the fetal brain (Meyer et al. 2009). It is believed that these cytokines can reach the fetus by transplacental passage leading to a fetal inflammatory response syndrome (FIRS). IL-6, a pro-inflammatory cytokine expressed by leucocytes, is known to transfer freely across the placenta in an ex vivo human model and raised serum levels in the fetus is the hallmark of FIRS (Young et al. 2002; Zaretsky et al. 2004). Interestingly, placental gene expression of IL-6 was similarly raised in both the *E.coli* K1 and *E.coli* K12 groups in this study and may represent the link between intrauterine inflammation and brain inflammation that we see.

As mentioned above, activated microglia are seen in the brains of both *E.coli* K1 and *E.coli* K12 exposed pups. They show an increased trend of expression in all the four brain regions assessed; cortex, hippocampus, striatum and thalamus for both strains, although they are only significantly increased in the cortex of *E.coli* K1 pups and the hippocampus and striatum of *E.coli* K12 pups. The probable mechanism of brain injury is a combination of direct injury of oligodendrocytes and neurons from pro-inflammatory cytokines (either via transplacental passage or secondary from FIRS) and indirect injury as a result of microglial activation by pro-inflammatory cytokines, for example, IL-1β has been shown to activate hippocampal microglia in rats *ex vivo* (Burd et al. 2012; Vogt et al. 2008; Hailer et al. 2005). Activated microglia confer injury by further release of pro-inflammatory cytokines and excitatory metabolites such as, glutamate, which can be cytotoxic or by the release of oxidative free radicals (Dommergues et al. 2003; Li et al. 2005; Vargas et al. 2005). In an intrauterine LPS rabbit model, microglial activation was seen in the hippocampus and periventricular nuclei regions of the neonatal brains

as well as a significant motor deficit phenotype (Saadani-Makki et al. 2008; Kannan et al. 2007). Microglial activation has been found to be associated with autism and may contribute to the high incidence of autistic spectrum disorder amongst premature children (Vargas et al. 2005; Zerrate et al. 2007; Lyall et al. 2017).

There was evidence of cellular apoptosis in all regions of the brain assessed in *E.coli* K1 and *E.coli* K12 infected brains. This is supported by data in which increased apoptosis was seen in the cortex and periventricular regions of neonatal rats exposed to intracervical LPS *in utero* (Bell & Hallenbeck 2002). For future studies, it would be interesting to determine the cells which undergo apoptosis as there is evidence that TNF-α signalling may have a role in LPS-induced microglial toxicity to pre-oligodendrocytes in rat brains (Li et al. 2008; Kim et al. 2011).

Intestinal colonization of E.coli K1

E.coli K1 is known to cause neonatal sepsis and meningitis in humans. The particular strain utilised in this study is currently being used to study patterns of *E.coli* K1 colonization and invasion in neonatal rats (Witcomb et al. 2015). *E.coli* K1 has been shown to cause lethal systemic infection in neonatal rats by translocation from the GI tract lumen into the bloodstream (Dalgakiran et al. 2014). The susceptibility to *E.coli* K1 gastrointestinal colonization is age-dependent with neonates infected at the early gestation P2 (rather than P9) being more susceptible (Witcomb et al. 2015). This is thought to be because of a poorly developed intestinal mucus barrier at this age and reduced α-defensin expression from Paneth cells (Birchenough et al. 2017; Birchenough et al. 2013). The data shown in the previous chapter complements this work, showing that gastrointestinal *E.coli* K1 colonization also occurs in the majority of fetal mice following maternal intravaginal infection and supports the concept that colonization and subsequent systemic infection occurs as a result of an immature mucus barrier (Figure 3.17).

Necrotizing enterocolitis (NEC) is seen commonly in premature infants and although its aetiology remains unclear; prematurity, bacterial colonization, enteral formula feeding and

hypoxia/ischaemia appear to play a role (Lin et al. 2008; Hunter et al. 2008). Villous atrophy is a common histological feature of NEC and is used to describe NEC in experimental models (Niinikoski et al. 2004; Yurttutan et al. 2014). Maternal administration of *E.coli* K1 did not induce villous atrophy in the pups in this chapter (Figure 4.4). As mentioned earlier, the cohort of pups that survived to one week of life may not have exhibited any intestinal disease as they were the "healthier pups" (that were possibly less infected with bacteria). Alternatively, prematurity and GI tract bacterial colonization may not be enough to induce villous atrophy or a NEC-like phenotype as other factors such as hypoxia/ischaemia may also need to be present.

The work in this chapter has several limitations. We measured cytokine levels in the whole brain which may not reflect the cytokine environment of different parts of the brain. Furthermore, cytokines have very short half-lives and so analysis on the day of birth may not be an accurate representation of the inflammatory response. The sample sizes were small (pups from 3 dams/group) for the one week analyses and this work did not take into account how premature the pups were in the *E.coli* K1 group. For future studies, I would like to assess the brain further by studying other regions including the external capsule, corpus callosum and the periventricular regions. These regions incorporate the white matter, which is commonly associated with the brain injury seen in premature babies, for example periventricular leukomalacia (Yoon et al. 1996; Yoon et al. 2003). I would also like to perform more thorough analysis of neuropathology (using Nissl, TUNEL, myelin basic protein immunohistochemistry), neuroinflammation (using Iba-1/CD68, GFAP immunohistochemistry) and oligodendrocyte maturation (using Olig2 and O4 immunohistochemistry).

In conclusion, this chapter demonstrates that intrauterine inflammation, regardless of whether it induces preterm birth in mice, can induce acute inflammation in the brain and possibly lead to long term brain injury.

Table 4.1: Mouse models of preterm brain injury.

Route of administration	Infectious or Inflammatory agent	Embryonic day	Brain injury	References
Intranasal (maternal)	Human influenza virus	E9.5	• Reduced hippocampal and cortical thickness • Cerebellar pathology • Deficits in behavioural tests; pre-pulse inhibition, acoustic reflex and social interaction	(Shi et al. 2003; Shi et al. 2009; Fatemi et al. 2008)
Intrauterine	LPS	E15.5	• Reduced MAP2 and dendrites in primary cortical neuronal cultures • Increased brain cytokine mRNA expression • Hypomyelination • Grey matter injury	(Elovitz et al. 2011; Burd et al. 2009; Burd et al. 2010; Leitner et al. 2014; Wang et al. 2007)
Intrauterine	LPS	E17.5	• Reduced dendrites in primary cortical neuronal cultures • Microglial activation • Increased brain cytokine mRNA expression • Brain injury improved with mesenchymal stem cell treatment	(Lei et al. 2015)
Intravenous	Poly I:C	E9.5 or 17.5	• Deficits in behavioural tests; open field, perseverative behaviour • Grey matter injury	(Meyer et al. 2006)
Intrauterine	IL-1β	E16.5	• Increased brain cytokine mRNA expression • Degeneration and atrophy of brain • Visual evoked potential abnormalities	(Nadeau-Vallée et al. 2017)

Chapter 5 Gene delivery to the murine cervix

5.1. Summary

The previous chapters describe the development of ascending models of vaginal infection and preterm birth. In this chapter, I move on to assessing if gene delivery to the murine cervix is a plausible therapeutic system that could be used to develop a topical therapy for preterm birth which may be tested on the models described in the previous chapters.

Gene transfer can be achieved by viral and non-viral vectors. Viral vectors have been more successful up to now as gene delivery vectors and have been used in numerous clinical trials (Bainbridge et al. 2015b; Nathwani et al. 2012). The most common viral vectors used are derived from lentiviruses, adenoviruses and adeno-associated viruses (AAV). AAV vectors have, however, been used to transduce human vaginal and cervical epithelial cells *in vitro* and they have successfully been used to transduce the lower reproductive tract of the rhesus macaque (Abdel-Motal et al. 2011; Abdel-Motal et al. 2014). However, delivering genes to the cervical epithelium in mice has not been done before.

This chapter tests the hypothesis that murine cervical epithelium can be transduced by topically applied viral vectors. The optimal gene delivery system is assessed using different viral vectors as well as examining administration methods to improve gene delivery to the cervical mucosa. In contrast to the human cervix, the entirety of the murine cervix comprises stratified squamous epithelium (Leppi 1964). Although little is known about the mouse cervix, we do know that one layer of the 28-layer human vaginal and ectocervical stratified squamous epithelium sheds every four hours (Anderson et al. 2014). Therefore, thermosensitive hydrogels were assessed as a method to prolong vector-epithelia contact time and thus improve transduction.

I show that viral vectors can transduce murine cervical epithelium *in vivo* leading to transient cervical protein expression lasting for up to 14 days. Thermosensitive hydrogels were found to improve transduction efficiencies, particularly when applied as an intravaginal plug.

5.2. *In vivo* transduction of the vagina and cervix is possible using viral vectors

Initial studies were carried out to determine if it was possible to transduce the upper vagina and cervix of the mouse by topical delivery of different viral vectors encoding a firefly luciferase marker gene driven by a CMV promoter. The three different viral vectors used were; AAV 8, adenovirus serotype 5 and VSV-g pseudotyped lentivirus (Figure 5.1A). This data showed that there was evidence that it was possible to transiently express the luciferase enzyme using all the viral vectors tested. However, expression was variable and appeared to diminish by one-week post-injection (Figure 5.1B)

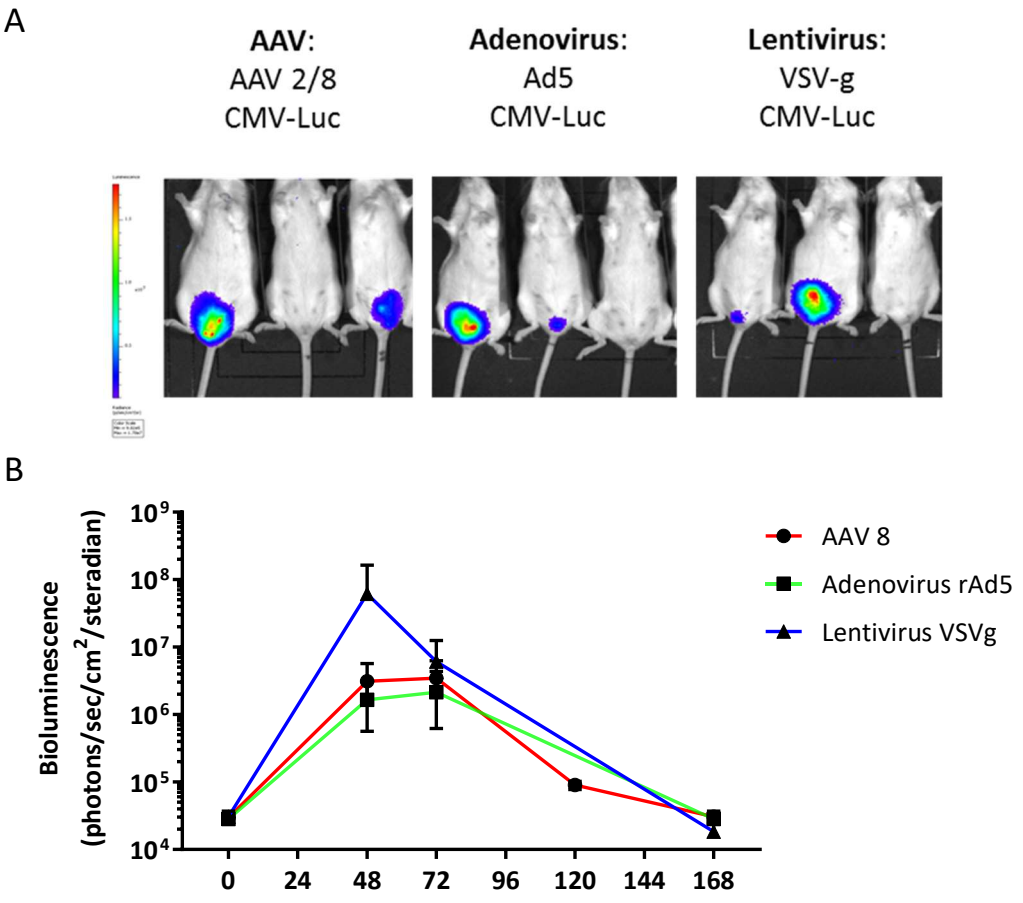

Figure 5.1: In vivo transduction of the vagina and cervix is possible using viral vectors; AAV, adenovirus and lentivirus. (A) Representative images of cervico-vaginal luciferase expression comparing the three different viral vectors at 72 hours after intravaginal application. **(B)** Cervicovaginal luciferase expression over time. n=3.

5.3. Luciferase expression is restricted to the vagina and cervix

In mice treated with recombinant adenovirus serotype 5 delivering the luciferase gene, *ex-vivo* luminometry was performed on the vagina, cervix, uterus and liver at 72 hours after administration to confirm localisation of expression and to assess for viral spread into the uterus or liver (Figure 5.2). *Ex vivo* bioluminescent signal from the vagina and cervix 72 hours after transduction show no obvious expression in the uterine cavity (Figure 5.2A). Using *ex vivo* luminometry there was significant luciferase expression in the upper vagina and cervix (*P<0.0001*); similarly, the liver and uterus had no detectable luciferase expression (Figure 5.2B).

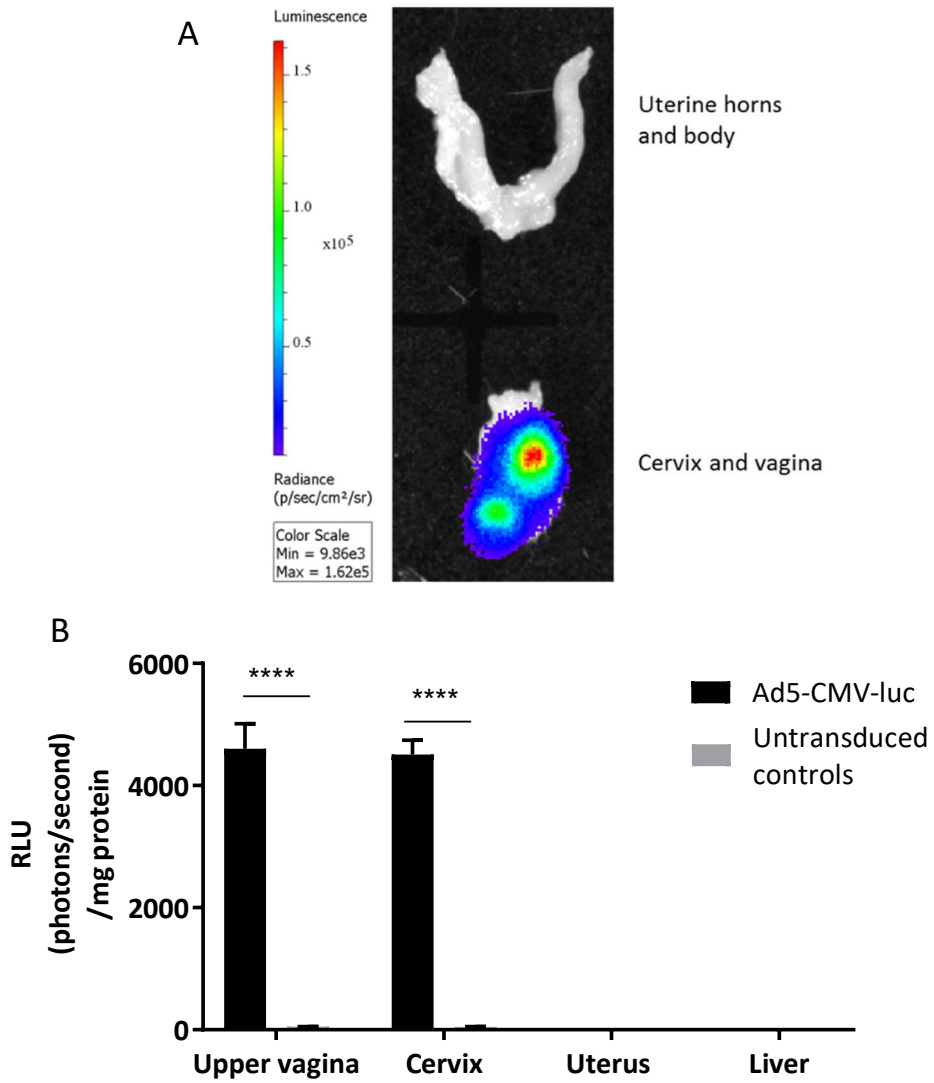

Figure 5.2: Luciferase expression is restricted to the vagina and cervix following transduction with Ad5 CMV-Luciferase. (A) Representative images of bioluminescence from the vagina, cervix and uterus 72 hours after transduction with Ad5 CMV-Luciferase (the cervix and vagina are detached from the uterus at the level of the uterine body just above the cervical canal). **(B)** *Ex-vivo* luminometry of luciferase expression in different organs 72 hours after intravaginal application of Ad5 CMV-Luciferase. n=3, data analysed with a two-way ANOVA with post-hoc bonferroni test ****$P<0.0001$.

5.4. AAV 6 and AAV 8 can transduce cervical epithelium *in vitro* and *in vivo*

AAV, rather than adenovirus or lentivirus, was chosen for the ensuing studies due to its relatively low immunogenicity, episomal-nature, thermostability and success in numerous clinical trials (Mingozzi et al. 2014; Gruntman et al. 2015; Schnepp et al. 2003). The most efficient application method for cervical epithelium transduction was determined. Numerous AAV serotypes have been identified with different cellular tropisms (Zincarelli et al. 2008). The two AAV serotypes assessed in this study were AAV 6 and AAV 8; this was based on studies in which AAV 6 was found to be most efficient serotype for transduction of human vaginal and cervical cell lines *in vitro* (Abdel-Motal et al. 2011) whilst AAV 8 has been successful in numerous clinical trials for Haemophilia (Nathwani et al. 2014) and is, therefore, clinically validated.

AAV 6 - and AAV 8- CMV luciferase vectors were used to transduce human endocervical cells (End1 E6/7) *in vitro* followed by luminometry 72 hours after transduction. There was a significant increase in transduction of AAV 6 at an MOI of 50, compared to AAV8 (*P=0.02*), however, other MOIs showed similar transduction efficiencies (Figure 5.3).

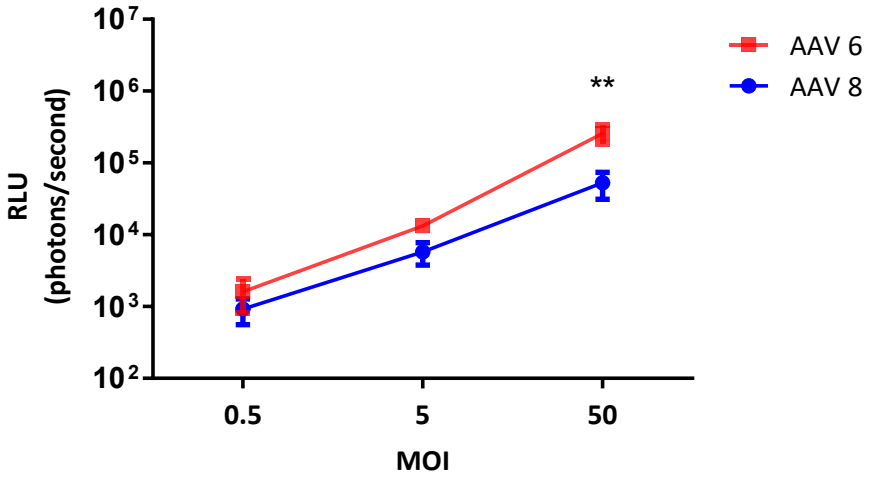

Figure 5.3: Luciferase expression in endocervical cells 72 hours after transduction with AAV CMV luciferase. n=6 (performed in triplicate); data analysed with a one-way ANOVA, ***P<0.01*.

In vivo experiments were subsequently performed by intracervical application of AAV 6- and AAV 8- CMV GFP in a diestrus (MPA-treated) female mouse. Mice were subcutaneously injected with medroxyprogesterone-acetate (2.5mg) 7 days prior to injection to ensure all mice were in the diestrus stage of the estrous cycle. This was performed to reduce variation amongst the mice as AAV transduction has been shown to be effected by hormones (Davidoff et al. 2003). To confirm that mice were in the diestrus stage, I performed a smear prior to viral vector application (Figure 5.4A).

There was no significant difference in the cervical expression of GFP for AAV6 or AAV8 serotypes (*p=0.35*) (Figure 5.4B), although AAV6 showed a tendency for higher expression. Nevertheless AAV 8 was used for the remaining experiments in this study as cervical expression was more consistent with this serotype (AAV 8; mean 63.1 SD±31, AAV 6; mean 158.2 SD±245.6). From a clinical translation point of view, AAV 8 also has lower prevalence of neutralising antibodies in humans, compared with AAV 6 (Boutin et al. 2010).

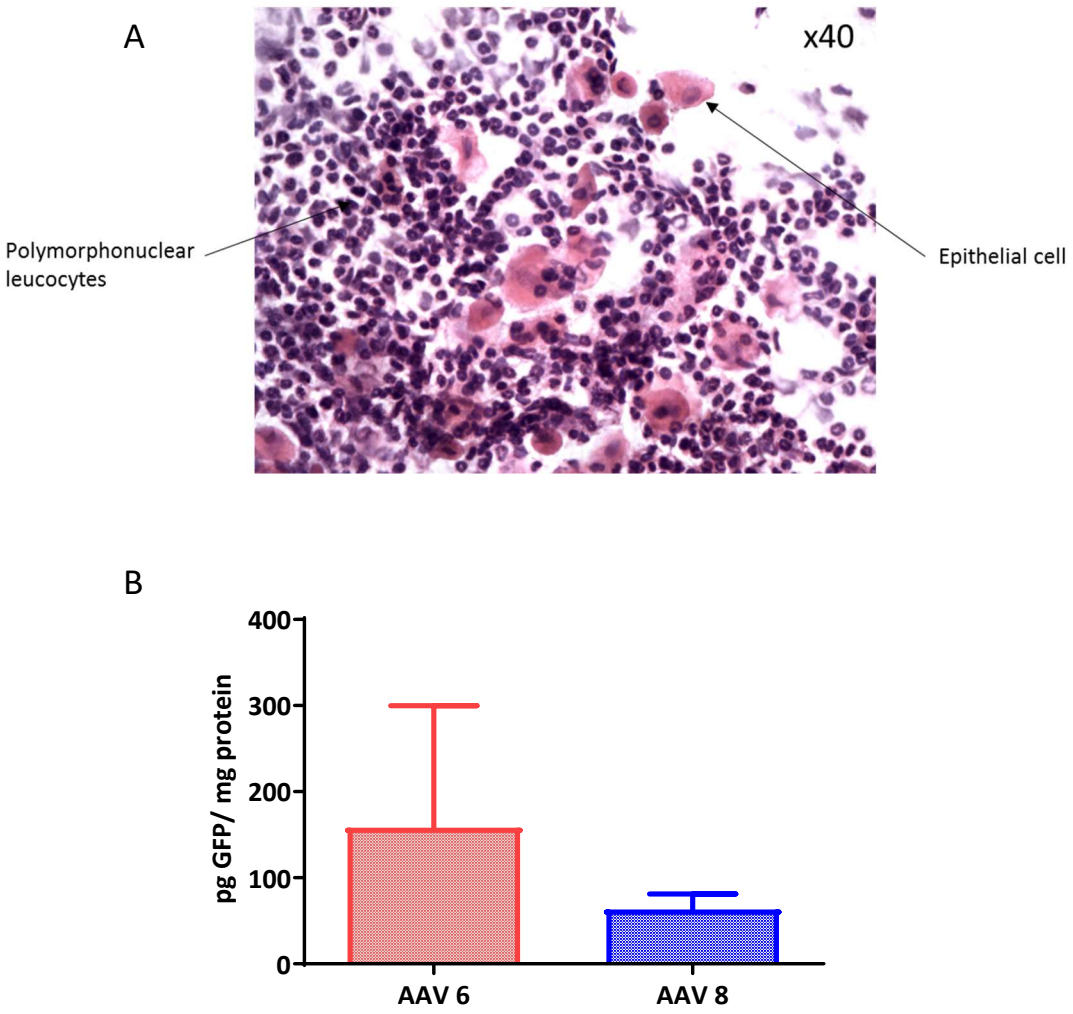

Figure 5.4: There is no difference in the cervical GFP expression between the AAV6 and AAV8 serotypes. (A) Murine diestrus vaginal smear; representative image of a H&E stained vaginal smear showing the predominant cells to be polymorphonuclear leucocytes with a few larger epithelial cells. **(B)** Cervical GFP expression with ELISA for comparison of AAV 6 and AAV 8 serotypes. n=3; data not normally distributed therefore analysed with a Mann-Whitney rank test.

5.5. Thermosensitive gels can improve protein expression

The use of thermo-sensitive gels to improve the efficiency of gene transfer to the mouse cervix was determined in the following experiments.

5.5.1. GFP expression appears increased when using AK12 pluronic gel

Intravaginal application of an AAV 8 viral vector encoding GFP (driven by a CMV promoter) was used for the following experiments. GFP expression comparing the use of AK12 pluronic gel with virus alone was assessed initially by direct fluorescence imaging. There appear to be more GFP expression following application of virus mixed with an AK12 pluronic gel compared to virus alone (Figure 5.5).

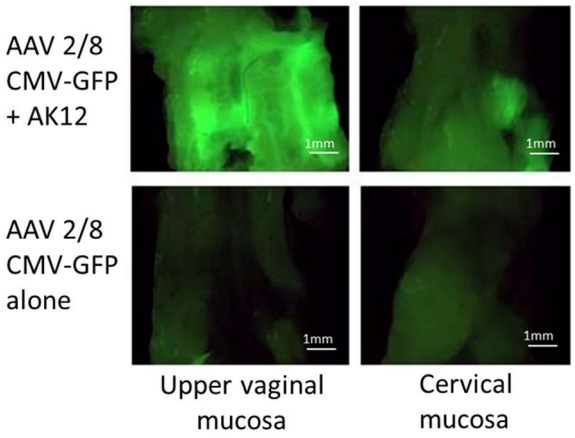

Figure 5.5: GFP expression appears increased when the AAV8-GFP viral vector is administered with an AK12 pluronic gel compared with AAV8-GFP viral vector alone. Direct GFP fluorescence imaging comparing a mixture of viral vector and pluronic gel AK12 (top) with direct application of viral vector (bottom).

5.5.2. Pluronic gels appeared to increase cervical GFP expression when administered in a mixture with the viral vector

Two different types of pluronic gel were tested; AK12 and F-127 pluronic gels. AK12 forms a gel at 20-25^{o}C, whilst F-127 works at 37^{o}C. GFP expression was compared following administration of AAV8-GFP combined with either of these two pluronic gels as well as a no gel control (Figure 5.6). There was a trend showing an increase in GFP expression when the viral vector was administered in a mixture with a pluronic gel (F-127 or AK12) compared with no pluronic gel, although this was not significant (*P=0.42*).

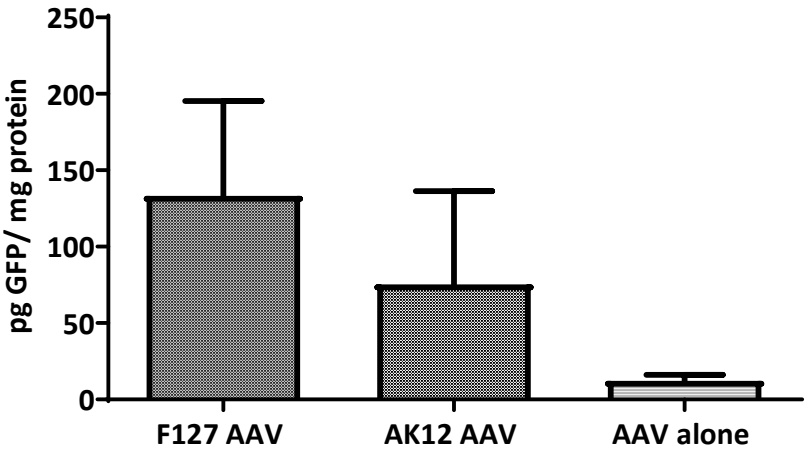

Figure 5.6: GFP expression was increased when the viral vector was administered in a mixture with pluronic gels (either F127 or AK12) compared with no gel although this was not statistically significant. Cervical GFP expression 72 hours after application of AAV 8 CMV-GFP; comparison between F-127 gel, AK12 gel and no gel. n=7 in the F-127 and AK12 groups, n=3 in the control group; data not normally distributed therefore analysed with a Kruskal-Wallis test with post-hoc Dunn's test.

Whilst carrying out the above experiments, GFP expression was found to be expressed along the whole length of the vaginal mucosa rather than, as would be ideal, targeting the epithelium of the upper vagina and cervix. Therefore, a plug method was developed in which viral vector was applied alone to the cervix and then the pluronic gel was used as a plug at the vaginal introitus so that the vector remained in place. I chose the AK12 gel for further experiments as its gelling temperature of 20-25°C means that it formed a gel much quicker than the F127 gel (which works best at 37°C) and it seemed more appropriate for a plug that would be exposed to the outside environment at the vaginal introitus. Using the AK12 gel in a plugging method, there was a significant increase in cervical GFP expression, compared to the original mix method (*P=0.0195*) (Figure 5.7). Furthermore, this method significantly increased cervical GFP expression compared with vector alone (*P=0.0244*) (Figure 5.7).

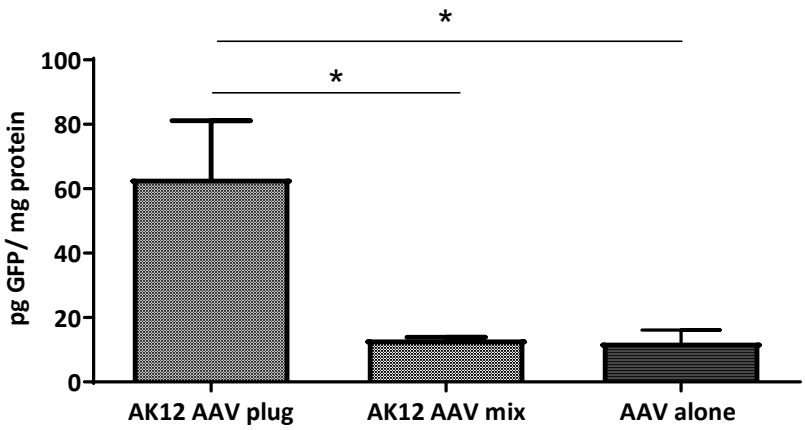

Figure 5.7: The AK12 AAV plug method significantly increased cervical GFP expression. Cervical GFP expression comparing AK12 pluronic gel plug, AK12 pluronic gel mix method and vector alone. n=4 in AK12 mix group, n=3 in AK12 plug and control group; data analysed with a one way ANOVA with post-hoc Bonferroni test, **P<0.05*.

5.6. Luciferase expression occurs after 24 hours *in vivo* and begins to diminish after 120 hours

Based on the above data, AAV 8 containing a luciferase gene driven by a CMV promoter was intravaginally administered using the AK12 plug method to determine time course of expression. Bioluminescence was detected at the earliest time point of assessment, 24 hours after injection, with peak signal occurring between 72 and 96 hours (Figure 5.8). Bioluminescent signal starts to diminish 120 hours after viral application and returns to background levels by 14 days after injection.

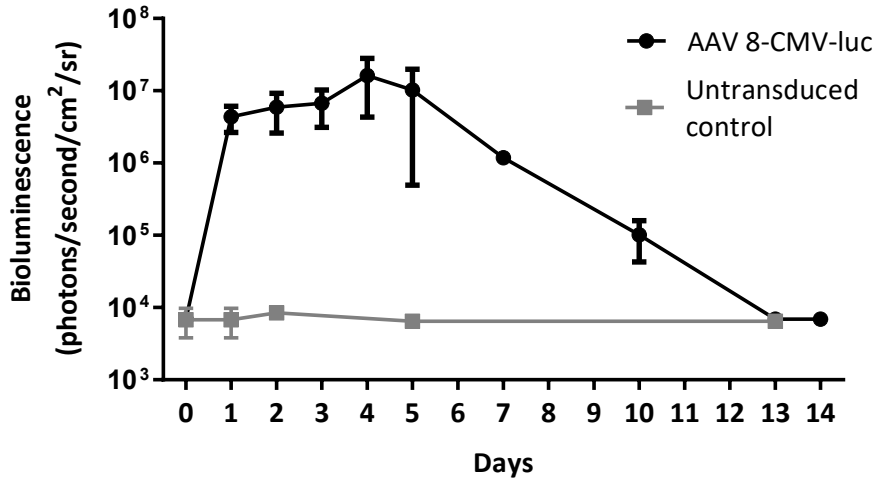

Figure 5.8: Luciferase expression from the lower reproductive tract occurs after 24 hours following vector administration and begins to diminish by 120 hours. Time course of luciferase expression using *in vivo* bioluminescence imaging. n=5.

5.7. GFP is expressed in the vaginal and cervical epithelium

GFP immunohistochemistry was performed to determine cellular location of GFP expression. GFP was detected in the epithelial cells, with most of the expression seen in the top epithelial cell layers (Figure 5.9). There appears to be some evidence of basal layer expression.

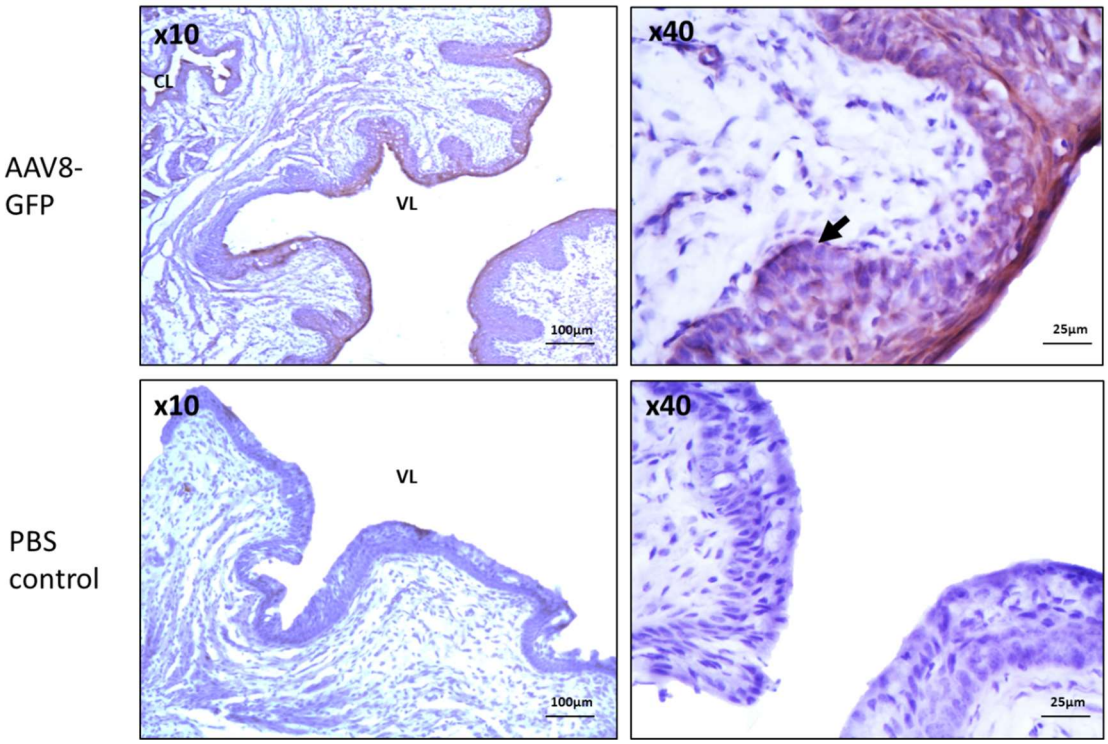

Figure 5.9: GFP is expressed in the upper vaginal and cervical epithelium. Representative images of GFP immunohistochemistry of transverse sections of the cervical and upper vaginal epithelium 72 hours following; AAV 8-GFP (top) or PBS (bottom) administration. Brown colouration depicts DAB-positive cells. Black arrow depicts basal epithelial cell layer. VL=vaginal lumen, CL=cervical lumen.

GFP immunofluorescence was performed to further assess expression. Using a cytokeratin antibody for co-localisation, GFP expression was only found in cytokeratin positive cells confirming that expression is confined to the stratified squamous epithelial cell layer (Figure 5.10).

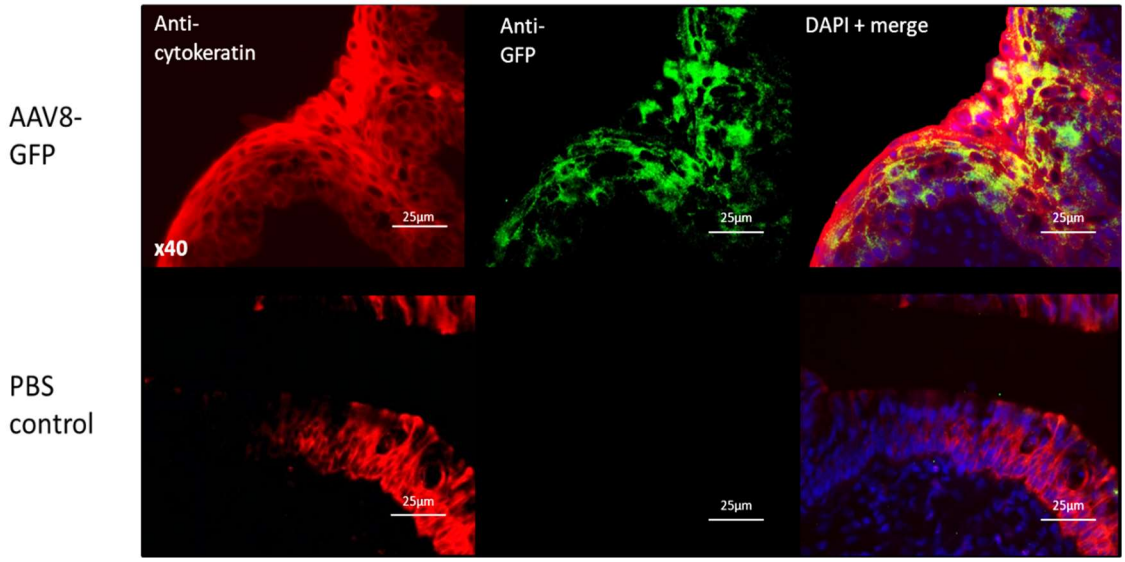

Figure 5.10: GFP co-localises with cytokeratin in the cervix, confirming that GFP expression is confined to the epithelial cell layers. Representative images of cytokeratin and GFP immunofluorescence staining of transverse sections of the cervical epithelium 72 hours following; AAV8-GFP (top) or PBS (bottom) administration. Red fluorescence represents cytokeratin positive cells, whilst green fluorescence represents GFP positive cells.

5.8. Discussion

This chapter explores the use of viral vectors to deliver genes to murine cervical epithelium *in vivo*. I find that it is possible to transduce the cervix and upper vagina using different types of viral vectors (Figure 5.1). Although no experiment comparing the transduction efficiency, localisation of expression and time course of expression between the different viral vectors was performed, initial data using viral vector transfer of the luciferase transgene shows direct expression after intravaginal administration of the three main viral vectors; a lentivirus (VSV-g), an adenovirus (rAd5) and an AAV (serotype 8) using bioluminescent imaging. There was no evidence of local vector spread into the uterine cavity or systemic spread into the liver on *ex vivo* luminometry (Figure 5.2). AAV was chosen as the viral vector for the remaining experiments in this thesis because of its immunogenicity profile and track record in preclinical research and clinical trials.

AAV serotypes and cervical gene delivery

Thirteen naturally occurring AAV serotypes of human and simian origin have been described so far (Zinn & Vandenberghe 2014). The multiple AAV serotypes are differentiated by their capsid proteins which appear to determine their cellular tropism (Zincarelli et al. 2008). The mechanism behind cellular tropism is still, however, poorly understood although it is becoming clear that AAV interaction with cell surface receptors is the first step to successful transduction. The recent discovery of a multi-serotype AAV receptor using genome wide screening is beginning to shed light on these mechanisms (Pillay et al. 2016). They have shown that different serotypes have evolved distinctive interactions with the receptor, for example AAV 8 requires interaction with both PKD-1 (polycystic kidney domain) and PKD-2 domains of the receptor for successful transduction, which may help to confer tropism. Furthermore cell infectivity and transduction is believed to be dictated by the ability of the capsid protein to attach to cell surface glycans as attachment receptors, with the interaction of AAV2 and heparan sulphate proteoglycan being

the best characterised (Kern et al. 2003). Cellular tropism is thought to be mediated in part by the differential glycan receptor usage for cell surface attachment (Pillay & Carette 2017).

AAV 6 has been found to have the best transduction efficiency *in vitro* in human endocervical and vaginal cells; in primary cells as well as in purchased cell lines (Abdel-Motal et al. 2011; Abdel-Motal et al. 2014). This was confirmed in my experiment comparing the luciferase expression from AAV 6 and AAV 8 transduced endocervical cells (Figure 5.3). Although luciferase expression from the AAV 8 transduced cells was much higher in my experiments than previously published, it was only significantly different from AAV 6 transduced cells at the highest MOI. *In vivo*, AAV 6 and AAV 8 transduction was comparable and importantly AAV8 transduction appeared less variable between mice (Figure 5.4). Apart from the use of AAV 6 in the rhesus macaque, there is no published animal data looking at other AAV serotypes in vaginal or cervical gene transfer *in vivo*. In the mouse, research describing viral vector gene transfer to other organs with stratified squamous epithelium, such as the cornea, has been published (Hippert et al. 2012). The cornea consists of an anterior stratified squamous epithelial cell layer, then a thick collagenous stromal centre with an endothelial cuboidal monolayer base. Interestingly after intrastromal injections of numerous AAV vectors delivering GFP (AAV 1,2,5,8), AAV 8 was found to be the most efficient at transducing the corneal squamous epithelium in mice as well as in human corneas *ex vivo* (Hippert et al. 2012; Sharma et al. 2010; Vance et al. 2016).

Thermosensitive pluronic gels

Thermosensitive pluronic gels have been developed for numerous functions, including vaginal drug delivery (Tuğcu-Demiröz et al. 2013; Ghahremankhani et al. 2008; Jeong et al. 2000). More specifically as a viral vector delivery system, the F127 gel has been used to deliver VEGF with an adenoviral vector to the uterine circulation as a treatment for fetal growth restriction (Mehta et al. 2014; Mehta et al. 2016). The benefits of these gels are that they are biodegradable, low in toxicity and they transfer from aqueous phase to gel phase on increasing temperature, often

body temperature. The F127 polymer becomes a gel at body temperature (37^{o}C) whilst the AK12 polymer gels at room temperature (20-25^{o}C). The use of AK12 and F127 gels in a mixture with the viral vector appeared to improve cervical viral vector transduction, although this was not significant and possibly because of the small sample size (Figure 5.6). Using a gel plugging method with the AK12 gel, however, there was a significant increase in cervical GFP expression (Figure 5.7). No studies have specifically compared these two gels for vaginal use, F127 gel has been compared with hydroxylpropyl-methylcellulose gel preparations for vaginal oxybutynin delivery (Tuğcu-Demiröz et al. 2013). Hydroxypropyl-methylcellulose preparations were found to show better muco-adhesive properties in a rabbit vaginal delivery model and therefore may be useful as a comparative gel and also perhaps as an additive to the AK12 or F-127 pluronic gels to prolong epithelial exposure time.

Location of protein expression

I show that the location of GFP expression following AAV8-GFP transduction is predominantly in the top epithelial cell layers of the upper vagina and cervical epithelium (Figure 5.9). Co-localisation immunofluorescence staining with a pan-cytokeratin antibody confirms that expression is confined to the epithelial cell layers (Figure 5.10). The basal layer of the epithelium consists of epithelial stem cells and so transduction of this layer would lead to long term expression. There is no evidence of significant basal layer transduction seen on immunofluorescent staining, consistent with the time course of expression data. In this experiment luciferase expression diminishes in all mice 14 days after application suggesting complete shedding of the transduced upper epithelial cell layers. Intravaginal administration of AAV 6 CMV-GFP in the rhesus macaque did, however, result in some basal layer transduction confirmed by p63 co-localisation (p63 is a transcription factor confined to the basal epithelial cells) (Abdel-Motal et al. 2014). Although in these experiments the vaginal and ectocervical mucosa were scarified using a cervical brush prior to viral vector application to encourage basal

layer transduction. As the ultimate aim for the viral vectors in this study is to deliver genes to the cervix during pregnancy, short term expression would be most appropriate for clinical translation.

Promoters for cervical gene delivery

The human cytomegalovirus major immediate-early promoter/enhancer (CMV promoter) was chosen as the promoter for these experiments and the remaining experiments in my thesis. I chose this promoter as it is a strong and common promoter which leads to high transduction rates in most cells (Boshart et al. 1985). Transcriptional silencing, is the main concern with this promoter, although this is unlikely to be a problem in this situation, as mentioned above, expression is transient (Kong et al. 2009; Brooks et al. 2004; Prösch et al. 1996). However, for future translational applications cervical cell-targeted promoters should be assessed to reduce the risk of ectopic expression. This has been explored in normal endometrial cells but not in endocervical and ectocervical cells, although a secretory leucocyte protease inhibitor promoter could be considered (Othman et al. 2016; Itaoka et al. 2015).

In conclusion, AAV viral vectors can be used to successfully deliver genes to the cervical epithelium and the optimal application method was determined with the use of thermosensitive pluronic gels.

Chapter 6 The effects of overexpressing antimicrobial peptide, human beta defensin-3, on the murine cervix

6.1. Summary

In the previous chapter I describe the development of an efficient gene transfer system for the delivery of genes to the murine cervical epithelium. In this chapter, I use that system to deliver a human antimicrobial peptide gene to the cervix and explore the effects of this gene on cervical mucosal immunity in the mouse.

During pregnancy, the cervix produces a specialised mucus plug which is believed to play a role in preventing pathogens from ascending into the uterine cavity. This plug is a large structure that fills the cervical canal during pregnancy and predominantly consists of mucins, negatively charged mucinous glycoproteins. Mucins provide the structural framework of the mucus plug and their immune properties include inhibition of bacterial diffusion, inhibition of viral replication and retention of positively charged molecules, such as antimicrobial peptides (Carlstedt et al. 1983; Habte et al. 2008). The mucus plug has been shown to have a high concentration of antimicrobial peptides; secreted from the surrounding endocervical cells and neutrophils (Hein et al. 2002; Hein et al. 2001; Becher et al. 2009).

The pathogenesis of infection-related preterm birth is still unknown. Accumulating evidence points towards immune dysfunction within the cervix; whether this is as a result of reduced epithelial surface area, as in women who have had cervical biopsies for cervical intra-epithelial

neoplasia or whether this is due to an inherent dysfunction in cervical mucosal immunity is yet to be clarified (Castanon et al. 2014; Stock et al. 2016; Kindinger et al. 2017; Kyrgiou et al. 2014).

This chapter tests the hypothesis that overexpressing an antimicrobial peptide in the cervix would result in a "super" mucus plug capable of preventing bacterial ascent into the uterine cavity *in vivo.* HBD-3 was chosen as the antimicrobial peptide of choice because of its potent antimicrobial activity, particularly to bacteria implicated in preterm birth, and its relative resistance to high salt environments found in bodily fluids, such as cervical mucus (Harder et al. 2001; Xiao et al. 2014).

I find that it is possible to express human beta-defensin 3 in the murine cervix *in vivo*. Interestingly, HBD-3 expression appears to have immunomodulation properties *in vivo* resulting in an influx of neutrophils to the cervical epithelium. I assessed the effect of HBD-3 overexpression on the vaginal microbiota of the mouse and found no significant changes in the microbial composition compared to untreated mice.

6.2. Transient transfection of HEK 293-T cells with pAAV-HBD3 leads to GFP expression

A bicistronic AAV plasmid containing the HBD-3 gene and a GFP marker gene under transcriptional control of separate CMV promoters was designed and made by Vector Biolabs (USA) (designated AAV-HBD3 for the rest of the chapter) (Appendix Figure 10.1). Transient transfections of the AAV-HBD3 plasmid were performed on HEK 293-T cells and cells were imaged with a fluorescence microscope to detect GFP expression. GFP expression was detected from 24 hours after transfection (Figure 6.1).

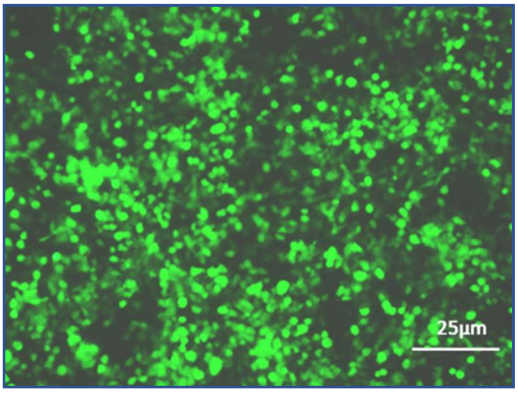

Figure 6.1: There was GFP expression 24 hours after transient transfection with the AAV HBD-3 plasmid. GFP expression in HEK293-T cells was visualised 24 hours after transfection**.**

6.3. HBD-3 peptide is expressed *in vitro*

To determine HBD-3 expression, cell supernatants and cell lysates were collected 72 hours after transfection and assessed using ELISAs.

6.3.1. HBD-3 is overexpressed in the supernatants and cell lysates of HEK 293-T transfected cells

HBD-3 was quantified in the cell supernatants and cell lysates. There was a significant increase in HBD-3 expression in the supernatants (p=0.0001) and the cell lysates (p=0.007) (Figure 6.2A & Figure 6.2B).

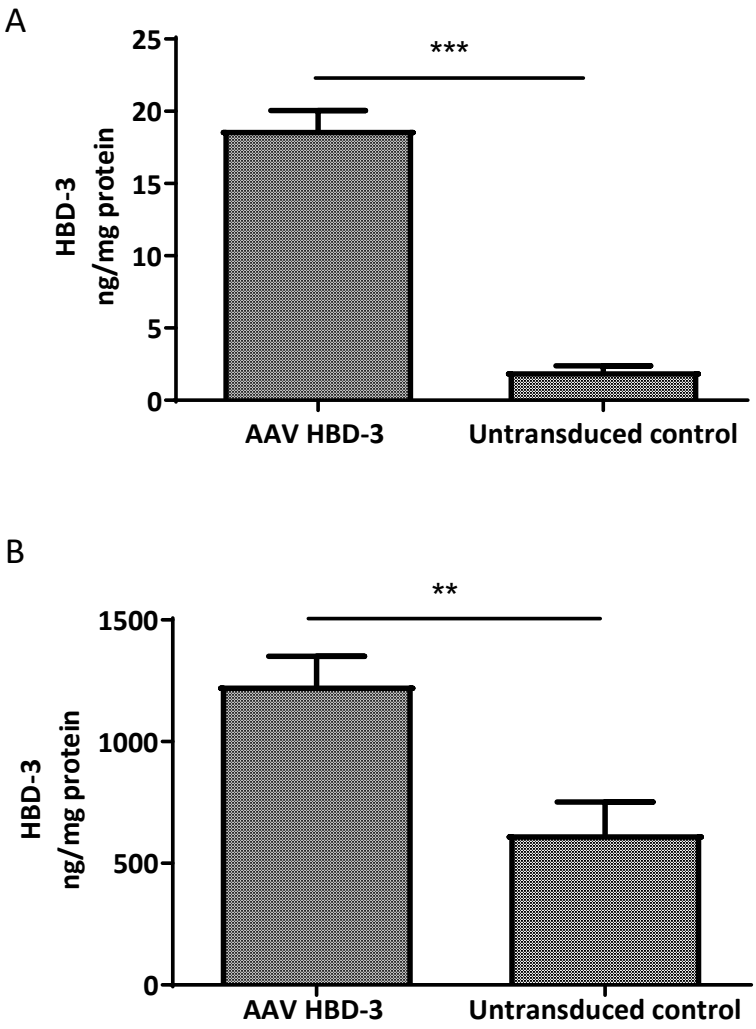

Figure 6.2: HBD-3 is overexpressed in the supernatants and cell lysates of HEK 293-T transfected cells. (A) Cell supernatant HBD-3 quantification 72 hours after transient transfection of AAV-HBD3 plasmid in HEK 293T cells. **(B)** Cell lysate HBD-3 quantification 72 hours after transient transfection of AAV HBD-3 plasmid in HEK 293-T cells. n=4; data analysed with an unpaired t-test, ***P<0.01*, ****P<0.001*.

6.3.2. Recombinant HBD-3 can kill *E.coli* K12

Killing assays using recombinant HBD-3 were performed using bioluminescent *E.coli* K12 bacteria (Figure 6.3). The anti-*E.coli* K12 activity of recombinant HBD-3 increases with increasing peptide concentration.

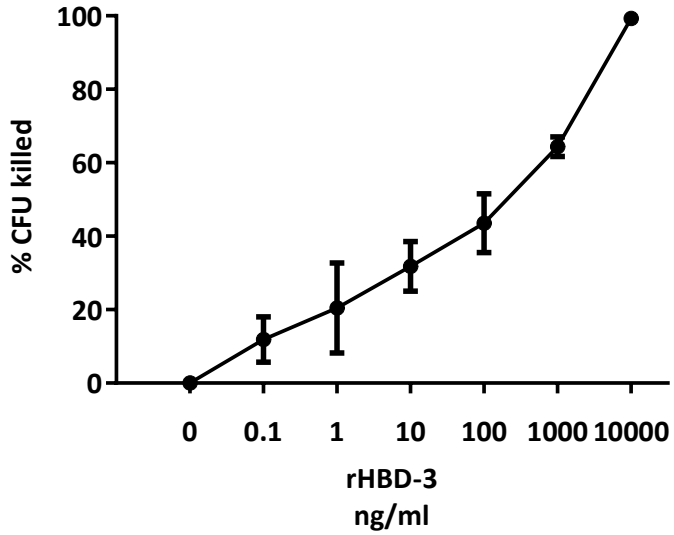

Figure 6.3: *E.coli* K12 kill increases with increased concentration of recombinant HBD-3. Total colony count on control plates with media alone was considered as 0%.

6.3.3. HBD-3 functions *in vitro*

Killing assays performed with the AAV transfected supernatants showed a significant reduction in absolute CFU numbers compared to control supernatants (*P=0.0003*) (Figure 6.4A). The percentage of *E.coli* K12 CFUs killed by undiluted AAV supernatants was 41.25% (data not shown here). Serial dilutions of HBD-3 (from AAV-HBD3 supernatants) were performed, based on levels of HBD-3 determined by ELISA, and a dose response of HBD-3 kill was performed (Figure 6.4B). There was a reduction in the absolute number of *E.coli* K12 CFUs with each fold dilution, except at the 5ng/ml concentration.

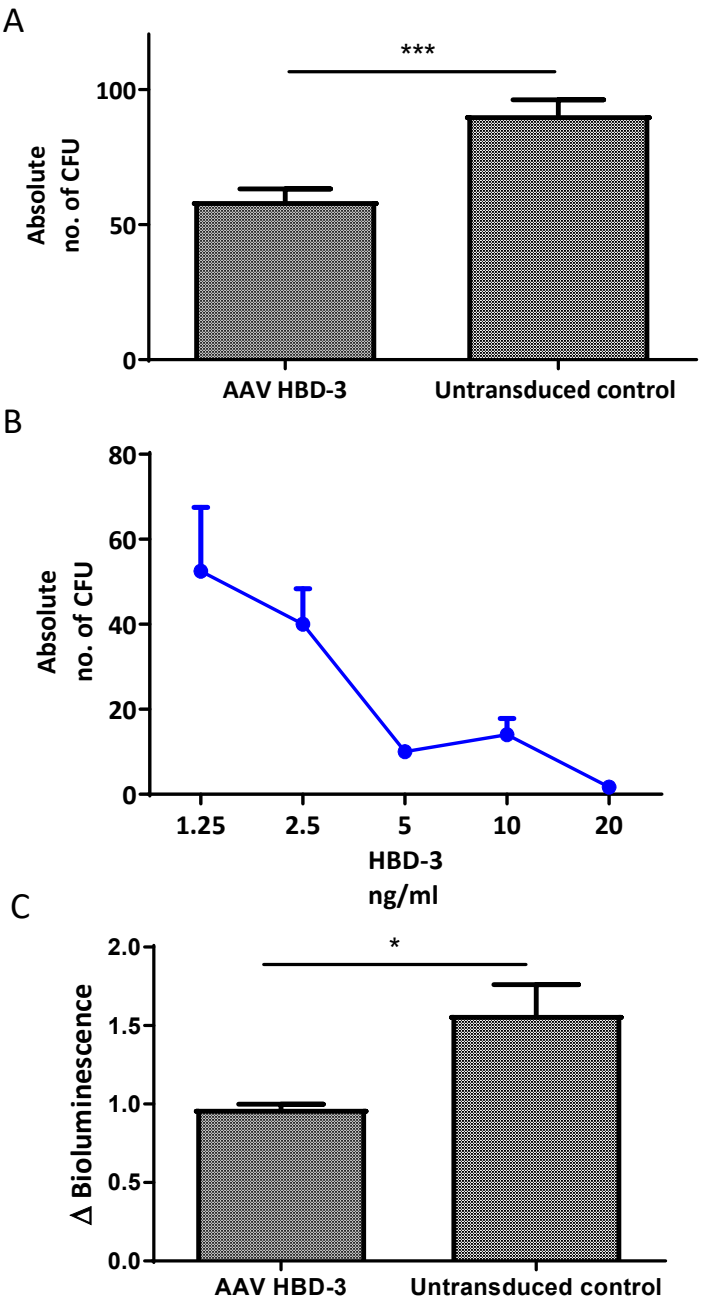

Figure 6.4: HBD3 from AAV-HBD3 transduced cell supernatants have antibacterial activity against *E.coli* K12. (A) Killing assay; absolute number of *E.coli* K12 CFUs following treatment with AAV HBD-3 supernatants and control supernatants. **(B)** Dose response of *E.coli* K12 kill (x values $\log_2$ transformed). HBD-3 was serially diluted from AAV-HBD-3 transduced after concentration was determined by ELISA. **(C)** Fold change in bioluminescence following *E.coli* K12 infection of AAV HBD-3 transfected cells**.** n=3, performed in triplicate; data analysed with an unpaired t-test, **P<0.05, ***P<0.001* (A,C).

As the *E.coli* K12 strain of bacteria used for killing assays is bioluminescent, luminometry was performed to determine the fold change in bioluminescence after infection of AAV-HBD3 transfected cells and control cells. There was no change in bioluminescent signal from the AAV HBD-3 transfected cells suggesting no bacterial growth, compared with a fold increase of 1.6 in bioluminescent signal in untransduced cells (*P=0.03*) (Figure 6.4C)

6.4. HBD-3 can be expressed *in vivo* following intravaginal application of AAV 8 HBD-3

HBD-3 expression was localised using HBD-3 immunofluorescence staining. Mature HBD-3 peptide was expressed in the upper layers of the vaginal and cervical epithelium of transduced mice (Figure 6.5). HBD-3 and GFP expression co-localised as expected and expression was confined to the upper epithelial cell layers, consistent with experiments in the previous chapter. There was no expression seen in control mice (data not shown).

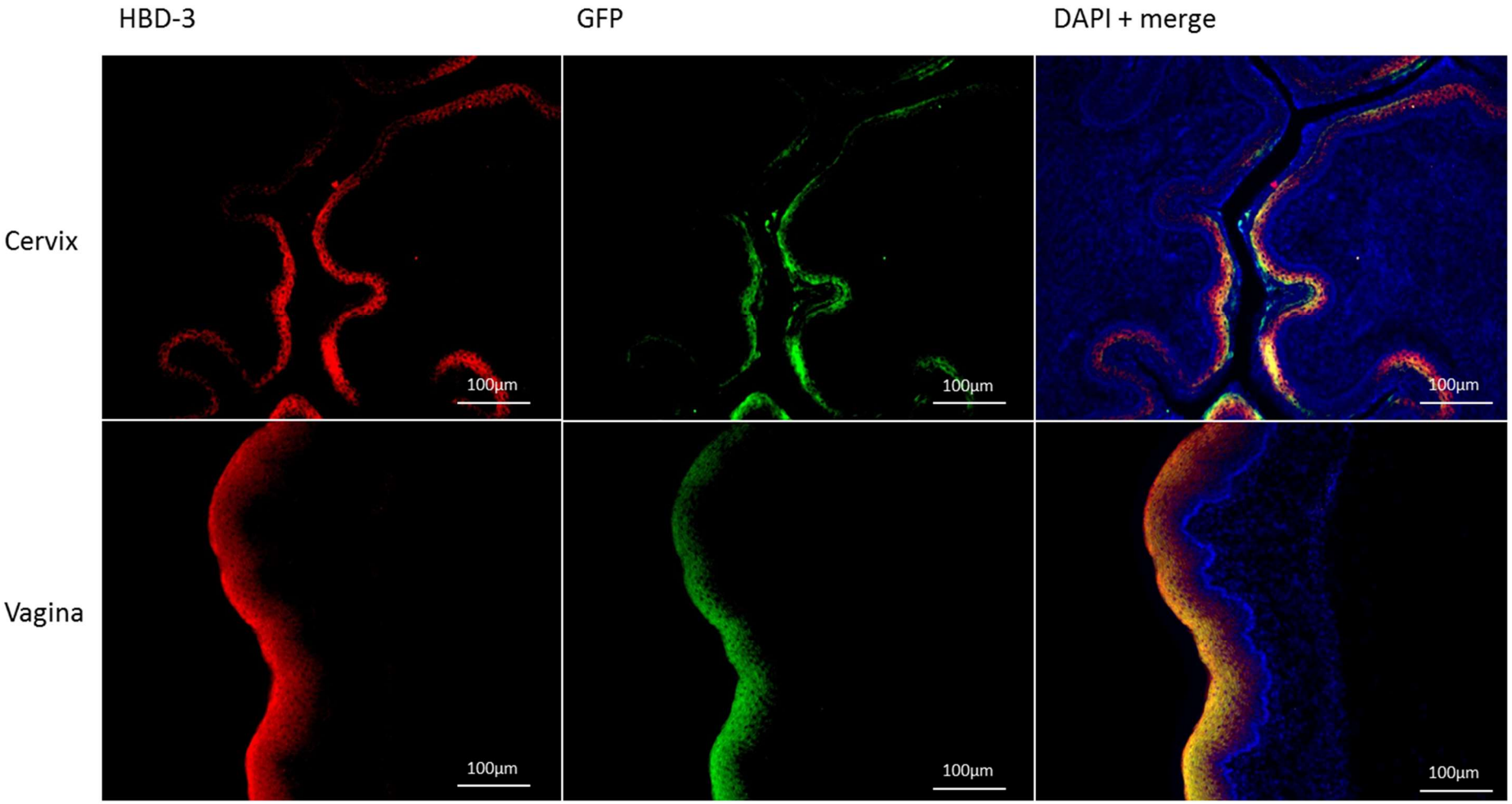

Figure 6.5: HBD-3 and GFP expression colocalised to the upper epithelial cell layers of the cervix and upper vagina of AAV HBD-3 transduced mice. Co-localisation immunofluorescence staining of cervix and upper vagina of AAV HBD-3 transduced mice. Organs were harvested 72 hours after vector administration. Untransduced controls showed no evidence of HBD-3 or GFP expression (sections not shown here).

6.5. HBD-3 is secreted into the vagina *in vivo*

Vaginal lavages were taken from mice 96 hours after transduction with AAV HBD-3 and from untransduced controls. There were increased levels of HBD-3 detected in vaginal lavages of AAV HBD-3 transduced mice, compared with controls (*P=0.04*) (Figure 6.6).

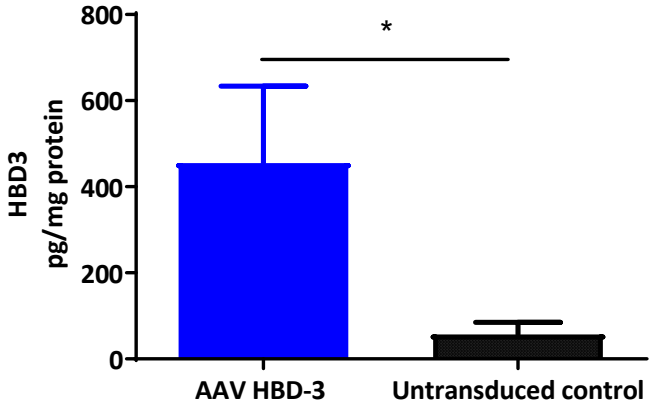

Figure 6.6: HBD-3 was detected in the vaginal lavage of AAV HBD-3 transduced mice. Vaginal lavages were taken from mice 96 hours after transduction with AAV HBD-3 and from untransduced controls. n=3; data analysed with an unpaired t-test, **P<0.05*.

6.6. Vaginal lavages from AAV HBD-3 transduced mice do not kill *E.coli* K12 or *E.coli* K1 *ex vivo*

Vaginal lavages were taken from mice 96-120 hours after transduction with AAV-HBD3, AAV-GFP and PBS. Unexpectedly, there was no difference in the *E.coli* K12 and *E.coli* K1 killing capability between the three groups (*P=0.06* and *P=0.66* respectively) (Figure 6.7).

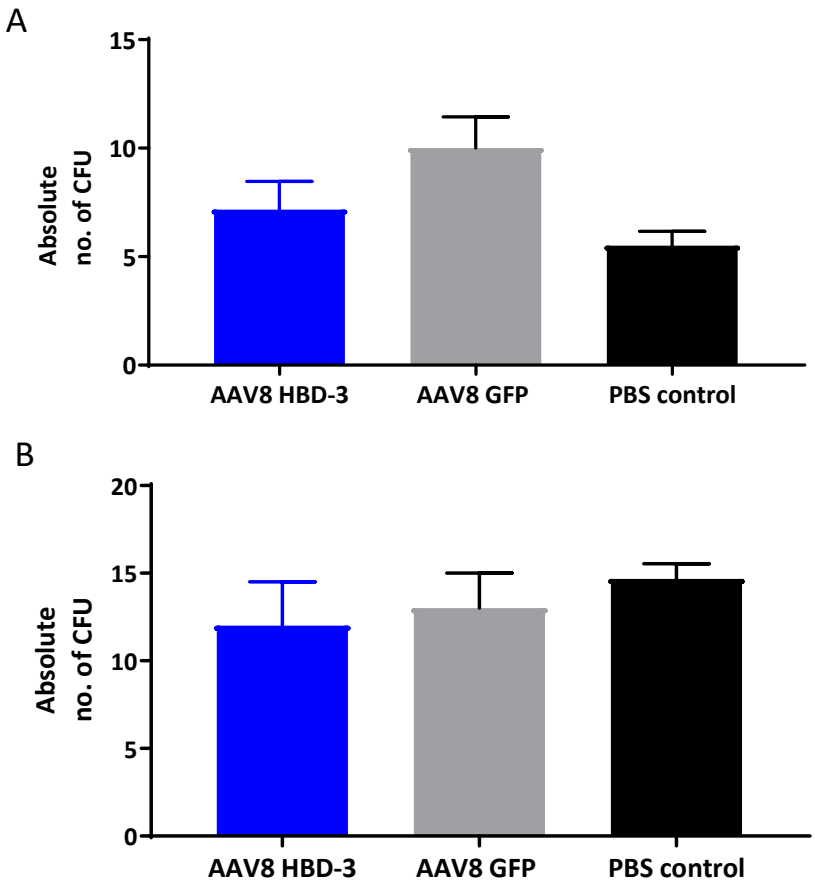

Figure 6.7: Vaginal lavages from AAV HBD-3 transduced mice do not kill *E.coli* K12 or *E.coli* K1 ex vivo. (A) E.*coli* K12 killing assays were performed with vaginal lavage from AAV8 HBD-3, AAV8 GFP and untransduced mice. There is no difference between the three groups. **(B)** *E.coli* K1 killing assays performed with vaginal lavage from AAV8 HBD-3, AAV8 GFP and untransduced mice. There is no difference between the three groups. n=5; data not normally distributed therefore analysed with a Kruskal-Wallis test with post hoc Dunn's test.

6.7. AAV HBD-3 induces an influx of neutrophils into the cervical epithelium within 72 hours after transduction

Cervices were harvested 72 hours after administration of AAV HBD-3, AAV GFP, *E.coli* K12 and PBS. They were stained for anti-Ly6g, a neutrophil surface marker, to determine neutrophil influx into the cervical epithelium and sub-epithelial stroma. There was an increase in neutrophils into the cervical epithelium 72 hours after AAV8 HBD-3 administration, compared with AAV8 GFP (*P=0.0077*), E.coli K12 (*P=0.0074*) and PBS (*P=0.016*) (Figure 6.8A). There was no difference in the number of neutrophils in the cervical stromal layer between the four groups (Figure 6.8B).

Macrophage influx, determined by CD68 immunohistochemistry, was also assessed but expression was minimal (≤ 1/section) in the cervix of all the groups so the data was not analysed. There was no obvious difference between the groups.

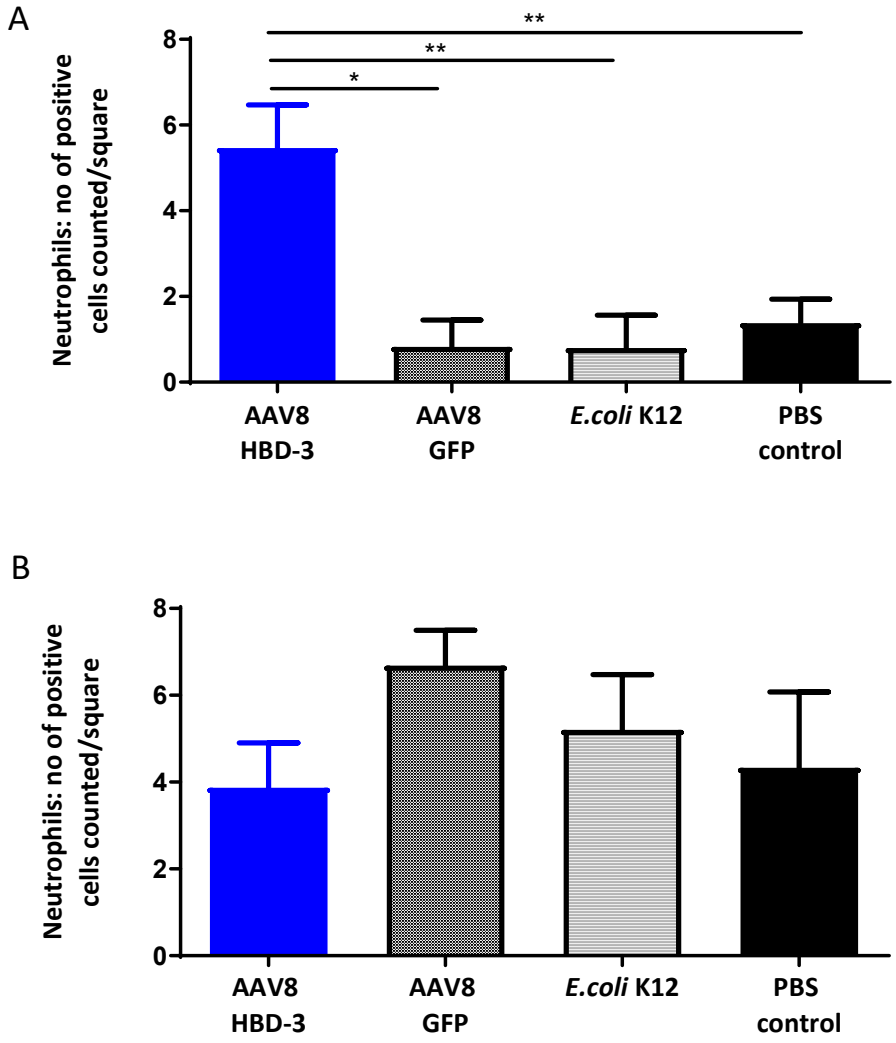

Figure 6.8: AAV HBD-3 induces an influx of neutrophils into the cervical epithelium within 72 hours after transduction. (A) Neutrophil influx into the cervical epithelium. There is an increase in neutrophils seen in the cervical epithelium 72 hours after administration of AAV HBD-3. **(B)** Neutrophil influx into the cervical sub-epithelial stroma**.** There is no difference in neutrophils seen in the cervical sub-epithelial stroma between the groups. n=3; data analysed with a one way ANOVA with post hoc Bonferroni test, **P<0.05*, ***P<0.01*.

6.8. There is a non-significant reduction in *Defb14* mRNA expression in cervices transduced by AAV HBD-3

qPCR was performed on cDNA obtained from cervices of AAV HBD-3 administered mice and AAV GFP administered control mice to detect inflammatory cytokine gene expression, as well as mouse β-defensin 14 gene (*Defb14*) which is the mouse orthologue of HBD-3 (Figure 6.9).

There is a non-significant trend of reduced expression of *Defb14* (4.2-fold), *Il1b* (2.5-fold) and *Tnf*a (1.7-fold) in AAV HBD-3 cervices, compared with controls. There was a non-significant trend of increased expression of *Il6* (1.96-fold) in AAV HBD-3 cervices, compared with controls.

6.9. Vector transduction is confined to the vagina and cervix in pregnant mice

Copy numbers of the HBD-3 gene were determined in the cervix of pregnant mice 96 hours after transduction with AAV HBD-3 (mean=3570 GC/µg cDNA). Negligible levels (below the limit of detection) were found in the uterus, placenta, ovaries, liver, spleen and fetal organs of AAV HBD-3 transduced mice (n=3), as well as in AAV8 GFP transduced control cervices (n=3).

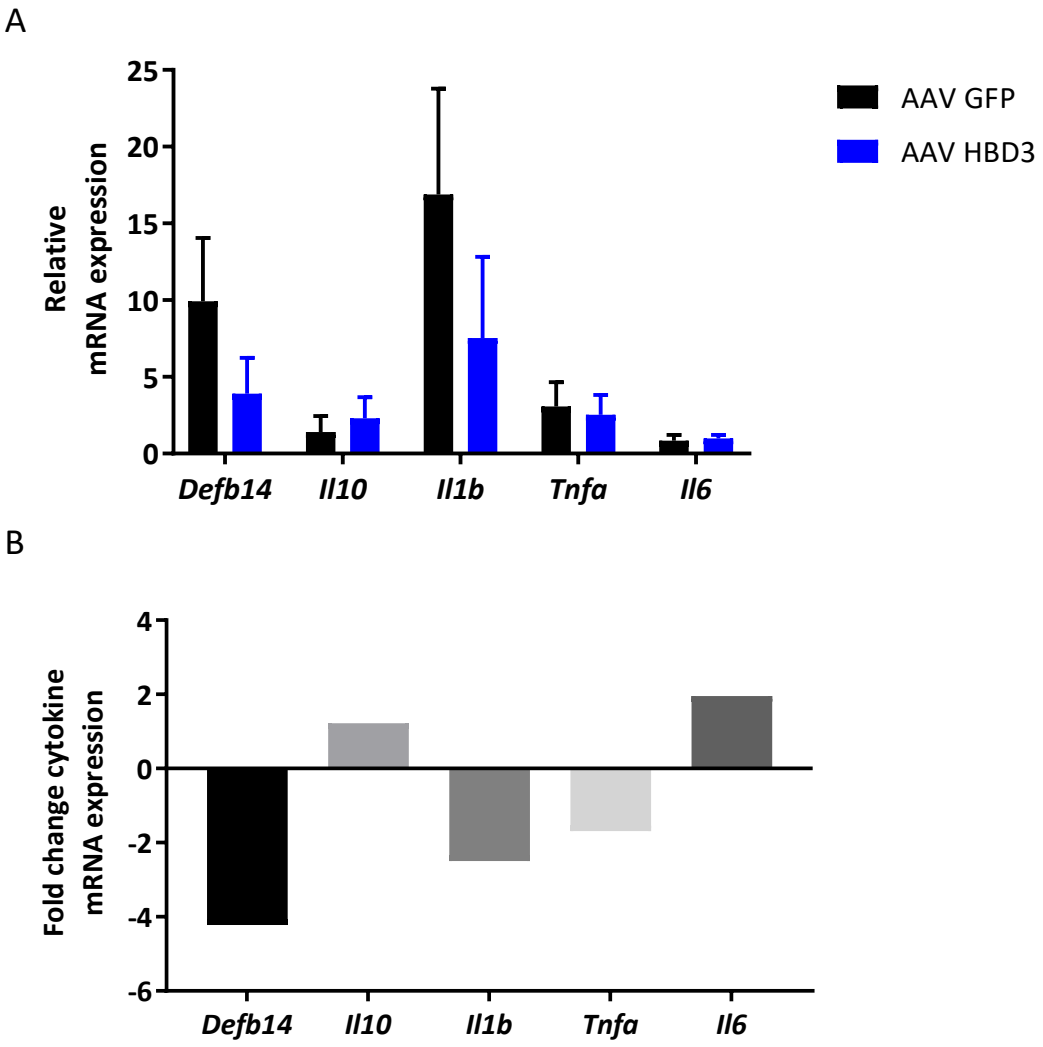

Figure 6.9: There is a non-significant reduction in *Defb14* mRNA expression in cervices transduced by AAV HBD-3. (A) Relative mRNA expression was determined in AAV HBD3 and AAV GFP cervices. n=6; data shown as $2^{-\Delta CT}$ data and analysed by two-way ANOVA with post hoc Bonferroni tests **(B)** Fold change in mRNA expression from AAV HBD-3 cervices compared with AAV GFP cervices**.** There is a non-significant reduction in *defb14* (4.2-fold), *Il1b* (2.5-fold) and *Tnfa* (1.7-fold) expression, whilst there is a non-significant increase in *Il6* (1.96-fold), compared with AAV8 GFP controls. n=6; data shown here as fold change (using the $2^{-\Delta\Delta CT}$ equation).

6.10. Vaginal microbiome studies

6.10.1. There is no difference in the diversity of bacterial species found in the vagina after administration of AAV HBD-3

Vaginal lavage samples were taken pre- and post- administration of AAV HBD-3, AAV GFP and PBS for 16s rDNA next generation sequencing. Species diversity within the vaginal microbiome of each group was calculated using the Shannon's diversity index (Figure 6.10). This diversity index describes the number of species within a microbial community as well as the abundance of those species. The post-administration groups contained pooled data from samples collected at 48 hours and 1 week after administration of vector or PBS. The data had to be pooled because the low bacterial load in the murine vagina meant that some samples had insufficient bacterial DNA for successful sequencing at all of the time points.

There was no difference in the pre- and post-administration indices for each group as well as no difference between groups (Figure 6.10A). Looking specifically at AAV HBD3 Shannon's entropy using unpooled post-administration data, we found no difference in the bacterial species diversity index following AAV HBD-3 administration (Figure 6.10B).

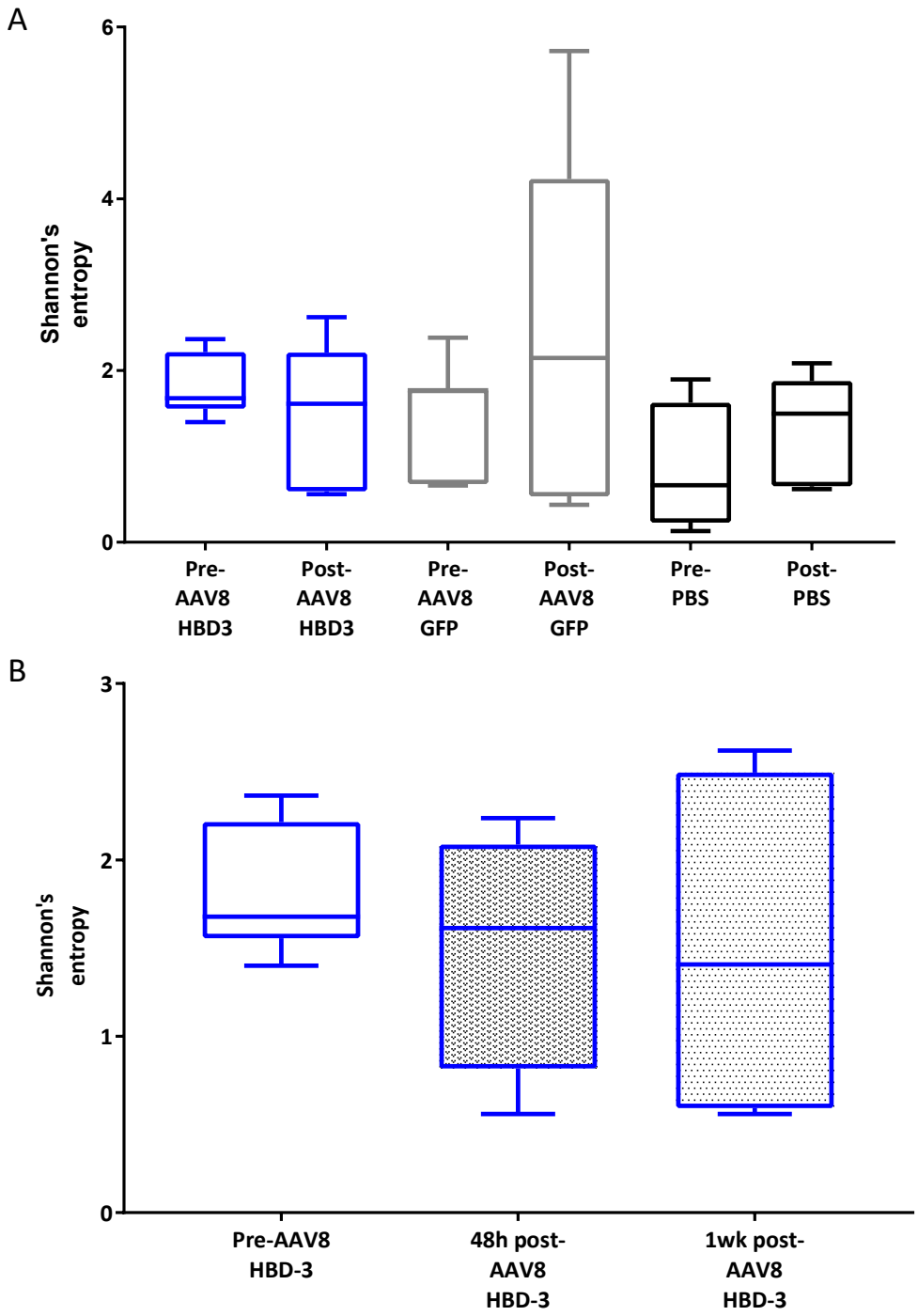

Figure 6.10: There is no difference in the diversity of bacterial species found in the vagina after administration of AAV HBD-3. (A) Shannon's entropy of the vaginal microbiome pre- and post-administration of AAV HBD3, AAV GFP and PBS. Post-administration samples were taken at 48 hours and 1 week, data is pooled here. (B) Shannon's entropy of vaginal microbiome before administration and following administration of AAV HBD3. n=5; data analysed with one-way ANOVA.

9 bacterial phyla were identified in the samples, with Firmicutes and Proteobacteria being the two most abundant phyla (>0.5% abundance) (Figure 6.11). There was minimal variation between the AAV HBD-3 and AAV GFP groups, however, there did appear to be a higher proportion of Proteobacteria in the PBS control group at both time points studied. Furthermore, there was an non-significant increase in the proportion of Proteobacteria following administration of vector or PBS in all groups (*P=0.15*, *P=0.28* and *P=0.23*) (Figure 6.12A). The Gammaproteobacteria, in particular Enterobacteriales and Pseudomonadales, were responsible for this increase (Figure 6.12B), although the differences were not statistically significant (*P=0.15* and *P=0.1* respectively).

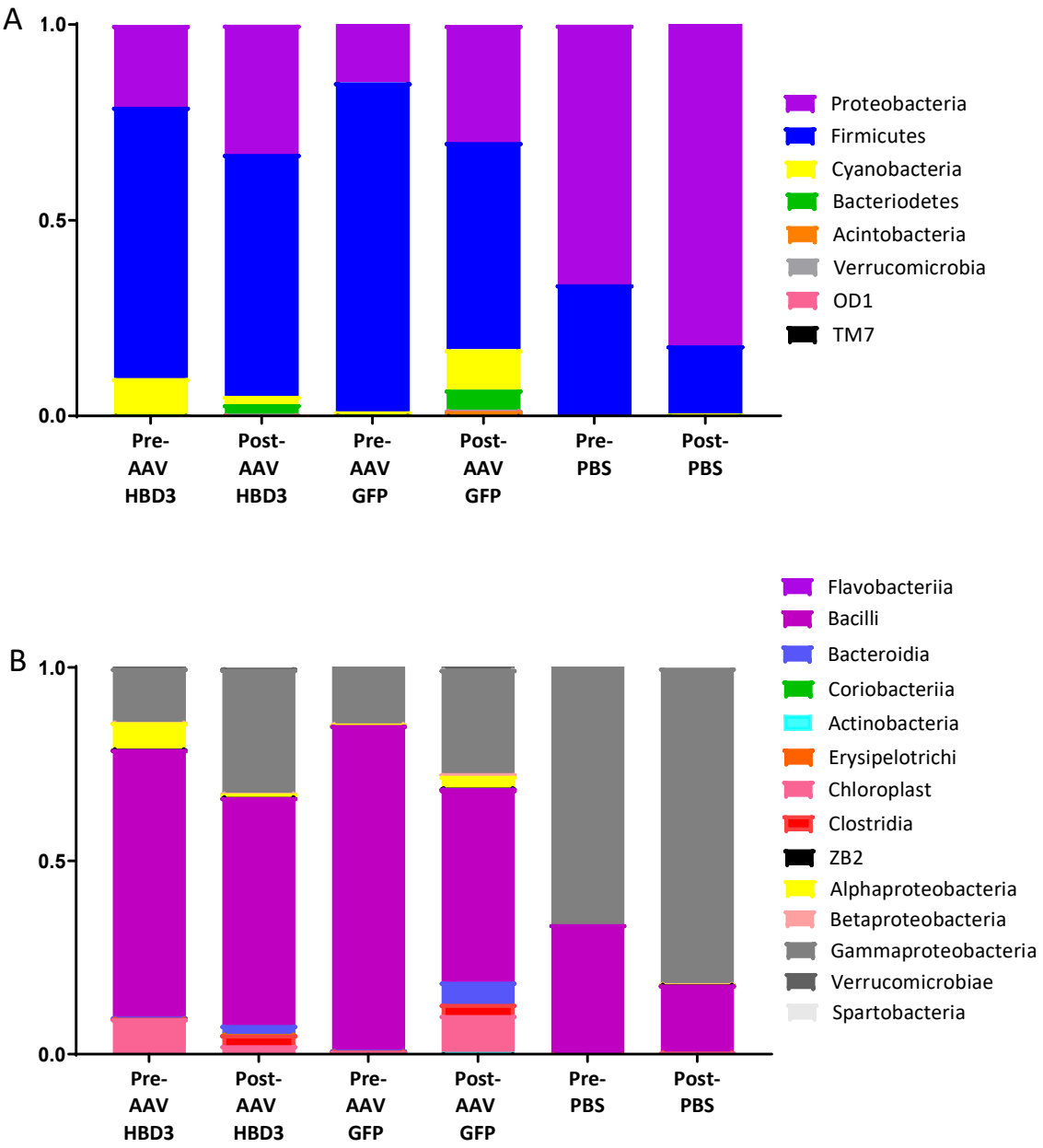

Figure 6.11: There is no difference in the proportion of bacterial classes and phyla between the AAV HBD-3, AAV GFP and PBS treated. (A) Proportion of bacterial classes within each group. There are no obvious differences in bacterial class between the vector groups, however there is a larger proportion of Gammaproteobacteria in the PBS controls at both time points. There also appears to be a increase in the proportion of Gammaproteobacteria after administration of vector or PBS. **(B)** Proportion of bacterial phyla within each group. There are no obvious differences in phyla between the vector groups, however there is a larger proportion of Proteobacteria in the PBS controls at both time points.

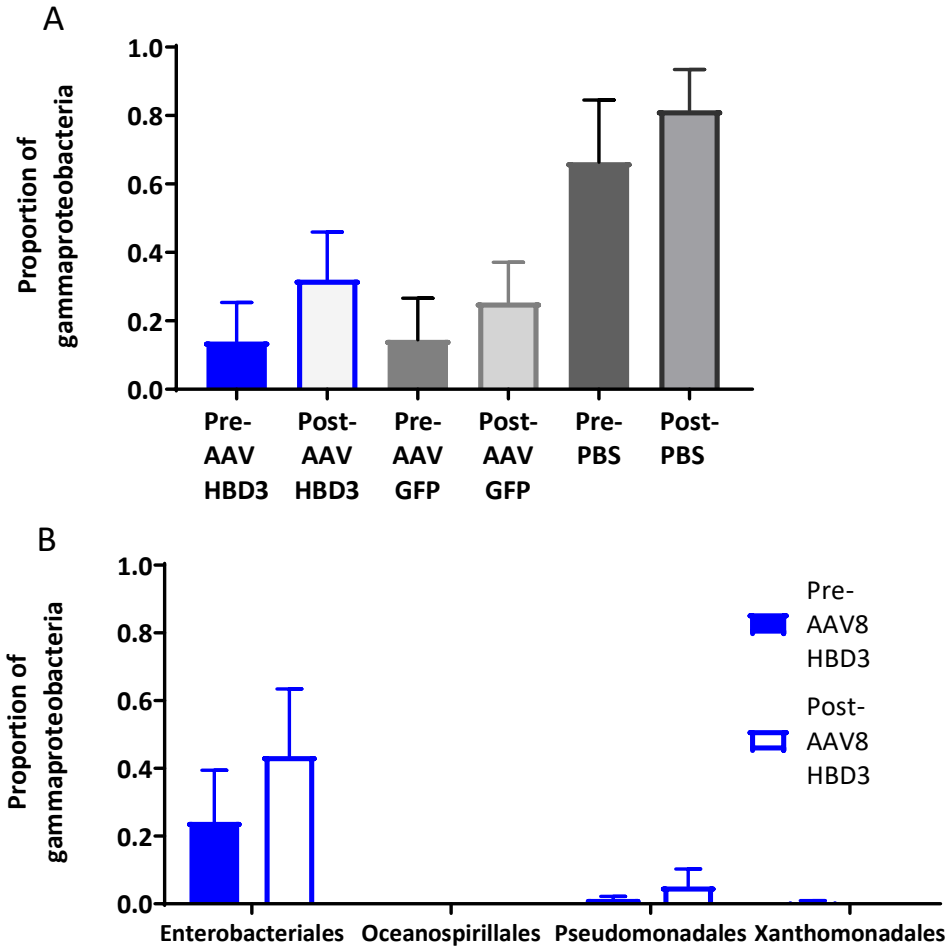

Figure 6.12: There is an increase proportion of Proteobacteria following administration of vector or PBS in all groups. (A) Proportion of Gammaproteobacteria pre- and post-administration of vector or PBS. There is an increase in proportions of gammaproteobacterial before and after administration of vector/PBS in all groups, although this was not significant. **(B)** Proportions of classes of Gammaproteobacteria pre- and post-administration of AAV HBD-3. There is an increase in proportions of Enterobacteriales and Pseudomonadales before and after administration of vector, although this was not significant. n=8, data arcsin transformed and analysed with unpaired t-tests.

6.10.2. *Lactobacillus* species are not reduced following AAV HBD-3 administration

During human pregnancy, the rise in oestrogen levels leads to a stable vaginal microbiome dominated by *Lactobacillus* species (MacIntyre et al. 2015; Romero et al. 2014). *Lactobacillus* species are thought to inhibit pathogen growth by secreting antimicrobial bacteriocins as well as producing lactic acid which helps to maintain a low, hostile pH (Borges et al. 2014). There is an association between *Lactobacillus* species depletion, vaginal dysbiosis and preterm birth (Hillier et al. 1995; DiGiulio et al. 2015; Kindinger et al. 2017). Therefore, the effect of AAV HBD3 on the proportion of *Lactobacillus* species was assessed at different time points before and after treatment (Figure 6.13). There is no significant difference between the proportion of lactobacilli species before and after administration of AAV HBD-3, suggesting that AAV HBD-3 treatment does not reduce lactobacilli species *in vivo* (*P=0.44*).

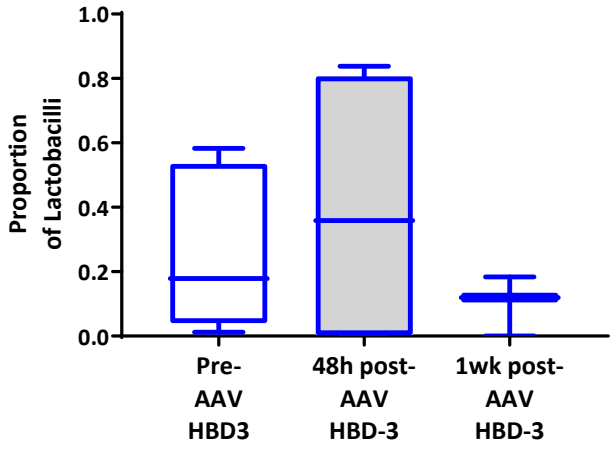

Figure 6.13: There is no difference in the proportion of *Lactobacillus* species before and after AAV HBD-3 administration. Proportion of *Lactobacillus* species pre- and post-administration of AAV HBD-3. n=6 pre-AAV group and n=4 both post AAV groups; data was arcsin transformed and analysed with a one-way ANOVA and post hoc Bonferroni test.

6.11. Discussion

This chapter shows that AAV8 HBD-3 can transduce murine cervical epithelium *in vivo* and produce peptide that is capable of inducing neutrophil influx. Furthermore, it shows that AAV8 HBD-3 treatment does not appear to have any deleterious effects on the vaginal microbiome.

HBD-3 detection

The detection of HBD-3 was initially problematic due to the small peptide size (5kDa) and instability, but lyophilisation and the use of acetic acid for lysis, rather than standard lysis buffers, helped to stabilise the peptide so that protein assays were much more reliable.

Transient transfection of the AAV HBD-3 plasmid in HEK 293-T cells resulted in overexpression of HBD-3 in supernatants and cell lysates (Figure 6.2). The HBD-3 in the supernatants was also functional leading to a dose-dependent killing of *E.coli*-K12 (Figure 6.4). Unexpectedly, even control supernatants exhibited detectable, albeit low, bactericidal activity. This could be due to endogenous AMP production from these cells or an antibacterial component in the cell media. There was also a significant reduction in *E.coli* K12 bioluminescence, signifying increased bacterial kill, in the *in vitro* killing assays (Figure 6.4C). A previously similar study in HBD-3 transfected keratinocytes did not show any difference in bacterial kill although bacterial kill was determined by plating and counting CFUs which may be less sensitive than the change in bioluminescence (Hirsch et al. 2009). Furthermore, they detected approximately 3 times less HBD-3 in their transfected supernatants which could also explain the difference in HBD-3 killing.

The upper vaginal and cervical epithelium expressed HBD-3 and GFP following *in vivo* AAV 8 HBD-3 administration (Figure 6.5). There was obvious GFP expression on direct fluorescence at 72 hours after intravaginal application. Interestingly, the expression seemed to be much more specific and localised to the cervical epithelium in the pregnant mouse on direct fluorescence, although HBD-3 immunohistochemistry was not performed in this study (images not shown).

Integrins are known to have a role in viral vector-endocytosis, specifically with the AAV 2 serotype and interestingly, certain integrins have been found to be upregulated in the pregnant mice cervix making them more susceptible to viral infection (Wickham et al. 1993; Kaminsky et al. 2012; Racicot et al. 2013). It is possible that the more specific cervical expression in the pregnant cervix may be mediated by this upregulation in integrins.

HBD-3 expression in the upper epithelial cell layers was detected using immunofluorescence (Figure 6.5). It is known that the HBD-3 gene encodes a pre-HBD-3 peptide which is cleaved by a signal peptidase prior to secretion to release the mature HBD-3 peptide (Beckloff et al. 2008). Quantification of HBD-3 protein in the vaginal lavage confirmed appropriate peptide processing and secretion in the mouse (Figure 6.6).

HBD-3 antimicrobial activity

E.coli killing assays performed with vaginal lavages collected in vivo from AAV8 HBD3 transduced mice showed no evidence of increased bacterial kill compared with AAV8 GFP controls (Figure 6.7). This result is unexpected and in contrast to the *in vitro E.coli* killing assays. It is possible that this is due to the lower concentrations of HBD-3 detected in lavage samples compared with lyophilized cell supernatants. Furthermore, lavage was performed with PBS, and although HBD-3 is known to be the least salt sensitive it is possible that storage in PBS may modify protein charge and therefore have a deleterious effect on its antimicrobial function (Harder et al. 2001; Klüver et al. 2005).

Immunomodulatory role of HBD-3

Emerging evidence suggests that human beta-defensins have a much more complex role in the immune system than just being natural antimicrobials. Human beta-defensins have the ability to chemoattract numerous immune cells, such as neutrophils, macrophages and dendritic cells (Niyonsaba et al. 2004; García et al. 2001). Following AAV8 HBD-3 administration *in vivo*,

neutrophils are recruited to the upper epithelial cell layers of the cervix (Figure 6.8). Neutrophils are critical effector cells of the innate and acquired immune system and are part of the first line of defence against microorganisms. Human beta defensin-2 has been shown to attract neutrophils via the G-protein phospholipase C-dependent pathway (Niyonsaba et al. 2004). The CCR6 receptor appears to be involved in activation of this pathway; HBD-3 and mouse beta-defensin 14 (mouse orthologue of HBD-3) are chemotactic for mouse CCR6-expression HEK 293 cells *in vitro* (Röhrl et al. 2008; Wu et al. 2003). Furthermore, the cysteine residues of the three disulphide bridge structure of HBD-3 appear to be necessary for this chemotactic role (Wu et al. 2003; Taylor et al. 2008). In addition to its chemotactic role, HBD-3 can prolong the lifespan of neutrophils at sites of infection by preventing apoptosis (Nagaoka et al. 2012; Nagaoka et al. 2008). This mechanism may also be contributing to the increased cervical neutrophil numbers seen here and exert an advantageous effect on cervical mucosal defence against bacterial infection.

Minimal macrophage influx into cervix was detected using CD-68 immunohistochemistry after vector administration in this study. This is not consistent with other studies that show HBD-3 to be a potent monocyte chemoattractor (García et al. 2001; Funderburg et al. 2007), although these studies were performed *in vitro*. It is possible that this time point (72 hours after vector administration) was too early to detect macrophage influx or alternatively, that HBD-3 expression in the murine cervix does not induce the same macrophage chemoattractant function that is seen *in vitro*.

HBD-3 was previously considered to be pro-inflammatory as its expression increases following TLR activation or IL-1β, TNF-α, IFN-ϒ release (Harder et al. 2001; García et al. 2001), however emerging data is recognising it more as a multifunctional effector of the immune system (Semple et al. 2011). It is possible that, similar to LL-37, HBD-3 may induce a strong chemoattractant and inflammatory response at high concentrations during infection and injury to respond to the

insult whilst at lower concentrations it has more of an anti-inflammatory, healing role (Scott et al. 2002). Interestingly, we show a trend towards reduced mRNA levels of *Defb14* (the gene for mBD14, the mouse orthologue of HBD-3) in the AAV8 HBD-3 treated cervices suggesting that HBD-3 may be involved in a negative feedback loop suppressing *Defb14* expression (Figure 6.9). *Il1b* and *Tnfa* also show a trend towards reduced expression in the AAV8 HBD-3 treated cervices, consistent with *in vitro* data (Semple et al. 2010; Semple et al. 2011). It would be interesting to determine expression of these genes following intravaginal infection as I hypothesise that the presence of bacteria or LPS would induce a significant pro-inflammatory cytokine response and possibly block this proposed negative feedback loop. In support of this, recent data has found that HBD-3 significantly augments the inflammatory response to bacterial DNA in human and mice cells via TLR-9 (McGlasson et al. 2017).

HBD-3 and the vaginal microbiome

Mice treated with AAV8 HBD-3 did not have an obvious effect on the vaginal microbiota compared with AAV8 GFP or PBS treated mice (Figure 6.10 & Figure 6.11). Furthermore, AAV8 HBD-3 does not appear to modify *Lactobacillus* species abundance in the vagina (Figure 6.12). These results are reassuring for clinical translation as the vaginal microbiota composition appears to be closely associated with preterm birth outcome (Kindinger et al. 2017). Very little data has been published on the mouse vaginal microbiome but vaginal bacterial phyla abundance appears consistent with the data presented here (Barfod et al. 2013; Jašarević et al. 2015). For further studies, it would be important to perform species-specific lactobacillus 16S qPCR to confirm the above findings. In support of these findings, HBD-3 does not exhibit antibacterial activity against lactic acid bacteria, including *L.rhamnosus*, suggesting that these bacteria may exhibit factors that protect them from host immune defence (Wang et al. 2015). Recent data has shown an association between an *L.iners*-dominant vaginal microbiome and an increased risk of preterm birth, whilst *L.crispatus*-dominance appears to be protective

(Kindinger et al. 2017). *L.crispatus* promotes epithelial cell defence against *Candida albicans in vitro* by increasing human beta defensin levels, in particular HBD-3 (Rizzo et al. 2013). This finding may play a role in linking the mechanism of *L.crispatus* dominant vaginal microbiome with its protective effect on preterm birth. It also importantly supports the clinical translation of the preventative therapy developed in this study.

The microbiome experiments did show evidence of increased abundance of Enterobacteriaceae following administration of either vector or PBS. It is possible that repeated vaginal lavage may have a damaging effect on the mucosa allowing colonisation of Enterobacteriaceae bacteria (which includes *E.coli*). Alternatively, repeated exposure to the animal house operating room, where *E.coli* is used for other experiments, may increase the risk of *E.coli* colonisation.

These experiments were limited by the fact that only small amounts of bacterial DNA were detected from vaginal lavage samples. This meant that, despite collecting samples at multiple time points, we were unable to create a sufficient library to sequence all the samples collected. Furthermore, these experiments were performed in non-pregnant mice resulting in a small risk of microbiome fluctuation due to hormonal changes in the estrous cycle. Variations in the vaginal microbiome, however, have only been shown in humans as a result of the hormonal fluctuations during the menstrual cycle and these hormonal changes may not have an effect on the much shorter rodent estrous cycle (Gajer et al. 2012; MacIntyre et al. 2015). Vaginal lavage samples from untreated pregnant mice were also sequenced to determine if there was much variation in vaginal bacterial communities between pregnant and non-pregnant mice and we reassuringly found similar bacterial abundance in these samples meaning that the non-pregnant data is likely to be translatable. These experiments were not designed to infer associative links between the mouse and human vaginal microbiome but as a means of determining treatment effects. Therefore, for future clinical translation studies of AAV8 HBD-3 it would be necessary to

perform *in vitro* experiments to determine the antimicrobial activity of HBD-3 on the *Lactobacillus* species commonly found in the pregnant human vaginal microbiome.

In conclusion, this chapter shows that it is possible to transduce cervical and upper vaginal epithelium of a mouse with AAV8 HBD-3 and this produces functional HBD-3 peptide which does not appear to have a deleterious effect on the commensal bacteria present in the mouse vagina.

Chapter 7 Cervical gene delivery of Human beta-defensin 3 for the prevention of ascending vaginal infection in pregnancy

7.1. Summary

This chapter assesses the effects of a cervical gene therapy, described in the previous chapter, on the models of ascending vaginal infection and preterm birth developed in Results Chapter 3 and Chapter 4. It tests the hypothesis that gene delivery of HBD-3 using an AAV8 viral vector can reduce bacterial ascent into the uterus and prolong gestation at delivery as well as improving pup survival and outcomes. This chapter focuses on pregnant mice but data from the experiments performed in non-pregnant mice can be found in the Appendix (10.7).

In this chapter, I show that there is a significant reduction in bacterial ascent into the pregnant uterus of both non-pathogenic *E.coli* K12 and a pathogenic *E.coli* K1 strain following AAV HBD3 treatment. Gestation was not prolonged in the AAV HBD3 treated dams following *E.coli* K1 administration but there was a statistically significant increase in the proportion of pups born alive.

7.1.1. Pregnant mice: Experimental plan

To assess the effect of cervical overexpression of HBD-3 on ascending vaginal infection in pregnant mice, AAV HBD3 was administered on embryonic day 13.5 and then 72 hours later on embryonic day 16.5 intravaginal *E.coli* K12 or *E.coli* K1 was injected (Figure 7.1).

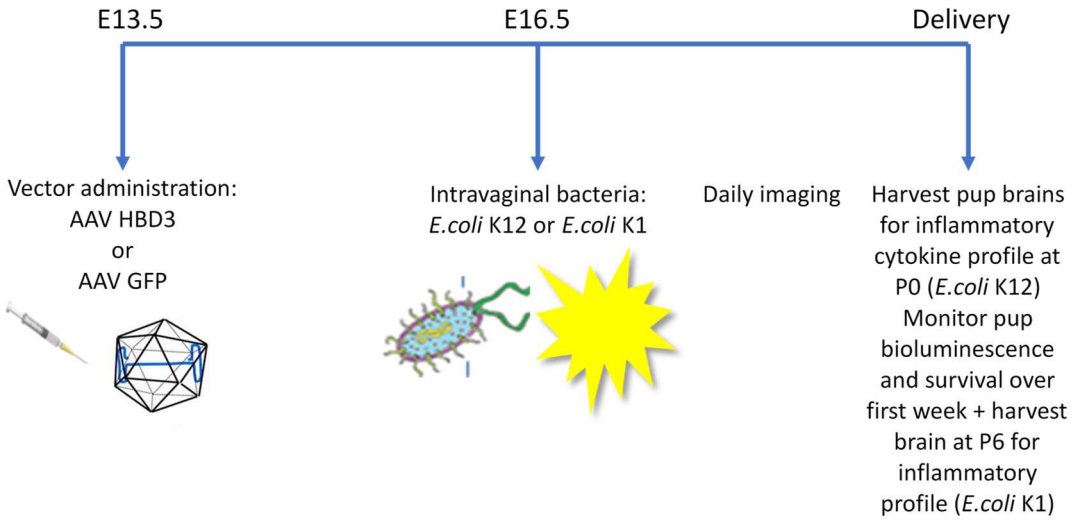

Figure 7.1: Summary of experimental plan for determining the effect of HBD-3 expression on intravaginal *E.coli* K12 or E.*coli* K1 infection in pregnant mice.

7.2. Non-pathogenic *E.coli* K12

7.2.1. HBD-3 reduces *E.coli* K12 bacterial ascent into the uterus of pregnant mice

There is a smaller increase in uterine bioluminescence in the AAV HBD3 dams compared with the AAV GFP control dams (overall *P=0.014*) (Figure 7.2). This was significant at 48 hours after bacterial administration (*P=0.03*), implying less bacterial ascent into the uterine cavity in the AAV HBD3 dams.

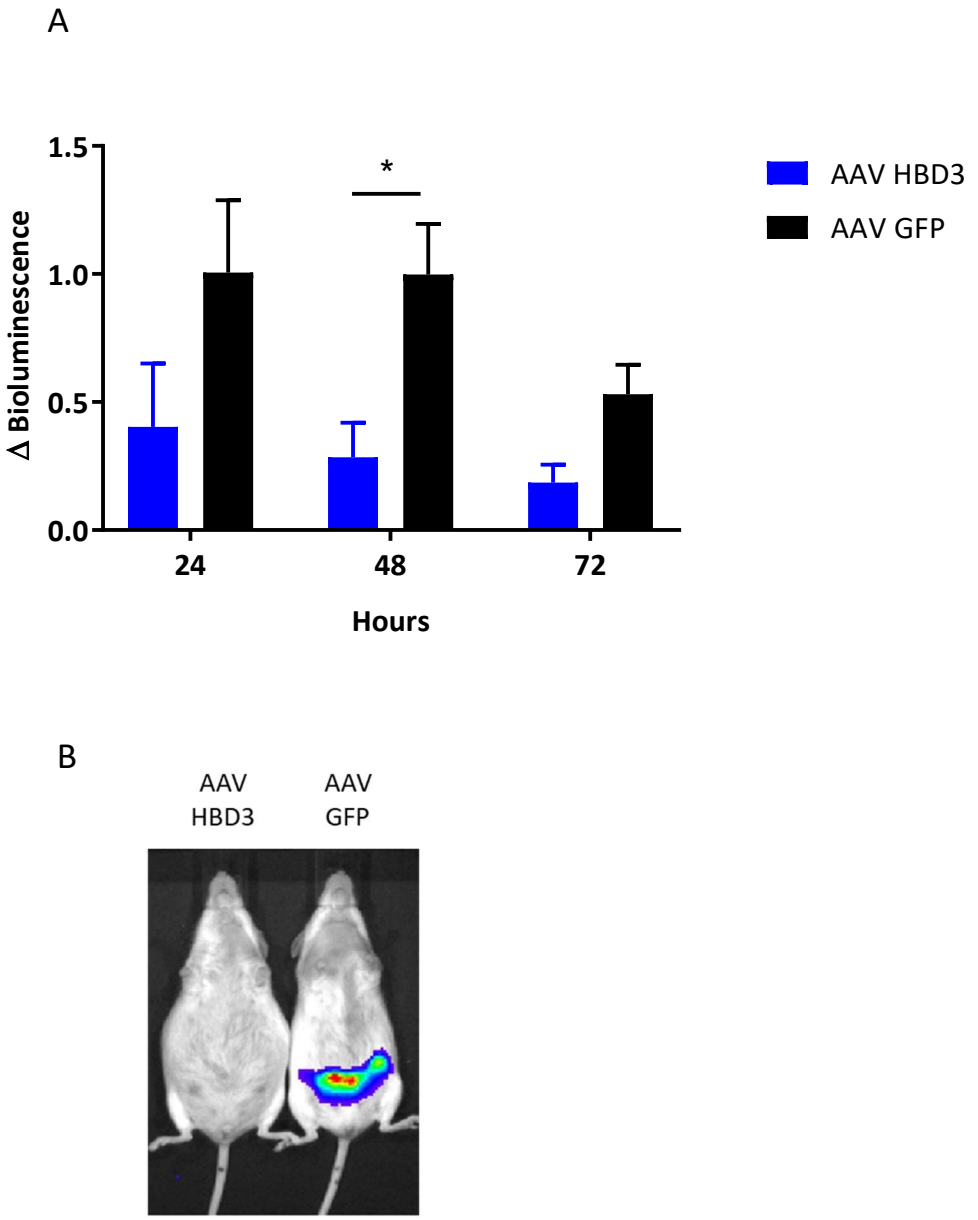

Figure 7.2: AAV HBD-3 treated dams have reduced *E.coli* K12 bacterial ascent into the uterus at 48 hours after infection. (A) Fold change in *E.coli* K12 bioluminescence over time (log transformed data shown). n=12; data log transformed and analysed with a repeated measures two-way ANOVA with post hoc Bonferroni test, *P<0.05. **(B)** Representative images at 48 hours after *E.coli* K12 infection in an AAV HBD3 and AAV GFP treated dam.

7.2.2. There is no difference in gestation at delivery or litter size between the AAV HBD3 and AAV GFP treated *E.coli* K12-infected dams

There was no difference between the gestation at the time delivery of the litter between all groups (P=0.23) (Figure 7.3A). Although there was an outlier in the AAV HBD3 group that delivered prematurely on embryonic day 17.5. This dam did not have increased bioluminescence (implying greater bacterial infection), compared with the other dams but did look systemically unwell so I suspect this was an incidental finding. The number of pups in each litter was comparable between the groups (P=0.6) (Figure 7.3B).

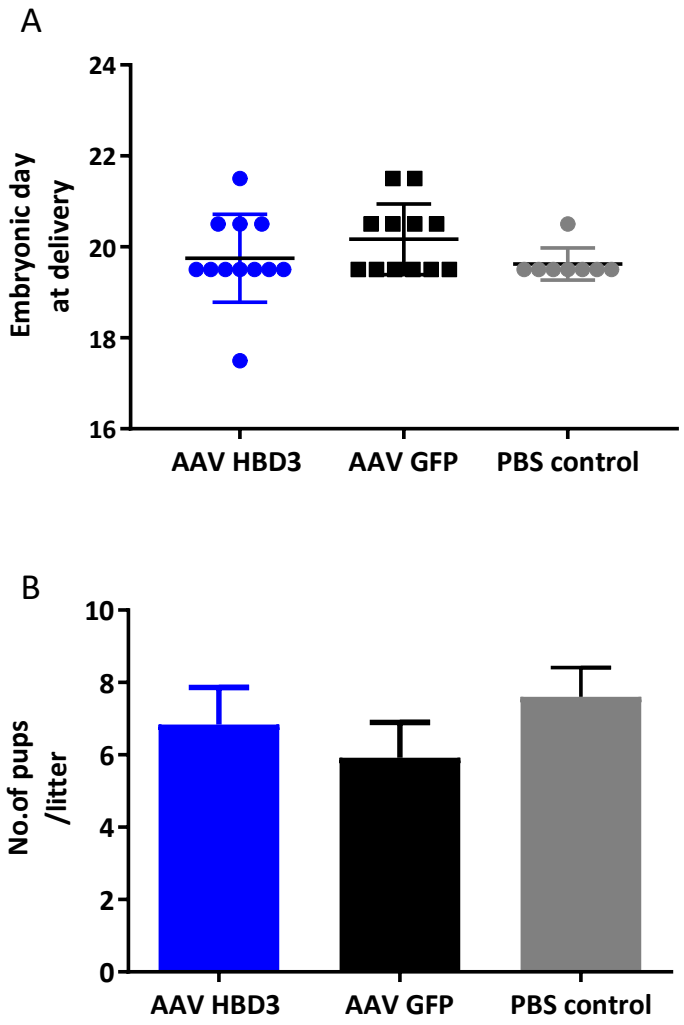

Figure 7.3: There is no difference in gestation at delivery or the number of pups in the littter between the AAV HBD3, AAV GFP and PBS control dams. (A) The gestation on the day of delivery between the groups. n=12 in AAV HBD3 and AAV GFP groups, n=8 in the PBS control group; data not normally distributed therefore, analysed with a Kruskal-Wallis test with post hoc Dunn's test. **(B)** The number of pups per litter from AAV HBD3, AAV GFP and PBS control dams. The litter size is comparable between the groups. n=12 in AAV HBD3 and AAV GFP groups, n=8 in the PBS control group; data not normally distributed, therefore analysed with a Kruskal-Wallis test with post hoc Dunn's test.

7.2.3. There is a non-significant increase in pro-inflammatory cytokines in the neonatal brains of pups from AAV GFP *E.coli* K12-infected control dams

Brains were harvested from pups on the day of birth of AAV HBD-3 and AAV GFP treated dams. These were analysed for pro-inflammatory cytokines; IL-1β, TNF-α and IL-6. There was no statistical difference in brain pro-inflammatory cytokine levels between the two groups, although there was a trend for increased inflammatory cytokine levels in AAV GFP treated dams (IL-1β, TNF-α and IL-6: *P=0.4*, *P=0.23* and *P=0.11* respectively) (Figure 7.4).

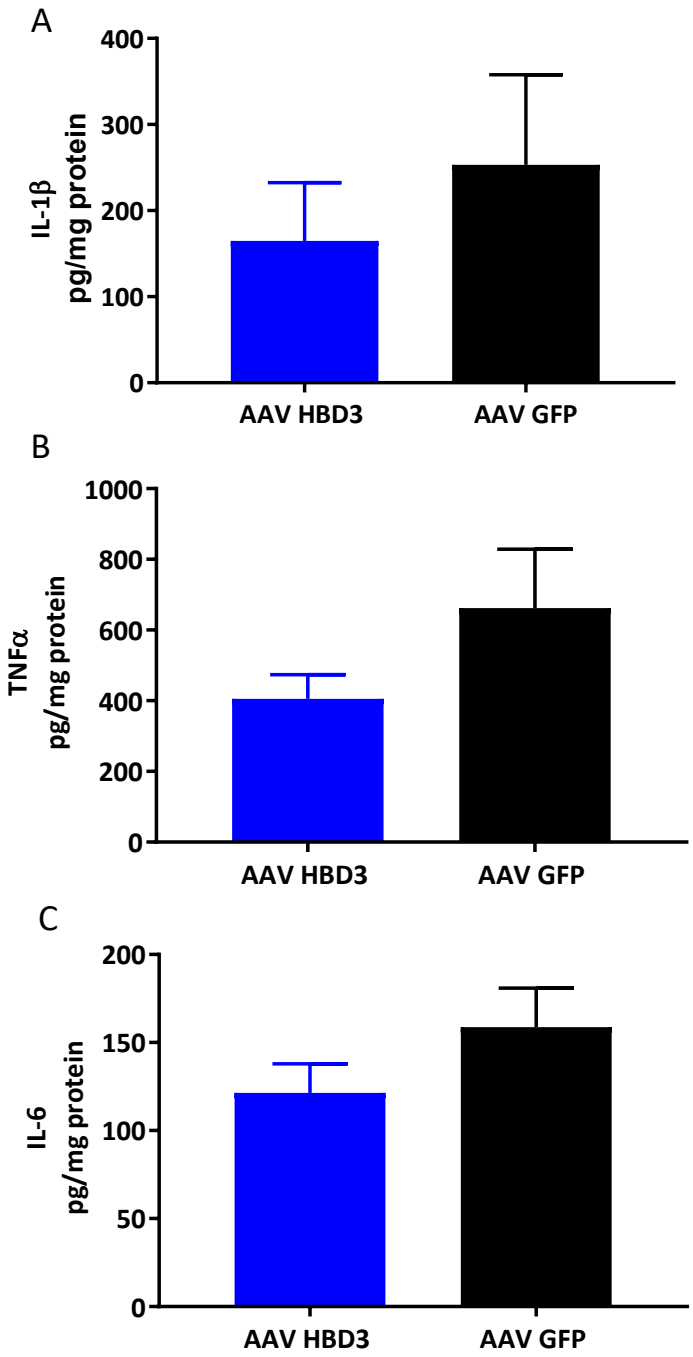

Figure 7.4: There is a non-significant increase in inflammatory cytokines in the pup brains from AAV GFP control dams, compared with pup brains from AAV HBD3 dams. (A) IL-1β brain levels in the brains from the newborn pups of AAV HBD3 and AAV GFP dams. **(B)** TNF-α brain levels in the brains from the newborn pups of AAV HBD3 and AAV GFP dams. **(C)** IL-6 brain levels in the brains from the newborn pups of AAV HBD3 and AAV GFP dams. n=12 from AAV GFP pups, n=18 from AAV HBD3 pups (from ≥ 3 dams); data not normally distributed therefore analysed by Mann Whitney rank test.

7.3. Pathogenic *E.coli* K1

7.4. *E.coli* K1: High CFU dose ($2x10^3$)

7.4.1. HBD-3 does not reduce high-dose *E.coli* K1 bacterial ascent into the uterus of pregnant mice

E.coli K1 was administered intravaginally on embryonic day 16.5 and pregnant mice were imaged daily until delivery. The bioluminescent signal from the uterus is similar between AAV HBD3 and AAV GFP treated groups, implying that AAV HBD3 does not reduce bacterial ascent into the uterus in these mice (Figure 7.5A). Confirming this, there is no difference in the fold change in uterine bioluminescence between the two groups (*P=0.47*) (Figure 7.5B).

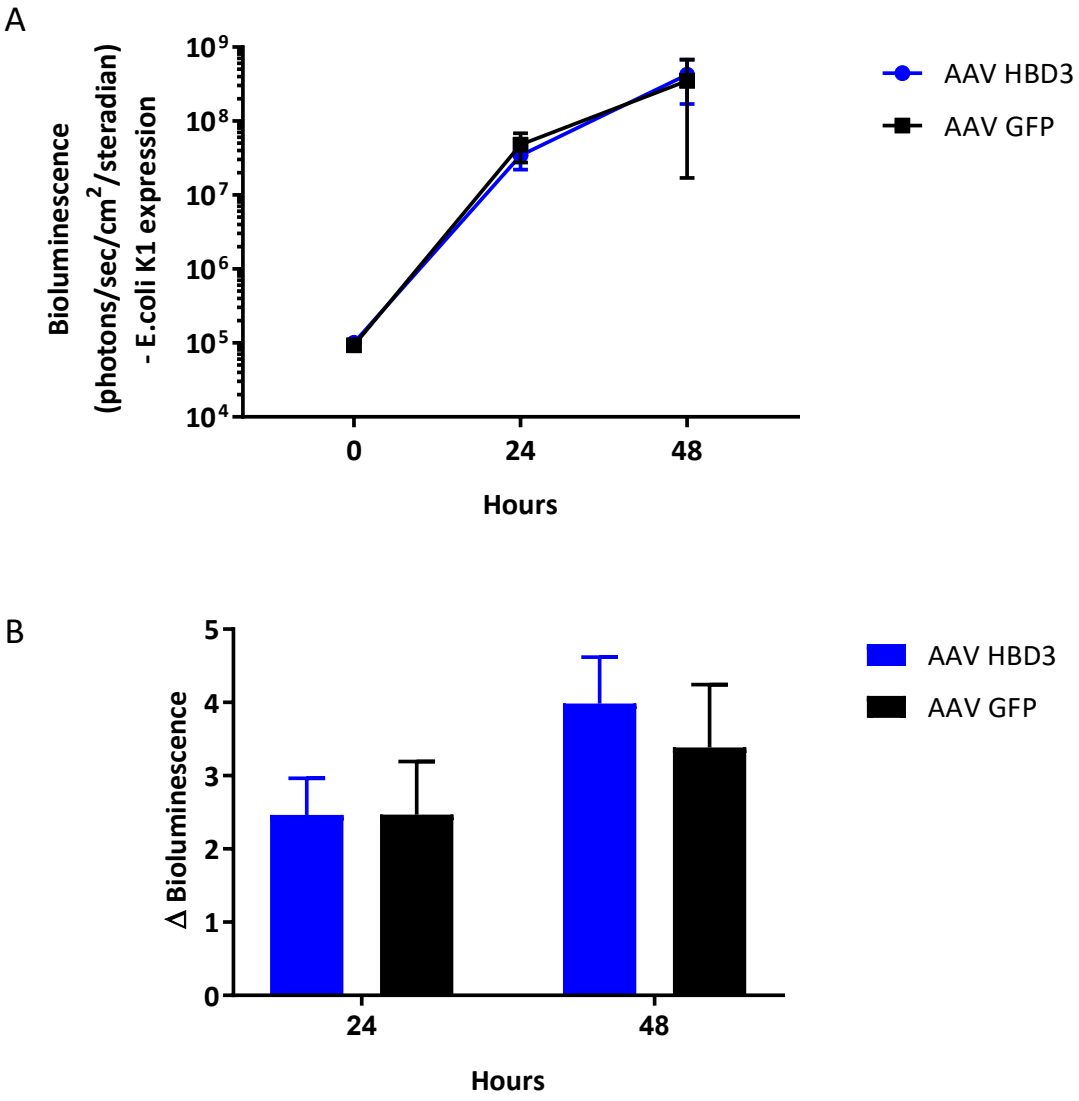

Figure 7.5: AAV HBD3 does not reduce high-dose *E.coli* K1 bacterial ascent into the uterus of pregnant mice. (A) Bioluminescence from the uterus of pregnant dams treated with AAV HBD3 or AAV GFP after administration of intravaginal *E.coli* K1. **(B)** Fold change in uterine *E.coli* K1 bioluminescence over time (log transformed data shown). There is no difference in the fold change in bioluminescence at 24 and 48 hours after bacterial administration between the two groups. n=4 in the AAV GFP group, n=5 in the AAV HBD3 group; data log transformed and analysed with a repeated measures two-way ANOVA with post hoc Bonferroni test.

7.4.2. AAV HBD3 treatment does not increase gestation length or increase the proportion of pups born alive following high dose *E.coli* K1 administration

The time of delivery of the first pup was determined following bacterial administration in the AAV HBD3 and AAV GFP groups and following PBS administration in the uninfected control. There is no increase in gestation length in the AAV HBD3 infected dams compared with the AAV GFP infected dams (*P=0.46*) (Figure 7.6A). The gestation length difference between *E.coli* K1 infected- AAV HBD3 or AAV GFP groups, and uninfected controls remains statistically significant (*P=0.02* and *P=0.0008* respectively). The proportions of pups born alive were determined in both AAV HBD3 and AAV GFP groups and were found to be no different (*P=0.48*) (Figure 7.6B).

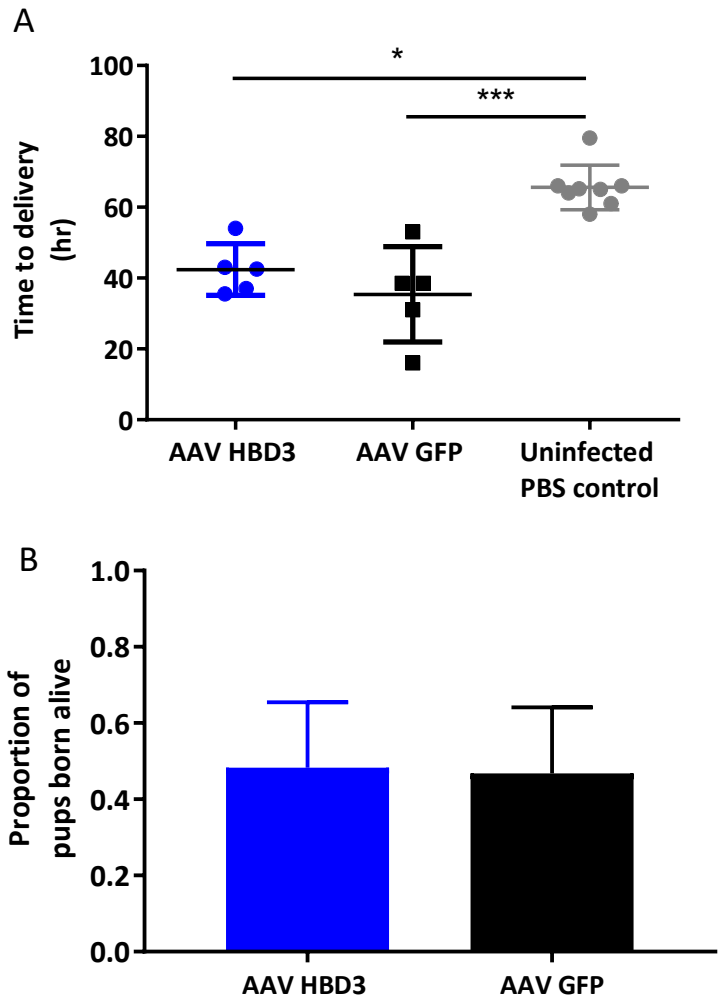

Figure 7.6: There is no difference in gestation at delivery or the proportion on pups born alive between the AAV HBD3 and AAV GFP groups. (A) Time to delivery from intravaginal *E.coli* K1 administration in AAV HBD3, AAV GFP and PBS control dams. n=5; data log transformed and analysed with a one-way ANOVA and post-hoc Bonferroni test. **(B)** Proportion of pups born alive from AAV HBD3 and AAV GFP dams. n=5; data arcsin transformed and analysed with an unpaired t-test. *$P<0.05$, ***$P<0.001$.

7.5. *E.coli* K1: Low CFU dose ($2x10^2$)

7.5.1. AAV HBD-3 significantly reduces low-dose *E.coli* K1 ascent into the uterus of pregnant mice

E.coli K1 (low dose) was administered intravaginally on E16.5 and pregnant mice were imaged daily until delivery as described in Figure 7.1. The bioluminescent signal from the uterus is lower in the AAV HBD3 groups compared with the AAV GFP treated group at the 24 hour time point, implying that AAV HBD3 does reduce bacterial ascent into the uterus in these mice (Figure 7.7) Confirming this, there is a significantly increased fold change in uterine bioluminescence in the AAV GFP control group at 24 hours compared with the AAV HBD3 treated group which is (*P=0.009*) (Figure 7.7B).

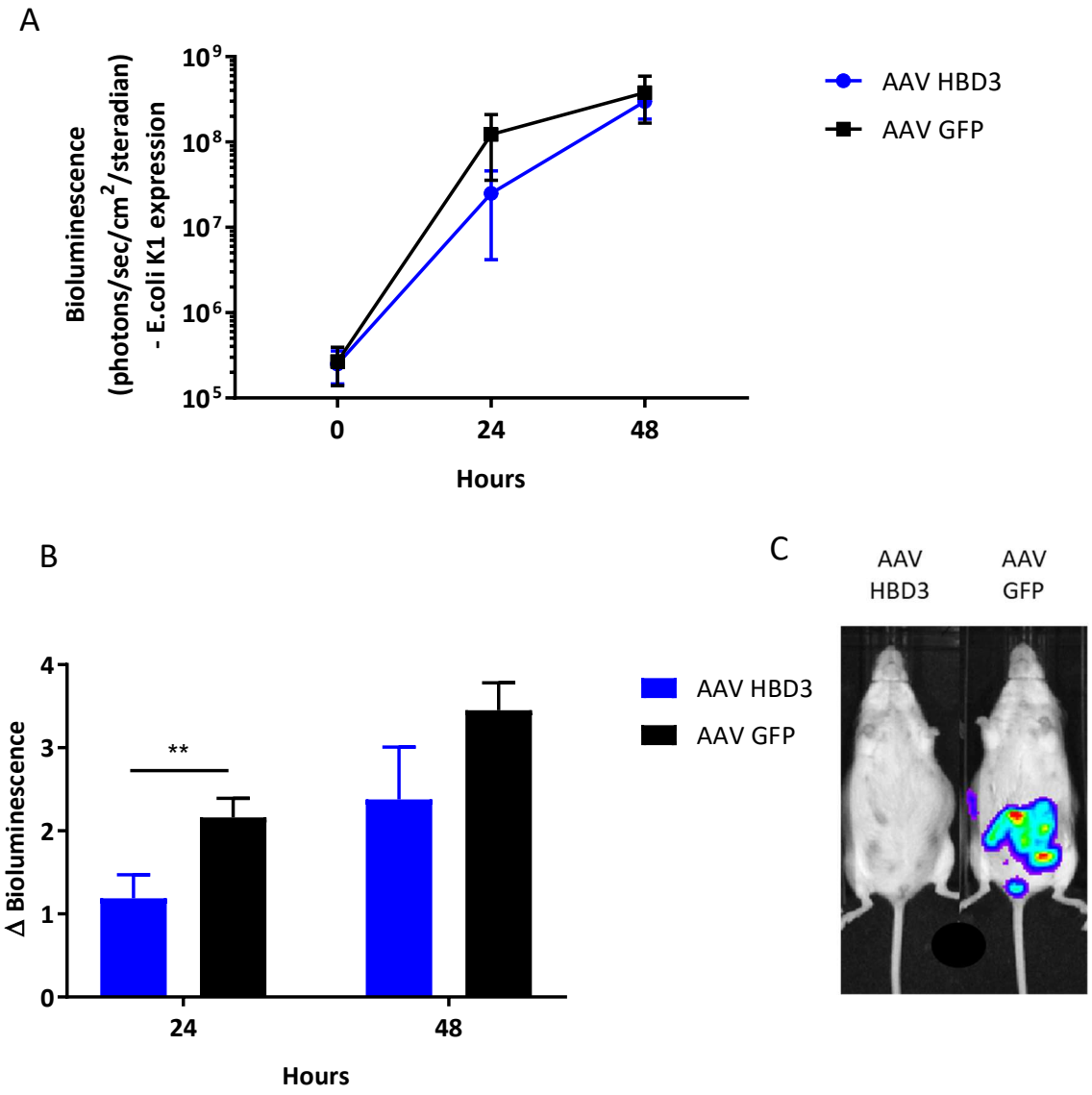

Figure 7.7: AAV HBD-3 significantly reduces low-dose *E.coli* K1 ascent into the uterus. (A) Bioluminescence from the uterus of pregnant dams treated with AAV HBD3 or AAV GFP after administration of intravaginal low dose *E.coli* K1. **(B)** Fold change in uterine E.coli K1 bioluminescence over time (log transformed data shown). There is a smaller fold increase in uterine bioluminescence in the AAV HBD3 group, compared with AAV GFP treated dams. **(C)** Representative images at 24 hours after infection in an AAV HBD3 and AAV GFP treated dam. n=9 in the AAV GFP group, n=10 in the AAV HBD3 group (postpartum dams excluded); data log transformed and analysed by unpaired t-tests (as sample size different at each time point), ***P<0.01*.

7.5.2. AAV HBD3 does not increase gestation length following low-dose *E.coli* K1 administration but it does significantly increase the proportion of pups born alive

The time of delivery of the first pup was determined following bacterial administration in the AAV HBD3 and AAV GFP groups and following PBS administration in the uninfected control. There is no increase in the gestation length in the AAV HBD3 dams compared with the AAV GFP dams (*P=0.94*) (Figure 7.8A). The gestation length difference between *E.coli* K1 infected-AAV HBD3 or AAV GFP groups, and uninfected controls remains statistically significant (*P=0.01* and *P=0.0001* respectively). The proportions of pups born alive were determined in both AAV HBD3 and AAV GFP groups and were found to be significantly increased in the AAV HBD3 group (*P=0.028*) (Figure 7.8B).

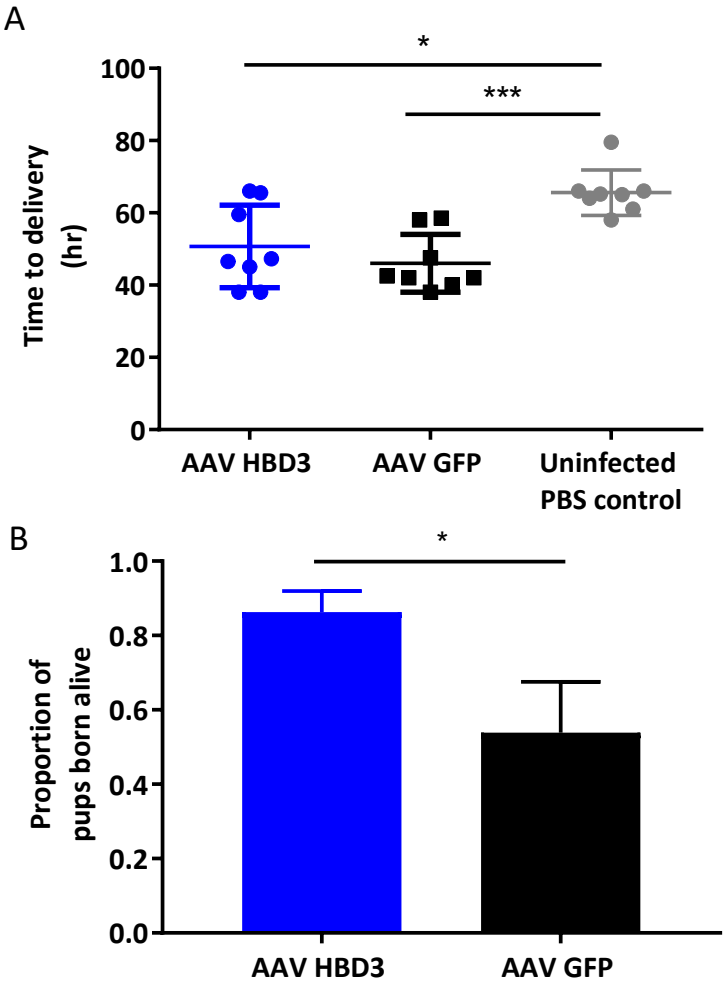

Figure 7.8: AAV HBD3 does not increase gestation length following low-dose E.coli K1 administration but it does significantly increase the proportion of pups born alive. (A) Time to delivery from intravaginal *E.coli* K1 administration in AAV HBD3, AAV GFP and PBS control dams. There is no difference in gestation at delivery between the AAV HBD3 and AAV GFP groups. **(B)** Proportion of pups born alive from AAV HBD3 and AAV GFP dams. n=9 in the AAV GFP group, n=10 in the AAV HBD3 group; data log transformed and analysed with a one-way ANOVA (A) and data arcsin transformed and analysed with an unpaired t-test (B), **P<0.05,* ****P<0.001*.

7.5.3. There was no difference in pup survival over the first week of life

The remaining pups were counted in the first week of life. There was no difference in the numbers by 7 days of life (*P=0.4*), although the AAV HBD3 pups have increased survival rates over the first 4 days of life (66% in the AAV HBD3 group versus 62% in the AAV GFP group) (Figure 7.9A). Separating the pups into those born preterm and those born term (48 hours after bacterial administration was defined as the term cut-off time point) revealed a trend towards increased survival in the term AAV HBD-3 treated pups, compared with AAV GFP control term pups, although this was not significant (*P=0.1*) Figure 7.9B). There was no difference between pup survival in the preterm AAV HBD3 and preterm AAV GFP groups (*P=0.8*) (Figure 7.9C). Pup bioluminescence, signifying *E.coli* K1 colonisation or infection, was assessed daily for the first week of life. There was no obvious difference in bioluminescence signal between AAV HBD3 and AAV GFP pups, consistent with the survival data (Figure 7.10).

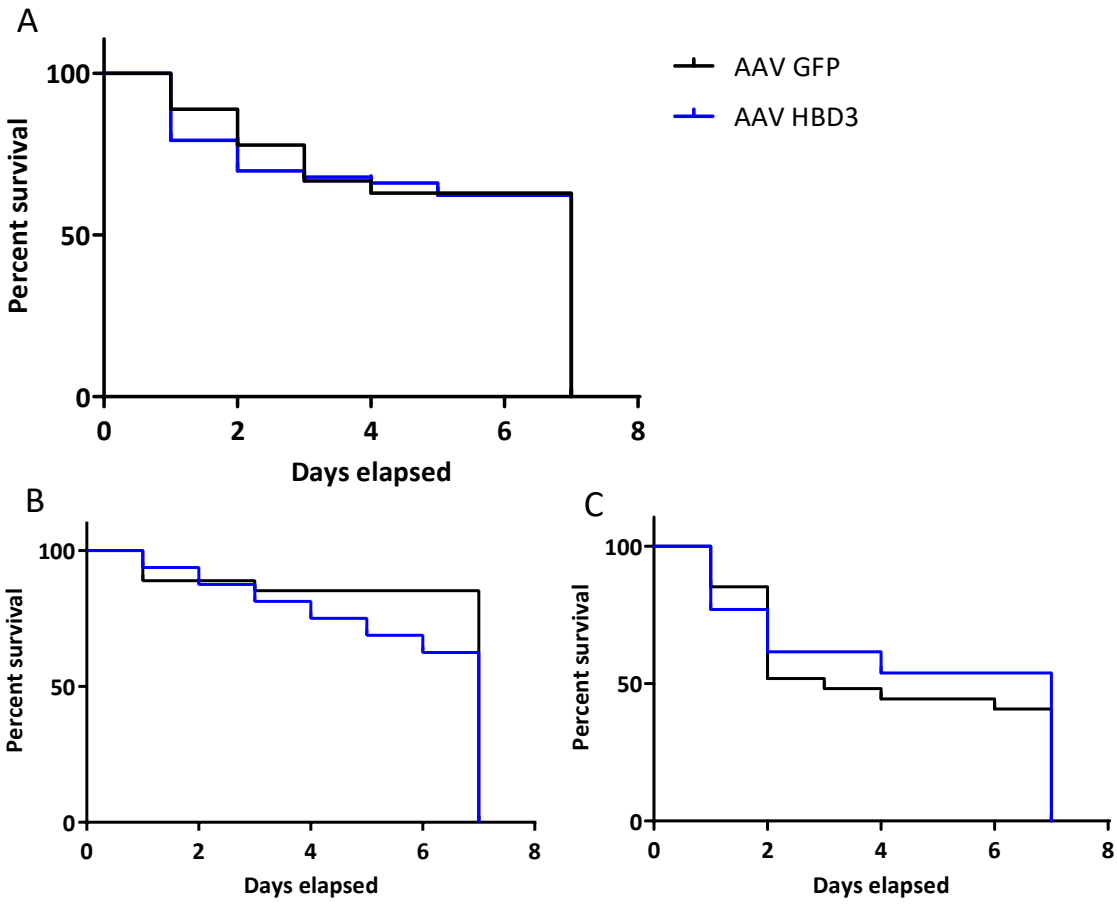

Figure 7.9: There is no difference in pup survival over the first week of life between AAV HBD3 and AAV GFP pups, although there is a trend for increased survival in the term AAV HBD-3 pups compared with term AAV GFP controls pups. (A) Overall pup survival over the first week of life. **(B)** Term pup survival over the first week of life. **(C)** Preterm pup survival over the first week of life Term pups were defined as those that were delivered > 48 hours after bacterial administration. n=27 in AAV GFP group, n=53 in the AAV HBD3 group. Data analysed by Log-rank Mantel-Cox test.

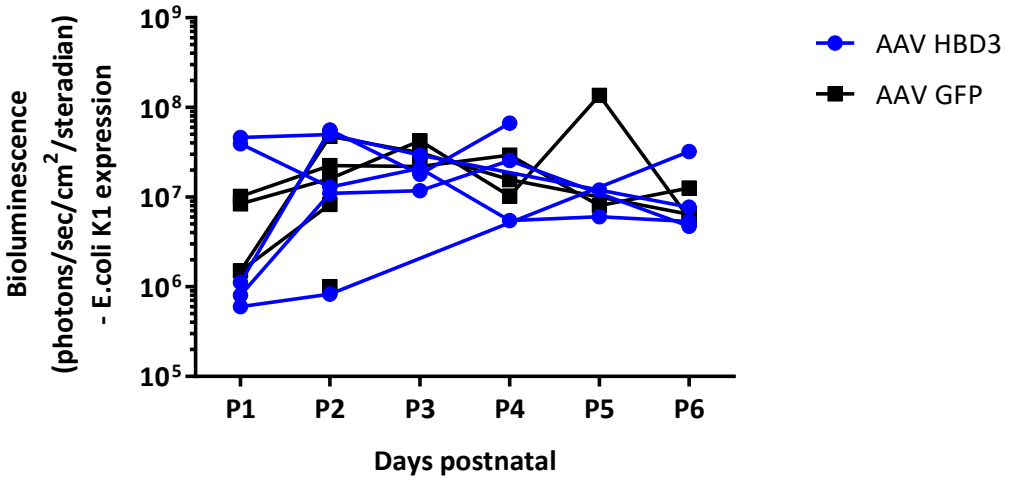

Figure 7.10: There is no difference in whole body pup bioluminescence between AAV HBD3 and AAV GFP pups. Whole body bioluminescence imaging data from the pups over the first week of life. n=5 dams; mean pup data from individual dams plotted.

7.6. Summary of results

Table 7.1 summarises the main findings in this chapter:

AAV HBD-3	**Uterine bacterial ascent**	**Gestational length**	**Proportion of pups born alive**	**Neonatal inflammatory brain cytokines**
E.coli K12	↓ **48h**, *24h 72h (non-significant)*	N/A	No change	↓ Non-significant
E.coli K1 high dose	No change	No change	No change	Not assessed yet
E.coli K1 low dose	↓ **24h**, *48h (non-significant)*	No change	↑	Not assessed yet

Table 7.1: Summary of the main AAV HBD-3 results in this chapter.

7.7. Discussion

This chapter describes the effect of a cervically-applied HBD-3 gene therapy for prevention of ascending vaginal infection and preterm birth. It shows that gene delivery of HBD-3 to the mouse cervix does appear to reduce the ascent of bacteria in pregnant models of ascending vaginal infection (Figure 7.2 & Figure 7.7). AAV HBD-3 treatment does not prolong gestational length in *E.coli* K1 (low dose) infected dams but it does cause an increase in pup survival at birth (Figure 7.8).

Preventing preterm birth

Unfortunately AAV HBD-3 did not significantly increase the gestational length in *E.coli* K1 infected dams. In both *E.coli* K1 dose groups (high and low), there is a slight increase in gestational length compared to the AAV GFP group although this is subtle and not statistically significant (Figure 7.6 & Figure 7.8). In order for the treatment to show effects on gestation length it will need to cause a drastic reduction in *E.coli* K1 ascent and infection for at least 48 hours. From observation during these experiments, I hypothesise that AAV HBD3 probably delays infection over the first 24 hours but then the virulent strain of *E.coli* becomes too much for the "augmented" mucosal immunity of the cervix to defend. This theory is consistent with the reduction in bacteria seen after 24 hours in the uterus of AAV HBD3 treated dams which then becomes less pronounced by 48 hours with the low dose *E.coli* K1 (Figure 7.7). For further studies, I would like to try a repeated application of AAV HBD3 prior to bacterial administration.

Increased pup survival with AAV HBD3

This study shows that AAV HBD-3 increases the proportion of pups born alive as well as a possibly increasing survival for neonates born at term following low dose *E.coli* K1 infection (Figure 7.8 and Figure 7.9). There is no improvement in preterm pup survival in the first week of life

suggesting that preterm pups are more susceptible to *E.coli* K1 infection than term pups (Figure 7.9).

Neonatal brains from AAV HBD-3 treated- *E.coli* K12 infected dams showed a non-significant reduction in inflammatory cytokine expression on the day of birth and future work would determine the effects of maternal AAV HBD-3 treatment on pup brain inflammation following *E.coli* K1 infection (Figure 7.4).

Mouse versus human immune systems

Although the mouse and human immune systems do share similarities there are some significant differences in immune system activation and response to challenge (Mestas & Hughes 2004). An important example of this includes the induction of an acute inflammatory response; mice require 250 times the amount of LPS endotoxin (per kg) than humans to mount the same IL-6 inflammatory response (Copeland et al. 2005). Therefore, we must practice caution when extrapolating immunological findings from mice to humans. The preterm birth model used here to mimic the human disease, is likely to represent a much simpler and more pathogenic process than what happens in the human disease. This is supported by the fact that the types of bacteria associated with premature chorioamnionitis clinically are generally minimally pathogenic bacteria that ordinarily colonise the vagina (Jones et al. 2009). Therefore, this treatment could potentially provide an effective means of augmenting local mucosal immunity without having a drastic effect on the vaginal microbiome or maternal and fetal systemic immune response. For future work, it would be important to determine the effects of cervical expression of HBD-3 on bacteria commonly associated with preterm birth, such as *U.urealyticum* or Group B streptococcus.

How does AAV HBD-3 reduce bacterial ascent?

The mechanisms by which HBD-3 in the murine cervix reduces bacterial ascent into the uterine cavity is intriguing. There are two ways in which HBD-3 could prevent bacterial ascent; by direct microbial killing action or by the recruitment of immune cells that kill the bacteria. I have shown that HBD-3 induces an influx of neutrophils into the cervical epithelium *in vivo*, but I have not been able to show that the vaginal lavage of AAV HBD-3 treated mice has direct *E.coli* killing activity (Figure 6.7 & Figure 6.8). Therefore, it is possible that HBD-3 mediated bacterial clearance is occurring solely through enhanced neutrophil action or alternatively that HBD-3 direct killing activity is only functional in physiological conditions *in vivo*. Furthermore, there is also a possibility that HBD-3 induces an endogenous murine mbd14 response on activation by local bacterial DNA which helps to increase direct bacterial killing *in vivo* (McGlasson et al. 2017). A study looking at the benefits of exogenously delivered human cathelicidin LL-37 in a murine model of *P.aeruginosa* lung infection found that cathelicidin LL-37 enhanced bacterial clearance *in vivo* (Beaumont et al. 2014). Interestingly, similar to results obtained in our study, there was no evidence of a direct microbicidal effect *in vivo* and the authors concluded that the likely mechanism of bacterial clearance is the peptide-mediated enhanced early neutrophil influx. For future studies it is important to determine the exact mechanisms of bacterial killing. The use of a neutrophil antibody to block neutrophil activity could be used, although this would be inappropriate in the *E.coli* K1 model as the mouse is likely to become overwhelmingly septic without adequate neutrophil function. However, it may work in the *E.coli* K12 model as its non-pathogenic nature is unlikely to lead to an overwhelming infection without neutrophil function. It has been shown that a HBD-3 peptide in which the six cysteine residues is replaced by alanine has antimicrobial function but without chemoattractant properties (Taylor et al. 2008). Therefore, another way to assess mechanisms would be to deliver a HBD-3 gene which produces this modified peptide.

Benefits of gene therapy

The use of synthetic recombinant antimicrobial peptide therapy would potentially avoid the ethical and immunological implications of a gene therapy approach. However, recombinant HBD-3 would be very costly to produce especially as it is likely to require multiple large dose applications and is very unstable in bodily fluids due to peptidase degradation (Svenson et al. 2008; Molchanova et al. 2017). However, it would be essential to compare topically applied recombinant HBD-3 with cervical gene delivery of HBD-3 in future studies to determine its efficacy at preventing ascending infection. This would also help us to understand more about mechanisms of action of HBD-3 as topically applied peptide may remain intraluminal and so exert different or reduced microbicidal actions and immunomodulatory effects.

Antimicrobial gene therapy

The use of antimicrobial gene therapy has been studied before, mainly as a way of treating infections with antibiotic resistant bacteria and treating certain wound infections where the skin epithelia has been severely damaged, such as burns (Jacobsen et al. 2005; Carretero et al. 2004; Sawamura et al. 2005). Gene delivery of HBD-3 to keratinocytes using adenoviral vectors has been performed in studies investigating novel treatments for wound infections (Hirsch et al. 2009; Carretero et al. 2004). They show that keratinocytes expressing HBD-3 *in vitro* have increased antimicrobial activity and interestingly found that the beta-defensins worked synergistically with the AMP, cathelicidin LL-37, in its antimicrobial activity against *E.coli* and *S.aureus* (Carretero et al. 2004). *In vivo*, in a model of infected diabetic wounds in pigs, adenoviral vectors delivering HBD-3 showed reduced bacterial load 4 days after vector administration and an improvement in re-epithelialization of the wound (Hirsch et al. 2009). The wound healing role of HBD-3 may also be of interest in women at high risk of preterm birth who have had previous cervical treatment for high risk precancerous cervical lesions. The expression of HBD-3, in combination with VEGF, in bone marrow derived stem cells resulted in improved

wound healing in a model of combined radiation-wound injury in rats (Xia et al. 2014). In particular, HBD-3 and VEGF promotes skin re-epithelialization, granulation tissue formation and collagen I deposition. In preterm birth, premature remodelling and shortening of the cervix involves degradation of cervical stromal collagen, particularly collagen I and III, by matrix metalloproteinases (Gonzalez et al. 2011; Kirby et al. 2016; Sundtoft et al. 2017). Therefore, this HBD-3 gene therapy may also help to inhibit this process in women at high risk of preterm birth by encouraging collagen I deposition. In further studies it would be interesting to determine the effects of the AAV HBD-3 treatment on cervical remodelling and collagen deposition following *E.coli* ascending infection.

In conclusion, AAV HBD3 does reduce *E.coli* K12 and *E.coli* K1 bacterial ascent into the uterine cavity, although it does not prevent preterm delivery in *E.coli* K1 infected dams. It does appear to have a beneficial effect on pup survival at birth whilst its effect on brain inflammation and injury needs to be explored further.

Chapter 8 Conclusion

This thesis describes the development of murine models of ascending vaginal infection and preterm birth as well as exploring the potential use of cervical gene therapy for the prevention of preterm birth in high risk women.

The main findings of this thesis are:

1. Bioluminescent *E.coli* can be used to model ascending vaginal infection and preterm birth in mice.
2. There is evidence of brain inflammation in the pups exposed to intra-uterine *E.coli*.
3. Viral vectors can be used to transduce the cervical epithelium.
4. Gene delivery of human beta-defensin 3 to the murine cervix induces neutrophil influx.
5. *E.coli* ascent into the uterine cavity can be reduced by AAV HBD-3 gene therapy.

This potential preventative therapy for preterm birth adds to the plethora of other promising therapies currently being investigated. These substances are broadly divided into those targeting cytokine or cytokine signalling and those suppressing inflammation. In particular, IL-1 receptor antagonists and statin therapies are showing promise at reducing preterm labour, cervical remodelling and adverse outcomes in neonates in mouse models of preterm birth (Nadeau-Vallée et al. 2015; Nadeau-Vallée et al. 2017; Pedroni et al. 2014; Gonzalez et al. 2014). A combination of these therapies may provide the key to the prevention of infection-associated preterm birth in humans in the future.

Despite the significant differences between humans and mice, mice models of preterm birth have been useful for understanding the mechanisms of preterm birth and testing specific novel therapies. Interestingly, the pathways regulating immune responses are highly conserved between mice and humans indicating that mice are a useful tool for examining inflammatory responses in preterm birth (Riley & Nelson 2010). However, brain development is different between mice and humans with postnatal day 1-5 in mice corresponding to 23 to 32 weeks gestation in humans. In particular, oligodendrocyte development and subsequent myelination occurs as a postnatal event in mice as opposed to occurring in utero in humans. Therefore, it is important to take this into account when extrapolating findings to human brain development.

The therapy developed in this thesis may have future clinical relevance in augmenting cervical immunity in women at high risk of infection-related preterm birth. The preterm birth syndrome is a complex multifactorial disorder and so this therapy is unlikely to be the "one size fits all" preventative treatment. Current research determining specific biomarkers for infection-related preterm birth may be helpful for identifying the women in which this type of cervical therapy may be beneficial. This study is limited to pre-treatment of animals with the therapy prior to introduction of the infectious and inflammatory agent. For this therapy to be clinically relevant in humans we would also ideally use this as a preventative treatment in women who are high risk of preterm birth before ascending infection occurs. However, we do not know when this infection actually occurs and although we can use cervical length and fetal fibronectin to predict preterm birth risk, this therapy is likely to be beneficial before any of these predictive tests become positive (i.e. short cervix, positive fetal fibronectin). Understanding why and when cervical shortening occurs is also imperative for understanding ascending infection and preventing preterm birth. The use and clinical benefits of this therapy would probably be guided by improved knowledge in this field.

The next steps in this work would be to carry out further pre-clinical experiments to determine the effects of AAV8 HBD-3 therapy on neonatal brain inflammation and injury as well as testing the efficacy of a repeated schedule of gene therapy administration. It would also be imperative to perform promotor and further AAV serotype studies to determine the most clinically translatable viral vector for this purpose. Furthermore, from a patient perspective, I plan to organise focus groups and interviews with patients who have experienced a preterm birth to determine the ethical and social acceptability of this type of maternal gene therapy.

In conclusion, gene delivery of HBD-3 to the murine cervix reduces bacterial ascent into the non-pregnant and pregnant uterine cavity. Whilst it does not delay premature delivery, it does improve neonatal survival at delivery. In the future, this type of therapy may have a potential role in boosting cervical mucosal immunity in women who are at high risk of preterm birth.

Chapter 9 References

Abbott, D.S. et al., 2013. Evaluation of a quantitative fetal fibronectin test for spontaneous preterm birth in symptomatic women. *American Journal of Obstetrics and Gynecology*, 208(2), p.122.e1-122.e6.

Abbott, D.S. et al., 2015. Quantitative Fetal Fibronectin to Predict Preterm Birth in Asymptomatic Women at High Risk. *Obstetrics & Gynecology*, 125(5), pp.1168–1176.

Abbott, D.S. et al., 2014. Raised trappin2/elafin protein in cervico-vaginal fluid is a potential predictor of cervical shortening and spontaneous preterm birth. *PLoS ONE*, 9(7), pp.10–12.

Abdel-Motal, U.M. et al., 2011. Anti-gp120 minibody gene transfer to female genital epithelial cells protects against HIV-1 virus challenge in vitro. *PLoS ONE*, 6(10), pp.1–9.

Abdel-Motal, U.M. et al., 2014. Prolonged expression of an anti-HIV-1 gp120 minibody to the female rhesus macaque lower genital tract by AAV gene transfer. *Gene Therapy*, 21(9), pp.802–810.

Adams Waldorf, K.M. et al., 2011. Choriodecidual Group B Streptococcal Inoculation Induces Fetal Lung Injury without Intra-Amniotic Infection and Preterm Labor in Macaca nemestrina M. M. Heimesaat, ed. *PLoS ONE*, 6(12), p.e28972.

Adams Waldorf, K.M. & McAdams, R.M., 2013. Influence of infection during pregnancy on fetal development. *Reproduction (Cambridge, England)*, 146(5), pp.R151-162.

Akgul, Y., Word, R.A., et al., 2014. Hyaluronan in cervical epithelia protects against infection-mediated preterm birth. *Journal of Clinical Investigation*, 124(12), pp.5481–5489.

Anahtar, M.N. et al., 2016. Inflammatory Responses in the Female Genital Tract. *Immunity*, 42(5), pp.965–976.

Andersen, J.M., Al-Khairy, D. & Ingalls, R.R., 2006. Innate Immunity at the Mucosal Surface: Role of Toll-Like Receptor 3 and Toll-Like Receptor 9 in Cervical Epithelial Cell Responses to Microbial Pathogens1. *Biology of Reproduction*, 74(5), pp.824–831.

Anderson, D.J., Marathe, J. & Pudney, J., 2014. The structure of the human vaginal stratum corneum and its role in immune defense. *American journal of reproductive immunology (New York, N.Y. : 1989)*, 71(6), pp.618–623.

Appaiahgari, M.B. & Vrati, S., 2015. Adenoviruses as gene/vaccine delivery vectors: promises and pitfalls. *Expert opinion on biological therapy*, 15(3), pp.337–351.

Aroutcheva A & al., 2001. Defense factors of vaginal lactobacilli. *American Journal of Obstetrics and Gynaecology*, 185(2), pp.375–379.

Atchison, R.W., Casto, B.C. & Hammon, W.M., 1965. Adenovirus-Associated defective virus particles. *Science (New York, N.Y.)*, 149(3685), pp.754–756.

Ba-Thein, W. et al., 2002. Vaginal Escherichia coli share common virulence factor profiles, serotypes and phylogeny with other extraintestinal E. coli. *Microbiology*, 148(9), pp.2745–2752.

Back, S.A., 2017. White matter injury in the preterm infant: pathology and mechanisms. *Acta Neuropathologica*, 134(3), pp.331-349.

Bainbridge, J.W.B. et al., 2015. Long-Term Effect of Gene Therapy on Leber ' s Congenital Amaurosis. *New England Journal of Medicine*, 372(20), pp.1887–1897.

Baldwin TO, Berends T, Bunch TA, Holzman TF, Rausch SK, Shamansky L, Treat ML, Z.M., 1984. Cloning of the luciferase structural genes from Vibrio harveyi and expression of bioluminescence in Escherichia coli. *Biochemistry*, 23(16), pp.3663–3667.

Baranger, K. et al., 2008. The antibacterial and antifungal properties of trappin-2 (pre-elafin) do not depend on its protease inhibitory function. *FEBS Journal*, 275(9), pp.2008–2020.

Barfod, K.K. et al., 2013. The murine lung microbiome in relation to the intestinal and vaginal bacterial communities. *BMC microbiology*, 13, p.303.

Beaumont, P.E. et al., 2014. Cathelicidin Host Defence Peptide Augments Clearance of Pulmonary Pseudomonas aeruginosa Infection by Its Influence on Neutrophil Function In Vivo. *PLoS ONE*, 9(6), p.e99029.

Becher, N. et al., 2009. The cervical mucus plug: structured review of the literature. *Acta obstetricia et gynecologica Scandinavica*, 88(5), pp.502–513.

Bedran, T.B.L. et al., 2014. Synergistic anti-inflammatory activity of the antimicrobial peptides human beta-defensin-3 (hBD-3) and cathelicidin (LL-37) in a three-dimensional co-culture model of gingival epithelial cells and fibroblasts. *PLoS ONE*, 9(9), pp.1–10.

Bell, M.J. & Hallenbeck, J.M., 2002. Effects of intrauterine inflammation on developing rat brain. *Journal of Neuroscience Research*, 70(4), pp.570–579.

Bell, M.J., Hallenbeck, J.M. & Gallo, V., 2004. Determining the fetal inflammatory response in an experimental model of intrauterine inflammation in rats. *Pediatric research*, 56(4), pp.541–546.

Berghella, V. et al., 2011. Cerclage for short cervix on ultrasonography in women with singleton gestations and previous preterm birth: a meta-analysis. *Obstetrics and gynecology*, 117(3), pp.663–671.

Bevins, C.L., Martin-Porter, E. & Ganz, T., 1999. Defensins and innate host defence of the gastrointestinal tract. *Gut*, 45(6), pp.911–915.

Bevis, K.S. & Biggio, J.R., 2011. Cervical conization and the risk of preterm delivery. *American Journal of Obstetrics and Gynecology*, 205(1), pp.19–27.

Binny, C.J. & Nathwani, A.C., 2012. Vector Systems for Prenatal Gene Therapy: Principles of Adeno-Associated Virus Vector Design and Production. In *Prenatal Gene Therapy*. Totowa, NJ: Humana Press, pp. 109–131.

Birchenough, G.M.H. et al., 2013. Altered Innate Defenses in the Neonatal Gastrointestinal Tract in Response to Colonization by Neuropathogenic Escherichia coli. *Infection and Immunity*, 81(9), pp.3264–3275.

Birchenough, G.M.H. et al., 2017. Postnatal development of the small intestinal mucosa drives age-dependent, regio-selective susceptibility to Escherichia coli K1 infection. *Scientific reports*, 7(1), p.83.

Blencowe, H. et al., 2013. Born too soon: the global epidemiology of 15 million preterm births. *Reproductive health*, 10 Suppl 1(Suppl 1), p.S2.

Blencowe, H. et al., 2012. National, regional, and worldwide estimates of preterm birth rates in the year 2010 with time trends since 1990 for selected countries: A systematic analysis and implications. *The Lancet*, 379(9832), pp.2162–2172.

Bohenzky, R.A., LeFebvre, R.B. & Berns, K.I., 1988. Sequence and symmetry requirements within the internal palindromic sequences of the adeno-associated virus terminal repeat. *Virology*, 166(2), pp.316–327.

Bollopragada, S. et al., 2009. Term labor is associated with a core inflammatory response in human fetal membranes, myometrium, and cervix. *American Journal of Obstetrics and Gynecology*, 200(1), p.104.e1-104.e11.

Bolton, C.E. et al., 2012. The EPICure Study: Association between Hemodynamics and Lung Function at 11 Years after Extremely Preterm Birth. *The Journal of Pediatrics*, 161(4), p.595–601.e2.

Bonacorsi, S. & Bingen, E., 2005. Molecular epidemiology of Escherichia coli causing neonatal meningitis. *International journal of medical microbiology : IJMM*, 295(6–7), pp.373–381.

Borges, S., Silva, J. & Teixeira, P., 2014. The role of lactobacilli and probiotics in maintaining vaginal health. *Archives of Gynecology and Obstetrics*, 289(3), pp.479–489.

Boshart, M. et al., 1985. A very strong enhancer is located upstream of an immediate early gene of human cytomegalovirus. *Cell*, 41(2), pp.521–530.

Boughter, J.D. et al., 2005. Inbred mouse strains C57BL/6J and DBA/2J vary in sensitivity to a subset of bitter stimuli. *BMC genetics*, 6, pp.36.

Boutin, S. et al., 2010. Prevalence of serum IgG and neutralizing factors against adeno-associated virus (AAV) types 1, 2, 5, 6, 8, and 9 in the healthy population: implications for gene therapy using AAV vectors. *Human gene therapy*, 21(6), pp.704–12.

Bradshaw, A.C. & Baker, A.H., 2013. Gene therapy for cardiovascular disease: Perspectives and potential. *Vascular Pharmacology*, 58(3), pp.174–181.

Brocklehurst, P. et al., 2013. Antibiotics for treating bacterial vaginosis in pregnancy (Review) Antibiotics for treating bacterial vaginosis in pregnancy. *Cochrane database of systematic reviews*, (1), pp.4–6.

Brooks, A.R. et al., 2004. Transcriptional silencing is associated with extensive methylation of the CMV promoter following adenoviral gene delivery to muscle. *Journal of Gene Medicine*, 6(4), pp.395–404.

Buckley, S.M.K. et al., 2015. In vivo bioimaging with tissue-specific transcription factor activated luciferase reporters. *Scientific reports*, 5, p.11842.

Burd, I. et al., 2009. Beyond white matter damage: fetal neuronal injury in a mouse model of preterm birth. *American Journal of Obstetrics and Gynecology*, 201(3), p.279.e1-279.e8.

Burd, I. et al., 2010. Inflammation-induced preterm birth alters neuronal morphology in the mouse fetal brain. *Journal of Neuroscience Research*, 88(9), pp.1872–1881.

Burd, I., Balakrishnan, B. & Kannan, S., 2012. Models of Fetal Brain Injury, Intrauterine Inflammation, and Preterm Birth. *American Journal of Reproductive Immunology*, 67(4), pp.287–294.

Campbell, J. et al., 2014. Bioluminescence Imaging of Chlamydia muridarum Ascending Infection in Mice. *PLoS ONE*, 9(7), p.e101634.

Cao, O. et al., 2007. Induction and role of regulatory CD4+CD25+ T cells in tolerance to the transgene product following hepatic in vivo gene transfer. *Blood*, 110(4), pp.1132–1140.

Carlstedt, I. et al., 1983. Isolation and characterization of human cervical-mucus glycoproteins. *The Biochemical journal*, 211(1), pp.13–22.

Carretero, M. et al., 2004. A cutaneous gene therapy approach to treat infection through keratinocyte-targeted overexpression of antimicrobial peptides. *The FASEB journal : official publication of the Federation of American Societies for Experimental Biology*, 18(15), pp.1931–1933.

Castanon A. et al., 2014. Risk of preterm delivery with increasing depth of excision for cervical intraepithelial neoplasia in England: nested case-control study. *BMJ (Clinical research ed.)*, 349, pp.6223.

Celik, H. & Ayar, A., 2002. Effects of erythromycin on pregnancy duration and birth weight in lipopolysaccharide-induced preterm labor in pregnant rats. *European Journal of Obstetrics Gynecology and Reproductive Biology*, 103(1), pp.22–25.

Challis, J.R.G. et al., 2000. Endocrine and Paracrine Regulation of Birth at Term and Preterm*. *Endocrine Reviews*, 21, pp.514–550.

Chang, E., 2015. Preterm birth and the role of neuroprotection. *BMJ*, 350(3), pp.6661.

Chang, H.H. et al., 2013. Preventing preterm births: trends and potential reductions with current interventions in 39 very high human development index countries. *Lancet*, 381(9862), pp.223–234.

Chapman MS, A.-M.M., 2006. Atomic structure of viral particles. In *Parvoviruses*. pp. 107–123.

Cnattingius, S. et al., 2013. Maternal Obesity and Risk of Preterm Delivery. *JAMA*, 309(22), p.2362.

Cook, J.R. et al., 2017. Cerclage position, cervical length and preterm delivery in women undergoing ultrasound indicated cervical cerclage: A retrospective cohort study R. C. Young, ed. *PLOS ONE*, 12(6), p.e0178072.

Copeland, S. et al., 2005. Acute Inflammatory Response to Endotoxin in Mice and Humans. *Clinical and Vaccine Immunology*, 12(1), pp.60–67.

Cronin, M. et al., 2016. Chapter 7 In Vivo Bioluminescence Imaging of Intratumoral Bacteria. , 1409, pp.69–77.

Cronin, M. et al., 2012. High resolution in vivo bioluminescent imaging for the study of bacterial tumour targeting. *PLoS ONE*, 7(1), e30940.

Cui, G. et al., 2013. Chloroquine pretreatment inhibits toll-like receptor 3 signaling after stroke. *Neuroscience Letters*, 548, pp.101–104.

Cunningham, S.C. et al., 2008. Gene Delivery to the Juvenile Mouse Liver Using AAV2/8 Vectors. *Molecular Therapy*, 16(6), pp.1081–1088.

Dada, T. et al., 2014. Mouse model of intrauterine inflammation: sex-specific differences in long-term neurologic and immune sequelae. *Brain, behavior, and immunity*, 38, pp.142–150.

Dalgakiran, F. et al., 2014. Non-invasive model of neuropathogenic Escherichia coli infection in the neonatal rat. *Journal of visualized experiments : JoVE*, (92), p.e52018.

Davidoff, A.M. et al., 2003. Sex significantly influences transduction of murine liver by recombinant adeno-associated viral vectors through an androgen-dependent pathway. *Blood*, 102(2), pp.480–488.

Demaison, C. et al., 2002. High-level transduction and gene expression in hematopoietic repopulating cells using a human immunodeficiency [correction of imunodeficiency] virus type 1-based lentiviral vector containing an internal spleen focus forming virus promoter. *Human gene therapy*, 13, pp.803–813.

Dhople, V., Krukemeyer, A. & Ramamoorthy, A., 2006. The human beta-defensin-3, an antibacterial peptide with multiple biological functions. *Biochimica et Biophysica Acta - Biomembranes*, 1758(9), pp.1499–1512.

Diamond, A.K. et al., 2007. Modulation of monocyte chemotactic protein-1 expression during lipopolysaccharide-induced preterm delivery in the pregnant mouse. *Reproductive sciences*, 14(6), pp.548–59.

DiGiulio, D.B. et al., 2008. Microbial prevalence, diversity and abundance in amniotic fluid during preterm labor: a molecular and culture-based investigation. *PloS one*, 3(8), p.e3056.

DiGiulio, D.B. et al., 2015. Temporal and spatial variation of the human microbiota during pregnancy. *Proceedings of the National Academy of Sciences*, 112(35), p.201502875.

Dommergues, M.-A. et al., 2003. Early microglial activation following neonatal excitotoxic brain damage in mice: a potential target for neuroprotection. *Neuroscience*, 121(3), pp.619–28.

Donders, G.G. et al., 2009. Predictive value for preterm birth of abnormal vaginal flora, bacterial vaginosis and aerobic vaginitis during the first trimester of pregnancy. *BJOG: An International Journal of Obstetrics and Gynaecology*, 116(10), pp.1315–1324.

Doyle, R.M. et al., 2017. Bacterial communities found in placental tissues are associated with severe chorioamnionitis and adverse birth outcomes. *PloS one*, pp.1–23.

Drouin, L.M. & Agbandje-McKenna, M., 2013. Adeno-associated virus structural biology as a tool in vector development. *Future virology*, 8(12), pp.1183–1199.

Dudley, D.J. et al., 1996. Induction of preterm birth in mice by RU486. *Biology of reproduction*, 55(5), pp.992–995.

Edey, L.F. et al., 2016. The Local and Systemic Immune Response to Intrauterine LPS in the Prepartum Mouse. *Biology of Reproduction*, 95(6), pp.125–125.

Elovitz, M.A. et al., 2003. A new model for inflammation-induced preterm birth: the role of platelet-activating factor and Toll-like receptor-4. *The American journal of pathology*, 163(5), pp.2103–2111.

Elovitz, M.A. et al., 2011. Intrauterine inflammation, insufficient to induce parturition, still evokes fetal and neonatal brain injury. *International Journal of Developmental Neuroscience*, 29(6), pp.663–671.

Elovitz, M. a. & Mrinalini, C., 2005. Can medroxyprogesterone acetate alter Toll-like receptor expression in a mouse model of intrauterine inflammation? *American Journal of Obstetrics and Gynecology*, 193(3 SUPPL.), pp.1149–1155.

Elovitz, M. & Wang, Z., 2004. Medroxyprogesterone acetate, but not progesterone, protects against inflammation-induced parturition and intrauterine fetal demise. *American Journal of Obstetrics and Gynecology*, 190(3), pp.693–701.

Elst, C.W. Vander et al., 1991. The role of chorioamnionitis and prostaglandins in preterm labor. *Obstet Gynecol*, 77(6), pp.672–676.

Fatemi, S.H. et al., 2008. Maternal infection leads to abnormal gene regulation and brain atrophy in mouse offspring: implications for genesis of neurodevelopmental disorders. *Schizophrenia research*, 99(1–3), pp.56–70.

Favaro, P. et al., 2009. Host and vector-dependent effects on the risk of germline transmission of AAV vectors. *Molecular therapy : the journal of the American Society of Gene Therapy*, 17(6), pp.1022–1030.

Favre, D. et al., 2001. Immediate and long-term safety of recombinant adeno-associated virus injection into the nonhuman primate muscle. *Molecular therapy : the journal of the American Society of Gene Therapy*, 4(6), pp.559–566.

Fawke, J. et al., 2010. Lung Function and Respiratory Symptoms at 11 Years in Children Born Extremely Preterm. *American Journal of Respiratory and Critical Care Medicine*, 182(2), pp.237–245.

Feikin, D.R. et al., 2001. Association between colonization with group B streptococci during pregnancy and preterm delivery among Danish women. *American journal of obstetrics and gynecology*, 184(3), pp.427–433.

Feng, Z. et al., 2006. Cutting edge: human beta defensin 3--a novel antagonist of the HIV-1 coreceptor CXCR4. *Journal of immunology*, 177(2), pp.782–786.

Ferrero, D.M. et al., 2016. Cross-Country individual participant analysis of 4.1 million singleton births in 5 countries with very high human development index confirms known associations but provides no biologic explanation for 2/3 of all preterm births. *PLoS ONE*, 11(9), pp.1–19.

Ferris, M.J. et al., 2007. Cultivation-independent analysis of changes in bacterial vaginosis flora following metronidazole treatment. *Journal of clinical microbiology*, 45(3), pp.1016–8.

Fidel, P. et al., 2003. The effect of antibiotic therapy on intrauterine infection-induced preterm parturition in rabbits. *J Matern Fetal Neonatal Med*, 14(1), pp.57–64.

Filipovich, Y. et al., 2015. Depletion of polymorphonuclear leukocytes has no effect on preterm delivery in a mouse model of Escherichia coli-induced labor. *American Journal of Obstetrics and Gynecology*, 213(5), p.697.e1-697.e10.

Filipovich, Y. et al., 2016. Maternal and fetal roles in bacterially induced preterm labor in the mouse. *Am J Obstet Gynecol*, 214(3), p.386.e1-9.

Frew, L. et al., 2014. Human Cathelicidin Production by the Cervix. *PLoS ONE*, 9(8), p.e103434.

Funderburg, N. et al., 2007. Human -defensin-3 activates professional antigen-presenting cells via Toll-like receptors 1 and 2. *Proceedings of the National Academy of Sciences of the United States of America*, 104(47), pp.18631–18635.

Funderburg, N.T. et al., 2011. The Toll-like receptor 1/2 agonists Pam3CSK4 and human β-defensin-3 differentially induce interleukin-10 and nuclear factor-κB signalling patterns in human monocytes. *Immunology*, 134(2), pp.151–160.

Gajer, P. et al., 2012. Temporal Dynamics of the Human Vaginal Microbiota. *Science Translational Medicine*, 2;4(132):132ra52.

Ganz, T., 2003. Defensins: antimicrobial peptides of innate immunity. *Nature reviews. Immunology*, 3(9), pp.710–720.

García, J.R. et al., 2001. Identification of a novel, multifunctional beta-defensin (human beta-defensin 3) with specific antimicrobial activity. Its interaction with plasma membranes of Xenopus oocytes and the induction of macrophage chemoattraction. *Cell and tissue research*, 306(2), pp.257–264.

Garfield, R.E., Gasc, J.M. & Baulieu, E.E., 1987. Effects of the antiprogesterone RU 486 on preterm birth in the rat. *American journal of obstetrics and gynecology*, 157(5), pp.1281–1285.

Gaspar, H.B. et al., 2011. Long-term persistence of a polyclonal T cell repertoire after gene therapy for X-linked severe combined immunodeficiency. *Science translational medicine*, 3(97), p.97ra79.

GBD 2015 DALYs and HALE Collaborators, N.J. et al., 2016. Global, regional, and national disability-adjusted life-years (DALYs) for 315 diseases and injuries and healthy life expectancy (HALE), 1990-2015: a systematic analysis for the Global Burden of Disease Study 2015. *Lancet*, 388(10053), pp.1603–1658.

Ghahremankhani, A.A., Dorkoosh, F. & Dinarvand, R., 2008. PLGA-PEG-PLGA tri-block copolymers as in situ gel-forming peptide delivery system: effect of formulation properties on peptide release. *Pharmaceutical development and technology*, 13(1), pp.49–55.

Ghorbani, M. et al., 2014. Factors associated with Posttraumatic Stress Disorder and Its Coping Styles in Parents of Preterm and Full-Term Infants. *Global Journal of Health Science*, 6(3), pp.65–73.

Ghosh, D. et al., 2002. Paneth cell trypsin is the processing enzyme for human defensin-5. *Nature immunology*, 3(6), pp.583–590.

Goldenberg, R.L. et al., 2008. Epidemiology and causes of preterm birth. *The Lancet*, 371(9606), pp.75–84.

Goldenberg, R.L., Hauth, J.C. & Andrews, W.W., 2000. Intrauterine infection and Preterm Delivery. *N Engl J Med*, 342(20), pp.1500–1507.

Gonzalez, J.M. et al., 2011. Complement activation triggers metalloproteinases release inducing cervical remodeling and preterm birth in mice. *American Journal of Pathology*, 179(2), pp.838–849.

Gonzalez, J.M., Pedroni, S.M.A. & Girardi, G., 2014. Statins prevent cervical remodeling, myometrial contractions and preterm labor through amechanism that involves hemoxygenase-1 and complement inhibition. *Molecular Human Reproduction*, 20(6), pp.579–589.

Greenough, A., 2012. Long term respiratory outcomes of very premature birth (<32 weeks). *Seminars in Fetal and Neonatal Medicine*, 17(2), pp.73–76.

Grigsby, P.L. et al., 2010. Choriodecidual inflammation: a harbinger of the preterm labor syndrome. *Reproductive sciences (Thousand Oaks, Calif.)*, 17(1), pp.85–94.

Gross, G. et al., 2000. Inhibition of cyclooxygenase-2 prevents inflammation-mediated preterm labor in the mouse. *American journal of physiology. Regulatory, integrative and comparative physiology*, 278(6), pp.R1415-23.

Gruntman, A.M. et al., 2015. Stability and compatibility of recombinant adeno-associated virus under conditions commonly encountered in human gene therapy trials. *Human gene therapy methods*, 26(2), pp.71–76.

Gupta, R. et al., 2014. In Vivo Whole Animal Body Imaging Reveals Colonization of Chlamydia muridarum to the Lower Genital Tract at Early Stages of Infection. *Molecular Imaging and Biology*, 16(5), pp.635–641.

Habte, H.H. et al., 2008. The inhibition of the Human Immunodeficiency Virus type 1 activity by crude and purified human pregnancy plug mucus and mucins in an inhibition assay. *Virology journal*, 5(1), pp.59.

Hailer, N.P. et al., 2005. Interleukin-1beta exacerbates and interleukin-1 receptor antagonist attenuates neuronal injury and microglial activation after excitotoxic damage in organotypic hippocampal slice cultures. *The European journal of neuroscience*, 21(9), pp.2347–2360.

Hamilton, S.A., Tower, C.L. & Jones, R.L., 2013. Identification of Chemokines Associated with the Recruitment of Decidual Leukocytes in Human Labour: Potential Novel Targets for Preterm Labour A. C. Zenclussen, ed. *PLoS ONE*, 8(2), p.e56946.

Han, Y.W. et al., 2009. Uncultivated bacteria as etiologic agents of intra-amniotic inflammation leading to preterm birth. *Journal of clinical microbiology*, 47(1), pp.38–47.

Handa, H. & Carter, B.J., 1979. Adeno-associated virus DNA replication complexes in herpes simplex virus or adenovirus-infected cells. *The Journal of biological chemistry*, 254(14), pp.6603–6610.

Harder, J. et al., 2001. Isolation and Characterization of Human ??-Defensin-3, a Novel Human Inducible Peptide Antibiotic. *Journal of Biological Chemistry*, 276(8), pp.5707–5713.

Hein, M. et al., 2001. An in vitro study of antibacterial properties of the cervical mucus plug in pregnancy. *American Journal of Obstetrics and Gynecology*, 185(3), pp.586–592.

Hein, M. et al., 2002. Antimicrobial factors in the cervical mucus plug. *American Journal of Obstetrics and Gynecology*, 187(1), pp.137–144.

Helderman, J.B. et al., 2010. Sepsis-associated electroencephalographic changes in extremely low gestational age neonates. *Early human development*, 86(8), pp.509–513.

Hensley, S.E. & Amalfitano, A., 2007. Toll-like receptors impact on safety and efficacy of gene transfer vectors. *Molecular therapy : the journal of the American Society of Gene Therapy*, 15(8), pp.1417–1422.

Hezelgrave, N.L. et al., 2016. Rationale and design of SuPPoRT: a multi-centre randomised controlled trial to compare three treatments: cervical cerclage, cervical pessary and vaginal progesterone, for the prevention of preterm birth in women who develop a short cervix. *BMC Pregnancy and Childbirth*, 16(1), pp.358.

Hillier, S.L. et al., 1995. Association between bacterial vaginosis and preterm delivery of a low-birth-weight infant. *The New England Journal of Medicine*, 333(26), pp.1737–1742.

Hippert, C. et al., 2012. Corneal transduction by intra-stromal injection of AAV vectors in vivo in the mouse and ex vivo in human explants. A. R. Janecke, ed. *PloS one*, 7(4), p.e35318.

Hirsch, E. & Muhle, R., 2002. Intrauterine bacterial inoculation induces labor in the mouse by mechanisms other than progesterone withdrawal. *Biology of reproduction*, 67(4), pp.1337–41.

Hirsch, T. et al., 2009. Human beta-defensin-3 promotes wound healing in infected diabetic wounds. *The journal of gene medicine*, 11(3), pp.220–228.

Hoggan, M.D., Blacklow, N.R. & Rowe, W.P., 1966. Studies of small DNA viruses found in various adenovirus preparations: physical, biological, and immunological characteristics. *Proceedings of the National Academy of Sciences of the United States of America*, 55(6), pp.1467–1474.

Honest, H. et al., 2002. Accuracy of cervicovaginal fetal fibronectin test in predicting risk of spontaneous preterm birth: systematic review. *BMJ (Clinical research ed.)*, 325(7359), p.301.

Hoover, D.M. et al., 2003. Antimicrobial characterization of human beta-defensin 3 derivatives. *Antimicrobial agents and chemotherapy*, 47(9), pp.2804–2809.

Hunter, C.J. et al., 2008. Understanding the Susceptibility of the Premature Infant to Necrotizing Enterocolitis (NEC). *Pediatric Research*, 63(2), pp.117–123.

Iams, J.D. et al., 2008. Primary, secondary and tertiary interventions to reduce the morbidity and mortality of preterm birth. *The Lancet*, 371(9607), pp.164-75..

Iams, J.D. et al., 1996. The Length of the Cervix and the Risk of Spontaneous Premature Delivery. *New England Journal of Medicine*, 334(9), pp.567–573.

Itaoka, N. et al., 2015. Cervical expression of elafin and SLPI in pregnancy and their association with preterm labor. *American Journal of Reproductive Immunology*, 73(6), pp.536–544.

Jacobsen, F. et al., 2005. Transient cutaneous adenoviral gene therapy with human host defense peptide hCAP-18/LL-37 is effective for the treatment of burn wound infections. *Gene Therapy*, 12(20), pp.1494–1502.

Janeway, C.A. & Medzhitov, R., 2002. Innate immune recognition. *Annual Review of Immunology*, 20(1), pp.197–216.

Jašarević, E. et al., 2015. Alterations in the vaginal microbiome by maternal stress are associated with metabolic reprogramming of the offspring gut and brain. *Endocrinology*, 156(9), pp.3265–3276.

Jeong, B., Bae, Y.H. & Kim, S.W., 2000. In situ gelation of PEG-PLGA-PEG triblock copolymer aqueous solutions and degradation thereof. *Journal of Biomedical Materials Research*, 50(2), pp.171–177.

Jiang, H. et al., 2006. Effects of transient immunosuppression on adenoassociated, virus-mediated, liver-directed gene transfer in rhesus macaques and implications for human gene therapy. *Blood*, 108(10), pp.3321–3328.

Jones, H.E. et al., 2009. Differing prevalence and diversity of bacterial species in fetal membranes from very preterm and term labor. *PLoS ONE*, 4(12), p.e8205.

Jooss, K. & Chirmule, N., 2003. Immunity to adenovirus and adeno-associated viral vectors : implications for gene therapy. *Gene therapy*, 10(11), pp.955–963.

Kaeppel, C. et al., 2013. A largely random AAV integration profile after LPLD gene therapy. *Nature medicine*, 19(7), pp.889–91.

Kaga, N. et al., 1996. Repeated administration of low-dose lipopolysaccharide induces preterm delivery in mice: a model for human preterm parturition and for assessment of the therapeutic ability of drugs against preterm delivery. *American journal of obstetrics and gynecology*, 174(2), pp.754–759.

Kalanda, B.F. et al., 2006. Adverse birth outcomes in a malarious area. *Epidemiology and infection*, 134(3), pp.659–666.

Kaminsky, P.M. et al., 2012. Directing Integrin-linked Endocytosis of Recombinant AAV Enhances Productive FAK-dependent Transduction. *Molecular Therapy*, 20(5), pp.972–983.

Kannan, S. et al., 2007. Microglial activation in perinatal rabbit brain induced by intrauterine inflammation: detection with 11C-(R)-PK11195 and small-animal PET. *Journal of nuclear medicine : official publication, Society of Nuclear Medicine*, 48(6), pp.946–54.

Kataoka, S. et al., 2006. Association between preterm birth and vaginal colonization by mycoplasmas in early pregnancy. *Journal of clinical microbiology*, 44(1), pp.51–55.

Kaul, A.K. et al., 1999. Experimental gestational pyelonephritis induces preterm births and low birth weights in C3H/HeJ mice. *Infection and Immunity*, 67(11), pp.5958–5966.

Kenyon, S. et al., 2008. Childhood outcomes after prescription of antibiotics to pregnant women with spontaneous preterm labour: 7-year follow-up of the ORACLE II trial. *The Lancet*, 372(9646), pp.1319–1327.

Kenyon, S.L., Taylor, D.J. & Tarnow-Mordi, W., 2001. Broad-spectrum antibiotics for spontaneous preterm labour: The ORACLE II randomised trial. *The Lancet*, 357(9261), pp.989–994.

Kern, A. et al., 2003. Identification of a heparin-binding motif on adeno-associated virus type 2 capsids. *Journal of virology*, 77(20), pp.11072–11081.

Khander, A. et al., 2017. The association between obstetrical history and preterm birth in women with uterine anomalies. *The Journal of Maternal-Fetal & Neonatal Medicine*, 9, pp.1–5.

Kia, A. et al., 2013. Inhibition of Histone Deacetylation and DNA Methylation Improves Gene Expression Mediated by the Adeno-Associated Virus/Phage in Cancer Cells. *Viruses*, 5(10), pp.2561–2572.

Kim, M.J. et al., 2009. Widespread microbial invasion of the chorioamniotic membranes is a consequence and not a cause of intra-amniotic infection. *Laboratory investigation; a journal of technical methods and pathology*, 89(8), pp.924–36.

Kim, S. et al., 2011. Astrocytes promote TNF-mediated toxicity to oligodendrocyte precursors. *Journal of Neurochemistry*, 116(1), pp.53–66.

Kindinger, L.M. et al., 2016. Relationship between vaginal microbial dysbiosis, inflammation, and pregnancy outcomes in cervical cerclage. *Science Translational Medicine*, 8(350), p.350ra102-350ra102.

Kindinger, L.M. et al., 2016. The effect of gestational age and cervical length measurements in the prediction of spontaneous preterm birth in twin pregnancies: an individual patient level meta-analysis. *BJOG : an international journal of obstetrics and gynaecology*, 123(6), pp.877–84.

Kindinger, L.M. et al., 2017. The interaction between vaginal microbiota, cervical length, and vaginal progesterone treatment for preterm birth risk. *Microbiome*, 5(1), p.6.

King, A.E. et al., 2007. Innate Immune Defences in the Human Uterus during Pregnancy. *Placenta*, 28(11–12), pp.1099–1106.

King, J. & Flenady, V., 2002. Prophylactic antibiotics for inhibiting preterm labour with intact membranes. *Cochrane database of systematic reviews (Online)*, (4), pp.CD000246.

Kirby, M.A. et al., 2016. Progesterone Receptor–Mediated Actions Regulate Remodeling of the Cervix in Preparation for Preterm Parturition. *Reproductive Sciences*, 23(11), pp.1473–1483.

Klüver, E. et al., 2005. Structure−Activity Relation of Human β-Defensin 3: Influence of Disulfide Bonds and Cysteine Substitution on Antimicrobial Activity and Cytotoxicity †. *Biochemistry*, 44(28), pp.9804–9816.

Koczot, F.J. et al., 1973. Self-complementarity of terminal sequences within plus or minus strands of adenovirus-associated virus DNA. *Proceedings of the National Academy of Sciences of the United States of America*, 70(1), pp.215–219.

Kong, Q. et al., 2009. Transgene expression is associated with copy number and cytomegalovirus promoter methylation in transgenic pigs. *PLoS ONE*, 4(8), p.e6679.

Korkmaz, B., Moreau, T. & Gauthier, F., 2008. Neutrophil elastase, proteinase 3 and cathepsin G: Physicochemical properties, activity and physiopathological functions. *Biochimie*, 90(2), pp.227–242.

Kotin, R.M. et al., 1990. Site-specific integration by adeno-associated virus. *Proceedings of the National Academy of Sciences of the United States of America*, 87(6), pp.2211–2215.

Koullali, B. et al., 2016. Risk assessment and management to prevent preterm birth. *Seminars in fetal & neonatal medicine*, 21(2), pp.80–88.

Kužnik, A. et al., 2011. Mechanism of Endosomal TLR Inhibition by Antimalarial Drugs and Imidazoquinolines. *The Journal of Immunology*, 186(8), pp.4794-4804.

Kyrgiou, M. et al., 2014. Proportion of cervical excision for cervical intraepithelial neoplasia as a predictor of pregnancy outcomes. *International Journal of Gynecology and Obstetrics*, 128(2), pp.141–147.

Lahra, M.M. & Jeffery, H.E., 2004. A fetal response to chorioamnionitis is associated with early survival after preterm birth. *American Journal of Obstetrics and Gynecology*, 190(1), pp.147–151.

Laughon, S.K. et al., 2014. The NICHD Consecutive Pregnancies Study: recurrent preterm delivery by subtype. *American Journal of Obstetrics and Gynecology*, 210(2), p.131.e1-131.e8.

Lawn, J.E. et al., 2010. Global report on preterm birth and stillbirth (1 of 7): definitions, description of the burden and opportunities to improve data. *BMC pregnancy and childbirth*, 10 Suppl 1(Suppl 1), p.S1.

Lee, P.R. et al., 2003. Therapeutic effect of cyclo-oxygenase inhibitors with different isoform selectivity in lipopolysaccharide-induced preterm birth in mice. *American Journal of Obstetrics and Gynecology*, 189(1), pp.261–266.

Lee, S.H. et al., 2010. Antibacterial and lipopolysaccharide (LPS)-neutralising activity of human cationic antimicrobial peptides against periodontopathogens. *International Journal of Antimicrobial Agents,* 35(2), pp.138-145.

Lee, Y. et al., 2015. Is there a stepwise increase in neonatal morbidities according to histological stage (or grade) of acute chorioamnionitis and funisitis?: effect of gestational age at delivery. *Journal of perinatal medicine*, 43(2), pp.259–267.

Lei, J. et al., 2015. Murine model: maternal administration of stem cells for prevention of prematurity. *American journal of obstetrics and gynecology*, 212(5), p.639.e1-10.

Leitich, H. et al., 2003. Bacterial vaginosis as a risk factor for preterm delivery: a meta-analysis. *American journal of obstetrics and gynecology*, 189(1), pp.139–147.

Leitner, K. et al., 2014. IL-1 Receptor Blockade Prevents Fetal Cortical Brain Injury but Not Preterm Birth in a Mouse Model of Inflammation-Induced Preterm Birth and Perinatal Brain Injury. *American Journal of Reproductive Immunology*, 71(5), pp.418–426.

Leppi, T.J., 1964. A study of the Uterine Cervix of the Mouse. *The Anatomical record*, 150, pp.51–65.

Leviton, A. et al., 2010. Microbiologic and Histologic Characteristics of the Extremely Preterm Infant's Placenta Predict White Matter Damage and Later Cerebral Palsy. The ELGAN Study. *Pediatric Research*, 67(1), pp.95–101.

Li, H. et al., 2011. Assessing the potential for AAV vector genotoxicity in a murine model. *Blood*, 117(12), pp.3311–3319.

Li, J. et al., 2005. Peroxynitrite generated by inducible nitric oxide synthase and NADPH oxidase mediates microglial toxicity to oligodendrocytes. *Proceedings of the National Academy of Sciences of the United States of America*, 102(28), pp.9936–9941.

Li, J. et al., 2008. Tumor Necrosis Factor Mediates Lipopolysaccharide-Induced Microglial Toxicity to Developing Oligodendrocytes When Astrocytes Are Present. *Journal of Neuroscience*, 28(20), pp.5321–5330.

Li, L.L. & Dinauer, 1998. Reconstitution of NADPH oxidase activity in human X-linked chronic granulomatous disease myeloid cells after stable gene transfer using a recombinant adeno-associated virus 2 vector. *Blood cells, molecules & diseases*, 24(4), pp.522–538.

Lin, P.W., Nasr, T.R. & Stoll, B.J., 2008. Necrotizing Enterocolitis: Recent Scientific Advances in Pathophysiology and Prevention. *Seminars in Perinatology*, 32(2), pp.70–82.

Liu, L. et al., 2015. Global, regional, and national causes of child mortality in 2000-13, with projections to inform post-2015 priorities: an updated systematic analysis. *The Lancet*, 385, pp.430–440.

Lucovnik, M. et al., 2011. Neutrophil defensins but not interleukin-6 in vaginal fluid after preterm premature rupture of membranes predict fetal/neonatal inflammation and infant neurological impairment. *Acta Obstetricia et Gynecologica Scandinavica*, 90(8), pp.908–916.

Lyall, K. et al., 2017. The Changing Epidemiology of Autism Spectrum Disorders. *Annual Review of Public Health*, 38(1), pp.81–102.

Lynch, A.M. et al., 2014. Association of extremes of prepregnancy BMI with the clinical presentations of preterm birth. *American Journal of Obstetrics and Gynecology*, 210(5), p.428.e1-428.e9.

MacIntyre, D.A. et al., 2014. Activator protein 1 is a key terminal mediator of inflammation-induced preterm labor in mice. *FASEB Journal*, 28(5), pp.2358–2368.

MacIntyre, D.A. et al., 2015. The vaginal microbiome during pregnancy and the postpartum period in a European population. *Scientific Reports*, 5(1), pp.8988.

Macones, G.A. et al., 2004. A polymorphism in the promoter region of TNF and bacterial vaginosis: Preliminary evidence of gene-environment interaction in the etiology of spontaneous preterm birth. *American Journal of Obstetrics and Gynecology*, 190(6), pp.1504–1508.

Mangham, L.J. et al., 2009. The cost of preterm birth throughout childhood in England and Wales. *Pediatrics*, 123(2), pp.e312-327.

Manno, C.S. et al., 2006. Successful transduction of liver in hemophilia by AAV-Factor IX and limitations imposed by the host immune response. *Nature medicine*, 12(3), pp.342–347.

Marlow, N. et al., 2005. Neurologic and Developmental Disability at Six Years of Age after Extremely Preterm Birth. *New England Journal of Medicine*, 352(1), pp.9–19.

Marlow, N. & Budge, H., 2005. Prevalence, causes, and outcome at 2 years of age of newborn encephalopathy. *Archives of disease in childhood. Fetal and neonatal edition*, 90(3), pp.193-194.

Martin, J.N. et al., 2017. In Pursuit of Progress Toward Effective Preterm Birth Reduction. *Obstetrics & Gynecology*, 129(4), pp.715–719.

McEniery, C.M. et al., 2011. Cardiovascular consequences of extreme prematurity: the EPICure study. *Journal of Hypertension*, 29(7), pp.1367–1373.

McGlasson, S.L. et al., 2017. Human β-defensin 3 increases the TLR9-dependent response to bacterial DNA. *European Journal of Immunology*, 47(4), pp.1–7.

Mehta, V. et al., 2016. Gene Targeting to the Uteroplacental Circulation of Pregnant Guinea Pigs. *Reproductive Sciences*, 23(8), pp.1087–1095.

Mehta, V. et al., 2014. Local over-expression of VEGF-DΔNΔCin the uterine arteries of pregnant sheep results in long-term changes in uterine artery contractility and angiogenesis. *PLoS ONE*, 9(6), p.E100021.

Mei-Dan, E. et al., 2015. The unborn smoker: association between smoking during pregnancy and adverse perinatal outcomes. *Journal of Perinatal Medicine*, 43(5), pp.553–558.

Meldrum, S.J. et al., 2013. Autism spectrum disorder in children born preterm—role of exposure to perinatal inflammation. *Frontiers in Neuroscience*, 7, pp.123.

Mendz, G.L., Kaakoush, N.O. & Quinlivan, J.A., 2013. Bacterial aetiological agents of intra-amniotic infections and preterm birth in pregnant women. *Frontiers in cellular and infection microbiology*, 16(3), pp.58.

Mestas, J. & Hughes, C.C.W., 2004. Of mice and not men: differences between mouse and human immunology. *Journal of immunology (Baltimore, Md. : 1950)*, 172(5), pp.2731–2738.

Meyer, U. et al., 2006. The time of prenatal immune challenge determines the specificity of inflammation-mediated brain and behavioral pathology. *The Journal of neuroscience : the official journal of the Society for Neuroscience*, 26(18), pp.4752–4762.

Meyer, U., Feldon, J. & Yee, B.K., 2009. A Review of the Fetal Brain Cytokine Imbalance Hypothesis of Schizophrenia. *Schizophrenia Bulletin*, 35(5), pp.959–972.

Meyer, U., Schwarz, M.J. & Müller, N., 2011. Inflammatory processes in schizophrenia: A promising neuroimmunological target for the treatment of negative/cognitive symptoms and beyond. *Pharmacology & Therapeutics*, 132(1), pp.96–110

Migale, R. et al., 2015a. Specific Lipopolysaccharide Serotypes Induce Differential Maternal and Neonatal Inflammatory Responses in a Murine Model of Preterm Labor. *American Journal of Pathology*, 185(9), pp.2390–2401.

Migale, R. et al., 2015b. Specific Lipopolysaccharide Serotypes Induce Differential Maternal and Neonatal Inflammatory Responses in a Murine Model of Preterm Labor. *American Journal of Pathology*, 185(9), pp.2390–2401.

Mingozzi, F. et al., 2013. Cellular Immune Responses To Vector In a Gene Therapy Trial For Hemophilia B Using An AAV8 Self-Complementary Factor IX Vector. *Blood*, 122(21), pp.717.

Mingozzi, F. et al., 2014. gene therapy Review Article Immune responses to AAV vectors : overcoming barriers to successful gene therapy. , 122(1), pp.23–36.

Mingozzi, F. et al., 2007. Modulation of tolerance to the transgene product in a nonhuman primate model of AAV-mediated gene transfer to liver. *Blood*, 110(7), pp.2334–2341.

Misund, A.R., Nerdrum, P. & Diseth, T.H., 2014. Mental health in women experiencing preterm birth. *BMC Pregnancy and Childbirth*, 14(1), pp.263.

Molchanova, N., Hansen, P.R. & Franzyk, H., 2017. Advances in Development of Antimicrobial Peptidomimetics as Potential Drugs. *Molecules*, 22(9), pp.1430.

Moore, T. et al., 2012. Neurological and developmental outcome in extremely preterm children born in England in 1995 and 2006: the EPICure studies. *British Medical Journal*, 345(12), pp.217–224.

Moutquin, J.M., 2003. Classification and heterogeneity of preterm birth. *BJOG: An International Journal of Obstetrics and Gynaecology*, 110(Suppl 20), pp.30–33.

Murphy, C. et al., 2017. Intratumoural production of TNFα by bacteria mediates cancer therapy P. L. Ho, ed. *PLOS ONE*, 12(6), p.e0180034.

Murphy, K. & Mitchell, C.M., 2016. The Interplay of Host Immunity, Environment and the Risk of Bacterial Vaginosis and Associated Reproductive Health Outcomes. *Journal of Infectious Diseases*, 214(Suppl 1), pp.S29–S35.

Nadeau-Vallée, M. et al., 2017. Antenatal Suppression of IL-1 Protects against Inflammation-Induced Fetal Injury and Improves Neonatal and Developmental Outcomes in Mice. *The Journal of Immunology*, 198(5):2047-2062.

Nadeau-Vallée, M. et al., 2015. Novel Noncompetitive IL-1 Receptor–Biased Ligand Prevents Infection- and Inflammation-Induced Preterm Birth. *The Journal of Immunology*, 195(7), pp.3402–3415.

Nagaoka, I. et al., 2008. Evaluation of the effect of human -defensins on neutrophil apoptosis. *International Immunology*, 20(4), pp.543–553.

Nagaoka, I. et al., 2012. Modulation of Neutrophil Apoptosis by Antimicrobial Peptides. *ISRN Microbiology*, 27(2012), pp.1–12.

Nakai, H. et al., 2001. Extrachromosomal recombinant adeno-associated virus vector genomes are primarily responsible for stable liver transduction in vivo. *Journal of Virology*, 75(15), pp.6969–6976.

Nathwani, A. et al., 2012. Adenovirus-associated virus vector-mediated gene transfer in hemophilia B. , 365(25), pp.2357–2365.

Nathwani, A.C. et al., 2014. Long-Term Safety and Efficacy of Factor IX Gene Therapy in Hemophilia B. *New England Journal of Medicine*, 371(21), pp.1994–2004.

Naumer, M. et al., 2012. Properties of the Adeno-Associated Virus Assembly-Activating Protein. *Journal of Virology*, 86(23), pp.13038–13048.

nc3Rs, 2014. The 3Rs. *The National centre for the replacement, refinement and reduction of animals in research*. Available at: https://www.nc3rs.org.uk/the-3rs.

Nguyen, D.P. et al., 2004. Mycoplasma hominis in mid-trimester amniotic fluid: relation to pregnancy outcome. *Journal of perinatal medicine*, 32(4), pp.323–6.

NICE, 2015. Preterm labour and birth. *Nice*, (November).

Niinikoski, H. et al., 2004. Onset of small intestinal atrophy is associated with reduced intestinal blood flow in TPN-fed neonatal piglets. *The Journal of nutrition*, 134(6), pp.1467–1474.

Niyonsaba, F., Ogawa, H. & Nagaoka, I., 2004. Human beta-defensin-2 functions as a chemotactic agent for tumour necrosis factor-alpha-treated human neutrophils. *Immunology*, 111(3), pp.273–281.

Norman, J.E. et al., 2016. Vaginal progesterone prophylaxis for preterm birth (the OPPTIMUM study): a multicentre, randomised, double-blind trial. *The Lancet*, 6736(16), pp.1–11.

O'Connor, A.R. & Fielder, A.R., 2007. Visual outcomes and perinatal adversity. *Seminars in Fetal and Neonatal Medicine*, 12(5), pp.408–414.

Oh, K.J. et al., 2017. Twenty-four percent of patients with clinical chorioamnionitis in preterm gestations have no evidence of either culture-proven intraamniotic infection or intraamniotic inflammation. *American Journal of Obstetrics and Gynecology*, 216(6), p.604.e1-604.e11.

Orzechowski, K.M. et al., 2014. A Universal Transvaginal Cervical Length Screening Program for Preterm Birth Prevention. *Obstetrics & Gynecology*, 124(3), pp.520–525.

Othman, E.R. et al., 2016. Enhancing Adenoviral-Mediated Gene Transfer and Expression to Endometrial Cells. *Reproductive Sciences*. 23(8), pp.1109-1115.

Owen, J. et al., 2001. Mid-trimester endovaginal sonography in women at high risk for spontaneous preterm birth. *JAMA*, 286(11), pp.1340–8.

Palliser, D. et al., 2006. An siRNA-based microbicide protects mice from lethal herpes simplex virus 2 infection. *Nature*, 439(7072), pp.89–94.

Pandey, S. et al., 2012. Obstetric and perinatal outcomes in singleton pregnancies resulting from IVF/ICSI: a systematic review and meta-analysis. *Human Reproduction Update*, 18(5), pp.485–503.

Paton, M.C.B. et al., 2017. Perinatal Brain Injury As a Consequence of Preterm Birth and Intrauterine Inflammation: Designing Targeted Stem Cell Therapies. *Frontiers in Neuroscience*, 11(April), pp.200.

Pazgier, M. et al., 2006. Human beta-defensins. *Cellular and Molecular Life Sciences*, 63(11), pp.1294–1313.

Pedroni, S.M.A. et al., 2014. Complement inhibition and statins prevent fetal brain cortical abnormalities in a mouse model of preterm birth. *Biochimica et Biophysica Acta - Molecular Basis of Disease*, 1842(1), pp.107–115.

Pestonjamasp, V.K., Huttner, K.H. & Gallo, R.L., 2001. Processing site and gene structure for the murine antimicrobial peptide CRAMP. *Peptides*, 22(10), pp.1643–1650.

Petricevic, L. et al., 2014. Characterisation of the vaginal Lactobacillus microbiota associated with preterm delivery. *Scientific reports*, 30(4), pp.5136.

Pillay, S. et al., 2017. AAV serotypes have distinctive interactions with domains of the cellular receptor AAVR. *Journal of Virology*, p.JVI.00391-17.

Pillay, S. et al., 2016. An essential receptor for adeno-associated virus infection. *Nature*, 530(7588), pp.108–112.

Pillay, S. & Carette, J.E., 2017. Host determinants of adeno-associated viral vector entry. *Current opinion in virology*, 24, pp.124–131.

Pingel, L.C. et al., 2008. Human beta-defensin 3 binds to hemagglutinin B (rHagB), a non-fimbrial adhesin from Porphyromonas gingivalis, and attenuates a pro-inflammatory cytokine response. *Immunology and cell biology*, 86(8), pp.643–649.

Pirianov, G. et al., 2009. The cyclopentenone 15-deoxy-delta 12,14-prostaglandin J(2) delays lipopolysaccharide-induced preterm delivery and reduces mortality in the newborn mouse. *Endocrinology*, 150(2), pp.699–706

Prösch, S. et al., 1996. Inactivation of the very strong HCMV immediate early promoter by DNA CpG methylation in vitro. *Biological chemistry*, 377(3), pp.195–201.

Racicot, K. et al., 2013. Viral infection of the pregnant cervix predisposes to ascending bacterial infection. *Journal of immunology*, 191(2), pp.934–41.

Randis, T.M. et al., 2014. Group B Streptococcus β-hemolysin/cytolysin breaches maternal-fetal barriers to cause preterm birth and intrauterine fetal demise in vivo. *Journal of Infectious Diseases*, 210(2), pp.265–273.

Reilly, R. et al., 2012. Birth outcomes following treatment for precancerous changes to the cervix: A population-based record linkage study. *BJOG: An International Journal of Obstetrics and Gynaecology*, 119(2), pp.236–244.

Reznikov, L.L. et al., 1999. Utilization of endoscopic inoculation in a mouse model of intrauterine infection-induced preterm birth: role of interleukin 1beta. *Biology of reproduction*, 60(5), pp.1231–1238.

Riley, J.K. & Nelson, D.M., 2010. Toll-like receptors in pregnancy disorders and placental dysfunction. *Clinical reviews in allergy & immunology*, 39(3), pp.185–193.

Rinaldi, S.F. et al., 2014. Decidual neutrophil infiltration is not required for preterm birth in a mouse model of infection-induced preterm labor. *Journal of immunology,* 192(5), pp.2315–2325.

Rinaldi, S.F. et al., 2015. Ultrasound-guided intrauterine injection of lipopolysaccharide as a novel model of preterm birth in the mouse. *American Journal of Pathology*, 185(5), pp.1201–1206.

Rizzo, A., Losacco, A. & Carratelli, C.R., 2013. Lactobacillus crispatus modulates epithelial cell defense against Candida albicans through Toll-like receptors 2 and 4, interleukin 8 and human β-defensins 2 and 3. *Immunology Letters*, 156(1–2), pp.102–109.

Röhrl, J. et al., 2008. Identification and Biological Characterization of Mouse β-Defensin 14, the Orthologue of Human β-Defensin 3. *Journal of Biological Chemistry*, 283(9), pp.5414–5419.

Romero, R., 2011. Preterm Labor: One syndrome, Many causes. *Science*, 18(11), pp.1492–1501.

Romero, R. et al., 2001. The role of infection in preterm labour and delivery. *Paediatric and Perinatal Epidemiology*, 15 (Suppl 2), pp.41–56.

Romero, R. et al., 2014. The vaginal microbiota of pregnant women who subsequently have spontaneous preterm labor and delivery and those with a normal delivery at term. *Microbiome*, 2(1), pp.18.

Romero, R. et al., 2016. Vaginal progesterone decreases preterm birth ≤ 34 weeks of gestation in women with a singleton pregnancy and a short cervix: an updated meta-analysis including data from the OPPTIMUM study. *Ultrasound in obstetrics & gynecology*, 48(3), pp.308–317.

Rose, J.A. et al., 1969. Evidence for a single-stranded adenovirus-associated virus genome: formation of a DNA density hybrid on release of viral DNA. *Proceedings of the National Academy of Sciences of the United States of America*, 64(3), pp.863–869.

Rose, J.A., Hoggan, M.D. & Shatkin, A.J., 1966. Nucleic acid from an adeno-associated virus: chemical and physical studies. *Proceedings of the National Academy of Sciences of the United States of America*, 56(1), pp.86–92.

Rubens, C.E. et al., 2014. Prevention of preterm birth: harnessing science to address the global epidemic. *Science translational medicine*, 6(262), p.262sr5.

Russell, S. et al., 2017. Efficacy and safety of voretigene neparvovec (AAV2-hRPE65v2) in patients with RPE65 -mediated inherited retinal dystrophy: a randomised, controlled, open-label, phase 3 trial. *The Lancet*, 390(10097), pp.849-860.

Saadani-Makki, F. et al., 2008. Intrauterine administration of endotoxin leads to motor deficits in a rabbit model: a link between prenatal infection and cerebral palsy. *American Journal of Obstetrics and Gynecology*, 199(6), pp.651.e1-651.e7.

Sabban, H. et al., 2017. Obstetrical and perinatal morbidity and mortality among in-vitro fertilization pregnancies: a population-based study. *Archives of Gynecology and Obstetrics*, 296(1), pp.107–113.

Sadowsky, D.W. et al., 2006. Preterm labor is induced by intraamniotic infusions of interleukin-1β and tumor necrosis factor-α but not by interleukin-6 or interleukin-8 in a nonhuman primate model. *American Journal of Obstetrics and Gynecology*, 195(6), pp.1578–1589.

Sahly, H. et al., 2006. Activity of human beta-defensins 2 and 3 against ESBL-producing Klebsiella strains. *Journal of Antimicrobial Chemotherapy*, 57(3), pp.562–565.

Samejima, T. et al., 2015. Elevated concentration of secretory leukocyte protease inhibitor in the cervical mucus before delivery. *American Journal of Obstetrics and Gynecology*, 214(6), pp.741.e1.

Samulski, R.J. et al., 1982. Cloning of adeno-associated virus into pBR322: rescue of intact virus from the recombinant plasmid in human cells. *Proceedings of the National Academy of Sciences of the United States of America*, 79(6), pp.2077–2081.

Sawamura, D. et al., 2005. Beta defensin-3 engineered epidermis shows highly protective effect for bacterial infection. *Gene Therapy*, 12(10), pp.857–861.

Schaaf, J.M. et al., 2013. Ethnic and racial disparities in the risk of preterm birth: a systematic review and meta-analysis. *American journal of perinatology*, 30(6), pp.433–450.

Scharf, S. et al., 2012. Streptococcus pneumoniae induces human β-defensin-2 and -3 in human lung epithelium. *Experimental Lung Research*, 38(2), pp.100–110.

Schnepp, B.C. et al., 2003. Genetic fate of recombinant adeno-associated virus vector genomes in muscle. *Journal of virology*, 77(6), pp.3495–3504.

Schuettrumpf, J. et al., 2006. Inadvertent germline transmission of AAV2 vector: findings in a rabbit model correlate with those in a human clinical trial. *Molecular therapy : the journal of the American Society of Gene Therapy*, 13(6), pp.1064–1073.

Scott, M.G. et al., 2002. The Human Antimicrobial Peptide LL-37 Is a Multifunctional Modulator of Innate Immune Responses. *The Journal of Immunology*, 169(7):3883-3891.

Semple, B.D. et al., 2013. Brain development in rodents and humans: Identifying benchmarks of maturation and vulnerability to injury across species. *Progress in neurobiology*, 106–107, pp.1–16.

Semple, F. et al., 2011. Human beta-defensin 3 affects the activity of pro-inflammatory pathways associated with MyD88 and TRIF. *European Journal of Immunology*, 41(11), pp.3291–3300.

Semple, F. et al., 2015. Human beta-defensin 3 Exacerbates MDA5 but Suppresses TLR3 Responses to the Viral Molecular Pattern Mimic Polyinosinic:Polycytidylic Acid. *PLoS Genetics*, 11(12), pp.1–21.

Semple, F. et al., 2010. Human beta-defensin 3 has immunosuppressive activity in vitro and in vivo. *European Journal of Immunology*, 40(4), pp.1073–1078.

Sen, G. & Sarkar, S., 2005. Transcriptional signaling by double-stranded RNA: role of TLR3. *Cytokine & Growth Factor Reviews*, 16(1), pp.1–14.

Shachar, B. et al., 2016. Interpregnancy interval after live birth or pregnancy termination and estimated risk of preterm birth: a retrospective cohort study. *BJOG: An International Journal of Obstetrics & Gynaecology*, 123(12), pp.2009–2017.

Sharma, A. et al., 2010. AAV serotype influences gene transfer in corneal stroma in vivo. *Experimental Eye Research*, 91(3), pp.440–448.

Shelburne, C.E. et al., 2005. Induction of beta-defensin resistance in the oral anaerobe Porphyromonas gingivalis. *Antimicrobial Agents and Chemotherapy*, 49(1), pp.183–187.

Shennan, A. et al., 2006. A randomised controlled trial of metronidazole for the prevention of preterm birth in women positive for cervicovaginal fetal fibronectin: The PREMET Study. *BJOG: An International Journal of Obstetrics and Gynaecology*, 113(1), pp.65–74.

Shi, L. et al., 2009. Activation of the maternal immune system alters cerebellar development in the offspring. *Brain, Behavior, and Immunity*, 23(1), pp.116–123.

Shi, L. et al., 2003. Maternal influenza infection causes marked behavioral and pharmacological changes in the offspring. *The Journal of neuroscience : the official journal of the Society for Neuroscience*, 23(1), pp.297–302.

Simonsen, K.A. et al., 2014. Early-Onset Neonatal Sepsis. *Clinical Microbiology Reviews*, 27(1), pp.21–47.

Somanathan, S. et al., 2010. AAV vectors avoid inflammatory signals necessary to render transduced hepatocyte targets for destructive T cells. *Molecular therapy : the journal of the American Society of Gene Therapy*, 18(5), pp.977–982.

Sondhi, D. et al., 2007. Enhanced Survival of the LINCL Mouse Following CLN2 Gene Transfer Using the rh.10 Rhesus Macaque-derived Adeno-associated Virus Vector. *Molecular Therapy*, 15(3), pp.481–491.

de Souza, A.P.D. et al., 2007. Genital CD8+ T cell response to HIV-1 gag in mice immunized by mucosal routes with a recombinant simian adenovirus. *Vaccine*, 25(1), pp.109–116.

Steel, J.H. et al., 2005. Bacteria and Inflammatory Cells in Fetal Membranes Do Not Always Cause Preterm Labor. *Pediatric Research*, 57(3), pp.404–411.

Stock, S.J. et al., 2016. Elafin (SKALP / Trappin-2 / proteinase inhibitor-3) Is Produced by the Cervix in Pregnancy and Cervicovaginal Levels Are Diminished in Bacterial Vaginosis. *Reproductive Sciences*, pp.1125–1134.

Streck, C.J. et al., 2005. Adeno-associated virus vector-mediated systemic delivery of IFN-beta combined with low-dose cyclophosphamide affects tumor regression in murine neuroblastoma models. *Clinical cancer research : an official journal of the American Association for Cancer Research*, 11(16), pp.6020–6029.

Su, L.L., Samuel, M. & Chong, Y.S., 2014. Progestational agents for treating threatened or established preterm labour. *Cochrane Database of Systematic Reviews*, (4), p.CD006770.

Subramaniam, A. et al., 2012. Antimicrobials for preterm birth prevention: An overview. *Infectious Diseases in Obstetrics and Gynecology*, 2012, 157159

Suff, N. & Waddington, S.N., 2017. The power of bioluminescence imaging in understanding host-pathogen interactions. *Methods*, 127, pp.69–78.

Summerford, C. & Samulski, R.J., 1998. Membrane-associated heparan sulfate proteoglycan is a receptor for adeno-associated virus type 2 virions. *Journal of virology*, 72(2), pp.1438–1445.

Sundtoft, I. et al., 2017. Cervical collagen is reduced in non-pregnant women with a history of cervical insufficiency and a short cervix. *Acta Obstetricia et Gynecologica Scandinavica*, 96(8), pp.984–990.

Svenson, J. et al., 2008. Antimicrobial Peptides with Stability toward Tryptic Degradation †. *Biochemistry*, 47(12), pp.3777–3788.

Takami, M. et al., 2014. A classification of congenital uterine anomalies predicting pregnancy outcomes. *Acta Obstetricia et Gynecologica Scandinavica*, 93(7), pp.691–697.

Takeda, K., Kaisho, T. & Akira, S., 2003. Toll-Like Receptors. *Annual Review of Immunology*, 21(1), pp.335–376.

Tamrakar, R. et al., 2007. Association between Lactobacillus species and bacterial vaginosis-related bacteria, and bacterial vaginosis scores in pregnant Japanese women. *BMC infectious diseases*, 7(1), p.128.

Taylor, K. et al., 2008. Analysis and separation of residues important for the chemoattractant and antimicrobial activities of β-defensin 3. *Journal of Biological Chemistry*, 283(11), pp.6631–6639.

Tejera, P. et al., 2009. Genetic polymorphisms of peptidase inhibitor 3 (elafin) are associated with acute respiratory distress syndrome. *American Journal of Respiratory Cell and Molecular Biology*, 41(6), pp.696–704.

Tewary et al., 2013. Beta-defensin 2 and 3 promote the uptake of self and CpG DNA, enhance IFN-alpha production by human plasmacytoid dendritic cells and promote inflammation. *Journal of immunology*, 73(4), pp.389–400.

Thompson, J.M.D. et al., 2006. Secular trends in socio-economic status and the implications for preterm birth. *Paediatric and Perinatal Epidemiology*, 20(3), pp.182–187.

Thwaite, R. et al., 2015. AAVrh.10 immunogenicity in mice and humans. Relevance of antibody cross-reactivity in human gene therapy. *Gene Therapy*, 22(2), pp.196–201.

To, M. et al., 2004. Cervical cerclage for prevention of preterm delivery in woman with short cervix: randomised controlled trial. *The Lancet*, 363, pp.1849–1853.

Tosi, M.F., 2005. Innate immune responses to infection. *Journal of Allergy and Clinical Immunology*, 116(2), pp.241–249.

Trempe, J.P., Mendelson, E. & Carter, B.J., 1987. Characterization of adeno-associated virus rep proteins in human cells by antibodies raised against rep expressed in Escherichia coli. *Virology*, 161(1), pp.18–28.

Tsukuba, T. et al., 2006. Cathepsin E-deficient mice show increased susceptibility to bacterial infection associated with the decreased expression of multiple cell surface Toll-like receptors. *Journal of Biochemistry*, 140(1), pp.57–66.

Tuğcu-Demiröz, F., Acartürk, F. & Erdoğan, D., 2013. Development of long-acting bioadhesive vaginal gels of oxybutynin: Formulation, in vitro and in vivo evaluations. *International Journal of Pharmaceutics*, 457(1), pp.25–39.

Tulone, C. et al., 2007. Natural cathepsin E deficiency in the immune system of C57BL/6J mice. *Immunogenetics*, 59(12), pp.927–935.

Valore, E. V., Wiley, D.J. & Ganz, T., 2006. Reversible deficiency of antimicrobial polypeptides in bacterial vaginosis. *Infection and Immunity*, 74(10), pp.5693–5702.

Vance, M. et al., 2016. AAV Gene Therapy for MPS1-associated Corneal Blindness. *Scientific Reports*, 6(1), p.22131.

Vargas, D.L. et al., 2005. Neuroglial activation and neuroinflammation in the brain of patients with autism. *Annals of Neurology*, 57(1), pp.67–81.

van der Ven, J. et al., 2015. The capacity of mid-pregnancy cervical length to predict preterm birth in low-risk women: a national cohort study. *Acta Obstetricia et Gynecologica Scandinavica*, 94(11), pp.1223–1234.

Verstraelen, H. et al., 2009. Longitudinal analysis of the vaginal microflora in pregnancy suggests that L. crispatus promotes the stability of the normal vaginal microflora and that L. gasseri and/or L. iners are more conducive to the occurrence of abnormal vaginal microflora. *BMC microbiology*, 9, p.116.

Vogt, C. et al., 2008. Successful inhibition of excitotoxic neuronal damage and microglial activation after delayed application of interleukin-1 receptor antagonist. *Journal of Neuroscience Research*, 86(15), pp.3314–3321.

Vornhagen, J. et al., 2016. Bacterial Hyaluronidase Promotes Ascending GBS Infection and Preterm Birth. *mBio*, 7(3), e00781-816.

Wagner, H., 2002. Interactions between bacterial CpG-DNA and TLR9 bridge innate and adaptive immunity. *Current opinion in microbiology*, 5(1), pp.62–69.

Waldorf, K.M.A., Rubens, C.E. & Gravett, M.G., 2011. Use of nonhuman primate models to investigate mechanisms of infection-associated preterm birth. *BJOG: An International Journal of Obstetrics & Gynaecology*, 118(2), pp.136–144.

Wallenius, M. et al., 2015. Secular trends of pregnancies in women with inflammatory connective tissue disease. *Acta Obstetricia et Gynecologica Scandinavica*, 94(11), pp.1195–1202.

Wang, G. & Guangshun, 2014. Human Antimicrobial Peptides and Proteins. *Pharmaceuticals*, 7(5), pp.545–594.

Wang, X. et al., 2007. Effects of intrauterine inflammation on the developing mouse brain. *Brain Research*, 1144, pp.180–185.

Wang, X.-F. et al., 2015. Antimicrobial activity of human β-defensins against lactic acid bacteria. *Natural Product Research*, 29(22), pp.2164–2166.

WHO, 2015. WHO | Preterm birth. *Fact sheet N°363*. Available at: http://www.who.int/mediacentre/factsheets/fs363/en/ [Accessed July 18, 2017].

Wickham, T.J. et al., 1993. Integrins alpha v beta 3 and alpha v beta 5 promote adenovirus internalization but not virus attachment. *Cell*, 73(2), pp.309–319.

Wierzbicki, A.S. & Viljoen, A., 2013. Alipogene tiparvovec: gene therapy for lipoprotein lipase deficiency. *Expert Opinion on Biological Therapy*, 13(1), pp.7–10.

Wiesner, J. & Vilcinskas, A., 2010. Antimicrobial peptides: the ancient arm of the human immune system. *Virulence*, 1(5), pp.440–464.

Witcomb, L.A. et al., 2015. Bioluminescent imaging reveals novel patterns of colonization and invasion in systemic Escherichia coli K1 experimental infection in the neonatal rat. *Infection and Immunity*, 83(12), pp.4528–4540.

Witkin, S.S. et al., 2013. Influence of vaginal bacteria and D- and L-lactic acid isomers on vaginal extracellular matrix metalloproteinase inducer: Implications for protection against upper genital tract infections. *mBio*, 4(4), pp.1–8.

Witt, A. et al., 2005. Increased intrauterine frequency of Ureaplasma urealyticum in women with preterm labor and preterm premature rupture of the membranes and subsequent cesarean delivery. *American Journal of Obstetrics and Gynecology*, 193(5), pp.1663–1669.

Wozniak, K.L. et al., 2005. Immunotherapeutic approaches to enhance protective immunity against Candida vaginitis. *Medical mycology*, 43(7), pp.589–601.

Wu, H.-C. et al., 2009. Subclinical Histologic Chorioamnionitis and Related Clinical and Laboratory Parameters in Preterm Deliveries. *Pediatrics & Neonatology*, 50(5), pp.217–221.

Wu, T.-L. et al., 2014. CD8+ T Cell Recognition of Epitopes Within the Capsid of Adeno-associated Virus 8–based Gene Transfer Vectors Depends on Vectors' Genome. *Molecular Therapy*, 22(1), pp.42–51.

Wu, Z. et al., 2003. Engineering disulfide bridges to dissect antimicrobial and chemotactic activities of human beta-defensin 3. *Proceedings of the National Academy of Sciences of the United States of America*, 100(15), pp.8880–8885.

Xia, Z. et al., 2014. Transplantation of BMSCs expressing hVEGF165 /hBD3 promotes wound healing in rats with combined radiation-wound injury. *International wound journal*, 11(3), pp.293–303.

Xiao, L. et al., 2014. Suppression of antimicrobial peptide expression by Ureaplasma species. *Infection and Immunity*, 82(4), pp.1657–1665.

Xiao, X., Li, J. & Samulski, R.J., 1996. Efficient long-term gene transfer into muscle tissue of immunocompetent mice by adeno-associated virus vector. *Journal of virology*, 70(11), pp.8098–8108.

Xu, J., Holzman, C. & Arvidson, C., 2008. Midpregnancy Vaginal Fluid Defensins, Bacterial Vaginosis, and Risk of Preterm Delivery. *Obstetrics and gynecology*, 112(3), pp.524–531.

Yoon, B.H., Romero, R., et al., 1997a. Amniotic fluid cytokines (interleukin-6, tumor necrosis factor-alpha, interleukin-1 beta, and interleukin-8) and the risk for the development of bronchopulmonary dysplasia. *American journal of obstetrics and gynecology*, 177(4), pp.825–830.

Yoon, B.H., Jun, J.K., et al., 1997b. Amniotic fluid inflammatory cytokines (interleukin-6, interleukin-1beta, and tumor necrosis factor-alpha), neonatal brain white matter lesions, and cerebral palsy. *American journal of obstetrics and gynecology*, 177(1), pp.19–26.

Yoon, B.H., Kim, C.J., et al., 1997c. Experimentally induced intrauterine infection causes fetal brain white matter lesions in rabbits. *American journal of obstetrics and gynecology*, 177(4), pp.797–802.

Yoon, B.H. et al., 1996. Interleukin-6 concentrations in umbilical cord plasma are elevated in neonates with white matter lesions associated with periventricular leukomalacia. *American journal of obstetrics and gynecology*, 174(5), pp.1433–1440.

Yoon, B.H., Park, C.-W. & Chaiworapongsa, T., 2003. Intrauterine infection and the development of cerebral palsy. *BJOG : an international journal of obstetrics and gynaecology*, 110 (Suppl 20), pp.124–127.

Young, A. et al., 2002. Immunolocalization of proinflammatory cytokines in myometrium, cervix, and fetal membranes during human parturition at term. *Biology of reproduction*, 66(2), pp.445–9.

Yurttutan, S. et al., 2014. Beneficial effects of Etanercept on experimental necrotizing enterocolitis. *Pediatric surgery international*, 30(1), pp.71–777.

Zaiss, A.-K. et al., 2002. Differential activation of innate immune responses by adenovirus and adeno-associated virus vectors. *Journal of virology*, 76(9), pp.4580–4590.

Zaragoza, D.B. et al., 2006. The interleukin 1beta-induced expression of human prostaglandin F2alpha receptor messenger RNA in human myometrial-derived ULTR cells requires the transcription factor, NFkappaB. *Biology of reproduction*, 75(5), pp.697–704.

Zaretsky, M. V et al., 2004. Transfer of inflammatory cytokines across the placenta. *Obstetrics and gynecology*, 103(3), pp.546–550.

Zerrate, M.C. et al., 2007. Neuroinflammation and behavioral abnormalities after neonatal terbutaline treatment in rats: implications for autism. *The Journal of pharmacology and experimental therapeutics*, 322(1), pp.16–22.

Zhang, Y. et al., 2000. CD40 ligand-dependent activation of cytotoxic T lymphocytes by adeno-associated virus vectors in vivo: role of immature dendritic cells. *Journal of virology*, 74(17), pp.8003–10.

Zhu, J., Huang, X. & Yang, Y., 2009. The TLR9-MyD88 pathway is critical for adaptive immune responses to adeno-associated virus gene therapy vectors in mice. *The Journal of clinical investigation*, 119(8), pp.2388–2398.

Zincarelli, C. et al., 2008. Analysis of AAV serotypes 1-9 mediated gene expression and tropism in mice after systemic injection. *Molecular therapy : the journal of the American Society of Gene Therapy*, 16(6), pp.1073–1080.

Zinn, E. & Vandenberghe, L.H., 2014. Adeno-associated virus: fit to serve. *Current opinion in virology*, 8, pp.90–97.

Chapter 10 Appendix

10.1. Reagents and buffers

10.1.1. *E.coli* culture and bacterial transformations

Ampicillin	*Life Technologies, Glasgow, UK*
Erythromycin	*Life Technologies, Glasgow, UK*
Kanamycin	*Life Technologies, Glasgow, UK*
ccdB chemically competent E.coli cells	*Life Technologies, Glasgow, UK*
One Shot Stbl3™	*Qiagen, Manchester, UK*
Luria-Bertani agar	*Life Technologies, Glasgow, UK*
Luria-Bertani Broth	*Life Technologies, Glasgow, UK*
Qiagen Maxi-prep kit	*Qiagen, Manchester, UK*
Qiagen Mini-prep kit	*Life Technologies, Glasgow, UK*
SOC medium	*Life Technologies, Glasgow, UK*
SIM medium agar	*Sigma Aldrich, Dorset, UK*

10.1.2. Immunohistochemistry and Immunofluorescence staining

30% H_2O_2	*Sigma Aldrich, Dorset, UK*
3,3'-Diaminobenzidine (DAB)	*Sigma Aldrich, Dorset, UK*
DAPI	*Invitrogen, California, USA*
Glacial Acetic Acid	*Sigma Aldrich, Dorset, UK*
Histoclear	*National Diagnostics, Yorkshire, UK*
Rabbit anti-mature HBD-3 antibody	*Abcam, Cambridge, UK*
Mouse anti-full HBD-3 antibody	*Abcam, Cambridge, UK*

Rat anti-Ly6g antibody	*Abcam, Cambridge, UK*
Rabbit anti-cytokeratin antibody	*Abcam, Cambridge, UK*
Hamster anti-ICAM-1 antibody	*Merck Millipore, Germany*
Chicken anti-GFP antibody	*Aves labs, Oregon, USA*
Goat anti-rat secondary antibody	*Vector Laboratories, Cambridge, UK*
Goat anti-mouse secondary antibody	*Vector Laboratories, Cambridge, UK*
Goat anti-rabbit secondary antibody	*Vector Laboratories, Cambridge, UK*
Goat anti-rabbit alexa fluor 488 dye	*Invitrogen, California, USA*
Goat anti-chicken alexa fluor 488 dye	*Invitrogen, California, USA*
Goat anti-rabbit alexa fluor 568 dye	*Invitrogen, California, USA*
Goat Serum	*Vector Laboratories, Cambridge, UK*
Mouse serum	*Vector Laboratories, Cambridge, UK*
Triton X-100	*Sigma Aldrich, Dorset, UK*
ABC Vectastain	*Vector Laboratories, Cambridge, UK*
DPX mounting solution	*Thermo-fisher scientific, Glasgow*
Fluoromount-G mounting solution	*Southern Biotech, Birmingham, USA*

10.1.3. Cell culture and *in vitro* experiments

0.05% Trypsin-EDTA	*Life Technologies, Glasgow, UK*
0.25% Trypsin-EDTA	*Life technologies, Glasgow, UK*
1x Phosphate buffered Saline	*Life Technologies, Glasgow, UK*
DMEM	*Life Technologies, Glasgow, UK*
Fetal Calf Serum	*Life Technologies, Glasgow, UK*
Keratinocyte serum free medium	*Life technologies, Glasgow, UK*
Bovine pituitary extract	*Life technologies, Glasgow, UK*
Human recombinant epidermal growth factor	*Life technologies, Glasgow, UK*

Calcium chloride	*Sigma Aldrich, Dorset, UK*
Penicillin-Streptomycin	*Life technologies, Glasgow, UK*

10.1.4. Viral vector production

Isopropanol	*VWR, Lutterworth, UK*
10% Acrylamide gel	*Life Technologies, Glasgow, UK*
2x Laemlli buffer	*Sigma Aldrich, Dorset, UK*
4-12% Polyacrylamide gel	*Life technologies, Glasgow, UK*
50KDa Polyethyleneimine (PEI)	*Sigma Aldrich, Dorset, UK*
PEI (AAV)	*Polyscience, Northampton, UK*
50x MOPS buffer	*Life Technologies, Glasgow, UK*
Benzonase	*Life Technologies, Glasgow, UK*
Ethanol	*VWR, Lutterworth, UK*
Gel Red	*Biotium, Cambridge, UK*
Glycine	*Sigma Aldrich, Dorset, UK*
Hyperladder 1	*New England Biolabs, USA*
Magnesium Sulphate	*Sigma Aldrich, Dorset, UK*
Optimem	*Life Technologies, Glasgow, UK*
p24 assay kit	*Zeptometric Corporation, New York, USA*
Protein ladder broad range	*New England Biolabs, USA*
Sodium dexycholate	*VWR, Lutterworth, UK*
Tris	*Sigma Aldrich, Dorset, UK*
Sodium Chloride	*Sigma Aldrich, Dorset, UK*

10.1.5. *In vivo* experiments

Isoflurane	*Abbott Laboratories, London, UK*
D-Luciferin (Potassium salt) (LUCK-1G-OPT2)	*Gold Biotechnology Inc, St Louis, USA*
Hydrochloric acid	*Fisher chemical, Loughborough, UK*
Lipopolysaccharide	*Life Technologies, Glasgow, UK*
Paraformaldehyde	*Sigma Aldrich, Dorset, UK*
Sodium Azide	*VWR, Lutterworth, UK*
Sucrose	*Sigma Aldrich, Dorset, UK*
Pluronic F127 gel	*Sigma Aldrich, Dorset, UK*
AK12 gel	*PolyVivo, USA*

10.1.6. Western blotting

4x laemelli buffer	*Sigma Aldrich, Dorset, UK*
Dithiothreitol (DTT)	*Sigma Aldrich, Dorset, UK*
SDS buffer	*BioRad, Hemel Hempstead, UK*
Mini-PROTEAN® TGX™ Precast Gels	*BioRad, Hemel Hempstead, UK*
Precision plus protein all blue ladder	*BioRad, Hemel Hempstead, UK*
PVDF membranes	*BioRad, Hemel Hempstead, UK*
Secondary rabbit HRP-conjugated antibody	*Abcam, Cambridge, UK*
Chemiluminescence kit	*BioRad, Hemel Hempstead, UK*
Skimmed milk powder	*Sigma Aldrich, Dorset, UK*

10.1.7. ELISAs

HBD-3 ELISA kit	*Peprotech, London, UK*
Recombinant HBD-3 protein	*Peprotech, London, UK*
Murine IL-1β ELISA kit	*R&D systems, Minneapolis, USA*
Murine TNF-α ELISA kit	*R&D, Minneapolis, USA*
Recombinant GFP protein	*Sigma Aldrich, Dorset, UK*
ABTS substrate solution	*Sigma Aldrich, Dorset, UK*
TMB substrate solution	*Sigma Aldrich, Dorset, UK*
Sulphuric acid	*Sigma Aldrich, Dorset, UK*
Streptavidin HRP	*Invitrogen, California, USA*
Monoclonal anti-GFP antibody	*Abcam, Cambridge, UK*
Biotinylated polyclonal anti-GFP antibody	*Abcam, Cambridge, UK*

10.2. Buffers

LB Broth	1L: 10g NaCl, 5g Yeast extract, 10g tryptone peptone. Autoclave
LB Agar	1L: 10g NaCl, 5g Yeast extract, 10g tryptone peptone, 15g bacto agar. Autoclave.
50 x TAE	1L: 242g Trisamine (Tris), 57.1 mL Glacial Acetic Acid, 100mL 0.5M EDTA
5x DNA loading dye (Orange G)	25mL: 6.75g Ficoll (15%), 0.25g Orange G, up to 25mL with dH_20

TD buffer	1L: 8.18g NaCl, 372.8mg KCl, 95.26mg K_2HPO_4, 333.23mg $MgCl_2$, 3.03g Tris; pH 7.5. Autoclave
MOPS buffer	1L: 50mL 20x MOPS buffer in 1L dH_20
Coomassie blue dye	1L: 500mL Methanol, 400mL dH_20, 100mL Acetic acid, 2.5g Coomassie Brilliant blue R-250
Destain solution	1L: 250mL Methanol, 680mL dH_20, 70mL Acetic acid
50x Alkaline Electrophoresis buffer	1L: 100g NaOH, 14.62g EDTA
Alkaline sample loading buffer	350µl: 200µl 20% Glycerol, 80µl 50x Alkaline electrophoresis buffer, 60µl of 20% SDS and dip pipette tip in Xylene Cyanol powder and mix in solution
4x Gelred	1L: 1 gel volume solution in to 5.8g NaCl; 20mL 5M NaCl of dH_20
4% Paraformaldehyde (PFA)	1L: 40g PFA in 1L 1x Phosphate-buffered saline (PBS)
30% Sucrose	1L: 300g Sucrose in 1L 1x PBS
10x Tris-buffered Saline (TBS)	1L: 64g Trisamine (Tris), 88g NaCl and 34mL Hydrochloric acid; pH 7.6
TBSAF	1L: 700mL 1x TBS, 3.5mL 10% Sodium Azide, 300mL Ethlyene Glycol and 150g Sucrose
TBS-T	1L: 0.1% of Triton X-100 in 1x TBS

TUNEL staining solution	13ml: 13µl TdT, 19.5µl biotinylated dUTP (deoxyuridine triphosphate), 1.3ml cacodylate buffer in 11.67ml ddH2O
Cacodylate buffer	100ml: 3.64g Tris in 80ml dH2O, add 29.96g Cacodylate (pH 7.5 with HCl), add 0.24g Cobalt chloride (pH 7.2 with HCl) and the final volume to 100ml with ddH2O (stored at 4°C)
TUNEL stop solution	200ml: 300mM NaCl (1753.2mg in 100ml dH_2O) + 30mM Sodium citrate (1882.3mg in 100ml dH_2O).
DAB cobalt-nickel solution	150ml 10mM PB: 75mg DAB, 1.5ml Cobalt-nickel, 1.5ml CaSO4, 50.1 µl H_2O_2
0.5M Phosphate buffer	1L: 20g NaOH, 71g NaH_2PO_4 in 1L ddH_20, pH adjusted to 7.4 with H_3PO_4
SIM medium agar	3g in 100ml ddH_20
Bicarbonate buffer	0.8g Na_2CO_3, 1.465g $NaHCO_3$ in 500ml ddH_20
Wash buffer	200µl TWEEN-20 in 400ml PBS
Block solution	4g BSA in 400ml PBS

10.3. Antibody dilutions

10.3.1. Immunohistochemistry

Primary antibody	**Dilution**	**Secondary Antibody**	**Dilution**
Rabbit Anti-GFP antibody (abcam 13970)	1:10000	Biotinylated Goat Anti-Rabbit IgG Antibody (Vector Biolabs)	1:1000
Rabbit Anti-wide spectrum cytokeratin antibody (abcam 9377)	1:2000	Biotinylated Goat Anti-Rabbit IgG Antibody (Vector Biolabs)	1:1000
Mouse CD68-antibody	1:500	Biotinylated Rabbit Anti-Mouse IgG Antibody (Vector Biolabs)	1:1000
Rat Anti-Ly6G antibody (abcam 25377)	1:500	Biotinylated Goat Anti-Rat IgG Antibody (Vector Biolabs)	1:1000
Rabbit Anti-HBD-3 antibody (Millipore 3478)	1:250	Biotinylated Goat Anti-Rabbit IgG Antibody (Vector Biolabs)	1:500
Hamster Anti-ICAM-1 antibody (VWR)	1:3000	Biotinylated Goat Anti-Hamster IgG Antibody (Vector Biolabs)	1:1000

10.3.2. Immunofluorescence

Primary antibody	**Dilution**	**Secondary Antibody**	**Dilution**
Chicken Anti-GFP antibody (abcam 13970)	1:1000	Goat anti-chicken IgY H&L (Alexa Fluor® 488 abcam 150169)	1:1000
Rabbit Anti-wide spectrum cytokeratin antibody (abcam 9377)	1:2000	Goat anti-rabbit IgG H&L (Alexa Fluor® 568 abcam 175471)	1:1000
Rabbit Anti-*E.coli* antibody (abcam 137967)	1:500	Goat anti-rabbit IgG H&L (Alexa Fluor® 488 abcam 150077)	1:1000
Rat Anti-Ly6G antibody (abcam 25377)	1:500	Goat anti-rat IgG H&L (Alexa Fluor® 568 abcam 175476)	1:1000
Rabbit Anti-HBD-3 antibody (Millipore 3478)	1:500	Goat anti-rabbit IgG H&L (Alexa Fluor® 568 abcam 175471)	1:500
Mouse Anti-FoxP3 antibody (abcam 20034)	1:500	Goat Anti-Mouse IgG H&L (Alexa Fluor® 488 abcam 150113)	1:1000

10.3.3. ELISAs

Antibody	**Dilution**
Anti-mouse TNF-α capture antibody	1:40
Biotinylated goat anti-mouse TNF- α detection antibody	1:125
Anti-mouse IL-1β capture antibody	1:120
Biotinylated goat anti-mouse IL-1β detection antibody	1:60
Anti-rabbit HBD3 capture antibody	1:100
Biotinylated anti-rabbit HBD3 detection antibody	1:200

10.4. Primer sequences

Primer	Sequence
GAPDH	
F	ACTCCACTCACGGCAAATTC
R	TCTCCATGGTGGTGAAGACA
IL-1β	
F	CAGGCAGGCAGTATCACTCA
R	AGCTCATATGGGTCCGACAG
TNF-α	
F	TATGGCTCAGGGTCCAACTC
R	CTCCCTTTGCAGAACTCAGG
IL-6	
F	AGTTGCCTTCTTGGGACTGA
R	TCCACGATTTCCCAGAGAAC
CXCL-1	
F	GCCTATCGCCAATGAGCTG
R	AAGGGAGCTTCAGGGTCAAG
CXCL-2	
F	CAGTGCCTCCAACAAGCTTC
R	CATTGACAGCGCAGTTCACT
CXCR-2	
F	TTCTGCTACGGGTTCACACT
R	TTAAGGCAGCTGTGGAGGAA
IL-10	
F	GGTGAGAAGCTGAAGACCCT

R	TGTCTAGGTCCTGGAGTCCA
HBD-3 F R	 GGTGAAGCCTAGCAGCTAGGATC GAGCACTTGCCGATCTGTTCCTCC
mBD-14 F R	 CCTCATCTTGTTCTTGGTGCC TCTTTCGGCAGCATTTTCGA
16S Broad range rRNA F R	 TCCTACGGGAGGCAGCAGT GGACTACCAGGGTATCTAATCCTGTT

10.4.1. Illumina amplicon barcoded primers and custom sequencing primers

A1	701	CGAGAGTT	501	ATCGTACG
A2	702	ACTATGTC	501	ATCGTACG
A3	703	ACGCTACT	501	ATCGTACG
A4	704	ACTCACTG	501	ATCGTACG
A5	705	TGAGTACG	501	ATCGTACG
A6	706	CTGCGTAG	501	ATCGTACG
A7	707	TAGTCTCC	501	ATCGTACG
A8	708	CGAGCGAC	501	ATCGTACG
A9	709	ACTACGAC	501	ATCGTACG
A10	710	GTCTGCTA	501	ATCGTACG
A11	711	GTCTATGA	501	ATCGTACG
A12	712	TATAGCGA	501	ATCGTACG
B1	701	CGAGAGTT	502	ACTATCTG
B2	702	ACTATGTC	502	ACTATCTG
B3	703	ACGCTACT	502	ACTATCTG

B4	704	ACTCACTG	502	ACTATCTG
B5	705	TGAGTACG	502	ACTATCTG
B6	706	CTGCGTAG	502	ACTATCTG
B7	707	TAGTCTCC	502	ACTATCTG
B8	708	CGAGCGAC	502	ACTATCTG
B9	709	ACTACGAC	502	ACTATCTG
B10	710	GTCTGCTA	502	ACTATCTG
B11	711	GTCTATGA	502	ACTATCTG
B12	712	TATAGCGA	502	ACTATCTG
C1	701	CGAGAGTT	503	TAGCGAGT
C2	702	ACTATGTC	503	TAGCGAGT
C3	703	ACGCTACT	503	TAGCGAGT
C4	704	ACTCACTG	503	TAGCGAGT
C5	705	TGAGTACG	503	TAGCGAGT
C6	706	CTGCGTAG	503	TAGCGAGT
C7	707	TAGTCTCC	503	TAGCGAGT
C8	708	CGAGCGAC	503	TAGCGAGT
C9	709	ACTACGAC	503	TAGCGAGT
C10	710	GTCTGCTA	503	TAGCGAGT
C11	711	GTCTATGA	503	TAGCGAGT
C12	712	TATAGCGA	503	TAGCGAGT
D1	701	CGAGAGTT	504	CTGCGTGT
D2	702	ACTATGTC	504	CTGCGTGT
D3	703	ACGCTACT	504	CTGCGTGT
D4	704	ACTCACTG	504	CTGCGTGT
D5	705	TGAGTACG	504	CTGCGTGT
D6	706	CTGCGTAG	504	CTGCGTGT
D7	707	TAGTCTCC	504	CTGCGTGT
D8	708	CGAGCGAC	504	CTGCGTGT
D9	709	ACTACGAC	504	CTGCGTGT
D10	710	GTCTGCTA	504	CTGCGTGT

D11	711	GTCTATGA	504	CTGCGTGT
D12	712	TATAGCGA	504	CTGCGTGT
E1	701	CGAGAGTT	505	TCATCGAG
E2	702	ACTATGTC	505	TCATCGAG
E3	703	ACGCTACT	505	TCATCGAG
E4	704	ACTCACTG	505	TCATCGAG
E5	705	TGAGTACG	505	TCATCGAG
E6	706	CTGCGTAG	505	TCATCGAG
E7	707	TAGTCTCC	505	TCATCGAG
E8	708	CGAGCGAC	505	TCATCGAG
E9	709	ACTACGAC	505	TCATCGAG
E10	710	GTCTGCTA	505	TCATCGAG
E11	711	GTCTATGA	505	TCATCGAG
E12	712	TATAGCGA	505	TCATCGAG
F1	701	CGAGAGTT	506	CGTGAGTG
F2	702	ACTATGTC	506	CGTGAGTG
F3	703	ACGCTACT	506	CGTGAGTG
F4	704	ACTCACTG	506	CGTGAGTG
F5	705	TGAGTACG	506	CGTGAGTG
F6	706	CTGCGTAG	506	CGTGAGTG
F7	707	TAGTCTCC	506	CGTGAGTG
F8	708	CGAGCGAC	506	CGTGAGTG
F9	709	ACTACGAC	506	CGTGAGTG
F10	710	GTCTGCTA	506	CGTGAGTG
F11	711	GTCTATGA	506	CGTGAGTG
F12	712	TATAGCGA	506	CGTGAGTG
G1	701	CGAGAGTT	507	GGATATCT
G2	702	ACTATGTC	507	GGATATCT
G3	703	ACGCTACT	507	GGATATCT
G4	704	ACTCACTG	507	GGATATCT
G5	705	TGAGTACG	507	GGATATCT

G6	706	CTGCGTAG	507	GGATATCT
G7	707	TAGTCTCC	507	GGATATCT
G8	708	CGAGCGAC	507	GGATATCT
G9	709	ACTACGAC	507	GGATATCT
G10	710	GTCTGCTA	507	GGATATCT
G11	711	GTCTATGA	507	GGATATCT
G12	712	TATAGCGA	507	GGATATCT
H1	701	CGAGAGTT	508	GACACCGT
H2	702	ACTATGTC	508	GACACCGT
H3	703	ACGCTACT	508	GACACCGT
H4	704	ACTCACTG	508	GACACCGT
H5	705	TGAGTACG	508	GACACCGT
H6	706	CTGCGTAG	508	GACACCGT
H7	707	TAGTCTCC	508	GACACCGT
H8	708	CGAGCGAC	508	GACACCGT
H9	709	ACTACGAC	508	GACACCGT
H10	710	GTCTGCTA	508	GACACCGT
H11	711	GTCTATGA	508	GACACCGT

10.5. AAV CMV HBD-3 CMV GFP plasmid map (Vector Biolab)

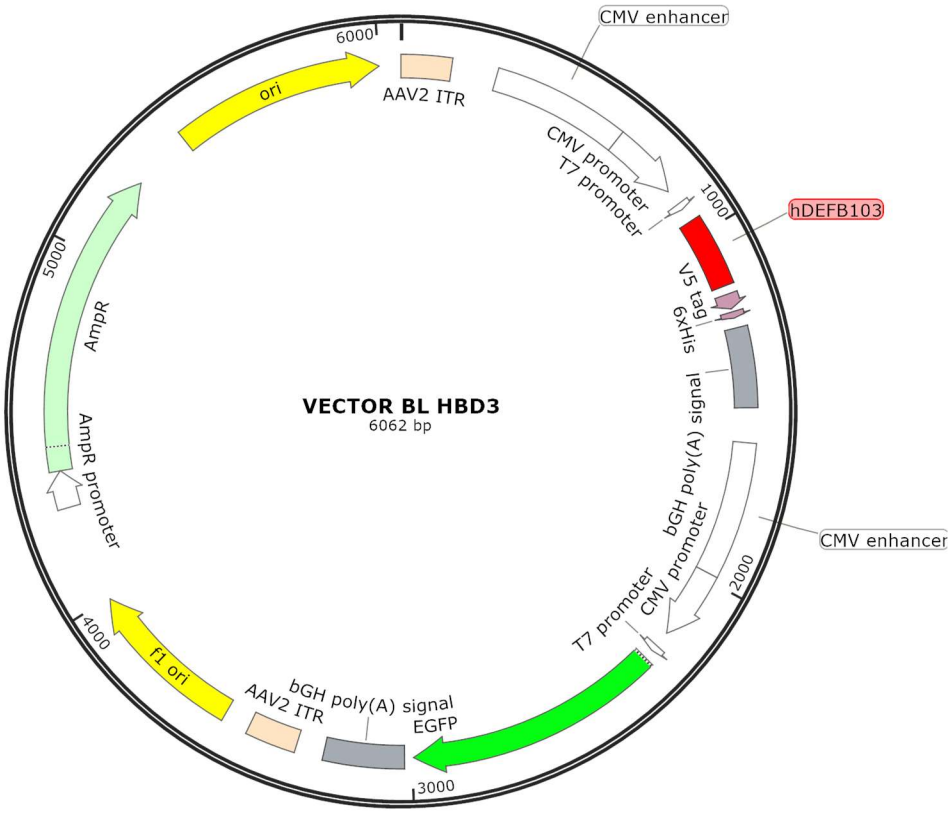

Figure 10.1: Bicistronic AAV HBD3 GFP plasmid map; *hDEFB103* (HBD-3 transgene) and *eGFP* run by separate CMV promoters. There is a *bGH*-polyA signal following each transgene.

10.6. Abbreviations

AAV	Adeno-associated virus
ABC	Avidin–biotin conjugates
Ad	Adenovirus
AMP	Antimicrobial peptide
bp	Base pair
BSA	Bovine serum albumin
CFU	Colony forming unit
CMV	Cytomegalovirus

DAB	Diaminobenzidine
DNA	Deoxyribonucleic acid
***E.coli*-k1**	*E.coli* K1 lux-operon
***E.coli*-k12**	*E.coli* K12 lux-operon
EDTA	Ethylenediaminetetraacetic acid
End1/E6E7	Human endocervical cells
GC	Genome copies
HBD	Human β-defensin
HEK 293-T	Human Embryonic Kidney 293-T cells
HNP	Human neutrophil peptide
HPLC	High Pressure Liquid chromatography
HRP	Horseradish Peroxidase
IP	Intraperitoneal
IV	Intravenous
IVag	Intravaginal
kb	Kilobases
kDa	Kilodaltons
LPS	Lipopolysaccharide
NF-κB	nuclear factor kappa-light-chain-enhancer of activated B cell
PBS	Phosphate buffered saline
PCR	Polymerase chain reaction
PFA	Paraformaldehyde
RAd	Recombinant adenovirus
RT	Reproductive tract
SFFV	Spleen focus forming virus

SLPI	Secretory leucocyte protease inhibitor
TBS	Tris buffered saline
VSV-g	Vesicular stomatitis virus glycoprotein G
WT	Wildtype

10.7. Additional data from Chapter 5: AAV HBD-3 treatment in a non pregnant model of ascending infection

10.7.1. HBD-3 reduces *E.coli* K12 vaginal infection in non-pregnant mice at 24 hours after infection

To assess the effect of cervical overexpression of HBD-3 on ascending vaginal infection, AAV HBD3 was administered and then 72 hours later intravaginal *E.coli* K12 was instilled (Figure 10.2). Mice were treated with medroxy-progesterone acetate 1 week prior to these experiments to ensure they were in the diestrus stage of the estrous cycle.

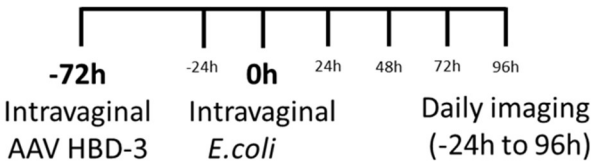

Figure 10.2: Summary of experimental plan for determining the effect of HBD-3 expression on intravaginal *E.coli* K12 infection in non-pregnant mice.

Following bacterial administration, *E.coli* bioluminescence remains close to baseline (0h time point) in the HBD-3 transduced group, except for one outlier, inferring that bacterial clearance is likely to have occurred in most of these mice. In the control group, bioluminescence did not remain at baseline signifying ongoing bacterial infection (Figure 10.3). As it was difficult to distinguish vaginal and uterine bacteria in the non-pregnant

mouse, fold change in bioluminescence signal from the whole reproductive tract was determined by comparing bioluminescent signal at different time points after infection to the bioluminescent signal prior to bacterial administration (Figure 10.4). There was no difference in the later time points (Figure 10.4).

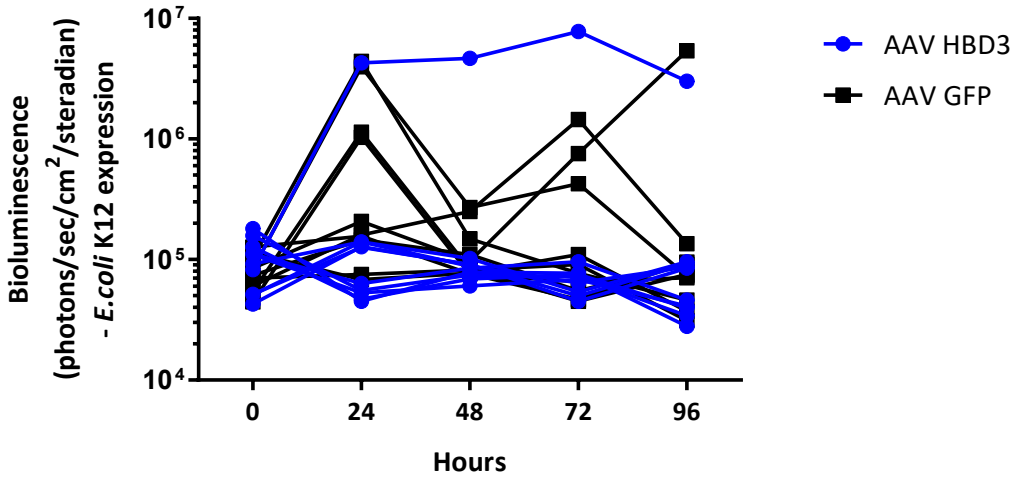

Figure 10.3: HBD-3 reduces *E.coli* K12 vaginal infection in non-pregnant mice at 24 hours after infection. Intravaginal *E.coli* K12 bioluminescence expression following cervical administration of AAV HBD3 or AAV GFP. 0h time point signifies baseline bioluminescent signal prior to bacterial administration. n=14 in the AAV GFP group, n=15 in the AAV HBD3 group.

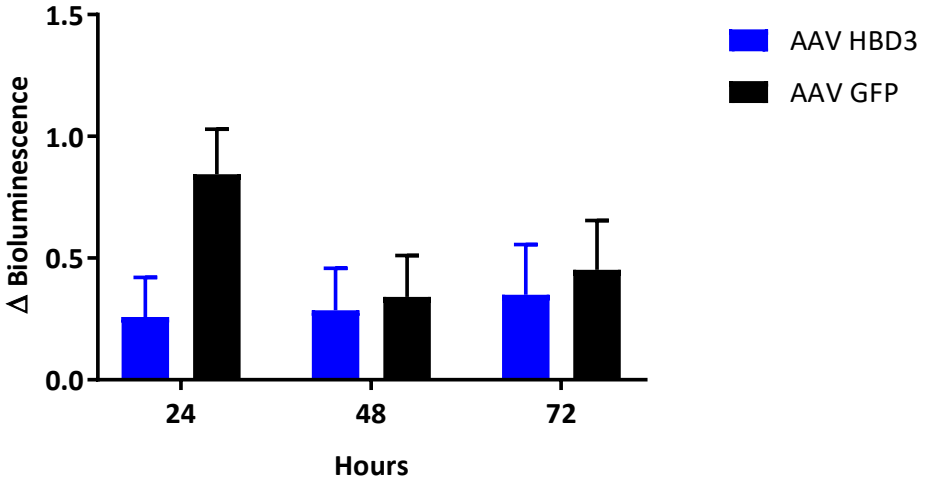

Figure 10.4: HBD-3 reduces *E.coli* K12 vaginal infection in non-pregnant mice at 24 hours after infection. Fold change in *E.coli* K12 bioluminescence over time (log transformed data shown here). n=14 in the AAV GFP group, n=15 in the AAV HBD3 group; data log transformed and analysed with repeated measures two-way ANOVA with post hoc Bonferroni test.